UNIVERSIDADE DE LISBOA

INSTITUTO SUPERIOR TÉCNICO

Fire behaviour of reinforced concrete structures strengthened with CFRP strips

João Pedro Lage da Costa Firmo

Supervisor: Doctor João Pedro Ramôa Ribeiro Correia

Co-Supervisor: Doctor Mário Rui Tiago Arruda

Thesis approved in public session to obtain the PhD Degree in Civil Engineering

Jury final classification: Pass with Distinction

Jury

Chairperson: **Chairman of the IST Scientific Board**

Members of the Committe:

Doctor Eduardo Nuno Brito Santos Júlio
Doctor José Manuel de Sena Cruz
Doctor João Pedro Ramôa Ribeiro Correia
Doctor João Paulo Correia Rodrigues
Doctor Carlos Manuel Tiago Tavares Fernandes
Doctor Mário Rui Tiago Arruda

2015

UNIVERSIDADE DE LISBOA

INSTITUTO SUPERIOR TÉCNICO

Fire behaviour of reinforced concrete structures strengthened with CFRP strips

João Pedro Lage da Costa Firmo

Supervisor: Doctor João Pedro Ramôa Ribeiro Correia
Co-Supervisor: Doctor Mário Rui Tiago Arruda

Thesis approved in public session to obtain the PhD Degree in Civil Engineering

Jury final classification: Pass with Distinction

Jury

Chairperson: Chairman of the IST Scientific Board

Members of the Committe:

Doctor Eduardo Nuno Brito Santos Júlio, Professor Catedrático do Instituto Superior Técnico da Universidade de Lisboa
Doctor José Manuel de Sena Cruz, Professor Associado da Escola de Engenharia da Universidade do Minho
Doctor João Pedro Ramôa Ribeiro Correia, Professor Associado do Instituto Superior Técnico da Universidade de Lisboa
Doctor João Paulo Correia Rodrigues, Professor Auxiliar (com Agregação) da Faculdade de Ciências e Tecnologia da Universidade de Coimbra
Doctor Carlos Manuel Tiago Tavares Fernandes, Professor Auxiliar do Instituto Superior Técnico da Universidade de Lisboa
Doctor Mário Rui Tiago Arruda, Investigador Pós-Doutoramento do Instituto Superior Técnico da Universidade de Lisboa

Funding Institutions

Fundação para a Ciência e a Tecnologia (SFRH/BD/74443/2010)
Fundação para a Ciência e a Tecnologia (PTDC/ECM/118271/2010)

2015

ABSTRACT

Carbon fibre reinforced polymer (CFRP) materials have been successfully used to strengthen civil engineering structures over the past 25 years, due to the advantages they present over traditional materials (concrete or steel), such as high strength-to-weight ratio, corrosion resistance and easy installation.

Although the structural effectiveness of CFRP strengthening techniques at ambient temperature has been widely confirmed in numerous investigations, their performance at elevated temperatures continues to hinder a more widespread application in buildings, where the fire action has to be considered at design. In fact, the strength and stiffness of CFRPs are severely deteriorated at moderately elevated temperature, namely when approaching the glass transition temperature (T_g) of the polymer matrix, which typically varies between 55 ºC and 120 ºC. The bond between CFRPs and the concrete substrate, which is critical to maintain the structural effectiveness of the strengthening system, is even more affected by temperature, since it is usually ensured by epoxy-based adhesives cured at ambient temperature, with lower T_g (typically ranging from 40 °C to 80 °C) than that exhibited by CFRPs. The available studies about this subject suggest that adequate fire protection systems need to be developed to allow extending the structural use of CFRP systems in buildings, pointing out that extensive research is needed to fill all the gaps in current knowledge.

The investigations developed in this thesis had two main objectives: (i) to obtain in-depth understanding about the behaviour at elevated temperature and under fire exposure of reinforced concrete (RC) structures strengthened with CFRP materials, and (ii) to develop a design method for the definition of tailored fire protection systems, thus allowing a widespread use of these strengthening systems in buildings. To achieve these goals, the research was conducted along the following two domains: (i) bond behaviour of CFRP-concrete interfaces at elevated temperature and (ii) fire behaviour of RC beams flexurally strengthened with CFRP strips.

The research on the bond behaviour of CFRP-concrete interfaces comprised double-lap shear tests at elevated temperatures (up to 150 °C) on four different types of concrete blocks strengthened with CFRP strips installed as follows: (i) as externally bonded reinforcement (EBR technique) using a current epoxy adhesive, (ii) EBR using a current epoxy adhesive and mechanically anchored to concrete with bolted steel plates, (iii) near surface mounted (NSM technique) using a current epoxy adhesive, and (iv) NSM using a mixed epoxy-cement adhesive. These tests allowed quantifying the stiffness and strength degradation with temperature for the most representative CFRP strengthening

techniques (EBR and NSM), obtaining temperature-dependent "bond stress *vs.* relative slip" laws and evaluating the influence of applying mechanical anchorages in EBR-CFRP strips and using different adhesives in NSM-CFRP strips on their bond performance with temperature. Additionally, numerical models of the above mentioned tests were developed, allowing deriving global bond *vs.* slip laws as a function of temperature for the CFRP-concrete interaction.

Regarding the second topic, the fire behaviour of RC beams strengthened with CFRP strips, in a first stage a preliminary methodology for the design of fire protection systems was proposed. The geometry of fire insulation schemes was optimized based on results of numerical thermal models and consisted of thicker insulation boards in the CFRP anchorages zones and thinner ones along the remaining length of the CFRP systems. This insulation strategy was based on the possibility of exploiting the mechanical contribution of the CFRP strengthening system through a cable behaviour (observed in previous tests), in which the CFRP system retains its structural effectiveness during fire even after the CFRP-concrete interaction is destroyed along its central length. Additional experimental and numerical studies about the flexural behaviour of partially bonded CFRP-strengthened RC beams at ambient temperature were performed to understand in further depth such cable behaviour. In a next stage fire resistance tests on insulated RC beams flexurally strengthened with CFRP systems (similar to those used in the double-lap shear tests) were performed. These tests, besides providing a better understanding of the structural effectiveness of CFRP strengthening systems in fire, validated the above-mentioned strategy for the design of fire protection systems. With the insulation schemes proposed, it was possible to exploit the CFRP mechanical contribution during fire exposure, in some case for more than 90 min, thus fulfilling stringent building code requirements. Finally, these fire resistance tests were numerically simulated, providing further validation to that insulation strategy as well as to the temperature dependent global bond *vs.* slip laws proposed for the CFRP-concrete interaction, showing they are adequate for simulating the behaviour of EBR-CFRP strengthening systems under fire exposure.

Keywords: Carbon fibre reinforced polymers (CFRP), reinforced concrete (RC), CFRP strengthening of RC structures, externally bonded reinforcement (EBR) technique, near surface mounted (NSM) technique, elevated temperatures, bond behaviour, fire behaviour, fire protection systems, experimental tests.

RESUMO

Os materiais poliméricos reforçados com fibras de carbono (CFRP) têm sido utilizados com sucesso no reforço de estruturas ao longo dos últimos 25 anos, sobretudo devido às vantagens que apresentam face aos materiais tradicionais (como o betão ou o aço), destacando-se o elevado rácio resistência/peso, a resistência à corrosão e a facilidade de instalação.

Apesar da eficácia estrutural das técnicas de reforço com CFRP a temperatura ambiente ter sido confirmada e objecto de bastantes estudos, o seu fraco desempenho a temperaturas elevadas continua a impedir uma crescente utilização em edifícios, onde a acção do fogo tem de ser considerada em projecto. De facto, a resistência e a rigidez dos CFRPs são severamente afectadas a temperaturas moderadamente elevadas, nomeadamente quando estas se aproximam da temperatura de transição vítrea (T_g) da sua matriz polimérica, que tipicamente varia entre 55 °C e 120 °C. A ligação entre o CFRP e o betão, essencial para manter a eficácia estrutural do sistema de reforço, é ainda mais afectada pela temperatura, uma vez que é normalmente assegurada por adesivos de base epoxídica com T_g inferior (tipicamente variando entre 40 °C e 80 °C) à dos CFRPs. Os estudos disponíveis sobre este assunto referem a necessidade de desenvolver sistemas de protecção adequados que permitam aumentar a utilização dos sistemas CFRP em estruturas de edifícios, mencionando também a necessidade de aprofundar a investigação neste domínio.

A investigação desenvolvida na presente tese teve os seguintes objectivos principais: (i) compreender detalhadamente o comportamento a temperatura elevada e ao fogo de estruturas de betão armado (BA) reforçadas com materiais CFRP e (ii) desenvolver um método de dimensionamento de sistemas de protecção ao fogo específicos para estes sistemas de reforço, contribuindo, assim, para alargar a sua utilização em edifícios. Para atingir estes objectivos, a investigação foi desenvolvida segundo os seguintes dois domínios: (i) comportamento da interface betão-CFRP a temperatura elevada e (ii) comportamento ao fogo de vigas de BA reforçadas à flexão com laminados de CFRP.

Relativamente ao comportamento da interface betão-CFRP, foram realizados ensaios de corte de junta dupla a temperaturas elevadas (até 150 °C) em quatro tipos de blocos de betão reforçados com laminados de CFRP instalados das seguintes formas: (i) exteriormente (técnica EBR) com adesivo epoxídico convencional, (ii) EBR com adesivo epoxídico convencional e ancorados mecanicamente com chapas de aço aparafusadas, (iii) em rasgos no betão de recobrimento (NSM) com adesivo epoxídico convencional, e (iv) NSM com adesivo misto (ligantes epoxídicos e

cimentícios). Estes ensaios permitiram quantificar a degradação da resistência e rigidez com a temperatura para as duas técnicas de reforço com CFRPs mais representativas (EBR e NSM), obter relações tensões de corte *vs*. escorregamento para diversas temperaturas e avaliar a influência no desempenho da ligação a temperaturas elevadas da aplicação de ancoragens mecânicas na técnica EBR ou da utilização de um adesivo misto na técnica NSM. Adicionalmente, foram desenvolvidos modelos numéricos dos ensaios mencionados que permitiram derivar relações globais tensões de corte *vs*. escorregamento em função da temperatura para a interface betão-CFRP.

Relativamente ao segundo domínio, o comportamento ao fogo de vigas de BA reforçadas com laminados de CFRP, numa primeira fase, foi proposta uma metodologia preliminar para o dimensionamento de sistemas de protecção ao fogo. A geometria dos esquemas propostos foi optimizada com base em resultados de modelos numéricos térmicos e consistiu em placas de isolamento de maior espessura na zona de ancoragem do sistema de reforço e de menor espessura na sua zona central. Esta estratégia de isolamento baseou-se na possibilidade de explorar a contribuição mecânica do CFRP através de um mecanismo de cabo (observado em ensaios anteriores), *i.e*, durante a exposição ao fogo, o sistema CFRP mantém a sua eficácia estrutural mesmo depois de a ligação betão-CFRP ter sido destruída na zona central. Complementarmente, para compreender com maior detalhe o referido comportamento de cabo, foram realizados estudos experimentais e numéricos a temperatura ambiente sobre o comportamento em flexão de vigas de BA reforçadas com CFRPs colados parcialmente. Numa fase seguinte, foram realizados ensaios de resistência ao fogo em vigas de BA reforçadas à flexão com sistemas CFRP semelhantes aos testados nos ensaios de corte com junta dupla. Estes ensaios, além de fornecerem resultados essenciais para a compreensão da eficácia estrutural dos sistemas CFRP durante a exposição ao fogo, permitiram validar a estratégia de dimensionamento de sistemas de protecção. Os resultados obtidos mostraram que, com recurso aos esquemas de isolamento propostos, é possível explorar a contribuição mecânica dos sistemas CFRP durante a exposição ao fogo, em alguns casos por mais de 90 min, permitindo, assim, cumprir os requisitos regulamentares exigentes para aplicação em edifícios. Por fim, estes ensaios de resistência ao fogo foram simulados numericamente, permitindo validar a metodologia de protecção e também as relações globais tensões de corte *vs*. escorregamento em função da temperatura para a interface betão-CFRP, mostrando a sua adequabilidade para simular o comportamento dos sistemas CFRP quando expostos ao fogo.

Palavras-chave: Polímeros reforçados com fibras de carbono (CFRP), betão armado (BA), estruturas de BA reforçadas com CFRP, técnica de reforço por colagem externa (EBR), técnica de reforço por instalação à superfície (NSM), temperaturas elevadas, comportamento da ligação betão-CFRP, comportamento ao fogo, sistemas de protecção ao fogo, ensaios experimentais.

ACKNOWLEDGEMENTS

I would like to use the following paragraphs to express my profound gratitude to the people who made my research work possible and remember that my accomplishments are also theirs, for this reason I dedicate this thesis to all of them.

First and foremost, I would like to thank my scientific supervisor, Professor João Ramôa Correia, for his constant availability, patience, friendship, generosity, and whose contribution was crucial for the development of this thesis. For his unmatched attention to people, his deep knowledge and incredible dedication to the research activity, Professor João Ramôa Correia has been a role model to me. It has been a great pleasure to work with him during the last 4 years.

I would like to express my gratitude to my co-supervisor, Doctor Mário Arruda, for his friendship, constant support and for lending his unique insight and experience to the numerical work presented herein. I would also like to thank to Professor Carlos Tiago for his support, willingness, suggestions and interesting discussions, particularly regarding the numerical problems.

I am also grateful to Professor Luke Bisby, from the *University of Edinburgh*, not only for welcoming me in the *BRE Centre for Fire Safety Engineering*, but also for the rich discussions about the results obtained in the experimental campaign, and for giving me the unique opportunity to contact, on a daily basis, with researchers and other PhD candidates working on the fire safety and on the fire behaviour of civil engineering structures.

I would also like to thank to my colleagues and fellow researchers at *Instituto Superior Técnico* (IST), namely José Gonilha, Mário Sá, Mário Garrido, Tiago Morgado, Luís Valarinho, David Martins, José Sampaio, Cristina López, Francisco Nunes, João Sousa, Daniel Ribeiro, Diogo Pitta, Taciano Correia and João Nunes, for their friendship, encouragement, for giving helpful suggestions and being always available to help me during the experimental campaign.

I would like to thank the valuable help of Professor Francisco Lemos, from the *Chemical Engineering Department* of IST, with the thermogravimetric (TGA) and differential scanning calorimetry (DSC) experiments. For the dynamic mechanical analyses (DMA), I would also like to thank the help of Dr. Susana Cabral Fonseca, from the *National Laboratory of Civil Engineering* (LNEC). For the double-lap shear tests, also performed at LNEC, I would like to express my gratitude to Doctor Helena Cruz and Doctor Manuel Pipa for making available the furnace used in the experiments and the laboratory facilities, respectively.

The present research was funded by the *Portuguese National Foundation for Science and Technology* (FCT) through a doctoral scholarship (SFRH/BD/74443/2010) and the *Carbofire* project (PTDC/ECM/118271/2010), whose support is greatly acknowledged. I would also like to thank to my research centre *Civil Engineering Research and Innovation for Sustainability* (CEris) and to the *Department of Civil Engineering, Architecture and Georesources* (DECivil) at IST for providing me the work conditions needed to develop this thesis.

I would also like to express my gratitude to the industrial partners who made the experimental campaign of this thesis possible by generously providing the materials, namely: *S&P Clever Reinforcement Ibérica*, in particular to Eng. Filipe Dourado, for supplying the CFRP strips and adhesives; *Secil* and *Unibetão* for supplying the concrete, HTecnic, in particular to Eng. João Farinha and Eng. Nuno Cerqueira, for preparing the test beams and all the formwork and steel reinforcement; and TRIA for supplying the fire protection materials.

I am also grateful to Mrs. Maria Helena Salvado for her patience, friendship, and indispensable help on solving all the bureaucratic problems. The work and help of the laboratory technicians Mr. Fernando Alves, Mr. Fernando Costa, Mr. João Lopes and Mr. Leonel Silva during the experimental campaign are gratefully appreciated, as they made the experimental campaign of this thesis possible.

I would like to thank my family for their understanding in some periods of absence and their support over the past 4 years, which were crucial for the progress and conclusion of this thesis. Finally, I would like to thank to my future wife, Carla, for being always present during my long periods of reclusion, for her unconditional love, support and encouragement on occasions far too numerous to mention.

TABLE OF CONTENTS

LIST OF FIGURES

LIST OF TABLES

NOTATION

Roman Lower Case

a	Length of the supports
a'	Parameter that describes the residual value for the mechanical properties
b	Width of the specimen
b'	Parameter empirically derived
b_f	FRP width
c	Cohesion
c'	Parameter empirically derived
d	Effective depth
f	Strength retention
f_{at}	Tensile strength of adhesive
f_c	Compressive strength of concrete
f_{cm}	Average compressive strength of concrete
f_{ct}	Tensile strength of concrete
f_{ctm}	Average tensile strength of concrete
f_{fu}	Tensile strength of FRP
f_{sy}	Yielding stress of steel
f_{syk}	Characteristic yielding stress of steel
f_{syu}	Ultimate yielding stress (post-hardening)
f_{sum}	Average failure stress of steel
f_t	Normal tensile resistance
h	Height of the specimen
h_c	Convection coefficient
k_b	Geometrical factor
k_m	Parameter obtained by fitting a hyperbolic tangent function to the experimental data
k_n	Elastic normal stiffness
k_t	Elastic tangential stiffness
l_e	Recommended FRP anchorage length
l_a	Adopted FRP anchorage length
m	Weibull exponent
n	Parameter that depends on the stress state

n'	Parameter empirically derived
r	Concrete cover
s	Slip
$\bar{s}_{i+1/2}$	Average slip between two consecutive strain gauges
s_{LM}	Slip corresponding to the maximum shear bond strength (τ_{LM})
s_{LO}	Ultimate slip
t	Time; insulation thickness at the central zone of the specimen
t_f	FRP thickness
x, y, z	Global reference axes of the structural element

Roman Capital

A	Parameter empirically derived; mechanical anchorage
A_f	Cross-sectional area of FRP
$A_{S,inf}$	Cross-sectional area of tensile steel reinforcing bars
$A_{S,sup}$	Cross-sectional area of steel reinforcing bars for compression
$A_{S,w}$	Cross-sectional area of shear reinforcing bars
B	Parameter empirically derived
B'	Interfacial brittleness index
C	Parameter empirically derived
$C_{p,CS}$	Specific heat capacity of calcium silicate (CS) boards
E	Elastic modulus retention
E'	Storage modulus
E_a	Elastic modulus of adhesive
E_c	Elastic modulus of concrete
E_{cm}	Average elastic modulus of concrete
E_f	Elastic modulus of FRP
E_s	Elastic modulus of steel
E_{sm}	Average elastic modulus of steel
E_{su}	Ultimate elastic modulus of steel (post-hardening)
F_u	Failure load
$F_{u,exp}$	Experimental failure load
$F_{u,num}$	Numerical failure load
G	Shear modulus
G_f	Interfacial fracture energy
G_{cf}	Fracture energy of concrete
K	Stiffness

L	CFRP laminate/strip; span; linear damage model; insulation length
NL	Non-linear damage model
P	Mechanical property; applied load
P_d	Design load
P_d^{RC}	Design load of the reinforced concrete beam
P_{fire}	Load applied during fire exposure
P_R	Relaxed property
P_u	Failure load
P_u^{RC}	Failure load of the reinforced concrete beam
P_U	Unrelaxed mechanical property
R	Residual resin content, CFRP rods
$R_{n\theta}$	Nominal strength at elevated temperature
$R_{n\theta,existing}$	Nominal strength of the unstrengthened member at elevated temperature
S	Steady state; CFRP sheets
S_{DL}	Dead load effect
S_{LL}	Live load effect
S_{LLO}	Other transient live load effect
S_{LLP}	Permanent live load effect
T	Transient state
T	Temperature; insulation thickness in the FRP anchorage zones
T_0	Relaxation temperature
T_d	Decomposition temperature
T_g	Glass transition temperature
$T_{g,mech}$	Parameter obtained by fitting a hyperbolic tangent function to the experimental data
W	Insulation width

Greek symbols

γ_f	Safety factor for FRP
γ_m	Safety factor for materials strength
Δ_{exp}	Relative difference between experimental and numerical results
Δv_c	Parameter from bi-linear softening law
δ	Deflection; phase angle (DMA experiments)
ε_f	FRP strain
ε_{fu}	Ultimate tensile strain of FRP
λ_{CS}	Thermal conductivity of calcium silicate (CS) boards
ν	Poisson ratio

ρ_{CS}	Density of calcium silicate (CS) boards
τ	Shear stress
$\bar{\tau}_{i+1/2}$	Average shear stress between two adjacent strain gauges
τ_{LM}	Maximum shear bond strength
ϕ	Diameter (in millimetres) of steel rebars
ϕ	Strength reduction factor for ambient conditions
Φ	Friction coefficient

Acronyms

2D	Two-dimensional
3D	Three-dimensional
ACI	American Concrete Institute
AFRP	Aramid fibre reinforced polymer
ASTM	American Society for Testing and Materials
BFRP	Basalt fibre reinforced polymer
CB	Cement-based mortar
CFRP	Carbon fibre reinforced polymer
CNR	National Research Council
CS	Calcium silicate
CSA	Canadian Standard Association
DMA	Dynamic mechanical analysis
DSC	Differential scanning calorimetry
EBL	Effective bonded length
EBR	Externally bonded reinforcement
EC	Eurocode
GB	Gypsum boards
GFRP	Glass fibre reinforced polymer
FCT	Fundação para a Ciência e a Tecnologia (Portuguese National Foundation for Science and Technology)
FE	Finite element
Fib	International Federation for Structural Concrete (*Fédération Internationale du Béton*)
FRP	Fibre reinforced polymer
IC	Intumescent coating
ISI	Institute for Scientific Information
ISIS	Intelligent Sensing for Innovative Structures
ISO	International Organization for Standardization

IST	Instituto Superior Técnico
LERM	Laboratório de Estruturas e Resistência de Materiais (Structures and Strength of Materials Laboratory)
LNEC	Laboratório Nacional de Engenharia Civil (Portuguese National Laboratory of Civil Engineering)
LVDT	Linear variable displacement transducer
NSM	Near surface mounted
PBO	Polybenzoxazole fibres
PC	Personal computer
RC	Reinforced concrete
RW	Rock wool
TB	Thermal blanket
TGA	Thermogravimetric analysis
VG	Vermiculite/gypsum mortar
VP	Vermiculite/perlite

Part I:

Introduction and state-of-the-art review

CHAPTER 1

INTRODUCTION

1.1 CONTEXT AND MOTIVATION

The repair and strengthening of deteriorated and substandard concrete structures has become one of the most important challenges for civil engineering worldwide. In fact, the rehabilitation needs are growing fast, especially in developed countries, which built most of their infrastructure in the middle of the last century. Therefore, a vast number of reinforced concrete (RC) structures require urgent repair or strengthening due to changes in use, structural degradation or modifications. Moreover, many of those structures were built prior to the introduction of modern design codes, hence do not comply with the corresponding requirements - strengthening is often needed due to the increase of design loads.

Traditional strengthening techniques for RC members include bonding steel plates to the tension and/or side faces of beams and slabs (increasing their flexural and shear capacities), steel jacketing of columns (increasing axial, flexural and shear capacities, as well as their ductility), and external post-tensioning of beams with steel tendons. These traditional techniques, which have been applied with varying degrees of success, all suffer from one disadvantage: the susceptibility to corrosion of steel, resulting in loss of cross-sectional area and often in loss of bond to concrete. Over the last three decades many of the above-mentioned approaches have been implemented using fibre reinforced polymer (FRP) materials instead of steel. These materials, first developed for the aerospace, naval and automotive industries, offer numerous advantages over steel, such as very high strength-to-weight ratio, resistance to electrochemical corrosion and ease of installation. Recent advances in the fabrication technologies of FRPs improved their quality and reduced their costs, making FRPs a viable alternative to steel for strengthening RC structures. In civil engineering applications, the three most commonly used FRPs are composed of carbon (CFRP), glass (GFRP) and aramid (AFRP) fibres. Although being the most expensive, CFRPs have been the first option for the rehabilitation of concrete structural elements, mainly due to their higher stiffness and strength, low relaxation, and superior fatigue and durability characteristics.

Research in the area of FRP-strengthened RC members has now advanced to a point where various design guidelines are available and a widespread acceptance of this strengthening technique was achieved. In fact, over the last two decades many RC structures have been strengthened with

externally bonded FRP strips and sheets. However, the use of these systems has been limited mainly to bridges and exterior structural members, where fire endurance is not a primary design concern. For building applications, although FRP strengthening systems also present a great potential, their performance during fire, as well as their ability to meet the fire endurance criteria defined in codes, still needs to be carefully understood and evaluated. Indeed, there are well-founded concerns with their fire behaviour - the strength, stiffness and bond properties of FRPs are severely reduced at only moderately increased temperatures, namely when approaching their glass transition temperature (T_g, typically ranging between 65 ºC and 120 ºC). Moreover, the bond between FRPs and concrete, which typically relies on epoxy adhesives and is critical to maintain the effectiveness of the strengthening system, is also severely reduced at temperatures above their T_g, usually lower than that of the FRPs' (generally within the 50-80 ºC range).

This issue, which is already reflected in design recommendations but is yet to be addressed in a comprehensive manner, has hampered the widespread use of FRP systems in buildings. The few studies about this subject suggest that adequate fire protection systems need to be developed to allow extending the structural use of FRP systems in buildings, pointing out that a great deal of further work is required to fill all the gaps in current knowledge. In fact, several international scientific organizations have unanimously recognized the behaviour of FRP materials/systems under elevated temperatures and fire as one of the most critical research needs [1-4].

1.1.1 Previous research at Instituto Superior Técnico

The MSc dissertation of the author [5] about the fire behaviour of the CFRP-strengthened RC beams (concluded in 2010 at *Instituto Superior Técnico* (IST) of the *University of Lisbon*) provided an important background knowledge for the research developed in the subsequent years and presented in this PhD thesis. In that exploratory study fire resistance tests were conducted in six RC beams strengthened with CFRP strips, using an intermediate scale furnace that reproduced the ISO 834 [6] standard fire. The soffits of the beams were protected with calcium silicate (CS) boards or vermiculite/perlite (VP) cementitious mortar, and the anchorage zones of the CFRP strips were additionally thermally insulated by the furnace walls, *i.e*., the extremities of the strengthening system (over a length of approximately 20 cm) were not directly exposed to the thermal action. It was empirically found that the insulation scheme allowed the heated length of the CFRP strip to transform into a "cable", fixed in the anchorage zones, where the CFRP-concrete bond remained relatively undamaged. This protection strategy led to a considerable extension of the fire endurance of the strengthening system, which in some specimens exceeded 2 hours. In spite of these relevant scientific contributions, this preliminary study did not provide in-depth understanding about the fire behaviour of CFRP-strengthened RC beams, in particular, concerning the above-mentioned cable behaviour, as well as the CFRP-concrete bond behaviour at elevated temperatures. Moreover, methodologies for the design of appropriate fire protection systems still needed to be developed.

The research initiated in that MSc dissertation was further developed in the present PhD thesis and in the framework of the *Carbofire* project, funded by the *Portuguese National Foundation for Science and Technology* (FCT), and promoted in partnership between IST, *University of Coimbra* and the *National Laboratory of Civil Engineering* (LNEC). *Carbofire* aimed at assessing the effectiveness of different fire protection systems in extending the fire endurance of RC members strengthened with CFRP systems, either externally bonded or near surface mounted. The first stage of the project consisted of a comprehensive study about CFRP-concrete bonded interfaces at elevated temperatures, whereas the second stage aimed at evaluating the effect of applying thick insulation in the CFRP anchorage zones, a procedure that proved to be very effective in the research developed during the above-mentioned MSc dissertation and that was expected to lead to considerable cost-savings in fire protection systems.

1.2 OBJECTIVES AND METHODOLOGY

The main objectives of this PhD thesis are two-fold: (i) to obtain in-depth understanding about the behaviour at elevated temperature and under fire exposure of RC structures strengthened with CFRP materials, and (ii) to develop a design method for the definition of tailored fire protection systems, thus allowing a widespread use of these strengthening systems in buildings. The research carried out in this thesis aimed at making a contribution to the following two domains:

1. Bond behaviour of CFRP-concrete interfaces at elevated temperature;
2. Fire behaviour of RC beams/slabs flexurally strengthened with CFRP strips.

Regarding the first topic, bond degradation with temperature of CFRP-concrete interfaces, the following objectives were defined:

- To quantify the stiffness and strength degradation with temperature for the most representative CFRP strengthening techniques – externally bonded reinforcement (EBR) and near surface mounted (NSM);
- To obtain temperature-dependent "bond stress *vs.* relative slip" laws for both EBR and NSM techniques;
- To evaluate the influence of applying mechanical anchorages in EBR-CFRP strips and using different adhesives in NSM-CFRP strips on their bond performance with temperature.

To achieve the aforementioned goals, an experimental campaign was conducted at LNEC comprising double-lap shear tests at elevated temperatures on four different types of concrete blocks strengthened with the following systems: (i) EBR-CFRP strips bonded to concrete with a current epoxy adhesive, (ii) EBR-CFRP strips bonded with a current epoxy adhesive and mechanically anchored to concrete with bolted steel plates, (iii) NSM-CFRP strips bonded to

concrete with a current epoxy adhesive, and (iv) NSM-CFRP strips bonded to concrete with a mixed epoxy-cement adhesive. The influence of the test procedure was also evaluated by performing both steady state and transient state tests. In the steady state tests, the specimens were first heated up a predefined temperature (maximum of 150 °C, measured in the adhesive) and then loaded up to failure; in the transient tests the specimens were loaded up to predefined fractions of their capacity at room temperature and then heated up to failure at a constant rate. Numerical models of these tests were developed, allowing to derive (based on an inverse analysis) global bond *vs.* slip laws as a function of temperature for the CFRP-concrete interaction.

In what concerns the second topic, fire behaviour of RC beams strengthened with CFRP strips, the following objectives were defined:

- To understand in further depth the CFRP cable behaviour empirically observed in the previous fire resistance tests;
- To compare the performance under fire of EBR and NSM-strengthened RC beams;
- To evaluate the influence on the fire response of applying mechanical anchorages in EBR-CFRP strips and using different bonding adhesives in NSM-CFRP strips;
- To develop a methodology for the design of fire protection systems for RC members strengthened with CFRP strips;

In order to achieve the above mentioned objectives, numerical simulations about the thermal response of insulated CFRP-strengthened RC slab strips were performed, aiming at the optimization of the geometry of fire insulation schemes. These thermal models, which allowed defining a preliminary methodology for the design of fire protection systems, assumed that it is possible to exploit the mechanical contribution of the CFRP strengthening system through a cable behaviour, *i.e.*, the CFRP system retains its structural effectiveness during fire even after the CFRP-concrete interaction is destroyed along its central length. This assumption was further investigated through experimental tests and numerical simulations performed at ambient temperature on partially bonded CFRP-strengthened RC beams, providing in-depth understanding of the CFRP cable behaviour empirically observed in the previous tests. The next stage of the methodology consisted of fire resistance tests on insulated RC beams flexurally strengthened with CFRP strips installed according to the following techniques (and bonding adhesives): (i) EBR with a current epoxy adhesive, (ii) EBR with a current epoxy adhesive and mechanically anchored to concrete with bolted steel plates, (iii) NSM with a current epoxy adhesive, and (iv) NSM with a mixed epoxy-cement adhesive. The beams were thermally insulated with different fire protection schemes, comprising thicker insulation boards in the CFRP anchorages zones and thinner ones along the remaining length of the CFRP systems. This extensive experimental campaign, conducted at the *Structures and Strength of Materials Laboratory* (LERM) of IST, besides providing a direct comparison between the performances under fire of the above-mentioned CFRP strengthening

techniques, allowed validating the methodology proposed for the design of fire protection systems. Finally, these fire resistance tests were numerically simulated, providing a further validation to that methodology and additional data for the understanding of the CFRP cable behaviour; these models also provided further validation to the global bond *vs.* slip laws proposed for the CFRP-concrete interaction and allowed evaluating the accuracy of those laws in the simulation of the structural response of CFRP-strengthened RC members under fire.

1.3 MAIN SCIENTIFIC CONTRIBUTIONS AND PUBLICATIONS

The research presented in this thesis provided scientific contributions regarding the behaviour of CFRP-strengthened RC structural members at elevated temperatures/fire. The results obtained are relevant for the scientific community, and the conclusions obtained have practical relevance regarding the application of CFRP strengthening systems in RC structures likely to be subjected to fire (buildings), which, ultimately, may allow to widespread their use in building applications.

Investigations performed on the CFRP-concrete bond behaviour at elevated temperatures provided a significant amount of experimental data, which were scarce in the literature when the experiments were performed. These data include the bond strength and stiffness degradations with temperature of CFRP-concrete interface for different CFRP strengthening techniques (EBR and NSM), different bonding agents (epoxy and mixed epoxy-cement adhesives, in the NSM technique), and also include the influence of applying mechanical anchors (EBR technique) in those interface properties. The numerical simulation of these experimental results by means of finite element (FE) models, allowed the definition of temperature-dependent global bond *vs*. slip laws for both EBR and NSM-CFRP-concrete interfaces, which can be implemented in numerical tools to predict the mechanical response of CFRP-strengthened RC members at elevated temperatures or fire. It is worth mentioning that from these studies, the following three ISI (Institute for Scientific Information) papers were published/submitted for publication:

1. J.P. Firmo, J.R. Correia, D. Pitta, C. Tiago, M.R.T. Arruda, "Experimental characterization of the bond between externally bonded reinforcement (EBR) CFRP strips and concrete at elevated temperatures", *Cement and Concrete Composites*, Vol. 60, pp. 44-54, 2015.
2. J.P. Firmo, J.R. Correia, D. Pitta, C. Tiago, M.R.T. Arruda, "Bond behavior at high temperatures between near surface mounted (NSM) CFRP strips and concrete", *Journal of Composites for Construction* (accepted for publication, doi: 10.1061/(ASCE)CC.1943-5614.0000535).
3. M.R.T. Arruda, J.P. Firmo, J.R. Correia, C. Tiago, "Numerical modelling of the bond between concrete and CFRP laminates at elevated temperatures", *Engineering Structures* (submitted for publication 24/7/2014).

The research on the fire behaviour of CFRP-strengthened concrete beams improved the understanding regarding the structural efficiency of the CFRP strengthening system during fire exposure, in particular in what concerns the definition of a "critical temperature" for CFRP systems. This had not been carefully assessed in the studies available in the literature, which focused mainly on the overall fire performance of structural members rather than in the CFRP system itself. As for the bond tests mentioned above, the fire resistance tests provided a significant amount of new experimental data, including a direct comparison between the fire performance of the EBR and NSM CFRP strengthening techniques, and provided a better understanding about the influence of applying mechanical anchors at the extremities of EBR-CFRP strips and using different bonding adhesives in NSM-strengthened beams.

The experimental and numerical investigations developed in this thesis on CFRP-strengthened RC beams or slabs at both ambient and fire conditions, besides improving the understanding about the CFRP cable behaviour, provided a comprehensive validation of a simplified methodology for the design of fire protection systems. The proposed methodology is based on the fulfilment of two main requirements: (i) the temperature of the CFRP strengthening element along the central zone must remain below a certain critical temperature, avoiding the tensile rupture of the CFRP; and (ii) the temperature of the CFRP-concrete interface along the anchorage length must be kept below the glass transition temperature (T_g) of the adhesive to prevent the CFRP debonding for the required time of fire exposure. Furthermore, the results obtained showed that in CFRP-strengthened RC beams/slabs fire-protected according with the proposed methodology it is possible to exploit the CFRP mechanical contribution for more than 2 hours of exposure to the standard fire, thus fulfilling the most stringent fire resistance ratings. These results may contribute to a revision of the existing design guidelines for FRP strengthening, which simply recommend neglecting the FRP mechanical contribution when applied to structures where the fire action has to be considered.

From the aforementioned research on the fire behaviour of CFRP-strengthened RC members the following six ISI papers were published or submitted for publication:

4. C. López, J.P. Firmo, J.R. Correia, C. Tiago, "Fire protection systems for reinforced concrete slabs strengthened with CFRP laminates", *Construction and Building Materials*, Vol. 47, pp. 324–333, 2013.
5. J.P. Firmo, M.R.T. Arruda, J.R. Correia, "Contribution to the understanding of the mechanical behaviour of CFRP-strengthened RC beams subjected to fire: experimental and numerical assessment", *Composites Part B: Engineering*, Vol. 66, pp. 15-24, 2014.
6. J.P. Firmo, M.R.T. Arruda, J.R. Correia, C. Tiago, "Flexural behaviour of partially bonded CFRP strengthened concrete beams: application to fire protection systems design", *Materials and Design*, Vol. 65, pp. 1064-1074, 2015.

7. J.P. Firmo, J.R. Correia, "Fire behaviour of thermally insulated RC beams strengthened with EBR CFRP strips: experimental study", Composite Structures, Vol. 122, pp. 144-154, 2015.
8. J.P. Firmo, J.R. Correia, "Fire behaviour of thermally insulated RC beams strengthened with NSM-CFRP strips: experimental study", *Composites Part B: Engineering*, Vol. 76, pp. 112-121, 2015.
9. J.P. Firmo, M.R.T. Arruda, J.R. Correia, "Numerical simulation of the fire behaviour of thermally insulated RC beams strengthened with EBR-CFRP strips", *Composite Structures*, Vol. 126, pp. 360-370, 2015.

This PhD thesis includes a comprehensive state-of-the-art review on the fire performance of FRP-strengthened RC structural elements, which also addresses the mechanical behaviour at high temperature of the constituent materials of FRPs and how their bond to concrete is affected when heated. It is worth pointing out that some of the above mentioned scientific contributions, developed in the present thesis, are included in this review, allowing to benchmark the novelty and relevance of the results obtained with those from the literature. This state-of-the-art review was included in the following ISI paper:

10. J.P. Firmo, J.R. Correia, L. Bisby, "Fire behaviour of FRP-strengthened reinforced concrete structural elements: a state-of-the-art review", *Composites Part B: Engineering* (submitted for publication 23/12/2014).

In addition to the above mentioned 10 ISI journal papers, the research developed in this thesis was published in 2 national journal papers [7, 8], 5 international conference papers [9-13] and 2 national conference papers [14, 15].

1.4 OUTLINE OF THE DOCUMENT

The present thesis is organized in nine chapters, which were grouped into four parts:

- Part I – Introduction and state-of-the-art review (chapters 1 and 2);
- Part II – Bond behaviour of CFRP-concrete interfaces at elevated temperature (chapters 3 and 4);
- Part III – Fire behaviour of RC beams/slabs flexurally strengthened with CFRP strips (chapters 5 to 8);
- Part IV – Conclusions and future developments (chapter 9).

This thesis was produced based on the 10 international journal papers mentioned in the previous section. However, their original content was slightly amended, avoiding unnecessary repetitions and further enhancing the connection between the topics assessed in each chapter. The main goal was to produce a synthetic document (quality inherent to the PhD thesis resulting from the

collection of articles) but with a logical sequence and interconnection between subjects (and conclusions) addressed in each chapter (inherent to a standard thesis). Table 1.1 shows the general organization of the document and the journal papers included in each chapter. The chapters' contents are summarized in the paragraphs below.

Table 1.1: General organization of the document including the journal papers associated with each chapter.

Thesis Parts	Chapters	Journal Papers[1]
I	1. Introduction	-
	2. State of the art review	10
II	3. Bond of CFRP to concrete at elevated temperature: experimental investigation	1, 2
	4. Bond of CFRP to concrete at elevated temperature: numerical modelling	3
III	5. Development of fire protection systems for RC members strengthened with CFRP strips	4
	6. Partially bonded CFRP-strengthened RC beams: flexural behaviour and applications to fire protection systems design	5, 6
	7. Fire resistance tests on RC beams flexurally strengthened with CFRP strips	7, 8
	8. Numerical simulation of the fire behaviour of EBR-CFRP-strengthened RC beams	9
IV	9. Conclusions and recommendations for future research	-

[1] Numbering defined in section 1.3.

The first and present chapter introduces the thesis theme in the general context of civil engineering, describing the main objectives, the methodology and the main scientific contributions of the research developed.

Chapter 2 presents a state-of-the-art review on the fire performance of FRP-strengthened RC structural elements. The review addresses first the mechanical behaviour at high temperature of the constituent materials of FRP strengthening systems and how their bond to concrete is affected when heated. Then the available experimental and numerical studies on the fire behaviour of FRP-strengthened RC beams, slabs, and columns are presented. Available design guidance is also discussed.

Chapter 3 refers to the experimental characterization of the CFRP-concrete interfaces at elevated temperatures. The first part of this chapter concerns the research on EBR-CFRP-concrete bonded connections, describing the test series and procedures, and presenting and discussing the experimental results. In the second part of this chapter a similar organization was adopted for the NSM-CFRP-concrete bonded connections. Finally, a comparison of the bond behaviour with temperature of both EBR and NSM techniques is provided.

Numerical simulations of the bond tests on CFRP-concrete bonded connections are presented in chapter 4. The numerical approach is described, with a particular focus on the modelling of CFRP-concrete interface at elevated temperature. Temperature-dependent global bond *vs.* slip

relationships are proposed and discussed. Comparisons with experimental results are provided to attest the accuracy and reliability of such relationships for modelling the CFRP-concrete bond at elevated temperatures.

Chapter 5 presents numerical investigations on the thermal response of RC slabs flexurally strengthened with CFRP strips, where a preliminary methodology for the design of fire protection systems is proposed. In the first part of the chapter, numerical results are compared with previous experimental data to validate the numerical procedure. In the second part of the chapter, the calibrated models are used to design different fire protection systems based on the proposed insulation strategy.

Chapter 6 refers to the study on the flexural behaviour of partially bonded CFRP-strengthened RC beams at ambient temperature. In the first part of this chapter, experimental and numerical investigations on small-scale beams are presented, allowing a better understanding of the CFRP cable behaviour observed in previous fire resistance tests. In the second part of the chapter, the numerical models are extended to intermediate and full-scale beams, in which the influence of the CFRP bonded length and the loading type (point or uniformly distributed) on the strength reduction was evaluated. These results are then incorporated in the simplified procedure that is proposed for the design of fire protection systems of CFRP-strengthened RC flexural members, which also includes the methodology presented in chapter 5.

The results of fire resistance tests on CFRP-strengthened RC beams are presented in chapter 7. The first part of this chapter concerns the experimental campaign on insulated EBR-CFRP-strengthened concrete beams, describing the test series and procedures, and presenting and discussing the experimental results. In the second part of the chapter, results from similar tests carried out on RC concrete beams strengthened with NSM-CFRP strips are presented and compared with those obtained from EBR-strengthened beams. Finally, the efficacy of the adopted insulation strategy is discussed.

Chapter 8 concerns the numerical simulation of the fire resistance tests on EBR-CFRP-strengthened concrete beams (chapter 7). To begin with, a detailed description of the numerical procedure is presented, in particular the temperature-dependent thermal and mechanical properties adopted for all materials, as well as the modelling approach for the CFRP-concrete interface. Subsequently, this chapter presents the comparison between numerical results and the corresponding experimental data. Additionally, supplementary numerical results are presented, providing a further validation of the proposed strategy for the design of fire protection systems and a better understanding about the fire behaviour of CFRP-strengthened RC members.

Chapter 9 summarizes the main conclusions of this research and presents recommendations for future developments.

CHAPTER 2

STATE OF THE ART REVIEW

2.1 INTRODUCTION

Started in the 1980s and experiencing an acceleration of research interest in the 1990s that has continued until now, applications of fibre reinforced polymer (FRP) materials in civil engineering structures are now widespread. Among the most common applications of FRPs in structural applications is bonding or wrapping FRP products (strips or sheets) to the exterior of reinforced concrete (RC) members to increase their strength, stiffness, and/or deformability. From early on in the development of FRP strengthening systems for RC elements, attempts to apply FRPs in buildings have been hindered due to concerns and unknowns surrounding the reduction in their mechanical and bond properties at elevated temperatures. Considerable research has therefore been undertaken in an attempt to better understand the response of FRP materials and FRP-strengthened RC elements at high temperatures or in fire.

This chapter presents a state-of-the-art review on the fire performance of FRP materials and FRP-strengthened RC structural elements. It begins by discussing available research on the performance of FRP-strengthening systems at elevated temperatures (including FRP composites and adhesives). The focus is on tensile and bond properties, since these are the most important in RC strengthening applications. Analytical models to predict FRP property reductions and to correlate mechanical and bond properties to glass transition of the resins and adhesives are presented and discussed. Possible advantages of near surface mounted (NSM) FRP strengthening systems, as compared with externally bonded reinforcement (EBR) systems, are reviewed with a focus on bond performance at high temperature. The available fire resistance tests on FRP-strengthened RC elements, including columns, slabs, and beams are reviewed and discussed, as are the available modelling studies which have attempted to predict the fire resistance and mechanical response of FRP-strengthened RC elements at elevated temperatures. Finally, international guidance for structural fire resistance design of FRP-strengthened concrete elements is summarized. It is worth mentioning that the main results and conclusions obtained in the present thesis are included in the review allowing benchmarking the novelty and relevance of the scientific contributions provided herein and described in detail in the following chapters.

2.2 BEHAVIOUR OF CONSTITUENT MATERIALS AT ELEVATED TEMPERATURE

Temperature affects the properties of all constituent materials of FRP-strengthened RC structural elements, namely concrete, steel, FRP components and adhesives. Particular emphasis is given herein to the strengthening materials, since details of temperature effects on the other constituents are widely available elsewhere.

The physical and mechanical properties of concrete as a function of temperature have been studied during the past century and, despite many remaining unknowns, are reported in various documents (*e.g.*, [16-23]). The variation of concrete properties with temperature (Figure 2.1) can be attributed to the evaporation of water and to changes in the chemical composition and physical structure of the material, occurring mostly in the cement paste. Other effects stem from changes in the pore structure, the development of vapour pressure in the pores, which may result in spalling in some cases, and the loss of bond between the cement past and the aggregates due to differential thermal expansion.

Steel reinforcement properties as a function of temperature have also been extensively studied and are given in several documents (*e.g.*, [16-18]). Figure 2.1 shows that the mechanical properties of steel decrease significantly at temperatures above 400 ºC, resulting in a "critical" temperature definition (representing 50% retention of short term yield strength) being 593 ºC (note that this apparently precise number is simply a hard conversion of 1100 ºF).

Typical structural strengthening systems, comprised of FRP and adhesive, are more affected by temperature than concrete or steel. The strength and stiffness of FRP materials are reduced at only moderately increased temperatures approaching their glass transition temperature (T_g) (discussed later). The bond between FRPs and concrete, which relies on the adhesive and is critical to maintain the effectiveness of the strengthening system in many cases, is also severely reduced at temperatures above T_g.

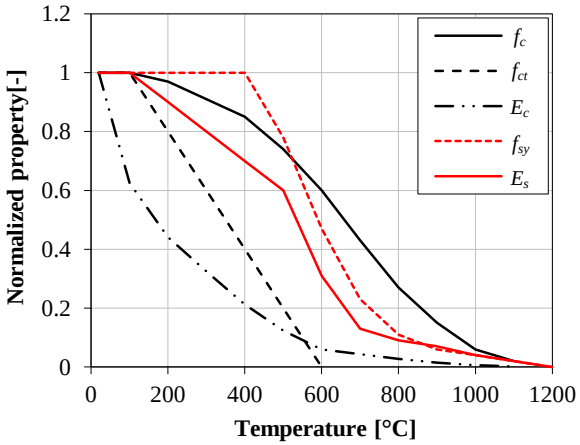

Figure 2.1: Typical mechanical properties of concrete (compressive strength, f_c, tensile strength, f_{ct}, and elastic modulus, E_c) and steel (yielding stress, f_{sy}, and elastic modulus, E_s) as a function of temperature, according to Eurocode 2 Part 1-2 [16].

2.2.1 FRP

When heated to moderately high temperatures, the resin of FRP composites used in structural strengthening applications changes from hard and brittle to viscous or rubbery, in a process called glass transition; this affects an FRP's thermal, mechanical and bond properties. The glass transition is typically identified by a single glass transition temperature value, T_g (generally within the 50-120 ºC range for ambient curing resins), which can be experimentally determined through dynamic mechanical analyses (DMA) or differential scanning calorimetry (DSC). T_g is commonly taken as a "critical temperature" in design decision making, although it is noteworthy that degradation in mechanical properties is observed before T_g is reached [24]. When exposed to higher temperatures (typically above 300-400 ºC) the FRP organic matrix decomposes thermally, possibly releasing heat, smoke, soot and toxic/combustible volatiles. Organic fibres (*e.g.* aramid, PBO, biofibres, etc.) used to reinforce some polymer composites may also decompose and contribute to the generation of heat, smoke and gases [25]. These decomposition processes typically cause further reduction of the mechanical and physical properties of FRPs due to the degradation of both matrix and (in some cases) fibres.

Bisby *et al.* [4] have previously presented a summary of high temperature mechanical property data for a wide variety of FRP materials available in the literature up to 2004. Since then, a number of additional relevant studies performed on tensile properties of FRPs specifically used for strengthening applications in civil engineering have been presented, including works of Cao *et al.* [26], Wang *et al.* [27], Chowdhury *et al*. [28], and Yu and Kodur [29]. Two basic types of test procedures were used in these prior studies: specimens were (i) heated up to a predefined temperature and then loaded up to failure (steady state (S) conditions); or (ii) loaded to a fraction of their ambient temperature strength and then heated up to failure (transient state (T) conditions). Table 2.1 summarizes the main features of these studies, and Figure 2.2 shows the results obtained in terms of tensile strength and elastic modulus with temperature.

Table 2.1: Main features of previous (tensile) tests on FRP strengthening materials at high temperature.

Source	FRP type	FRP shape	Glass transition		Tensile property	Temperature range [°C]
			T_g [°C]	Method		
Cao *et al.* [26]	CFRP	Sheets	38	DMA (onset *E'*)	f_{fu} [1]	16-200
Wang *et al.* [27]	CFRP	Strips		n.a.	f_{fu}	20-700
Chowdhury *et al*. [28]	GFRP	Sheets	75	DSC	f_{fu}; E_f [2]	20-200
Yu and Kodur [29]	CFRP	Strips; rods		n.a.	f_{fu}; E_f	20-600

[1] FRP tensile strength; [2] FRP elastic modulus

Cao *et al.* [26] performed a series of tensile tests on CFRP and hybrid (carbon/glass fibre) FRP sheets from ambient temperature up to 200 ºC under steady state (S) conditions. Figure 2.2a shows

that at temperatures below 55 ºC (approximately T_g for this system) the tensile strength experienced a significant reduction, and then remained almost constant up to 200 ºC (about 67% of the tensile strength at ambient temperature). The authors observed that increasing temperatures significantly affected the tensile failure modes. At ambient temperature the specimens failed at a single cross-section by brittle behaviour; however, at higher temperatures loss of bond between the fibres and the matrix occurred, due to the softening of the epoxy resin.

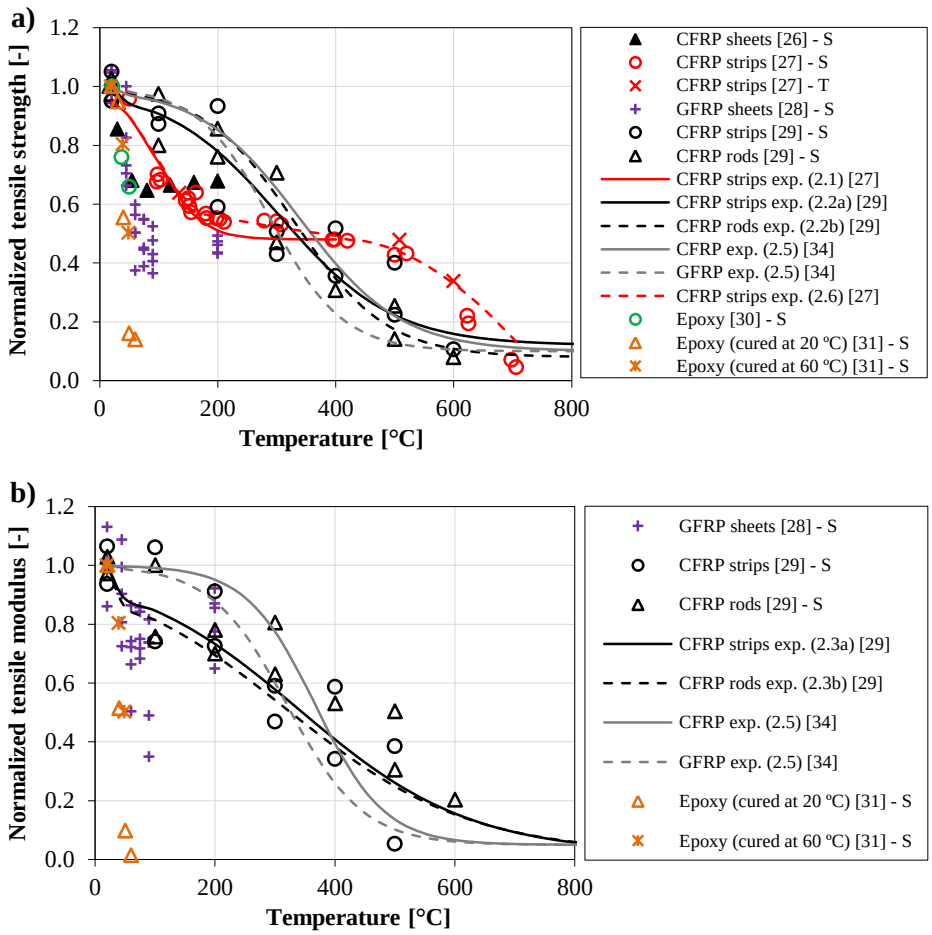

Figure 2.2: Normalized tensile properties vs. *temperature of FRPs and epoxy adhesives commonly used to strengthen RC elements: a) tensile strength; b) elastic modulus (S-steady-state conditions; T-transient conditions).*

Wang *et al.* [27] measured the tensile strength of CFRP pultruded strips at temperatures ranging from room temperature up to 700 ºC, in both steady-state (S) and transient conditions (T). Results obtained for both series (Figure 2.2a) exhibit two considerable reductions on the tensile strength: (i) one in the range 20-150 ºC, decreasing to 60% of the room temperature strength; and (ii) the other in the range 450-700 ºC, decreasing from 45% to less than 10% of the room temperature strength. Between 150 ºC and 450 ºC a gradual reduction in strength took place, with about 50% of the room temperature strength at 300 ºC. The results obtained from the transient-state series were similar to those of the steady-state series, the former being slightly higher than the latter.

Chowdhury *et al.* [28] conducted tensile tests on GFRP unidirectional sheets between room temperature and 200 °C under both steady-state (S) and transient thermal (T) conditions. The specimens tested at 60 °C (15 °C lower than T_g, determined through DSC) under steady state conditions experienced reductions in tensile strength (Figure 2.2a) and elastic modulus (Figure 2.2b) of about 50% and 70%, respectively. However, little additional degradation of both properties was found at temperatures up to 200 °C. This behaviour is similar to that observed by Wang *et al.* [27], and likely stems from the loss of interaction between fibres due to matrix softening. Indeed, the results obtained at the highest temperature are similar to those that would be obtained by testing dry fibres without a resin matrix. The specimens tested under transient conditions were in close agreement with steady-state tests.

Yu and Kodur [29] studied the effect of temperature on the tensile strength and elastic modulus of two types of CFRP pultruded products (strips and rods) for near surface mounted (NSM) strengthening under steady-state (S) conditions. As shown in Figure 2.2a, the tensile strength degradation with temperature of both strips and rods was roughly similar, presenting only 50% strength retention at 300 ºC; this is approximately the decomposition temperature of the polymer matrix. For both CFRP materials, the reduction of the elastic modulus with temperature (Figure 2.2b) followed a similar trend to that of tensile strength, with the elastic modulus presenting slightly higher retention.

It is worth mentioning that the results presented above are specific to the types of epoxy resin and fibres used, as well as to the fibre volume fraction and manufacturing conditions of the FRPs tested; therefore they cannot be directly compared. Whilst the test data cannot be extrapolated to other strengthening systems, the results reviewed are representative of the mechanical behaviour at elevated temperatures of FRPs used to strengthen RC structures. The results reviewed prompt the following comments: (i) the tensile strength and modulus of FRPs are significantly affected by temperature, presenting a first steep reduction due to the glass transition of the resin matrix, a subsequent more gradual (less pronounced) reduction during the decomposition of the matrix, and a final steep reduction due to the oxidation of the fibres, which starts for temperatures above ~500 ºC and is more intense in the 600-800 ºC range [25]; (ii) even after the glass transition and decomposition processes of the resin matrix are complete, the fibres are able to retain a considerable fraction of their ambient temperature tensile properties.

2.2.2 Adhesives

Since there are a wide variety of epoxy adhesive formulations available in the construction industry, it is rather difficult to provide generalizations on their behaviour under elevated temperatures. Furthermore, most prior studies have focused on the bond behaviour between FRP

strengthening systems and concrete (discussed in Section 2.3), rather than on the characterization of the adhesives themselves.

Bascom and Cottington [30] presented one of the first studies on temperature effects on the mechanical properties of epoxy adhesives; they reported a tensile strength reduction of about 35% at 50 ºC (the maximum temperature tested), which was slightly lower than the specific system's T_g (68 ºC, with the T_g test method not reported).

Moussa *et al.* [31] investigated the physical and mechanical properties of a commercial epoxy adhesive (used in CFRP strengthening systems) during heating/cooling at temperatures in the range of T_g (48 ºC, determined through DSC). Figure 2.2 shows that at a moderate temperature of 60 ºC the strength and stiffness of the adhesive were almost negligible, *i.e.* below 20% of the ambient temperature values. It was concluded that thermal exposures up to 60 °C, followed by a cooling phase to room temperature, improved the adhesive performance due to post-curing effects.

2.2.3 Prediction models

Alongside available experimental studies, various analytical models have also been developed to simulate the behaviour of FRP materials and adhesives at elevated temperatures. Most of these models involve semi-empirical curve fitting procedures.

For instance, Gibson *et al.* [32] have proposed a general model that takes the form of a hyperbolic tangent function, and considers the extent of thermal damage as follows,

$$P(T) = R^n \left[\frac{P_U + P_R}{2} - \frac{P_U - P_R}{2}\tanh\{k_m(T - T_{g,mech})\}\right] \quad (2.1)$$

where $P(T)$ is a mechanical property (*e.g.*, tensile strength, elastic modulus) at temperature T, P_U is the "unrelaxed" mechanical property (*i.e.*, before glass transition, generally at room temperature), P_R is the "relaxed" property (*i.e.*, after the glass transition process, but before decomposition); k_m and $T_{g,mech}$ are parameters obtained by fitting the experimental data and are related to the breadth of the relaxation process and the temperature around which the curve is nearly symmetrical, respectively; R is the residual resin content (between 0 and 1); n is a parameter that depends on the stress state (in FRPs, it has been suggested that $n = 1$ for resin dominated properties and $n = 0$ for fibre dominated properties) [32].

Wang *et al.* [27] calibrated the model of Gibson *et al.* [32] with their data (discussed above) for pultruded CFRP strips. In this calibration P_R was 0.48 (strength at 395 ºC), P_U, k_m and $T_{g,mech}$ were 1.0, 0.0139 and 100 ºC, respectively. As the tensile strength of this FRP product was a fibre dominated property, $R^n = 1.0$. The resulting curve is shown in Figure 2.2a and closely matches the experimental data [27].

Yu and Kodur [29] also calibrated the model of Gibson *et al.* [32] with their experimental data for CFRP pultruded strips and rods. The following relations were derived for strength (*f*) and elastic modulus (*E*) retention of both CFRP products as a function of temperature (*T*):

$$f(T) = \begin{cases} 0.56 - 0.44\tanh[0.0052(T-305)], & \text{CFRP strips} \\ 0.54 - 0.46\tanh[0.0064(T-330)], & \text{CFRP rods} \end{cases} \quad \begin{matrix} (2.2a) \\ (2.2b) \end{matrix}$$

$$E(T) = \begin{cases} 0.51 - 0.49\tanh[0.0035(T-340)], & \text{CFRP strips} \\ 0.51 - 0.49\tanh[0.0033(T-320)], & \text{CFRP rods} \end{cases} \quad \begin{matrix} (2.3a) \\ (2.3b) \end{matrix}$$

Mahieux *et al*. [33] suggested the following functional relationship based on Weibull distribution to compute the strength as a function of temperature (in Kelvin),

$$P(T) = P_R + (P_U - P_R) \times \exp[-(T/T_0)^m] \quad (2.4)$$

where T_0 is the relaxation temperature, and *m* is the Weibull exponent, both parameters being fitted to the experimental data.

The two models described above (from Gibson *et al*. [32] and Mahieux *et al*. [33]) were both successfully used by Moussa *et al*. [31] to describe the degradation in the tensile properties of epoxy adhesives.

Bisby [34] proposed the following semi-empirical sigmoid function to describe the reductions in FRP mechanical properties with temperature,

$$\frac{P(T)}{P_U} = \left(\frac{1-a'}{2}\right)\tanh[-b'(T-c')] + \left(\frac{1+a'}{2}\right) \quad (2.5)$$

where *a'* is an assumed constant that describes the residual value for the mechanical properties under consideration, and *b'* and *c'* are empirically derived parameters. Based on a database of experimental data on various FRP products collected from the pre 2004 literature, Bisby [34] derived the coefficients listed in Table 2.2 for the tensile strength and elastic modulus of CFRP and GFRP materials at high temperature (fittings plotted in Figure 2.2).

Table 2.2: Models of Bisby [34], equation (2.5): Derived coefficients for tensile strength and elastic modulus of CFRP and GFRP at high temperature.

Material	**Tensile property**	**Coefficient**		
		a'	b' ($\times 10^{-3}$)	c'
CFRP	Strength	0.10	5.83	339.54
	Elastic modulus	0.05	8.68	367.41
GFRP	Strength	0.10	8.10	289.14
	Elastic modulus	0.05	7.91	320.35

Wang *et al*. [27] recently proposed the following model, originally developed for metals, which the authors applied to describe the tensile strength of CFRP pultruded strips at high temperatures:

$$P(T) = P_U \times \left[A - \frac{(T-B)^{n'}}{C}\right] \tag{2.6}$$

The coefficients *A*, *B*, *C* and *n* in equation (2.6), calibrated for different temperature ranges with the test data presented in section 2.2.1, are given in Table 2.3. Figure 2.2a confirms that the model provides good agreement with the experimental data.

The summaries presented in the above sections confirm that epoxy adhesives are more susceptible to the mechanical (tensile) degradation when exposed to high temperatures compared with FRP materials. Since the adhesives are responsible for the bond between FRPs and concrete, when strengthening is bond-critical, the structural efficacy of the strengthening system can be severely affected during a high temperature exposure.

Table 2.3: Model of Wang et al. [27], equation (2.6) - Coefficients for the strength of CFRP pultruded strips.

Temperature range [°C]	**Coefficients**			
	A	***B***	***C***	***n'***
$22 \leq T < 150$	1.00	22	200	0.9
$150 \leq T < 420$	0.59	150	490	0.7
$420 \leq T < 706$	0.48	420	76000	1.8

2.3 BOND OF FRP TO CONCRETE AT ELEVATED TEMPERATURE

The bond behaviour of FRP-concrete interfaces at elevated temperatures has been addressed in a limited number of studies. Most of these (*e.g.* [35-41]) have been performed on specimens strengthened using the externally bonded reinforcement (EBR) technique. Studies on the bond behaviour of CFRP-concrete interfaces installed using the near surface mounted (NSM) technique are also available (*e.g.* [42-45]). Table 2.4 summarizes the main features of the experimental campaigns reviewed in this section. Analytical studies on this topic (*e.g.* [46, 47]) are also discussed in this section but are exclusively focused on EBR applications, since for NSM technique none is reported in the literature.

2.3.1 EBR strengthening

Blontrock [35] performed double lap shear tests on concrete blocks strengthened with CFRP strips bonded with an epoxy adhesive (T_g quoted as 62 ºC) at temperatures ranging from 20 ºC to 70 ºC. The bond strength retention at 40 ºC, 55 ºC and 70 ºC were 141%, 124% and 82%, respectively, thus featuring a non-monotonic variation with temperature, notably increasing for elevated

temperatures below T_g. At ambient temperature concrete cohesive failure occurred, while at elevated temperature adhesive failure was observed at the concrete-adhesive interface.

Table 2.4: Summary of prior bond tests on CFRP-concrete interfaces at elevated temperature.

Authors	Strengthening technique	CFRP shape	Test setup	Glass transition		Temperature range [°C]	Pre-conditioning
				T_g [°C]	Method		
Blontrock [35]	EBR	Strips	Double lap	62	n.a.	20 to 70	-
Klamer *et al*. [36]	EBR	Strips	Double lap	62	n.a	10 to 75	12 hours heating
Klamer [37]	EBR	Strips	Double lap	62	n.a	-20 to 90	12 hours heating
Wu *et al*. [38]	EBR	Sheets	Double lap	34 to 38	n.a	26 to 50	-
Gamage *et al*. [39]	EBR	Sheets	Single lap	n.a.	n.a.	20 to ~140	-
Leone *et al*. [40]	EBR	Strips and sheets	Double lap	55	DSC	20 to 80	-
Firmo *et al*. [41]	EBR	Strips[1]	Double lap	47	DMA (onset E')	20 to 120	-
Palmieri *et al*. [42]	NSM	Strips and rods	Double lap	65	n.a.	20 to 100	At least 12 hours heating
Burke *et al*. [43]	NSM and EBR	Strips and sheets	Beam tests[2]	59 and 69	DMA (tan δ)	21 to 200	-
Yu and Kodur [44]	NSM	Strips and rods	Pull-out	82 and 120	n.a.	100 to 400[3]	-
Firmo *et al*. [45]	NSM	Strips	Double lap	44 and 47	DMA (onset E')	20 to 150	-

[1] with and without mechanical anchorage.

[2] four-point bending tests on CFRP-strengthened RC beams.

[3] temperature at the adhesive surface (average temperatures at the CFRP-concrete interface not specified).

Klamer *et al*. [36] conducted similar double lap shear tests using normal strength concrete and CFRP strips bonded with epoxy adhesive (T_g quoted as 62 ºC) for temperatures between 10 ºC and 75 ºC. The specimens tested at elevated temperature were heated for at least 12 hours before being loaded. As for the work by Blontrock [35], similar failure modes were observed, as were bond strength increases below T_g (110% at 50 ºC) and moderate strength retention above T_g (64% at 75 ºC). Klamer [37] presented results of a further campaign, with specimens made of both normal and high strength concrete and tested from −20 ºC up to 90 ºC; similar results were obtained to those encountered in Klamer *et al.*'s initial study.

Wu *et al*. [38] performed double lap shear tests at temperatures varying from 26 ºC to 50 ºC on concrete blocks strengthened with CFRP sheets externally bonded with an epoxy adhesive with relatively low T_g (quoted as 34 ºC to 38 ºC, depending on the curing conditions). A consistent

decreasing failure load was observed with increasing temperature above T_g (only 40% retention at 50 ºC). The failure mode again changed with temperature, from mixed cohesive-adhesive at ambient temperature to exclusively adhesive (in the primer-adhesive interface) at elevated temperature.

Gamage *et al*. [39] performed single lap shear tests between concrete and CFRP sheets bonded with epoxy adhesive (T_g not reported). Results obtained were consistent with those of Wu *et al*. [38]; the bond strength demonstrated considerable strength reductions with temperature, being particularly steep in the 50-75 ºC temperature range after which the normalized bond strength dropped to less than 25% of ambient values. This reduction occurred together with a change in the failure modes, from a combination of bond failure and concrete rupture (up to 50 ºC) to peeling-off adhesive failure (above 60 ºC).

Leone *et al*. [40] performed double lap shear tests on concrete blocks strengthened with either CFRP strips or sheets, both externally bonded with epoxy adhesive (T_g quoted as 55 ºC). Tests were performed at temperatures ranging from 20 ºC to 80 ºC. In addition to a high scatter, a non-monotonic variation of bond strength with temperature was reported for the CFRP strips; this differed from results from Blontrock [35], Klamer *et al*. [36], and Klamer [37]. Bond strength retentions below and above T_g respectively decreased (85% at 50 ºC) and increased (109% at 80 ºC). For CFRP sheets, Leone *et al*. [40] observed a strength increase up to 65 ºC (24% increase at 50 ºC and 7% at 65 ºC), whereas at 80 ºC a 11% reduction was observed.

Firmo *et al*. [41] have recently performed double lap shear tests on concrete blocks with CFRP strips externally bonded with epoxy adhesive (T_g of 47 ºC, determined by DMA) from 20 ºC up to 120 ºC (a detailed description is provided in section 3.2 – page 48). The effect of using a mechanical anchorage on the extremities of the CFRP strips was also investigated. The influence of the test procedure was studied – both steady state and transient tests were performed. Increasing temperature caused (i) consistent reduction of bond strength, (ii) much more linear axial strain distributions at the interface due to softening of the adhesive, (iii) higher effective bond length, and (iv) changes in the failure mode (from cohesive to adhesive). Bond-slip relationships were determined for all temperatures tested, with the corresponding stiffness and maximum shear stress suffering considerable reductions at elevated temperature. Similar results were obtained for steady state and transient conditions, with bond strength retention at 120 ºC being 23%.

Regarding analytical studies of bond performance at elevated temperature, Gao *et al.* [46] presented a closed-form solution for the full-range behaviour of FRP-to-concrete bonded joints under combined thermal and mechanical loading; this being an extension of the model by Yuan *et al.* [48] for mechanical loading only. The results predicted by applying this typical bilinear local bond-slip relationship for the FRP-concrete interaction were compared with data obtained by

Klamer *et al.* [36] and Klamer [37]. Close agreement was obtained, including the temperature-induced interfacial stresses developed during heating, however only up to temperatures in the region of the adhesive T_g. This limitation is due to the assumptions that: (i) the concrete-adhesive interface is linear elastic; and (ii) the material properties are not affected by temperature. This model is therefore limited by the adhesive T_g.

Dai *et al.* [47] developed a non-linear local bond-slip model for FRP strips externally bonded to concrete at elevated temperatures, based on an existing two-parameter analytical approach for FRP-to-concrete interfaces at ambient temperature [49]. The two parameters considered, namely the interfacial fracture energy (G_f) and the interfacial brittleness index (B'), were related to the ultimate pull load and the global load-displacement response of FRP-to-concrete bonded joints obtained in experiments at elevated temperatures (double lap or single lap shear tests), respectively. The influences of both temperature induced thermal stresses and bond degradation were considered. The authors collected experimental data from the literature and used a regression analysis to propose equations for G_f and B'. The temperature-dependent bond-slip model showed reasonable agreement with the test data upon which it was based. The main advantage over the model of Gao *et al.* [46] is that softening of the adhesives at elevated temperature can be reflected in the two parameters, theoretically allowing the application of the model for temperatures above the adhesive T_g (provided that the necessary experimental data are available).

2.3.2 NSM strengthening

Palmieiri *et al.* [42] have presented the results of double lap shear tests at temperatures between 20 ºC and 100 ºC on concrete blocks with NSM CFRP rods and strips bonded with an epoxy resin (T_g quoted as 65 ºC). Tests were similar to those by Klamer *et al.* [36] and Klamer [37] (specimens were heated for at least 12 hours and then loaded to failure), as so were the results: the bond strength increased for elevated temperature below the adhesive T_g and decreased for temperatures equal to or above T_g, with reasonable bond strength retention at the maximum temperature (41% to 48%). The failure modes again changed with temperature, in this case from debonding with splitting of the resin (below T_g) to debonding at the CFRP-epoxy interface with pull-out of the strips/bars (above T_g).

Burke *et al.* [43] compared the effects of elevated temperatures on NSM and EBR systems through beam tests. Six RC beams were flexurally strengthened with NSM-CFRP strips using a typical epoxy adhesive (T_g = 69 °C, determined by DMA) or a cementitious grout adhesive. Three identical RC beams were strengthened with EBR wet lay-up carbon/epoxy sheets (T_g = 59 °C, DMA). The flexural strength increases ranged between 104% and 190% (higher than the recommended limit, usually 40-60%), thus allowing to study the structural effectiveness of the CFRP systems under elevated temperatures. All beams were first loaded up to a load higher than

the flexural strength of the un-strengthened members, and then heated up to 100 °C or 200 °C until failure. The NSM-epoxy system remained effective over 40 min at 100 °C but for less than 10 min at 200 °C. With the NSM-grout system it was possible to resist the sustained load for more than 240 min at 100 °C and for 70 min at 200 °C. A better performance was achieved by the EBR system, which maintained its structural effectiveness for more than 240 min at 100 °C and for more than 80 min at 200 °C. This unexpected result stemmed from the much lower average bond stresses in the adhesive for the EBR system. The results obtained in this study did not allow drawing definitive correlations between the adhesive T_g and the loss of structural effectiveness of the CFRP systems, although it appeared that for short-term exposures such temperature can be exceeded without compromising the strengthening effectiveness.

Yu and Kodur [44] performed pull-out tests on concrete blocks strengthened with NSM-CFRP strips and rods, embedded in two types of epoxy adhesive, with T_g of 82 ºC and 120 ºC, respectively. The surface of the epoxy adhesive was heated to 100 ºC, 200 ºC, 300 ºC, or 400 ºC. Although the average temperature of the adhesive (inside the groove) was not reported, the results obtained indicate a consistent and continuous reduction of bond strength with temperature, different from that reported by Palmieri *et al.* [42]. As expected, the adhesive with the highest T_g also gave the highest bond strength retention.

Firmo *et al.* [45] conducted double lap tests on concrete blocks strengthened with NSM CFRP strips at temperatures between 20 ºC and 150 ºC (a detailed description is provided in section 3.3 – page 66). Two bonding materials were used, an epoxy adhesive (T_g of 47 ºC, determined by DMA) and a mixed grout with both cement and epoxy binders (T_g of 44 ºC, determined by DMA). Regardless of the adhesive used, as in the companion study on EBR CFRP-concrete interfaces [41], elevated temperature caused a consistent reduction of bond strength, more linear strain distributions along the bonded length, an increase of effective bond length, bond-slip relationships with lower stiffness and maximum shear stress, and a change in the failure mode (from cohesive within the concrete block to adhesive at the CFRP-adhesive interface). The mixed grout presented considerably worse performance; this was attributed not only to its lower T_g, but also to its inferior mechanical properties as well as its fine filler particles that were unable to promote friction at the bonded interface comparable to those developed with the epoxy adhesive (containing coarse filler). At the maximum temperatures tested the bond strength retentions obtained with the two adhesive materials were 33% (epoxy at 150 ºC) and 10% (mixed grout at 90 ºC).

2.3.3 Summary of results and discussion

The studies discussed above show that CFRP-concrete interfaces are affected by exposure to elevated temperatures in magnitude that may be attained in civil engineering applications. Regardless of the strengthening technique and FRP shape (strip, sheet, or rods), the available data

are broadly similar in terms of (i) the influence of elevated temperature on the axial strain distributions along a bonded length (these become more linear due to the adhesive softening), (ii) an increase of the effective bond length with increasing temperature, and (iii) a change in failure mode from cohesive (typically in the concrete) to adhesive. However, as illustrated in Figure 2.3, the aforementioned studies are contradictory regarding bond strength variation with temperature, particularly for temperatures below T_g; in some cases bond strength increases up to T_g (*e.g.* [35-37, 42]), whereas it decreases in others (*e.g.* [38, 39, 41, 44, 45]).

In the cases where the bond strength increases at elevated temperatures below T_g this may be due to: (i) the effects of thermally induced stresses arising from differential thermal expansion of the constituent materials; or (ii) the more uniform shear stresses at the bonded interfaces with increasing temperature due to adhesive softening. The first issue should be pursued in future studies as its influence on bond strength has yet to be confirmed and quantified. The second issue has been confirmed in various studies [41, 45], however in which bond strength decreased within this temperature range. It is noteworthy that a common feature to all studies in which the bond strength increased at elevated temperatures below T_g is that the specimens in these studies were all conditioned at elevated temperature for long durations (12 hours or more) prior to structural testing. It is thus likely that the pre-conditioning promoted post-curing of the resin, which probably improved bond performance.

The results in Figure 2.3 show that generally, at temperatures moderately above T_g, the bond strength may remain considerable. Firmo *et al*. [41, 45] have attributed such bond strength reserves to frictional forces at the bonded interface. Unsurprisingly, the available literature also confirms the superior bond performance at elevated temperature with either anchorage systems or adhesives with higher T_g. Finally, these studies [41, 45] have also confirmed the superior bond performance at elevated temperature of NSM as compared with EBR systems.

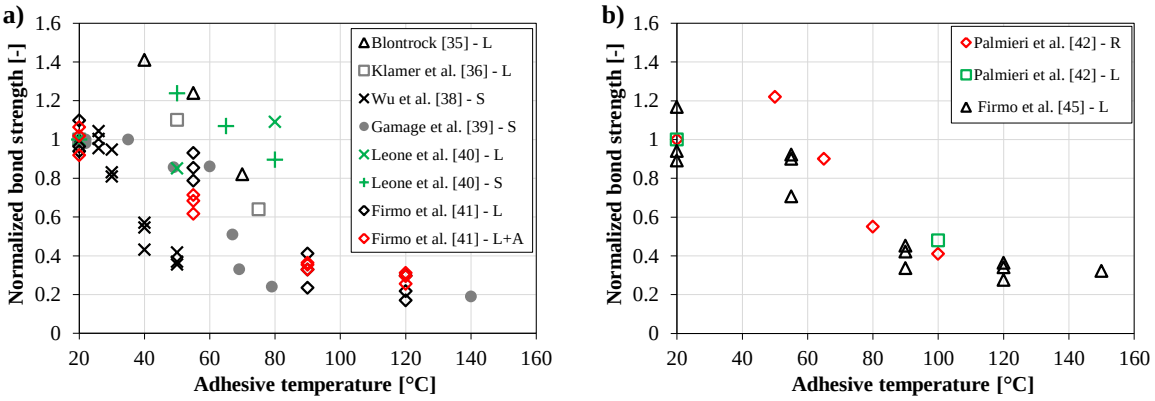

Figure 2.3: Comparison of normalized bond strength as a function of adhesive temperature for studies on a) EBR and b) NSM specimens (L – CFRP laminates/strips; L+A – CFRP laminates/strips with mechanical anchorages; S – CFRP sheets; R – CFRP rods).

2.4 FIRE RESISTANCE OF FRP-STRENGTHENED RC MEMBERS

The fire resistance of structural members is typically defined based on three performance criteria: (i) load bearing capacity (the ability to support the applied loads, without failure or excessive deformations); (ii) integrity (the capacity to maintain the separating function, without emission or passage of flames or combustible gases); and (iii) insulation (the ability to keep the unexposed surface at sufficiently low temperature); all for the required duration of exposure to a standard fire. The ability to meet these criteria is generally assessed using furnace tests in which isolated structural members are subjected to sustained service load levels during exposure to a standard time-temperature curve, which is generally presumed to simulate a credible worst case heating scenario. Table 2.5 presents a summary of available fire resistance tests on FRP-strengthened RC elements; these are summarized below.

2.4.1 Columns

Only a few studies have investigated the fire resistance behaviour of full- or intermediate-scale columns simultaneously subjected to axial load and fire (*e.g.* [50-53]). Bisby *et al.* [50] performed standard furnace tests on two full-scale CFRP-wrapped circular RC columns with a diameter of 0.40 m and an overall height of 3.81 m (Figure 2.4a). The CFRP wrap consisted of a single layer of a unidirectional carbon/epoxy system (T_g quoted as 93 °C), providing a theoretical axial strength increase of approximately 26% according to ISIS (2001) [54]. Both columns were thermally insulated with a spray-applied cementitious plaster (thickness of 32 mm or 57 mm) and an intumescent epoxy coating. The specimens were loaded up to 73% of their ultimate design load and subjected to the ASTM E119 [55] standard fire for 5 h. Both columns achieved more than 5 h of fire endurance according to ASTM E 119 requirements. The temperature of the steel reinforcement and concrete was maintained below 200 °C and therefore these columns were able to retain the vast majority of their room temperature strength. With the 57 mm thick insulation the temperature of the FRP was maintained below 100 °C (slightly higher than its T_g) for approximately 180 min (*cf.* Figure 2.4c). The FRP T_g was exceeded after 82 min and 182 min for the columns with 32 mm and 57 mm of thermal insulation, respectively. Unfortunately, it was not possible to state conclusively when or if the FRP wrap became ineffective as a confining mechanism for the concrete.

A similar experimental campaign is presented by Chowdhury *et al.* [51], who tested two CFRP-wrapped RC circular columns, one of which was protected with a 53 mm thick spray-applied cementitious mortar. Both columns were wrapped with two layers of a CFRP system (T_g quoted as 71 °C) that theoretically increased their axial strength by 63% based on ACI 440 guidelines [56]. During the ASTM E 119 fire exposure, a load of about 56% of the predicted ultimate design capacity of the strengthened member was applied on both columns. The unprotected column failed after 210 min, whereas the insulated specimen lasted for more than 300 min. The temperature at the

CFRP level exceeded T_g relatively early in the fire exposure for both columns (34 min in the insulated column and essentially instantaneously for the uninsulated column); however, as in the previous study [50] it was impossible to precisely identify if/when the CFRP system lost its mechanical efficiency.

Kodur *et al.* [52] performed a fire test on an insulated square column strengthened with three GFRP sheets (cross section illustrated in Figure 2.4b), which theoretically increased the axial strength of the column by about 10%. The results were similar to those obtained by Bisby *et al.* [50] and Chowdhury *et al.* [51]: the column achieved a fire endurance of more than 240 min, although the T_g of the strengthening system was exceeded early in the test (Figure 2.4c). Similar conclusions were also obtained by Bénichou *et al.* [53] from fire tests on full-scale CFRP-strengthened concrete square columns. Again, it was not possible to identify if/when the FRP system lost effectiveness.

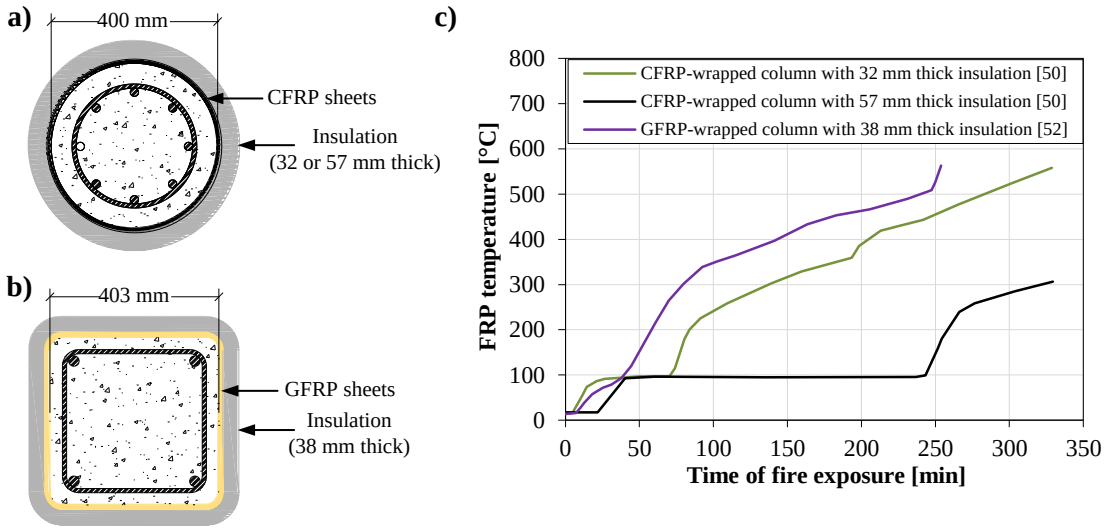

Figure 2.4: Cross section of the columns tested by (a) Bisby et al. [50], (b) Kodur et al. [52] and (c) the corresponding FRP temperatures as a function of the time of fire exposure.

2.4.2 Slabs

Blontrock *et al.* [57] evaluated the fire endurance of seven FRP-strengthened concrete slabs under exposure to the ISO 834 fire curve. The slabs were strengthened in flexure with one or two CFRP sheets, which provided a strength increase at ambient temperature of 20 and 51%, respectively. The specimens were protected with either (i) gypsum boards only or (ii) gypsum boards combined with rock wool, with total thicknesses varying from 15 mm to 40 mm. For one slab the insulation system was applied only over a length of 800 mm in the anchorage zones of the CFRP sheets. All the slabs were loaded in 4-point bending (in a span of 2850 mm) up to a service load corresponding to about 37% of their ambient temperature capacity. Although the FRP bond interaction was lost after between 24 and 55 min of fire exposure (depending on the insulation), the protected slabs achieved fire endurances ranging from at least 70 to 120 min due to only mild temperature increases in the concrete and steel reinforcement. When the CFRP-concrete interaction was lost the temperature in

the adhesive was between 47 and 69 °C (T_g quoted as 67 °C in this study). The performance of the partial protection (*i.e.* only in the anchorage zones) was shown to perform similarly to the full protection case.

Williams *et al.* [58] tested four intermediate-scale insulated FRP-strengthened RC slabs (95 × 133 × 15 cm) exposed to standard fire conditions (ASTM E119). Two strengthening systems were studied consisting of different CFRP sheets externally bonded to the bottom surfaces of the slabs with epoxy adhesives (T_g quoted as 82 °C). The specimens were thermally insulated with (i) a spray-applied cementitious plaster (19 or 38 mm thick) combined with an intumescent coating, similar to that used by Bisby *et al.* [50], or (ii) a cement-based mortar incorporating lightweight fillers (38 mm thick). During the fire exposure, the slabs were subjected to self-weight only, thus preventing any realistic assessment of the FRPs' structural effectiveness, rather the purpose of these tests was to estimate the thermal performance of the insulation systems used, namely with respect to the time for the temperatures at the CFRP-concrete interface to attain the adhesive T_g. Depending on the protection system applied, the time to exceed T_g varied between 42 and 104 min. More recently, Adelzadeh *et al.* [59] conducted a similar campaign in which unloaded FRP-strengthened slabs were insulated with a cement-based mortar (40 and 60 mm thick); the adhesive T_g was exceeded in approximately 30 min in this case.

Stratford *et al.* [60] evaluated the performance of insulated FRP-strengthened members subjected to a real fire. A compartment of a building with 15 cm thick RC ceiling slabs was strengthened with EBR-CFRP strips (100 mm × 1.4 mm) and NSM-CFRP bars (diameter of 12 mm, installed in 20 mm wide and 15 mm deep grooves), and bonded with an epoxy adhesive (T_g quoted as 60°C based on DMA testing). The theoretical strength increase at ambient temperature was not presented. The slab was not subjected to additional imposed loads during fire exposure. The protection included (i) an intumescent coating (120 °C activation temperature) or (ii) two layers of gypsum boards (each layer was 12 mm thick). The fire load, consisting of ordinary office furnishings, was estimated to be equivalent to 32 kg/m^2 of wood cribs over the floor area. The test demonstrated the vulnerability of FRP strengthening during a real compartment fire. The adhesive T_g was exceeded for both strengthening techniques and protection schemes after less than 6 min of fire exposure, far more quickly than furnace-based testing had suggested (the temperatures measured in this real fire presented high spatial scatter, particularly after flashover that occurred after 5 min). The unprotected and intumescent protected strips debonded after about 10 minutes of fire exposure. The test confirmed that the intumescent protection was ineffective due to its low activation temperature. The authors inferred that the NSM strengthening system appeared to have superior fire performance, as it remained in position and there was less visible degradation of the bonding adhesive. However, similar to the work by Williams *et al.* [58], these tests did not permit the assessment of the structural effectiveness of the strengthening systems during the fire event.

2.4.3 Beams

Most of the available experimental studies addressing the fire behaviour of RC beams strengthened with FRP materials have involved flexural strengthening with externally bonded CFRP strips or sheets (Section 2.4.3.1). Much less information is available concerning the fire performance of systems installed using an NSM technique (Section 2.4.3.2).

2.4.3.1 EBR strengthening

Deuring [61] tested a series of 5.0 m span RC beams (0.3 m deep, 0.4 m wide) strengthened in flexure with CFRP strips and loaded to approximately 55% of their theoretical ambient load capacity. Two of these were protected with calcium silicate (CS) boards (40 mm or 60 mm thick) that were mechanically fixed to the undersides of the beams along their entire length. One beam tested without protection achieved a fire endurance of 81 min, although the interaction between the concrete and CFRP was thought to be lost after 20 min. On both insulated beams, the fire resistance exceeded 120 min and debonding of the strengthening system was considerably delayed, presumed to take place when the CFRP temperature was approximately 83 °C (after 65 min) and 85 ºC (after 62 min) in the beams with 60 mm and 40 mm of insulation, respectively. Similar results have recently been reported by Grace and Bebawy [62].

Williams *et al.* [63] investigated the fire performance of two large-scale CFRP-strengthened RC T-beams (3.9 m long, 0.4 m deep) flexurally strengthened with CFRP sheets (15% predicted flexural strength increase) and protected with vermiculite/gypsum fire resistant cementitious insulation, applied on the lateral and bottom faces of the beams with thicknesses of 25 mm (Beam 1) or 38 mm (Beam 2). These were loaded to 48% of their predicted ambient strength with the ends of the beams remaining axially restrained during the tests. Both specimens achieved 240 min of fire endurance; however, in both cases the adhesive T_g (quoted as 93 °C) was exceeded between 16 and 36 min in Beam 1 and between 55 and 57 min in Beam 2 (Figure 2.5); it was not possible to identify when the CFRP system lost effectiveness. Adelzadeh *et al.* [59] extended this study with tests on two additional T-beams following a similar test procedure. The beams were CFRP-strengthened in flexure and insulated with 40 mm of cement-based, spray-applied mortar on their lateral and bottom faces. The specimens were loaded up to 71% of their theoretical ultimate ambient capacity and subjected to the ASTM E119 fire. The results were similar to those obtained by Williams *et al.* [63]; despite the adhesive T_g (quoted as between 50 °C and 60 °C) being exceeded in less than 30 min, none of the beams failed. Indeed, both beams achieved 240 min of fire endurance. These high fire ratings can be explained by the low flexural strength increase provided by the strengthening system and by the fact that the applied insulation systems maintained low temperatures in the pre-existing RC beams, essentially guaranteeing that they would not

collapse even if the CFRP was lost. Axial restraint provided to the beams' ends also might have enhanced their fire endurance.

Blontrock *et al.* [64] tested six CFRP-strengthened RC beams subjected to the ISO 834 fire and loaded to 38% of their ambient flexural capacity. These beams were protected with gypsum board/rock wool combinations and the influence of the total thickness, location, method of bonding and length of insulation was studied. In all cases debonding of the CFRP occurred when the strengthening material reached approximately 66 to 81 °C, which was in the range of the reported T_g of the epoxy adhesive used. Depending on the applied fire protection scheme, loss of composite action was observed after between 10 and 60 min of fire exposure. A U-shaped protection scheme performed better than one applied only on the beam's soffit due to the additional thermal protection given to the internal reinforcing steel; furthermore, when this U-shaped insulation was applied only in the anchorage zones, with the middle portion of the strengthening system directly exposed to fire, the bond was preserved and the CFRP strip was able to maintain its mechanical contribution for a similar duration to the case when its entire length was insulated. Similar results were reported by Kexu *et al.* [65].

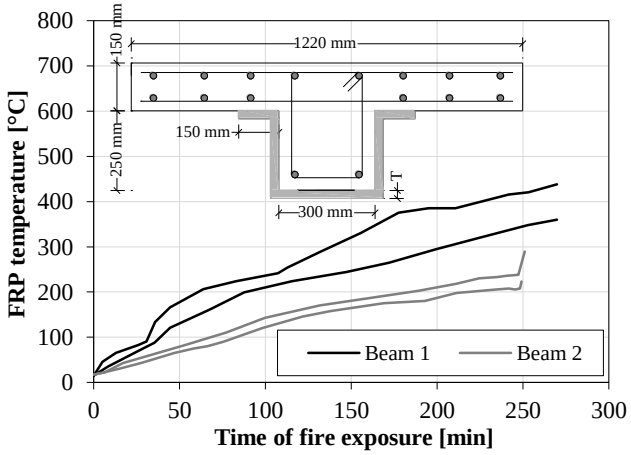

Figure 2.5: FRP temperature in Beam 1 (T = 25 mm) and Beam 2 (T = 38 mm) in two different positions as a function of time of fire exposure (adapted from Williams et al. [63]).

Ahmed and Kodur [66] tested four loaded RC beams strengthened with CFRP sheets (increasing their predicted flexural strength by 50%) exposed to either the ASTM E119 curve or a design fire defined using Eurocode 1 [67] for a typical office compartment. They investigated: (i) the presence of cool anchorages; (ii) the insulation type; and (iii) the axial restraint conditions. All beams were simply supported at the ends of an unsupported span of 3.66 m and loaded up to 50% of their capacity (computed based on ACI 440-2R-08 [56]) in a 4-point bending configuration. To study the influence of cooler anchorages, the CFRP was applied along the entire unsupported length of two beams, whereas for the remaining two beams only the central length (2.44 m directly exposed to fire) was retrofitted with CFRP. Two U-shaped 25 mm thick fire insulation systems, composed by different types of vermiculite-gypsum plaster and a top layer of intumescent coating, were spray-

applied on the bottom and lateral faces of the beams along their entire unsupported lengths. The results showed that the insulated FRP-strengthened RC beams could sustain either of the fire exposures for more than 3 h, although CFRP debonding occurred between 20 and 25 min of fire exposure when the temperature in the concrete-CFRP interface was around the adhesive T_g (quoted as 82 °C based on DMA). The fire-induced axial restraint forces reduced the deformability of the strengthened beams; in terms of fire resistance, none of the beams failed and no differences were reported in terms of time to FRP debonding. Regarding the influence of cooler anchorages, it was concluded that this detail plays a critical role in limiting the deflections of the strengthened beam after debonding of the CFRP in its central length; the unbonded continuous fibres on the beams' soffits continued to contribute to the strength of the beam by catenary action.

Firmo *et al*. [68] performed six fire resistance tests on RC beams strengthened with CFRP strips and loaded up to about 50% of their predicted ambient temperature strength, in which the effect of thermally insulating the anchorage zones of the strengthening system was further investigated. The soffits of the beams were protected with CS boards or vermiculite/perlite cementitious mortar (25 or 40 mm thick), and the anchorage zones of the CFRP strips were additionally thermally insulated by the furnace walls, *i.e.*, the extremities of the strengthening systems (over a length of approximately 200 mm) were not directly exposed to the ISO 834 thermal action. This insulation scheme allowed the heated length of the CFRP strip to transform into a "cable", fixed in the anchorage zones, where the CFRP-concrete bond remained relatively undamaged.

As the temperature increased, the overall stiffness of the beam decreased and, consequently, the beam deflection increased together with the tensile force in the CFRP cable. The strengthening system failed when one of the anchorage zones lost its bond strength, and this was associated with the average temperature in these areas attaining the adhesive T_g (quoted as 55 °C based on DMA). Bond failure of the CFRP system was clearly identified by a sudden midspan deflection increase (due to the loss of stiffness). It can be seen that the protection strategy led to a considerable extension of the fire endurance of the strengthening system in this case, with the increase varying between 23 min (when only the anchorage zones were insulated – beam CFRP) and 167 min (combining the insulation of the anchorage zones with 40 mm thick VP mortar applied along the entire length of the beam soffit – beam VP40).

Firmo and Correia [69] have presented results from nine fire resistance tests on RC beams strengthened with externally bonded CFRP strips in a similar setup to that used by Firmo *et al*. [68], however with the full length of the CFRP exposed to fire. Calcium silicate boards with different thicknesses in the anchorage (T in Figure 2.6) and central zones of the strips (t in Figure 2.6) extended the structural effectiveness of the CFRP strengthening system beyond 70 min (depending on the geometry of the insulation), again by taking advantage of the cable behaviour. This study also confirmed that using an alternative adhesive with a higher T_g, or using a mechanical

(bolted) anchorage, both proved to delay detachment of the CFRP. It was also found that debonding of the strengthening system occurred when the average temperature in the adhesive in the anchorage zones attained values ranging from 1.2 × T_g to 1.5 × T_g, with T_g defined as the onset value from the storage modulus curve from DMA. Whilst much higher temperatures were measured at the interface in the central zone of the beams (above 400 ºC), tensile failure of the CFRP never occurred. A detailed description of this study is provided in section 7.2 – page 143.

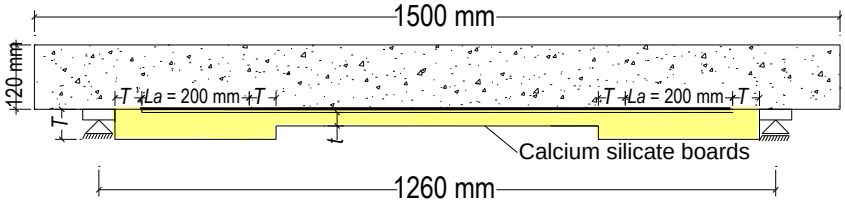

Figure 2.6: Longitudinal geometry of the fire protection system of the beams tested by Firmo and Correia [69].

2.4.3.2 NSM strengthening

The NSM technique has been gaining increasing interest in recent years mainly due to its higher bond efficiency compared with EBR. The fire performance of NSM strengthening systems is also widely thought to be superior to EBR, since the surrounding concrete provides additional thermal insulation to the FRP and its adhesive.

Palmieri *et al.* [70, 71] evaluated the fire behaviour of insulated RC beams with a span of 3.15 m, strengthened in flexure with NSM FRP strips or rods (in GFRP or CFRP) bonded to the concrete with either an epoxy adhesive (T_g quoted as between 62 and 65 °C based on DSC), a high T_g epoxy (82 °C based on DSC) or an expansive cementitious mortar. U-shaped insulation systems were applied along the beams' length, comprising five different materials with constant thicknesses (between 20 and 100 mm). The beams were first loaded up to a service load, which depending of the FRP type varied between 37% and 54% of their ultimate load at room temperature, and were then subjected to the ISO 834 fire. All beams were able to sustain the applied load without failure for 2 h of fire exposure. Although temperature measurements indicated that the adhesive T_g was exceeded in the early stages of the tests, none of the strengthening systems visibly detached nor was any evidence of debonding in the mechanical response.

Zhu *et al.* [72] tested four RC beams NSM-strengthened in flexure with high T_g (quoted as 174 °C) basalt fibre reinforce polymer (BFRP) bars bonded with an epoxy adhesive (T_g not reported), simultaneously subjected to the ISO 834 fire and loaded to 60% of their predicted ambient temperature capacity in a 4-point bending configuration. The effect of insulating the bonded ends of the BFRP bars was evaluated by applying a U-shaped system only along the anchorage zones or by extending the end of the bars to the beams' supports (where there was no direct heating). Both measures provided efficient insulation of the anchorage zones and allowed the NSM strengthening

system to perform for a longer duration of fire exposure. As a consequence, both specimens achieved fire resistances of about 100 min. It was also found that combining the effect of cooler anchorage zones, by extending the end of the bars to the supports, with U-shaped insulation (25 mm thick calcium silicate boards) applied along the entire length of the beams, led to more than 120 min of fire resistance. However, neither the instant when the strengthening system lost its effectiveness, nor the temperature in the adhesive, were reported.

Yu and Kodur [73] tested four full-scale RC T-beams NSM-strengthened with CFRP strips and subjected to the ASTM E119 fire when loaded in a 4-point bending configuration. The test variables included (i) the load level (50% or 65% of the predicted ambient capacity of the strengthened beams, determined according to ACI 440.2R-08 [56]), (ii) the presence of a 25 mm thick U-shaped fire insulation system (vermiculite gypsum plaster), and (iii) the effect of the axial restraint. Similarly to the tests by Firmo *et al.* [68], the anchorage zones of the CFRP were thermally insulated by the furnace walls over a length of 37 cm. Again it was observed that the CFRP strips debonded from the central zone of the beam early in the fire exposure, but continued to carry tension due to the cool anchorages. Consequently, the strengthening system maintained its structural effectiveness during the full 210 min of fire exposure in all cases. Beams with an insulation layer away from the anchorage zones had a reduced rate of deflection.

Firmo and Correia [74] have tested NSM-CFRP-strengthened RC beams insulated by calcium silicate boards with different thicknesses in the anchorage (*T* in Figure 2.6) and central zones of the strengthening system (*t* in Figure 2.6). These were similar to the EBR-strengthened ones tested by Firmo and Correia [69], thus allowing direct comparison of the fire performance of EBR and NSM systems. As for the EBR strengthened beams, with the insulation schemes adopted, it was possible to maintain the structural effectiveness of the CFRP strengthening system for long periods of standard fire exposure (up to 114 min depending on the geometry of the insulation), again by activation of the aforementioned cable behaviour. Comparing the fire behaviour of EBR- and NSM-strengthened RC beams confirmed the better performance of the NSM technique - CFRP debonding occurred after considerably longer periods of fire exposure and for much higher average temperatures in the adhesive in the CFRP anchorage zones, which in the case of NSM strengthening ranged from $2.2 \times T_g$ to $5.6 \times T_g$ (*vs.* $1.2 \times T_g$ to $1.5 \times T_g$ for EBR). Again T_g was determined by the onset of the storage modulus reduction curve from DMA. A detailed description of this study is provided in section 7.3 – page 159.

2.4.4 Discussion

For all types of RC members (beams, slabs or columns), the available research has clearly shown that FRP-strengthened structural elements can retain the necessary load bearing capacity in a fire scenario for the requisite durations. However, in most of the available studies loss of effectiveness

of the strengthening system was insufficient to cause failure of the strengthened member under sustained service loads. Indeed, if the pre-existing structural element is over-designed in terms of fire resistance and the strength increase provided by the strengthening system is low, the member may still be able to carry the applied load for the required duration[1]. In most of the investigations described above the FRP systems provided comparatively low strength increases, which explains the long fire endurances obtained in many cases. In addition, when supplementary fire insulation was applied over the FRP systems (delaying the loss of effectiveness of the FRP in some cases) the load-carrying capacity of the pre-existing member was preserved for even longer durations of fire exposure.

Few of the aforementioned furnace tests have contributed to an in-depth understanding of the stress-temperature-strength dependency of different FRP systems at elevated temperatures; this is mainly due to the relatively low strength increases provided by the FRP systems, together with the difficulty in detecting the loss of interaction with concrete (whether visually or from changes in the structural response) during fire. Only a few studies have provided useful data regarding the stress-temperature dependency of FRP systems at elevated temperatures [57, 64, 66, 68, 69, 74], and the majority of these have studied EBR-strengthened RC members in bending (beams or slabs). It has been found that loss of composite action seemed to occur when the temperatures at the FRP-concrete interface were in the range of the FRP systems' T_g (*i.e.* lowest T_g of the FRP strengthening system). In many studies, however, the precise test method and definition assumed for T_g are not disclosed.

Some of the available studies have attempted to associate loss of effectiveness of the strengthening systems with a so-called "critical" temperature, and some have suggested that T_g could be used to define a conservative limit. Notwithstanding the difficulties in establishing a universally accepted (and defensible) standard procedure to define T_g for FRP strengthening systems – namely the different tests (DMA and DSC) and methods (onset of storage modulus loss, peak in loss modulus, Tan δ, etc. – some studies [70, 71] have suggested that the critical temperature might be considerably higher than the T_g if the stress in the FRP or adhesive is sufficiently low. Additional research is needed to determine how to rationally define a critical temperature, the possible link(s) with T_g, the method and definition used to assign T_g, and the effects of the strengthening technique and stress level during heating.

In several of the above studies [57, 64-66, 68, 69, 72-74] the presence of cold anchorages, achieved either by extending the FRP into cold regions or by applying thermal insulation in the anchorage zones, have played important roles in prolonging the effectiveness of the FRP strengthening. In

[1] In this regard, it is worth mentioning that design codes/guidelines suggest strengthening limits that lead to situations in which the mechanical contribution of the FRP system during a fire event is not needed to insure the necessary load bearing capacity (further discussion is presented in section 2.6).

Table 2.1: Main features of previous fire tests on FRP-strengthened RC members found in the literature

Authors	Structural element	Technique	FRP material	Adhesive glass transition		Thermal insulation (thickness in mm)[1]	Strength increase [%]	Applied load/ultimate capacity [%]	Temperature in the FRP when the strengthening system debonded [°C]	Time of fire exposure at the FRP system debonding [min]
				T_g [ºC]	Method					
Bisby *et al.* [50]	Column	EBR	CFRP sheets	93	n.a.	VG, IC (32-57)	26	73	n.a.	n.a.
Chowdhury *et al.* [51]	Column	EBR	CFRP sheets	71	n.a.	CB (53)	63	56	n.a.	n.a.
Kodur *et al.* [51]	Column	EBR	GFRP sheets	82	n.a.	VG (38)	10	75	n.a.	n.a.
Bénichou *et al.* [53]	Column	EBR	CFRP sheets	60	n.a.	CB (40-51)	n.a.	n.a	n.a.	n.a.
Blontrock et al. [57]	Slab	EBR	CFRP sheets	67	n.a.	GB, RW (15-40)	20 - 51	37	47 - 69	24 - 55
Williams *et al.* [58]	Slab	EBR	CFRP sheets	82	n.a.	VG, CB (19-38)	n.a.	None	n.a.	n.a.
Adelzadeh *et al.* [59]	Slab	EBR	CFRP sheets	50 - 60	n.a.	CB (40-60)	n.a.	None	n.a	n.a.
Stratford *et al.* [60]	Slab	EBR and NSM	CFRP strips and bars	60	DMA	IC, GB (24)	n.a.	None	n.a.	n.a.
Deuring [61]	Beam	EBR	CFRP strips	n.a.	n.a.	CS (40-60)	n.a	55	83 - 85	20 - 65
Williams *et al.* [63]	Beam	EBR	CFRP sheets	93	n.a.	VG (25-38)	15	48	n.a.	n.a.
Adelzadeh *et al.* [59]	Beam	EBR	CFRP sheets and strips	50 - 60	n.a.	CB (40)	n.a.	71	n.a.	n.a.
Blontrock *et al.* [64]	Beam	EBR	CFRP strips	67	n.a.	GB, RW (25-60)	n.a	38	66 - 81	10 - 60
Kexu *et al.* [65]	Beam	EBR	CFRP sheets	n.a.	n.a.	CB (20-50)	n.a.	n.a	n.a.	n.a.
Ahmed & Kodur [66]	Beam	EBR	CFRP sheets	82	DMA	VG (25)	50	50	≈ 82	20 - 25
Firmo *et al.* [68]	Beam	EBR	CFRP strips	55	DMA (tan δ)	CS, VP (25-40)[5]	94	47	52[3]	23 - 167
Firmo & Correia [69]	Beam	EBR	CFRP strips	47	DMA (E' decay)	CS (25-75)[6]	74	36	58-69[3]	2[4] - 70
Palmieri *et al.* [70, 71]	Beam	NSM	CFRP/GFRP rods and CFRP strips	62, 65 or 82[3]	DSC	CB, CS, (20-100)	27 - 78	37 - 54	n.a.	n.a.
Zhu *et al.* [72]	Beam	NSM	BFRP bars	n.a.	n.a.	CS (25), RW (30)	16	60	n.a.	n.a.
Yu and Kodur [73]	Beam	NSM	CFRP strips	n.a.	n.a.	VG (25)[5]	49	50 – 65	n.a.	n.a.
Firmo & Correia [74]	Beam	NSM	CFRP strips	47	DMA (E' decay)	CS (25-50)[6]	111	37	117-239[3]	18[4] - 114

[1] GB - gypsum boards; CS - calcium silicate boards; VG - vermiculite/gypsum mortar; CB - cement based mortar; VP - vermiculite/perlite mortar; TB - thermal blanket; RW - rock wool; IC - intumescent coating; [2] Depending on type of adhesive used; [3] Average temperature in the anchorage zone (much higher temperatures in the central zone); [4] Without thermal insulation; [5] Anchorages thermally insulated by furnace walls; [6] Insulation thickness in anchorage zones higher or equal to that in the central length.

these cases the FRP seems able to function as an anchored cable, maintaining its structural effectiveness, even if the central portion of the FRP experiences extreme heat, provided that a sufficient length of anchorage remains below a certain critical temperature. The questions of what is sufficient length and what is a critical temperature remain largely open for the range of FRP strengthening systems currently being applied in practice.

Firmo and Correia [69, 74] have confirmed superior retention of structural effectiveness of NSM strengthening systems comprising CFRP strips in fire. For similar insulation schemes, not only were the critical temperatures in the anchorages considerably higher with an NSM system, but so were the fire endurance times obtained. This is attributed both to the thermal insulation provided by the NSM's partial embedment in the concrete, to the mechanical confinement conferred by the surrounding concrete, and to the better bonding performance.

2.5 NUMERICAL ANALYSIS OF THE FIRE BEHAVIOUR OF FRP-STRENGTHENED RC MEMBERS

Studies on numerical modelling of FRP-strengthened RC structures under fire are relatively scarce, likely as a consequence of the considerable complexities involved. The most relevant numerical studies on this issue are presented in the following sections.

2.5.1 Columns

Bisby *et al*. [75] developed a numerical model to evaluate the fire behaviour of FRP-wrapped RC circular columns, including thermal insulation. The model accounts for the variation of thermo-physical properties with temperature (for FRP, as proposed by Griffis *et al*. [76] and Bisby [34]) and comprises a two-stage procedure: (i) a finite-difference heat transfer analysis; and (ii) a strain-equilibrium load capacity analysis. Bisby *et al.* [75] assume axisymmetric heat transfer and neglect the contribution of steel rebars to heating. The axial load capacity is determined at all times during standard fire exposure based on a strain-equilibrium analysis. Buckling and crushing strength are determined by accounting for the temperature-dependent (i) stress-strain compressive response of concrete, and (ii) the confining pressure exerted by the FRP wrap, based on a modified version of the confinement model developed earlier by Spoelstra and Monti [77] (the model accounts for the variation of concrete properties over the cross-section due to thermal degradation). Output includes load *vs*. mid-height deflection plots for a range of fire exposure durations and thus axial capacity *vs*. time. The experimental results obtained by Bisby *et al.* [50] (described in section 2.4.1) were used to validate the model, which was shown to be able to predict the temperature profiles of the columns during fire exposure, as well as their axial deflection. Additional validation of this model was performed by Chowdhury *et al.* [51] using data from additional furnace tests on insulated FRP-

wrapped RC columns (Section 2.4.1). Reasonable agreement between predicted and measured temperatures was reported; however, the numerical predictions for load capacity were conservative (Figure 2.7).

Chowdhury *et al.* [78] extended the above model to enable it to simulate the structural behaviour of short or slender, concentrically or eccentrically loaded FRP-wrapped RC rectangular columns under both ambient and fire conditions. A finite-difference method similar to that adopted by Bisby *et al*. [75] was used for the heat transfer analysis. The structural behaviour was modelled using the column deflection method originally proposed by Chen and Atsuta [79] and implemented in a two-dimensional fibre-element analysis. The model accounts for the temperature-dependent non-linear thermal and mechanical response of the column's constituent materials, the partial confinement effect of the FRP wraps, and the second-order moments created due to lateral deflections. The FRP mechanical contribution is assumed to be totally ineffective at temperatures above 200 °C based on material tests performed by the authors [28]. The model was validated by comparing its predictions against experimental results on FRP-unwrapped and wrapped RC square columns under both ambient [80, 81] and fire conditions [52, 82]. It was shown to provide accurate predictions of the temperatures near the corners of FRP-wrapped and insulated square columns tested by Kodur *et al.* [52], mainly when the presence of cracks in the insulation was considered (according to experimental observations). In addition to predicting the evolution of the axial load capacity of the columns, the model is also able to predict the duration of the effectiveness of the FRP confinement (Figure 2.8).

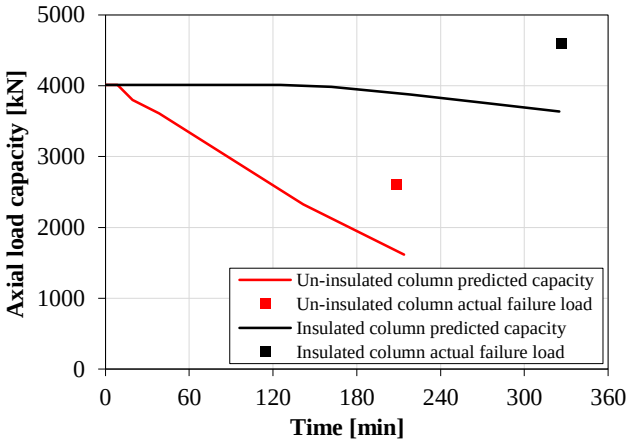

Figure 2.7: Predicted and observed variation of axial capacity with increasing time of fire exposure of FRP-wrapped RC circular columns (adapted from Chowdhury et al. [51]).

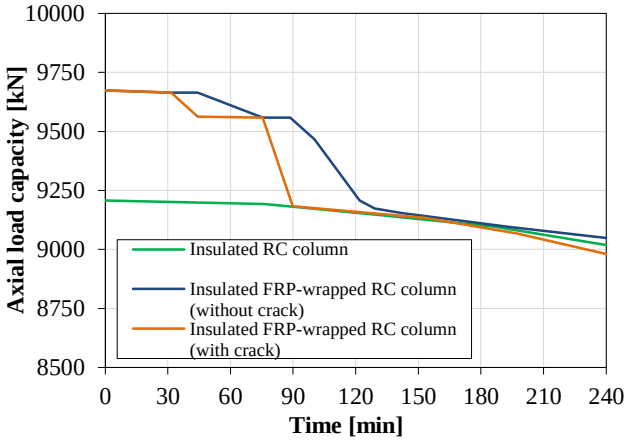

Figure 2.8: Predicted axial capacity of insulated RC square column, insulated FRP-wrapped RC square columns with and without cracking of the insulation (adapted from Chowdhury et al. [78]).

2.5.2 Slabs

A numerical study addressing the fire resistance behaviour of CFRP-strengthened RC slabs was presented by López *et al.* [83]. Three-dimensional thermal models of CFRP-strengthened slabs were developed using commercial FE software. The non-linear transient simulation accounted for the variation of thermo-physical material properties with temperature, defined as suggested by Firmo *et al.* [68]. The models were first validated based on comparison against temperature distributions measured in fire resistance tests (Firmo *et al.* [68]), and then used to assess the efficacy of different fire protection system configurations in which the thickness of the insulation was increased in the FRP anchorage zones. To maintain the effectiveness of the CFRP system the insulation schemes were aimed at: (i) maintaining the temperature of the CFRP along its central length below some critical temperature, defined on the basis of the stress in the CFRP together with its residual strength as a function of temperature; and (ii) maintaining the temperature of the CFRP-concrete interface along the anchorage zones below the T_g of the adhesive [84]. A detailed description of this study is provided in chapter 5.

2.5.3 Beams

Hawileh *et al.* [85] developed a three-dimensional FE model of the CFRP-strengthened T-section RC beams tested by Williams *et al.* [63]. The FE model, developed using a commercial FE package, accounts for the variation in thermal and mechanical properties of the constituent materials and performs the thermal and structural analyses separately. For the thermal model, the furnace temperature and the ambient temperature were applied directly on the bottom and top surfaces of the beams, respectively. Concrete was modelled using multi-linear nonlinear stress-strain curves for different temperatures. Failure of the strengthening system owing to either delamination or adhesive degradation was simulated using a simplistic element-killing procedure that was applied when: (i) the temperature in the CFRP exceeds 250 ºC (for which a 50% strength

reduction in the CFRP is assumed, based on Wang and Evans [86]) and (ii) the shear stress at the CFRP-concrete interface exceeds 4.5 MPa (based on work by Varastehpour and Hamelin [87]). The model agreed well with experimental temperatures, however it was not possible to obtain validation of the structural model because reliable test data were available only for a short duration of testing.

Kodur and Ahmed [88] and Ahmed and Kodur [89] presented similar numerical procedures capable of simulating the thermal and mechanical responses of fire-exposed RC beams strengthened with CFRP strips according to the EBR technique. The procedures were implemented through a macroscopic FE model which accounts for temperature-dependent material properties (namely those of the adhesive, including the shear modulus, and the CFRP as suggested by Bisby [34]), arbitrary thermal insulation, fire scenarios and loading schemes, load and restraint conditions, material and geometric nonlinearity, and appropriate failure criteria. The main innovation of the work presented in [89] is that the model explicitly simulates the bond degradation at the CFRP-concrete interface, particularly the bond-slip as a function of temperature (in [88] no bond degradation was considered). After performing a two-dimensional heat transfer analysis of the cross-section, the model involves: (i) calculation of the slip strain at the CFRP-concrete interface; and (ii) generation of moment *vs*. curvature curves for each beam segment and time step, and subsequent computation of internal forces and deflections from beam analysis. Failure is evaluated through any of the following criteria: (i) the applied moment exceeds the beam's capacity; (ii) the temperature in the internal steel rebar exceeds 593 ºC; (iii) the beam deflection exceeds $L/20$, with L being the span; (iv) the rate of beam deflection exceeds $L^2/9000d$ (mm/min), where d (in mm) is the effective depth of the beam (with L in mm); and (v) the temperature in the FRP layer exceeds T_g. The model was validated by comparison with experimental data presented by Blontrock *et al*. [64] and Ahmed and Kodur [66]. Good agreement was generally obtained in terms of temperatures, deflections (Figure 2.9), and the time to delamination of the strengthening system. It was also shown that attaining T_g in the CFRP might not lead to failure in CFRP-strengthened RC beams, and that more realistic fire limit states needed to be defined.

Kodur and Yu [90] extended the previous numerical model to predict the fire response of RC beams strengthened with NSM FRP materials. The model includes the same features as above – the main difference being that failure is now evaluated based only on criteria i), iii) and iv). The bond-slip relationship proposed by Sena-Cruz and Barros [91] is incorporated into the numerical model and its variation with temperature is assumed to follow test data reported by Katz *et al*. [92]. Model validation was achieved by comparison with data reported in the literature (*e.g.* [70, 73, 93]). Based on the successful validation of their model (Figure 2.10), Kodur and Yu [90] performed a parametric study in which they evaluated the influence of: (i) the strengthening technique (NSM *vs*. EBR); (ii) the position of the strengthening element in the cross-section; and (iii) the use and

geometry of a thermal insulation layer. Results obtained suggested that the NSM technique is likely to lead to higher fire resistances as compared with EBR.

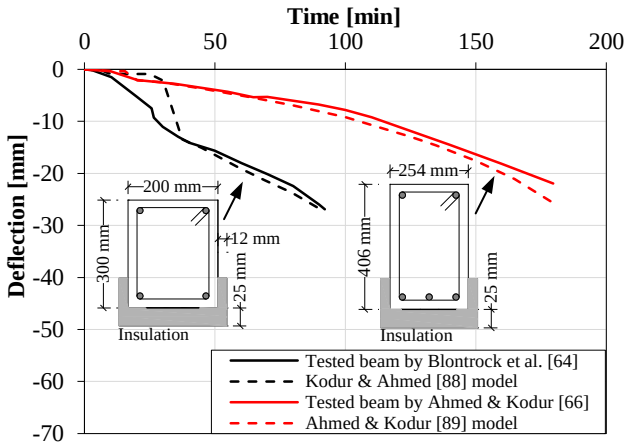

Figure 2.9: Measured and predicted deflections as a function of time of fire exposure for the beams tested by Blontrock et al. [64] and Ahmed and Kodur [66] (adapted from [88, 89]).

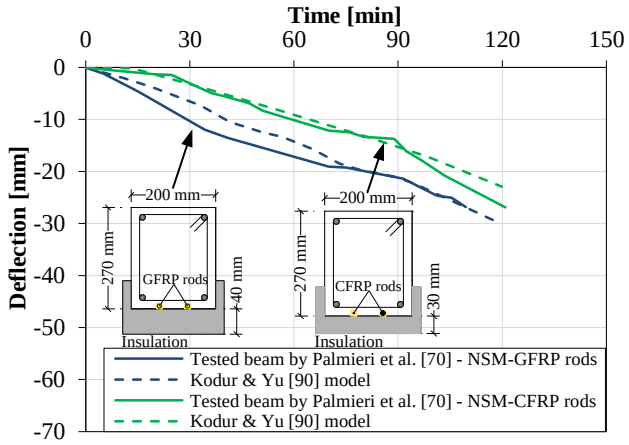

Figure 2.10: Measured and predicted deflections as a function of time of fire exposure for the beams tested by Palmieri et al. [70] (adapted from Kodur and Yu [90]).

Dai *et al.* [94] developed the only 3D FE model to date that simulates the thermal and structural behaviour of insulated FRP-strengthened RC beams exposed to fire accounting for bond degradation with temperature (both for the internal steel and the external FRP reinforcement). This modelling, developed using a commercial FE package, was validated using data from fire tests by Blontrock *et al.* [64] and Williams *et al.* [63]. The temperature-dependent thermo-physical properties of concrete and steel were defined according to Eurocode 2 – Part 1-2 [16]; for the FRP the variations in properties suggested by Griffis *et al.* [95] were adopted; and for the fire insulation materials the properties reported in the corresponding fire tests were used. The temperature-dependent mechanical properties of concrete and steel suggested in the Eurocode 2-Part 1-2 [16] were adopted, whereas for the FRP the authors calibrated sigmoidal functions for the tensile strength and elastic modulus based on test data reported in the literature. Regarding the bond behaviour between the concrete

and the steel reinforcement, the bond-slip model suggested in Model Code 90 [96] for ambient temperature was implemented; reductions in bond strength and interfacial fracture energy (calibrated by Gao *et al.* [97]) were then incorporated to reflect the bond degradation at elevated temperatures. For the FRP-concrete interface, the bond-slip model developed by Dai *et al.* [47] was implemented and represents the most innovative feature of this study. These FE models provided accurate predictions of both thermal and structural responses obtained in [63, 64], highlighting the importance of considering appropriate temperature-dependent bond-slip constitutive models.

2.6 DESIGN GUIDANCE

Existing guidelines specifically addressing FRP strengthening (*e.g.*, CAN/CSA S806-12 [98], fib Bulletin 14 [99], CNR-DT 200/2013-R1 [100], ACI 440.2R-08 [56]) generally provide little guidance on fire design and protection. These documents address some or all of the following issues: (i) general fire design recommendations; (ii) contribution of the FRP strengthening system in a fire situation and consideration of fire protection systems; (iii) combinations of loads for fire design and definition of strengthening limits; and (iv) reaction-to-fire recommendations.

2.6.1 General fire design recommendations

Recognizing the comparatively poor specific performance at elevated temperature of both FRP strengthening materials and polymer adhesives, the available design guidelines suggest that if no special provisions are taken, the strengthening system will be rapidly lost during a fire. If no fire protection is applied, the unstrengthened element must meet the required fire resistance rating by itself (*i.e.*, disregarding the strengthening system but subjected to the intended increased service loads) when considering an accidental design situation (for which the load combinations defined in Section 2.6.3. shall be used). In this case, general fire design rules for reinforced concrete members (*e.g.*, those defined in EC2 Part 1-2 [16]) are applicable.

2.6.2 Contribution of FRP strengthening system in a fire situation and use of fire protection systems

ACI 440.2R-08 [56] specifies that in the event of a fire the contribution of externally bonded FRP strengthening systems should be assumed to be lost, unless it can be demonstrated that the FRP temperature remains below its "critical temperature". The critical temperature is stated as being the lowest T_g of the components of the strengthening system (however not specifying the test method or procedure for determination of T_g).

When insulation systems are used, it is possible that the contribution of the FRP strengthening system could be used in a fire situation. Fib Bulletin 14 [99], one of the earliest design guidelines to

be published, mentions the possibility of using special measures, such as protective linings, and recommends that fire resistance be determined using a "refined calculation method" based on a thermal analysis followed by a mechanical analysis considering temperature-dependent material properties. It further recommends the dimensioning of the protection layer to be made based on keeping the adhesive within a certain "temperature limit" (between 50 ºC and 100 ºC in this document). Unfortunately, no information is provided on how to determine the temperature limit, nor the temperature-dependent properties of the materials, for any specific FRP system.

2.6.3 Load combinations and strengthening limits

For the general case in which no fire protection is used, fib Bulletin 14 [99] recommends verifying the safety of the unstrengthened element based on the accidental load combination of the strengthened element. This verification is to be performed with partial material safety factors (γ_m = 1.0) taking into account the partial load safety coefficients and combination factors defined in Eurocode 1 – Part 1-2 [67]. Such a combination gives,

$$R_{n\theta,existing} \geq 1.0S_{DL} + 0.9S_{LLP} + 0.5S_{LLO} \quad (2.7)$$

where $R_{n\theta,existing}$ is the nominal resistance of the unstrengthened member at elevated temperature, S_{DL} is the dead load effect, S_{LLP} is the permanent live load effect, and S_{LLO} is the other transient live load effect on the strengthened structure.

The Italian guidelines [100] suggest the following situations, considering the residual mechanical properties (for a certain duration of fire exposure or envisaged fire rating) and partial factors pertaining to exceptional situations (for FRP, γ_f = 1.0): (i) when the strengthening system has been designed to withstand fire exposure, all loads acting on the structure for the frequent combination are to be considered; (ii) when the strengthening system contribution is disregarded, applied loads are to be considered for the quasi-permanent combination. Unfortunately, as for the other documents, no quantitative information is provided on the reduction of mechanical or bond properties of FRPs with temperature.

To account for fire, ACI 440.2R-08 [56] recommends that the nominal strength at high temperature must be higher than the strengthened service load on the member defined as follows:

$$R_{n\theta} \geq 1.0S_{DL} + 1.0S_{LL} \quad (2.8)$$

This is considerably more restrictive than that defined in the Eurocodes (above).

Design guidelines recommend limiting the amount of strengthening in order to prevent catastrophic failure of the concrete member stemming from the loss of or damage to the strengthening system. As an example, the Italian guidelines recommend keeping low (although not specifying any limit)

the contribution of the FRP to the member capacity "as long as comprehensive information about the fire behaviour of strengthening and protection materials is not available" [100]. ACI 440.2R-08 [56] recommends that the capacity of the existing member that is to be strengthened allows resisting a substantial fraction of the future load defined as follows,

$$\phi R_{n\theta,existing} \geq 1.1 S_{DL} + 0.75 S_{LL} \tag{2.9}$$

where ϕ is the strength reduction factor for ambient conditions. The maximum permissible FRP strengthening is therefore typically between 25% and 100%, depending on the ratio between live loads and dead loads, and the load and resistance factors used in design.

2.6.4 Reaction-to-fire recommendations

FRP-strengthened structures must comply with applicable building and fire codes, however the information and design guidance with respect to fire reaction behaviour of FRP-strengthened RC structures is limited[2]. ACI 440.2R-08 [56] mentions that smoke generation and flame spread ratings of the assembly shall fulfil applicable requirements, and also refers to coatings and insulation systems in limiting smoke and flame spread. Similar requirements are specified by CAN/CSA S806-12 [98]. The Italian guidelines (CNR-DT 200/2013-R1 [100]) include a general recommendation concerning the capability of coatings at reducing the spread of flames and smoke production.

2.7 CONCLUDING REMARKS

This chapter has presented a detailed review of the state-of-the-art on the fire performance of FRP strengthening systems for RC structures. It has shown that the mechanical and bond properties of both EBR and NSM FRP systems are now reasonably well understood, with the research developed in this thesis presenting important contributions in this field (detailed descriptions are provided in chapters 3 and 4). Analytical models exist that are able to reasonably predict short-term reductions in tensile and bond properties of FRP materials at elevated temperatures, in the region of the systems' T_g. The review has also suggested that the short-term tensile and bond property degradation experienced by FRP materials at elevated temperature can be correlated to the results of DMA testing on FRP materials.

A wide range of fire resistance tests on FRP-strengthened RC elements (columns, slabs, and beams) are now available in the literature, and have confirmed the susceptibility of FRP strengthening systems to reductions in mechanical and bond properties at elevated temperatures,

[2] Although FRP strengthening systems are combustible, releasing heat and smoke during combustion, in most applications the total FRP exposed surface is low, particularly taking into account the typical combustible load of building compartments.

whilst demonstrating the need to provide thermal insulation to the FRP systems to prevent rapid loss of the FRPs' structural effectiveness. Research (in particular the one developed in the present thesis, *cf.* chapters 5 to 8) has also shown, however, that large thicknesses of thermal insulation are generally only needed in the FRPs' anchorage zones, and that well-anchored FRP materials are able to retain large proportions of their tensile strength and stiffness even at temperatures greatly exceeding T_g. This, combined with reasonable strengthening limits that should be applied during design of FRP strengthening systems (also discussed herein, and needed for protection against multiple hazards, including fire), generally means that FRP-strengthened RC elements are capable of achieving fire resistances which should be satisfactory in most conceivable applications.

Part II:
Bond behaviour of CFRP-concrete interfaces at elevated temperature

CHAPTER 3

BOND OF CFRP TO CONCRETE AT ELEVATED TEMPERATURE: EXPERIMENTAL INVESTIGATION

3.1 INTRODUCTION

The literature review presented in chapter 2 showed that although very pertinent for the design of CFRP-strengthened RC structures, the problem of the behaviour of CFRP-concrete interfaces at elevated temperature has only been addressed in a very limited number of experimental studies. Furthermore, some of the results reported are contradictory, in particular regarding the bond strength variation for temperatures below the T_g of the adhesives. In fact, such bond strength increased in some cases, decreased in others and even presented a non-monotonic variation with temperature. In addition, most of the studies mentioned in section 2.3 (page 20) were performed for relatively limited temperature ranges (only slightly exceeding the T_g of the adhesives) and have addressed mostly the bond between concrete and precured or wet lay-up CFRP systems applied according to the EBR technique. Concerning the bond behaviour with temperature of NSM-CFRP systems, for which better results are expected *a priori* due to the higher bonding area and the insulation effected provided by the concrete cover, only three studies [42-44] were reported.

This chapter presents experimental investigations on the bond between concrete and CFRP strengthening systems at moderately elevated temperatures (from 20 °C up to 150 °C) when installed according to either EBR (section 3.2) or NSM (section 3.3) techniques.

Concerning the former technique, the experiments consisted of double-lap shear tests performed on concrete blocks strengthened with CFRP strips externally bonded with a conventional epoxy adhesive. Bond tests were performed for both steady-state and transient conditions. In some of the specimens, a mechanical anchorage was applied on the extremities of the CFRP strips. Regarding the experimental characterization of the bond behaviour with temperature of latter technique, the test programme comprised double-lap shear tests performed on concrete blocks strengthened with CFRP strips inserted into slits and bonded with two different adhesives: a conventional epoxy one and a mixed grout with cement and epoxy binders. The tests on NSM-strengthened concrete blocks were performed only under steady-state conditions. Both experimental campaigns allowed quantifying the strain distributions, the bond-slip relationships, the overall stiffness and the strength

of CFRP-concrete interfaces for a wide range of elevated temperatures across the glass transition of the adhesives and for the two most representative CFRP strengthening techniques used with RC structural elements.

3.2 EBR STRENGTHENING

3.2.1 Description of the test programme

3.2.1.1 Test series

The following two types of tests were performed on concrete blocks strengthened with externally bonded CFRP strips: (i) steady state tests (series S1 and S1A), in which specimens were first heated up to a predefined temperature (20 °C, 55 °C, 90 °C and 120 °C) and then loaded up to failure; and (ii) transient tests (series S2), in which specimens were first loaded up to a fraction of the ambient temperature strength (25%, 50% and 75%) and then heated at a constant rate up to failure. The above-mentioned temperatures used in series S1/S1A were chosen as they cover most of the temperature range of the glass transition process underwent by the epoxy adhesive, with test temperatures respectively below (20 ºC), around (55 ºC), above (90 ºC) and well above (120 ºC) the adhesive T_g.

Two types of specimens were used in the steady state tests: (i) without (series S1), and (ii) with (series S1A) mechanical anchorage at the extremity of the CFRP strips. For each series, 3 specimens were tested for each temperature or fraction of ambient temperature strength. The following nomenclature was adopted: S1A-T55-sp2 (series S1 with mechanical anchorage, temperature of 55 °C, specimen 2) and S2-50-sp1 (series S2, loaded up to 50% of ambient temperature strength, specimen 1).

3.2.1.2 Materials

The following materials were used in the test programme: (i) concrete; (ii) steel rebars; (iii) CFRP strips; (iv) epoxy adhesive; and (v) steel plates and bolts.

The ready-mixed concrete, produced with limestone aggregates (maximum size of 22 mm) and Portland cement type CEM II/A-L 42.5 R, presented an average compressive strength in cylinders of f_{cm} = 27.4 MPa, average splitting tensile strength of f_{ctm} = 2.5 MPa and average elastic modulus of E_{cm} = 28.7 GPa, all at the age of testing (51 days).

Steel bars type A500 NR SD with a diameter of 16 mm were used for internal reinforcement of the concrete blocks, as well as for the load application system. The mechanical properties reported by the manufacturer are as follows: characteristic yielding strength of f_{syk} = 546 MPa; average failure stress of f_{sum} = 703 MPa; average elastic modulus of E_{sm} = 193 GPa.

The CFRP strips used as externally bonded reinforcement, with the commercial designation *S&P Laminates CFK 150/2000*, have a cross-section of 20 mm (width) × 1.4 mm (thickness). This material is constituted by unidirectional carbon fibres (about 70% in weight) embedded in an epoxy resin matrix. The average tensile properties of the CFRP strips, determined according to ISO 527-5 [101], are as follows: tensile strength of f_{fu} = 2076 MPa, Young's modulus of E_f = 189 GPa, and ultimate tensile strain of ε_{fu} = 11 ‰. The conventional two-component epoxy adhesive used to bond the CFRP strips, with the commercial designation *S&P Resin 220*, presents average values of tensile modulus and tensile strength of E_a = 10.0 GPa and f_{at} = 14.2 MPa, respectively, determined according to ISO 527-2 [102]. The glass transition temperatures of the CFRP strips (T_g = 83 °C) and the epoxy adhesive (T_g = 47 °C; 3 months age, cured at 20 ºC) were determined from dynamic mechanical analyses (DMA, dual cantilever setup, heating rate of 1 °C/min), based on the onset of the storage modulus curve decay (Figure 3.1a). Thermogravimetric analysis (TGA) and differential scanning calorimetry (DSC) measurements were also performed on both materials according to ISO 11357 [103], providing the mass variation and the energy changes as a function of temperature. Tests were run from ambient temperature (approximately 25 ºC) to about 800 ºC, in air atmosphere, at a heating rate of 10 ºC/min. Based on the middle temperature of the sigmoidal mass change (*cf.* Figure 3.1b), the decomposition temperature (T_d) of both the CFRP strips and the epoxy adhesive was defined as being approximately 380 ºC.

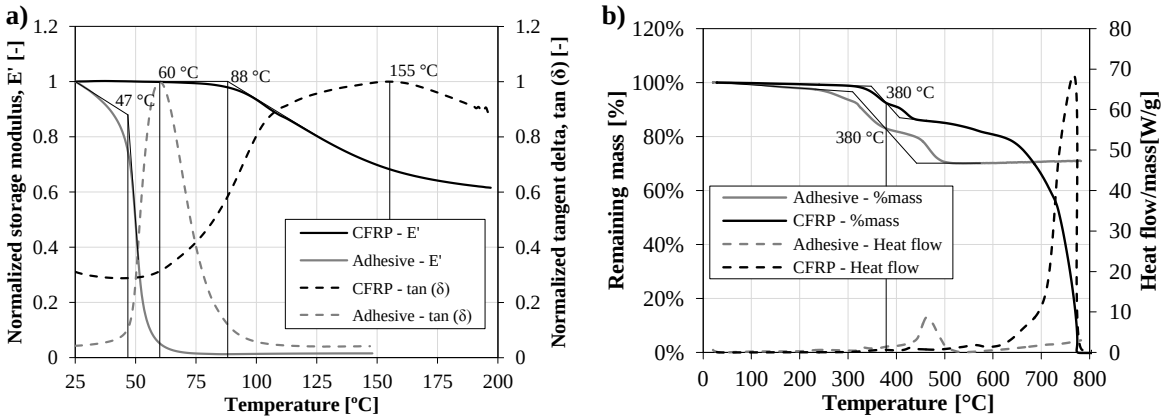

Figure 3.1: (a) DMA and (b) DSC/TGA curves for CFRP and epoxy adhesive.

The mechanical anchorage used in specimens from series S1A comprised 5 mm thick steel (class S235) plates and steel self-screwing bolts (grade 19MnB4) with diameter of 6 mm and length of 60 mm, with the commercial designation *Walraven - BIS TSM Concrete Screws*.

3.2.1.3 Specimens geometry and preparation

Figure 3.2 illustrates the geometry of the test specimens. The two concrete blocks are parallelepiped, with cross-section of 120 mm × 120 mm and length of 350 mm, and are internally reinforced with 2 U-shaped steel bars (diameter of 16 mm); the straight part of the rebars,

protruding from the concrete blocks, was threaded in a length of 50 mm in order to allow for the application of the mechanical load (*cf.* section 3.2.1.4). The CFRP strips (1.4 mm × 20 mm) were 600 mm long, with a bonded length of 2 × 250 mm (unbonded length of 100 mm). It is worth noting that the bonded length defined is higher than the anchorage length determined from different guidelines, namely ACI 440.2R-08 [56] (201 mm), fib Bulletin 14 [99] (205 mm) and CNR-DT 200/2013 [100] (also 205 mm). The adhesive layer thickness was approximately 2 mm.

The anchorage system used in specimens from series S1A comprised a square steel plate (60 mm × 60 mm, 5 mm thick), which was fixed to the concrete blocks by means of 4 self-tapping screws (diameter of 6 mm). The centre of the anchoring plate was positioned at a distance of 3 cm from the end of the CFRP strip.

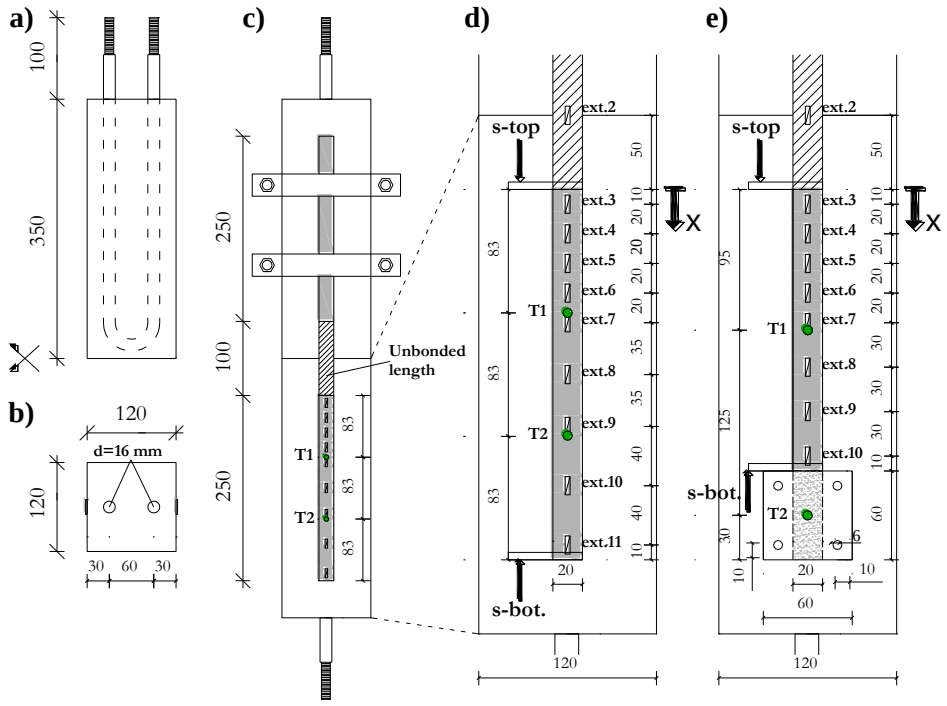

Figure 3.2: Geometry of test specimens (a, b and c) and detail of instrumentation (d – series S1; e – series S1A), dimensions in mm.

After the execution of the concrete blocks, the preparation of the test specimens involved the following procedure (*cf.* Figure 3.3): (i) preparation/roughening of the concrete surface with needle scalers in order to improve the bonding performance (Figure 3.3a); (ii) drilling the concrete blocks in the positions corresponding to the self-screwing bolts (Figure 3.3b - only in series S1A); (iii) cleaning of the dust and loose particles with a steel brush and compressed air jet (Figure 3.3c); (iv) positioning and alignment of the pairs of concrete blocks; (v) cleaning (with acetone) and bonding the CFRP strips (Figure 3.3d), with removal of the squeezed adhesive; (vi) positioning of the anchorage plate (with the epoxy adhesive still wet) and tightening of the self-screwing bolts with a torque of 20 N.m (Figure 3.3e - only in series S1A).

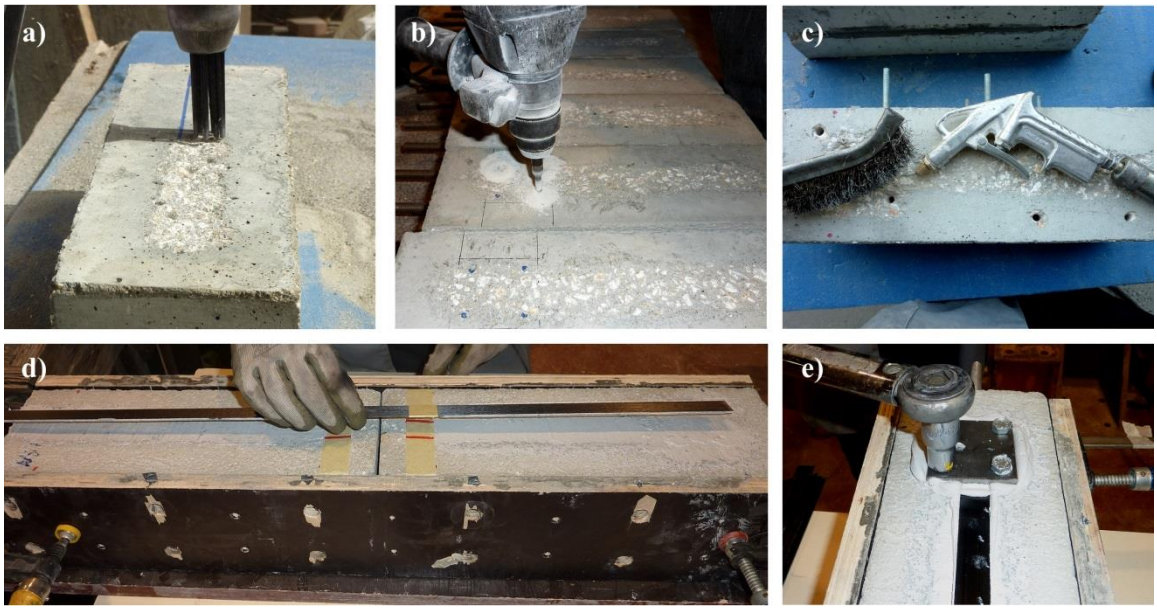

Figure 3.3: EBR specimens preparation – a) concrete surface preparation; b) drilling the blocks for the self-screwing bolts (only in series S1A); c) removing particles from the concrete surface; d) bonding the CFRP strips; e) tightening the self-screwing bolts (only in series S1A).

3.2.1.4 Test setup, instrumentation and procedure

The specimens were loaded in tension using a universal testing machine with a load capacity of 500 kN (Figure 3.4a). The mechanical load was applied using a 24 mm diameter auxiliary rebar, which was bolted to the internal rebars of the specimens and gripped by the clamps of the testing machine. In the tests conducted at elevated temperature, a thermal chamber with inner dimensions of 1100 mm × 280 mm × 340 mm was used (Figure 3.4b).

The instrumentation used in the tests of series S1 and S1A allowed monitoring the following parameters: (i) the load and cross-head displacement of the test machine; (ii) the temperature at the centre of the bonded interface, using 2 thermocouples type K with a diameter of 1.2 mm (T1 and T2 - positions marked in Figure 3.2c to e); (iii) the slip along the bonded length of the CFRP strip, with 2 high-temperature LVDTs (precision of 0.5%), positioned at the beginning and end of the bonded length (*cf*. Figure 3.2d and e); and (iv) the axial strains at the centre and along the bonded length of the CFRP strip, with 11 *TML* electrical strain gauges, model *BFL-5-5*, with a measuring range from -20 ºC up to +200 ºC (bonded to the upper surface of the CFRP strip and positioned as showed in Figure 3.2d and e). Since only one of the concrete blocks was instrumented, it was decided to prevent the failure of the strengthening system at the other concrete block. This was accomplished by (i) applying 2 steel plates in the central part of the CFRP strip, and (ii) wrapping the concrete block with ceramic wool to provide thermal insulation (in the tests at elevated temperature, *cf*. Figure 3.4b). The instrumentation used for series S2 included only the load and the cross-head displacement of the test machine, as well as the temperatures at the centre of the CFRP-concrete interface (Figure 3.2c).

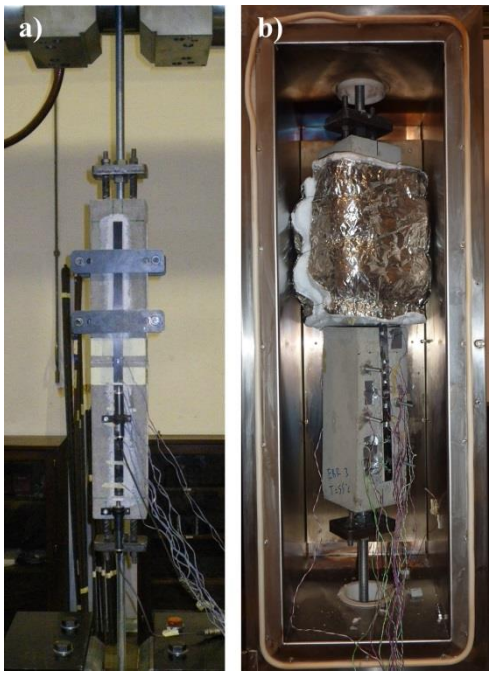

Figure 3.4: Test setup for tests at a) ambient temperature and b) elevated temperature.

The test procedure for series S1 and S1A involved the following steps: (i) specimens were first positioned inside the thermal chamber and were fixed only at the upper clamp of the test machine; (ii) specimens were heated up to the predefined temperature (20 ºC, 55 ºC, 90 ºC and 120 ºC) at variable speed (higher at initial stages, and lower when approaching the target temperature in the adhesive, *cf.* Figure 3.5); (iii) specimens were fixed to the lower clamp of the test machine; (iv) the strain gauges measurements and slip values were set to zero; and (v) specimens were loaded up to failure, under displacement control at a speed of 0.2 mm/min. Figure 3.5 shows the average temperature in the adhesive (average of temperatures from thermocouples T1 and T2, *cf.* Figure 3.2d) during the heating stage of three representative specimens from series S1. The average temperature increase rate ranged from 0.6 °C/min (specimens S1-T55) to 1.0 °C/min (specimens S1-T120). It can be seen that during the loading stage of the specimens, the average temperature in that interface was approximately constant.

For series S2, the following test procedure was adopted: (i) specimens were positioned inside the thermal chamber, at ambient temperature; (ii) specimens were loaded up to the predefined tensile force (25%, 50% or 75% of the average failure load at ambient temperature, previously determined from series S1); (iii) specimens were heated at a rate of 5 ºC/min (set for the air temperature inside the thermal chamber) up to failure. Figure 3.5 shows the average temperature in the adhesive of three representative specimens from series S2. It can be seen that the temperature increase rate was very similar for the different specimens, presenting an average value of 1.8 °C/min.

The heating rates adopted in both series were sufficiently but not excessively low in order (i) to guarantee a uniform temperature distribution at the CFRP-concrete interface and avoid excessive temperature gradients, and (ii) to minimize post-curing phenomena.

The recording of the applied load, cross-head displacement, upper and bottom slip at the CFRP-concrete interface, axial strains in the CFRP strip and temperatures in the adhesive was carried out in a PC using built-in data loggers with an acquisition rate of 10 Hz.

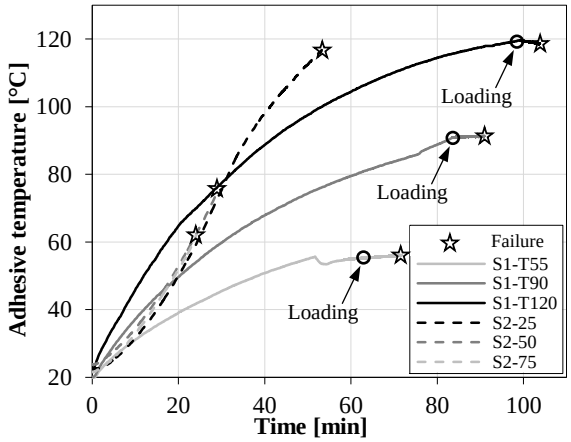

Figure 3.5: Average temperature at the bonded interface vs. time of specimens from series S1 and S2.

3.2.2 Results and discussion

3.2.2.1 Load vs. displacement curves

Figure 3.6 presents the load *vs*. (cross-head) deflection curves of specimens from series S1 (without anchorage) and S1A (with anchorage). For both series, load *vs*. deflection curves reflect a roughly linear overall response of the specimens, with a slight loss of stiffness prior to failure. Specimens from series S1A tested at ambient temperature exhibit several stiffness reductions (with minute deflection increase and load reduction), which were most likely due to the progressive slip of the CFRP strip. As expected, for both series, the temperature increase caused a considerable reduction of the (overall) stiffness and strength. The comparison of specimens from series S1 and S1A tested for similar temperatures highlights the increase of both stiffness and strength provided by the mechanical anchorage.

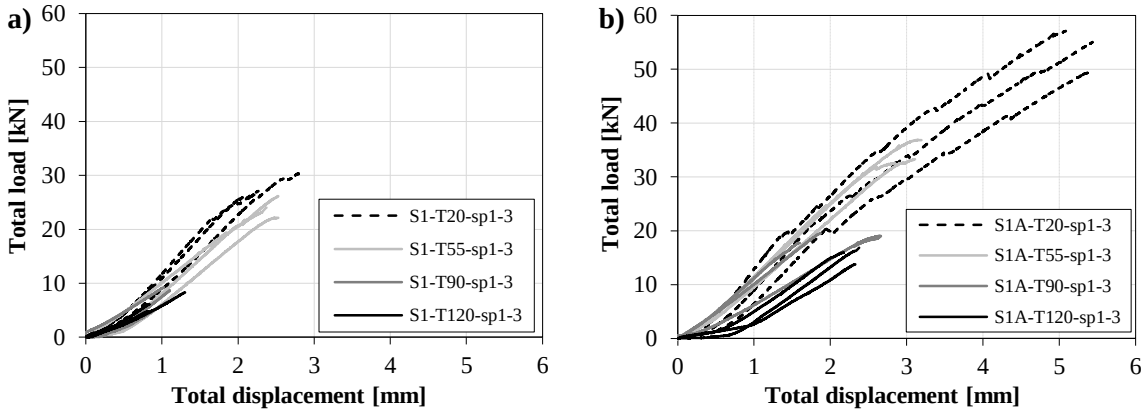

Figure 3.6: Load vs. cross-head deflection curves of specimens from a) series S1; and b) series S1A.

Figure 3.7 presents the increase in the cross-head deflection and the average temperature at the bonded interface, both as a function of time, of specimens from series S2. For all load fractions, the cross-head deflection continuously increased, which can be attributed mainly to the loss of stiffness experienced by the epoxy adhesive. Initially, the cross-head deflection variation presented an increasing rate which was similar for the specimens loaded at the different fractions of ambient temperature strength. For the lowest load fraction, after about 22 min, when the interface temperature was 60 ºC (*i.e.* already beyond the adhesive T_g) the rate of cross-head deflection started to decrease; this trend is believed to be due to the fact that after glass transition, the stiffness (and strength) degradation of the adhesive with increasing temperature is lower, as attested by DMA measurements (*cf.* Figure 3.1). The cross-head deflection of specimens tested at the highest load fraction did not exhibit such inflection and failed precisely at a temperature of about 54 ºC; this different behaviour should stem from the increased stress level installed in these specimens. The specimens tested at the intermediate load level presented also an intermediate behaviour compared to the previous two. As expected, the average time to failure and interface temperature at failure decreased with the load level: 55 min, 28 min and 22 min, and 114 ºC, 71 ºC and 54 ºC, respectively for specimens loaded at 25%, 50% and 75% of ambient temperature strength.

3.2.2.2 Load vs. slip curves

Figure 3.8 depicts the load *vs.* slip curves (measured with the LVDTs positioned at the top and bottom extremities of the CFRP strip, *cf.* Figure 3.2) of a representative specimen from series S1 and S1A for all temperatures tested.

For series S1 (without anchorage, Figure 3.8a), at ambient temperature, it can be seen that regardless of the applied load, there was no slip at the bottom extremity of the CFRP strip, which is consistent with the test setup designed, *i.e.* the bonding length of the CFRP strip (250 mm) was higher than the minimum anchorage length (computed with the designed guidelines) necessary to maximize the capacity of the strengthening system. For increasing test temperatures, slip also

occurred at the bottom of the CFRP strip, which is in agreement with the strain distributions presented next (*cf*. section 3.2.2.3); furthermore, for a given load level, such slip increased with the test temperature. At the top of the CFRP strip, slip was measured for all test temperatures and, for a given load level, it consistently increased with temperature.

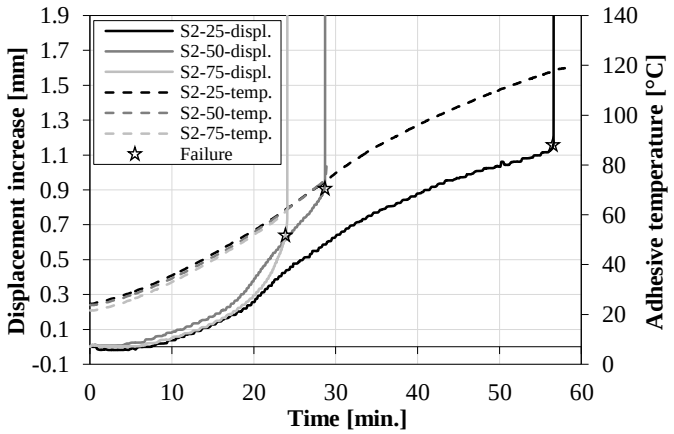

Figure 3.7: Cross-head deflection increase and average temperature at the bonded interface vs. time of specimens from series S2.

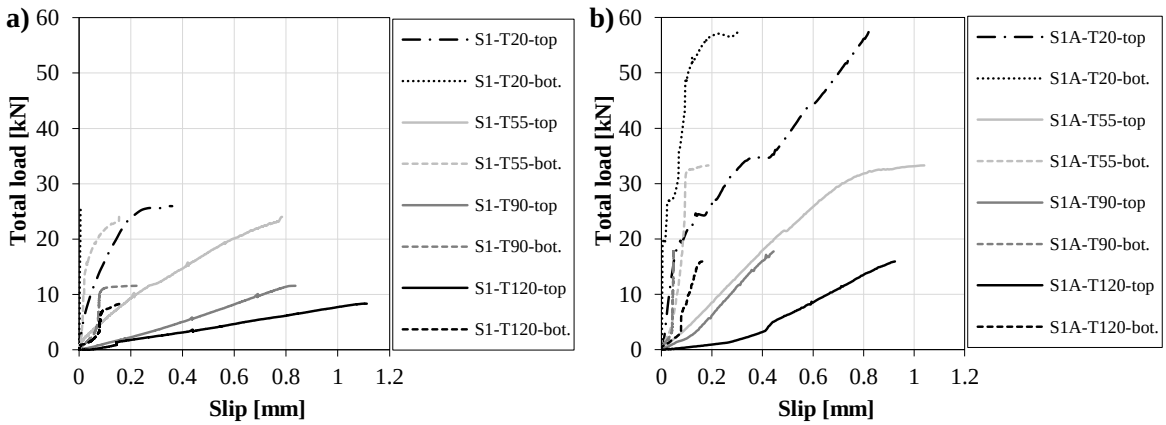

Figure 3.8: Load vs. slip curves of representative specimens from a) series S1; and b) series S1A.

For series S1A (with anchorage, Figure 3.8b), at ambient temperature, for a load level between 20 and 25 kN (roughly the capacity of the corresponding specimen from series S1), slip started to be measured at the bottom of the CFRP strip, although presenting very low magnitude (below 0.05 mm); for increasing load, the bottom slip continuously increased (as well as the top slip), sometimes presenting instantaneous variations (also reflected in the load *vs*. cross-head deflection curves, *cf*. Figure 3.6b); in the brink of collapse, a progressive and significant stiffness reduction occurred, corresponding to the slippage of the CFRP strip below the mechanical anchorage. Regarding the other curves plotted in Figure 3.8b, it can be seen that compared to series S1, at elevated temperature the average stiffness of specimens from series S1A is moderately higher.

These curves highlight again the strength increase provided by the mechanical anchorage for all temperatures tested.

3.2.2.3 Strain distributions

Figure 3.9 presents the axial strain distributions along the bonded length of specimens from series S1 caused by the axial load (*i.e.* neglecting the residual strains developed during the heating stage), for different fractions of the failure load (F_u) and for all temperatures tested. Although high-temperature strain gauges (and adhesive) were used in all experiments, some axial strain measurements were not valid. In these (very limited) cases, dotted lines are plotted in Figure 3.9.

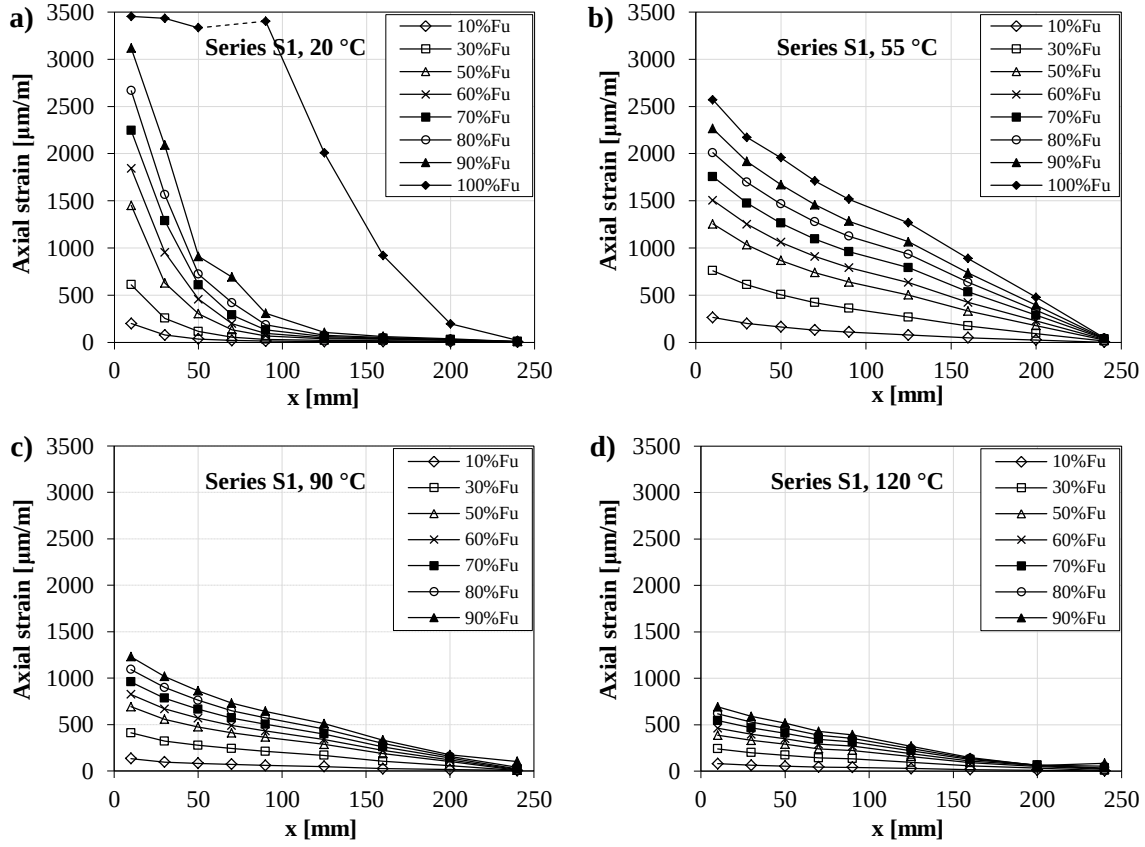

Figure 3.9: Axial strain distributions along the bonded length (x) of representative specimens from series S1 for varying fractions of the failure load at a) 20 ºC, b) 55 ºC, c) 90 ºC, and d) 120 ºC.

At ambient temperature, the axial strain distributions plotted in Figure 3.9a present a typical non-linear development along the bonded length, with null deformations at the end of the CFRP strips (x = 250 mm) for all load levels (due to the aforementioned design concerning the bonded length) and a peak at the opposite extremity. The strain measurements capture a change in the strain distribution pattern for a load level between 90% and 100% of the failure load; in fact, it can be seen that prior to collapse, strains present a considerable relative increase in the central part, becoming almost constant in about 40% of the bonded length. This effect is well explained in

previous analytical and numerical studies (*e.g.* [48, 104-106]), but not always captured experimentally.

For elevated temperature, it can be seen that the overall magnitude of the strain distributions plotted in Figure 3.9 is considerably lower when compared to the ambient temperature one and the maximum axial strains measured consistently decrease with temperature; this is naturally due to the reduction of strength and stiffness experienced by the materials, in particular the epoxy adhesive. It can also be seen that the axial strains distribution along the bonded length changes with increasing temperatures in two aspects: (i) for low to moderate loads, the distribution becomes closer to linear, *i.e.* there is no longer a peak at the top extremity of the CFRP strip; this is explained by the stiffness reduction of the adhesive, which is known to smooth the shear stress/strain distributions in bonded joints (*e.g.* [107]); (ii) for the highest load levels (in the brink of failure), this type of strain distribution (close to linear) is maintained, *i.e.* the trend for a more uniform distribution is no longer observed.

Results plotted in Figure 3.9 also show that the effective bond length (EBL, distance from the loaded end required for the axial strain to become negligible[3]) consistently increases with temperature. At ambient temperature, the EBL was significantly lower than the bonded length, at 55 ºC it roughly matched the bonded length, while at 90 ºC and 120 ºC it actually exceeded the bonded length, although the strain at the end of the CFRP strip was very low (but not negligible). Similar results had been reported earlier by Leone *et al*. [40].

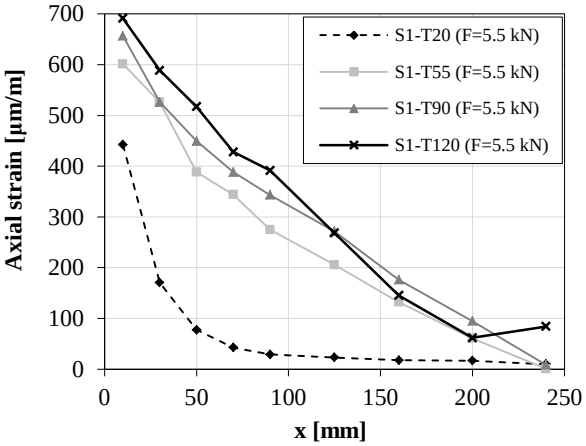

Figure 3.10: Axial strain distributions along the bonded length (x) of specimens from series S1.

Figure 3.10 presents, as an illustrative comparison, the axial strain distributions along the bonded length of specimens from series S1 for an axial load of 5.5 kN (corresponding to about 90% of the failure load at 120 ºC). This figure confirms some of the previous remarks, showing that (i) the axial strains at ambient temperature and elevated temperatures exhibit different patterns (due to the

[3] There is no standard definition for the limit strain below which it can be considered negligible, however the value of 1% of the strain measured at the CFRP loaded end is often used as reference (*e.g.* Leone *et al.* [40]).

stiffness reduction of the adhesive), and that (ii) for the same load level the axial strains increase with temperature (due to the stiffness reduction of the adhesive).

Figure 3.11 presents the axial strain distributions along the bonded length of specimens from series S1A, for different fractions of the failure load and for all temperatures tested. Due to the aforementioned measuring problems, parts of some curves are plotted as dashed lines. In this case, due to the presence of the mechanical anchorage, it was not possible to measure the axial strains along the entire length of the CFRP strip (*cf.* Figure 3.2d).

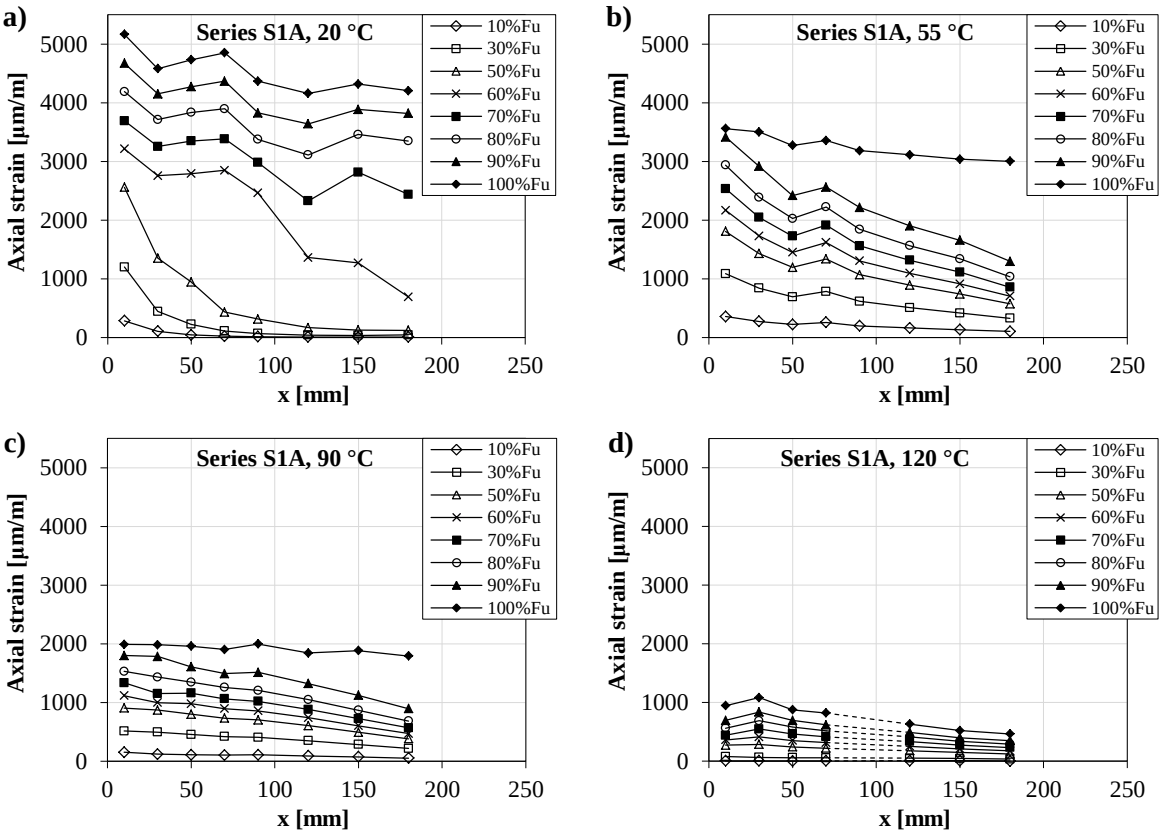

Figure 3.11: Axial strain distributions along the bonded length (x) of representative specimens from series S1A for varying fractions of the failure load at a) 20 ºC, b) 55 ºC, c) 90 ºC, and d) 120 ºC.

At ambient temperature, up to about 50% of the failure load (approximately the strength without anchorage), the axial strain distributions and magnitudes are roughly similar to those of series S1. However, for increasing loads, there is a significant change in the pattern of axial strains distribution: they become progressively more uniform along the bonded length, presenting much higher relative magnitude at the strain gauge closest to the mechanical anchorage (x = 180 mm). This change stems from the progressive debonding of the CFRP strengthening system that takes place in the current bonding area; at this stage, the load transfer between the CFRP strip and concrete is mostly guaranteed by the friction at the mechanical anchorage.

For elevated temperatures, as for series S1, the axial strain distributions became closer to linear, *i.e.* without peaks at the loaded extremity of the CFRP strip; unlike series S1, for temperatures of 55 ºC

and 90 ºC, axial strains are no longer null at the strain gauge closest to the mechanical anchorage, even for low levels of the applied load (for ambient temperature, this was only observed for loads higher than 50% of ambient strength). As for ambient temperature, axial strains tend to become more uniform with increasing load, particularly in the brink of failure.

Finally, it is worth highlighting the fact that for all temperatures tested, the maximum axial strains attained in series S1A are much higher compared to those measured in series S1; this naturally stems from the higher CFRP-concrete bond capacity provided by the mechanical anchorage.

3.2.2.4 Bond vs. slip relationships

Shear stress (τ) *vs*. slip (s) curves were computed based on the axial strain measurements, namely considering the results from pairs of adjacent strain gauges. The procedure described in Ferracutti *et al*. [108] was followed, which considers the following basic assumptions: (i) the deformation of the concrete specimen far from the external cover is negligible compared to that of the CFRP strip; (ii) the variation of axial strains between consecutive strain gauges is linear. By integrating the strain distribution starting from the bottom strain gauge (next to the CFRP free-end, $x = x_m$, where $s(x_m)$ = slip measured by the bottom LVDT), the following equation is obtained for the slip at a general position x, with $x_i \leq x \leq x_{i+1}$, and $\xi = x_m - x$:

$$s(x) = s(x_{i+1}) + \int_{\xi_{i+1}}^{\xi} \varepsilon\,(\xi) d\xi \tag{3.1a}$$

$$s(x) = s(x_{i+1}) - \frac{(\varepsilon_{i+1} - \varepsilon_i)}{(x_{i+1} - x_i)} \frac{(x_{i+1} - x)^2}{2} + \varepsilon_{i+1}(x_{i+1} - x) \tag{3.1b}$$

The average slip between two consecutive strain gauges is determined as follows:

$$\bar{s}_{i+1/2} = \frac{s(x_{i+1}) + s(x_i)}{2} \tag{3.2}$$

Considering that the CFRP strip displays an elastic behaviour, the average shear stress between two adjacent strain gauges ($\bar{\tau}_{i+1/2}$) can be readily obtained from the difference between the axial strains measured at such pair of readings (ε_{i+1} - ε_i), the elastic modulus of the CFRP strip (E_f) for the test temperature (as defined in [34]), its cross-section (A_f) and width (b_f):

$$\bar{\tau}_{i+1/2} = -\frac{E_f A_f (\varepsilon_{i+1} - \varepsilon_i)}{b_f (x_{i+1} - x_i)} \tag{3.3}$$

Figure 3.12 presents the bond-slip curves obtained for specimens from series S1 and S1A and for all the tested temperatures (as a high acquisition rate was adopted in the tests (10 Hz), the points were connected with lines in order to provide a clear visualization of those relations). These curves correspond to pairs of adjacent strain gauges (from all specimens) in which valid strain

measurements were obtained. It must be stressed that the strains were measured at the outer (external) surface of the CFRP strips, therefore the slip measured with the LVDT at $x = 0$ does not necessarily match the slip at the same position derived from the strain measurements. In fact, those results should be different as the latter slip encompasses the overall flexibility of the CFRP-concrete bonded connection, *i.e.* it is affected by the distortion of the epoxy adhesive.

Results obtained for series S1 (without anchorage, Figure 3.12a) at ambient temperature, were consistent and in agreement with other results reported in the literature (*e.g.* [48, 104-106], although lower shear stress were reported), providing the full bond-slip relationship, namely the ascending and descending branches of the shear stress *vs*. slip response. The set of bond-slip curves obtained present some scatter among each other (also reported in several other earlier works, *e.g.* Leone *et al*. [40]), and this can be attributed to several causes, namely the local nature of the measurements and the irregularity of the concrete surface, causing a non-uniform thickness of the adhesive and hence a variation of the interface stiffness along the bonded length. However, it is worth mentioning that the maximum shear stresses of three curves obtained at ambient temperature in series S1 are higher than expected (> 15 MPa - higher than those reported in the literature *e.g.* [48, 104-106]); this might be related to the following aspects: (i) the relatively low width of the CFRP strip – it is well known (and mentioned in design guidelines [99, 100]) that lower CFRP widths lead to higher maximum shear stresses; and (ii) the influence of localized effects - those curves were obtained from pairs of strain gauges that might be located in a length that is not fully representative of the overall behaviour of the CFRP-concrete connection.

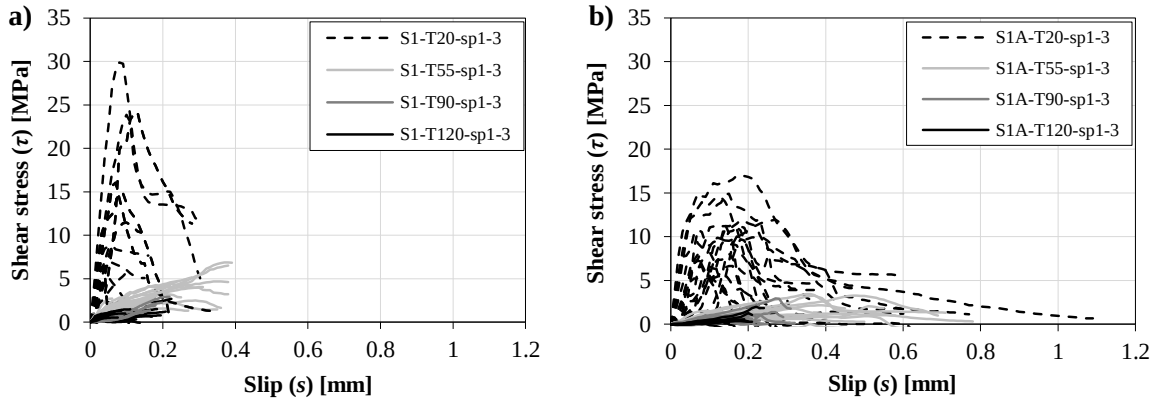

Figure 3.12: Shear stress vs. slip curves for a) series S1 and b) series S1A for all temperatures tested.

At elevated temperatures, due to the aforementioned difficulties encountered with some strain measurements, results were less consistent and presented higher scatter. In addition, in most cases, it was not possible to trace a descending branch of the bond *vs*. slip curve. Nevertheless, results obtained clearly showed a consistent reduction of both stiffness and maximum shear stress with temperature.

The shear stress *vs*. slip curves obtained for series S1A (with mechanical anchorage, Figure 3.12b) present a similar overall pattern to those of series S1 for all temperatures tested. It can be seen that the mechanical anchorage allowed attaining higher slip values, which is in agreement with the slip measurements obtained from the LVDTs (*cf*. section 3.2.2.2). For ambient temperature, it can also be seen that the maximum shear stresses are lower compared to those of series S1; this should be due to the effect of the mechanical anchorage, which is deemed to be (at least partly) mobilized, even for lower levels of applied load.

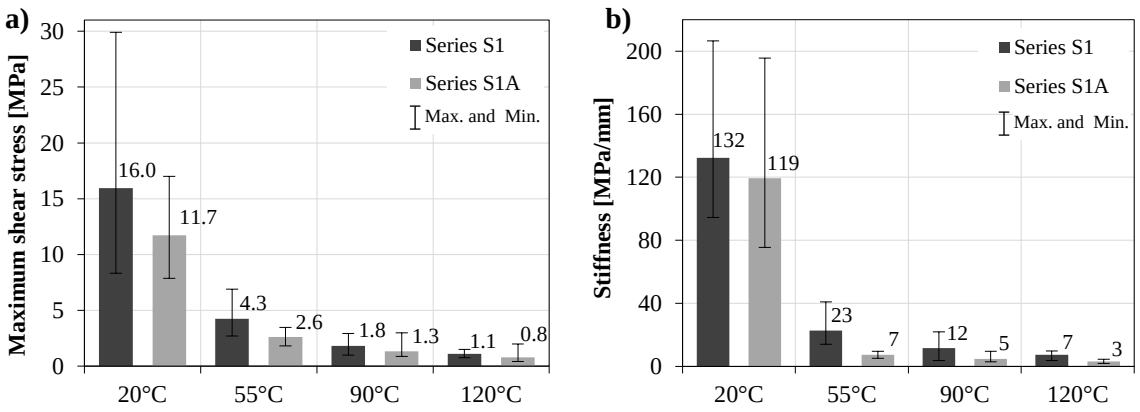

Figure 3.13: Average values of a) shear stress and b) stiffness from bond-slip relationships of series S1 and S1A (error bars correspond to maximum and minimum values).

Figure 3.13 summarizes the variation of the stiffness and the maximum shear stress at the different temperatures for series S1 and S1A (computed based on the individual bond-slip curves, Figure 3.12). The error bars correspond to the minimum and maximum values determined at each temperature. Although the results obtained present relatively high variability (due to the aforementioned reasons), they clearly indicate that for both series S1 and S1A the most substantial reductions of maximum shear stress and stiffness occur when temperature increases from 20 ºC to 55 ºC. It is interesting to note that those reductions are much higher than that suffered by the normalized bond strength (*cf*. section 3.2.2.6 and Figure 3.15). This difference is due to the change in the axial strain distribution along the bonded length, which, as discussed in section 3.2.2.3, becomes close to linear at elevated temperature.

3.2.2.5 Failure modes

For specimens from series S1 and S1A, tested in steady state condition, the failure modes were different at ambient temperature and elevated temperatures. For series S1, cohesive failure occurred in specimens tested at ambient temperature (Figure 3.14a), with the failure surface located a few millimetres inside the concrete substrate. At elevated temperature, adhesive failure occurred at the concrete-adhesive interface (Figure 3.14b). For series S1A, specimens tested at ambient temperature presented shear failure of the concrete block in the anchorage zone (Figure 3.14c), which means that the anchorage system was successful in preventing premature debonding of the

CFRP system. At elevated temperature, failure was caused by the progressive slip of the CFRP system under the anchorage plate, which took place after the occurrence of adhesive failure at the concrete-adhesive interface outside the anchorage area (Figure 3.14d).

For specimens from series S2, tested in transient condition, the failure modes were similar to those of series S1 tested at elevated temperature, *i.e.* involved adhesive failure at the concrete-adhesive interface.

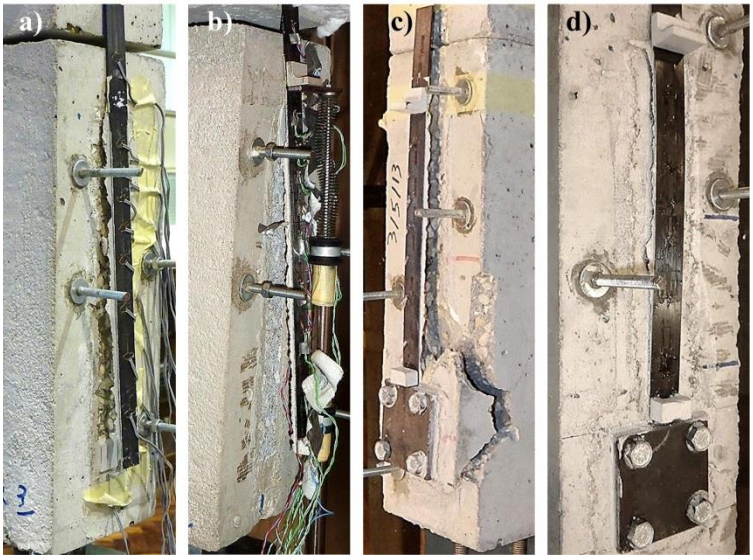

Figure 3.14: Failure modes for series S1 at a) 20 ºC and b) 55 ºC, and series S1A at c) 20 ºC and d) 55 ºC.

3.2.2.6 Bond strength

Figure 3.15 presents the failure load *vs*. interface temperature for all test series. The average failure loads obtained in series S1 and S1A are also presented in Table 3.1. The comparison of results obtained for series S1 and S1A shows that for all temperatures, the anchorage system provided considerably higher bond strength (between 56% and 139%). For both series, it can also be seen that there is a significant reduction of bond strength with temperature, which naturally stems from the glass transition process underwent by the epoxy adhesive applied at the CFRP-concrete interface. This reduction was roughly similar for both test series, as it was caused by the softening of the epoxy adhesive. It is worth mentioning that for temperatures of 90 ºC and 120 ºC (much higher than the T_g of the adhesive, determined from the onset of the storage modulus curve), the residual tensile strengths (compared to the ambient temperature one) were as much as 32% and 23%, respectively. Since the glass transition process of the adhesive was complete for those temperatures (from a mechanical viewpoint), it is likely that friction forces at the concrete-adhesive interface as well as chemical adhesion promoted such relatively high residual strength.

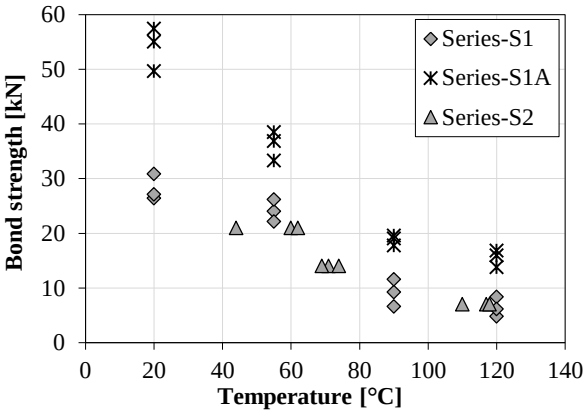

Figure 3.15: Bond strength vs. temperature for all test series.

Table 3.1: Failure load as a function of temperature obtained in EBR specimens (average ± standard deviation).

Series	Specimens	Failure load [kN]
S1	S1-T20	28.1 ± 2.4
	S1-T55	24.1 ± 2.0
	S1-T90	9.1 ± 2.5
	S1-T120	6.4 ± 1.8
S1A	S1A-T20	54.0 ± 4.0
	S1A-T55	37.7 ± 2.7
	S1A-T90	19.3 ± 0.9
	S1A-T120	15.3 ± 1.6

The comparison of results obtained for series S1 and S2 shows that the influence of the test condition (steady-state or transient) was very limited. In fact, the bond strength as a function of temperature of specimens from series S2 is roughly similar to that of specimens from series S1, particularly for the highest temperatures.

Figure 3.16 plots the normalized bond strength of specimens from series S1 and S1A, *i.e.* the ratio between the bond strength at a given temperature and the corresponding strength at ambient temperature, and the adhesive storage modulus curve (from Figure 3.1). The experimental data from both series are plotted alongside two simulation curves fitted with the Gibson *et al.*'s [32] relaxation model (presented in section 2.2.3 - page 18). P_R was taken as the average strength at the maximum temperature tested; k_m and $T_{g,mech}$ (listed in Table 3.2) were obtained by fitting the experimental data (the least squares criterion was adopted).

Results plotted in Figure 3.16 show that the experimental data from both series is reasonably well described by Gibson's relaxation law. The experimental and modelling results depicted in Figure 3.16 also indicate that the initial bond strength reduction (*e.g.*, for a temperature of 55 ºC) with the mechanical anchorage is higher compared to that of the simply bonded system; a possible explanation for this higher relative bond strength decrease of series S1A could be the tightness

reduction of the self-screwing bolts due to their thermal expansion, thus decreasing the pressure in the anchoring plate. On the other hand, for the highest temperatures, both test and modelled data presented in Figure 3.16 show that the mechanical anchorage provides higher residual bond strength; this improved performance should stem from the residual friction provided by the steel anchoring plate at elevated temperature. Figure 3.16 also shows that there is no direct correlation between the bond strength degradation and the adhesive storage modulus curve, with the latter property presenting a higher reduction that takes place for lower temperatures than those obtained in the bond strength of the specimens. As mentioned above, the high residual tensile strengths obtained at temperatures significantly higher than the adhesive T_g might be due to friction forces and chemical adhesion at the concrete-adhesive interface.

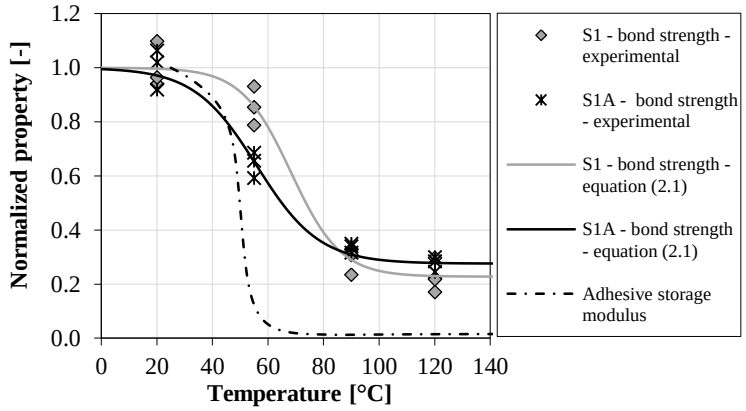

Figure 3.16: Normalized bond strength vs. temperature for series S1 and S1A: experimental data and modelling.

Table 3.2: Fitted parameters of the bond strength as a function of temperature simulation curves (Gibson et al.'s [32] model).

Series	k_m [-]	$T_{g,mech}$ [°C]	R^2 [-]
S1	0.0559	68.3	0.97
S1A	0.0444	55.9	0.98

3.2.3 Summary of results

This section presented an experimental investigation on the bond between concrete and EBR-CFRP strips at moderately elevated temperatures. The following main results were obtained:

- Elevated temperature caused significant changes in the strain distributions along CFRP-concrete bonded interfaces: while at ambient temperature typical non-linear distributions were observed, at elevated temperature the strain distributions were closer to linear, which is explained by the stiffness reduction of the adhesive, promoting the smoothing of shear stresses along the bonded length. The incorporation of the mechanical anchorage led to more uniform strain distributions for all temperatures tested.

- For specimens without mechanical anchorage, the effective bond length consistently increased with temperature: at ambient temperature, it was significantly lower than the bonded length, at 55 ºC it roughly matched the bonded length, while at 90 ºC and 120 ºC it exceeded the bonded length.
- Bond-slip relationships determined at ambient temperature present the typical pattern reported in the literature, with well-defined ascending and descending branches. At elevated temperature, in most cases, it was only possible to trace the ascending branch; however, the obtained results clearly highlight a consistent reduction of both stiffness and maximum shear stress with temperature. The bond-slip relationships with incorporation of a mechanical anchorage generally feature lower maximum shear stresses, which was attributed to the (at least partial) mobilization of the mechanical anchorage.
- As in previous studies, with elevated temperature the failure modes of specimens without anchorage changed from cohesive in the concrete substrate (at ambient temperature) to adhesive at the concrete-adhesive interface (at elevated temperature). When the mechanical anchorage was used, failure at ambient temperature occurred due to shear in the concrete, whereas at elevated temperature the mechanical anchorage was less effective, with adhesive failure occurring at the concrete-adhesive interface outside the anchorage area.
- Elevated temperature caused a significant and continuous reduction of bond strength, due to the glass transition process underwent by the epoxy adhesive. The application of a mechanical anchorage at the extremities of the CFRP strips allowed obtaining higher bond strength for all temperatures tested; however, specimens with mechanical anchorage experienced comparable strength reductions with temperature compared to those without such constructive detail. The bond strength degradation with temperature of specimens with and without mechanical anchorage is reasonably well described by Gibson's relaxation law.
- The bond strength as a function of temperature of specimens tested under steady-state conditions (series S1 - constant temperature with increasing load) was similar to that obtained in specimens tested under transient conditions (series S2 - sustained load with increasing temperature), showing that the influence of the test procedure adopted in this study was very limited.
- It was shown that significant bond strength is kept for temperatures higher than the T_g of the adhesive and this was attributed to friction forces and chemical adhesion at the concrete-adhesive interface. According to Gibson *et al.*'s [32] relaxation model, for a temperature corresponding to the adhesive T_g (based on the onset of the storage modulus curve decay, from DMA tests) the bond strength is about 93% of that at ambient temperature. This result is particularly relevant for practical applications, since it indicates

that for both service and fire conditions a critical temperature considerably higher than the adhesive T_g can be defined, depending on the stress level installed on the strengthening system. Additional investigations are still needed in order to obtain in-depth understanding about the stress-temperature dependency of EBR-CFRP strengthening systems and to define such upper temperature limits.

3.3 NSM STRENGTHENING

3.3.1 Description of the test programme

3.3.1.1 Test series

The experimental programme presented in this section comprised double-lap shear tests between concrete blocks and CFRP strips installed according to the NSM technique and bonded with two different types of adhesives: a conventional epoxy adhesive (series EP), and a mixed grout with cement and epoxy binders (series MG). This latter adhesive was chosen for incorporating cement binders, since it was expected that its mechanical and bond properties would be less affected by temperature compared to the conventional epoxy one (in a recent study [71] adhesives with cement binders had presented good performance at elevated temperature when compared to epoxy). The tests were carried out in steady state condition, *i.e.* specimens were first heated up to a predefined temperature (20 ºC, 40 ºC, 55 ºC, 90 ºC, 120 ºC and 150 ºC) and then loaded up to failure. Specimens from series EP were tested up to 150 ºC (and excluding 40 °C), whereas those from series MG were tested only up to 90 ºC, as for this temperature the remaining strength compared to ambient temperature was already very low. For each series and test temperature, 3 specimens were tested. The following nomenclature was used: *EP-T55-sp1* stands for specimen 1 (sp1) of series EP, tested at 55 ºC.

3.3.1.2 Materials

As for the EBR specimens (section 3.2), the concrete blocks used in this experimental campaign were cast with ready-mixed concrete and internally reinforced with steel bars with a diameter of 16 mm; the corresponding mechanical properties were indicated in section 3.2.1.2.

The CFRP strips used as strengthening materials, with the same commercial designation of those used in the EBR specimens (*S&P Laminates CFK 150/2000*), have a smaller cross-section: 10 mm (width) × 1.4 mm (thickness). The average tensile properties of these CFRP strips (determined according to ISO 527-5 [101]), are as follows: tensile strength of f_{fu} = 2850 MPa, Young's modulus of E_f = 168 GPa, and ultimate strain of ε_{fu} = 16 ‰. A similar glass transition temperature (T_g = 83 °C) to that determined for the EBR-strips was obtained from DMA (dual cantilever setup,

heating rate of 1 °C/min) based on the onset of the storage modulus curve decay (Figure 3.17a), as well as the decomposition temperature (T_d = 380 °C), determined from TGA measurements (air atmosphere; heating rate of 10 °C/min from 25 °C to 800 °C; according to ISO 11357 [103]) based on the middle temperature of the sigmoidal mass change (*cf.* Figure 3.17b).

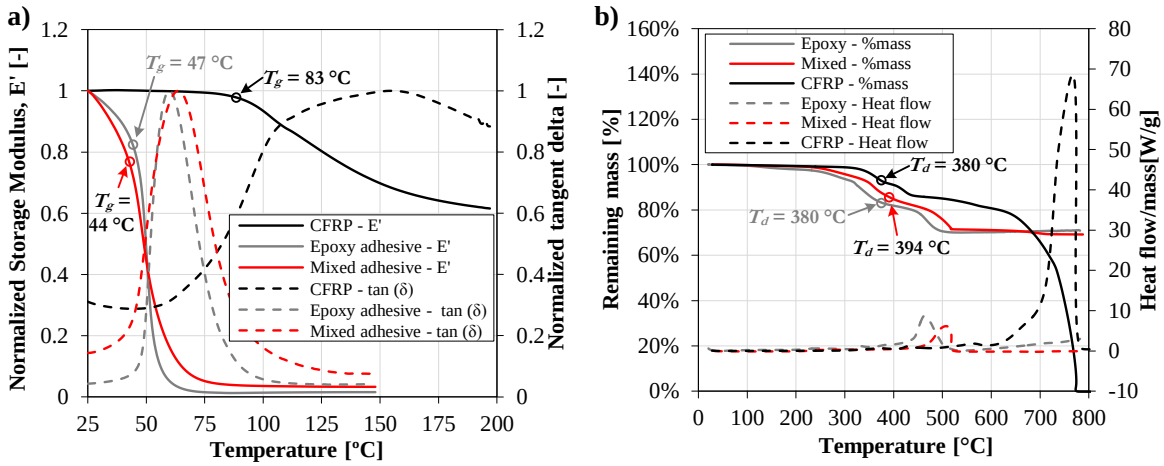

Figure 3.17: (a) DMA and (b) DSC/TGA curves for CFRP, epoxy adhesive and mixed grout.

In series EP the same two-component epoxy adhesive used in the EBR-specimens was adopted (properties provided in section 3.2.1.2). It is worth pointing out that this adhesive comprises a relatively high content of additions and filler, with relatively coarse grading.

In series MG a three-component grout, with the commercial designation *ATFloor ER* (supplied by *Quimidois*), was used as an alternative to the epoxy adhesive. This bonding agent is made of both cement and epoxy binders, containing also additions and filler, but with a much finer grading compared to that of the epoxy adhesive. This adhesive presents average tensile modulus and strength of E_a = 1.6 GPa and f_{at} = 6.6 MPa, respectively (determined according to ISO 527-2 [102]), both at ambient temperature, and a T_g of 44 ºC (Figure 3.17a). It is worth mentioning that although it presents a lower T_g, the storage modulus curve of the mixed grout exhibits a lower reduction rate with temperature than the epoxy adhesive (T_g = 47 °C, *cf.* Figure 3.17a). This result indicates that the degradation of its mechanical properties starts at a (slightly) lower temperature, but the reduction (with temperature) is slower. Regarding the decomposition temperature, T_d = 394 °C (*cf.* Figure 3.17b, also determined from TGA measurements using similar test conditions to those described for the CFRP), it is slightly higher than that obtained for the epoxy adhesive (T_d = 380 °C).

3.3.1.3 Specimens geometry and preparation

Figure 3.18 presents the geometry of the test specimens that comprised two parallelepiped concrete blocks similar to those of the EBR specimens, which were internally reinforced with two U-shaped

steel bars. The CFRP strips (1.4 mm × 10 mm) were 600 mm long, being bonded in a total length of 2 × 250 mm (unbonded length of 100 mm), as adopted in the EBR specimens. The slits pre-cut into the concrete cover were 15 mm deep and 5 mm width; such dimensions fulfil the ACI 440.2R-08 [56] recommendations. According to [56], the anchorage length needed to maximize the resistance of the strengthening system was 159 mm. The following two reasons explain the adoption of a higher value: (i) to allow for a direct comparison with the EBR specimens; (ii) at elevated temperatures, one expected the anchorage length to increase.

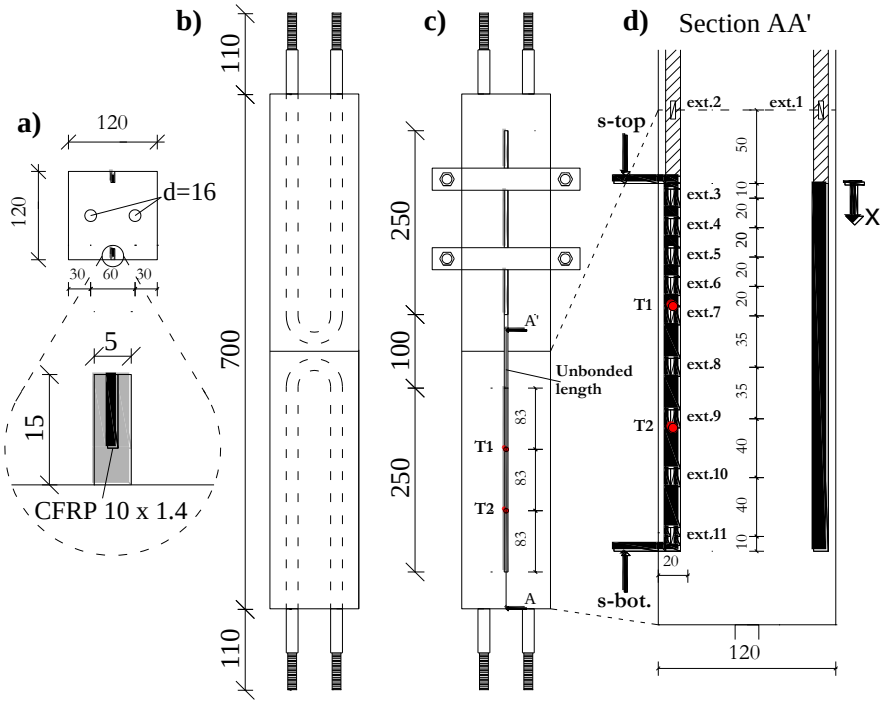

Figure 3.18: a) Cross-section and position of the slits and CFRP strips; b), c) specimens geometry; d) and detail of instrumentation, dimensions in mm.

After casting the concrete blocks, the test specimens were prepared according to the following procedure: (i) execution of slits inside the concrete cover (Figure 3.18a), with dimensions of 15 mm (depth) × 5 mm (width) (according to the recommendations of ACI 440.2R-08 [56]), using a diamond slit cutter (Figure 3.19a); (ii) cleaning the dust and loose particles with a compressed air jet gun; (iii) positioning and alignment of the pairs of concrete blocks; (iv) cleaning (with acetone) the CFRP strips, and application of the instrumentation (thermocouples and strain gauges, *cf*. next section); (v) preparation and introduction of the adhesives into the slits; (vi) application of a thin layer of adhesive into the surfaces of the CFRP strips; (vii) insertion of the CFRP strips inside the slits with application of pressure and removal of the squeezed adhesive (Figure 3.19b and c).

Figure 3.19: NSM specimens preparation – a) execution of the slits in the concrete cover; b) detail of the CFRP strips' instrumentation before insertion inside the slits; c) insertion of the CFRP strips inside the slits.

3.3.1.4 Test setup, instrumentation and procedure

The test setup adopted in the present bond tests was similar to that described for the EBR strengthening campaign (*cf.* section 3.2.1.4); the same universal testing machine (Figure 3.20a) and thermal chamber were used (Figure 3.20b). Hence, in what concerns the instrumentation, the following parameters were monitored in one block (using the measuring devices described in section 3.2.1.4): (i) the load and cross-head deflection of the test machine; (ii) the temperature at the centre (mid-depth) of the bonded interface in two positions (*cf.* Figure 3.18c); (iii) the slip along the bonded length of the CFRP strips at the beginning and end of the bonded length (Figure 3.18d); and (iv) the axial strains along the bonded length and in the (unbounded) centre of the CFRP strip, with 11 electrical strain gauges (positioned depicted in Figure 3.18d). Since the instrumentation was applied in only one of the concrete blocks, as for the EBR specimens, in order to prevent failure at the other concrete block it was decided (i) to apply a clamping system made of steel plates to delay the failure of the CFRP strengthening system (at that side of the specimen), and (ii) to wrap the concrete block with ceramic wool to provide thermal insulation in the tests at elevated temperature.

As mentioned, in this experimental campaign the tests were performed only under steady-state conditions. The following experimental procedure was adopted: (i) specimens were positioned inside the thermal chamber and fixed by the upper clamp of the test machine; (ii) the thermal chamber was turned on, thus starting to heat the interface at a speed of about 0.8 ºC/min until the average temperature in the thermocouples equalled the predefined temperatures; (iii) specimens were fixed by the lower clamp of the test machine and tested under displacement control at a rate of 0.6 mm/min until failure. The measurements provided by the instrumentation (applied load, cross-head displacement, upper and bottom slip, axial strains and temperatures) were recorded in a PC using built-in data loggers.

It is worth mentioning that although the total area of the strain gauges represented only 7% of the total contact area between the CFRP and the bonding adhesive, the influence of applying the referred number of sensors along the CFRP bonded length on the bond behaviour between the

CFRP strip and the adhesive was addressed in a preliminary experimental campaign performed on specimens identical to those described herein. In this study it was concluded that their influence on the overall stiffness and bond strength of the bonded connection was not significant: for both parameters, the relative differences for specimens with and without strain gauges were well within the experimental scatter. These results demonstrated the suitability of using such sensor arrangement on double-lap shear tests between NSM CFRP strips and concrete at elevated temperatures.

Figure 3.20: Setup for tests at a) ambient temperature and b) elevated temperature.

3.3.2 Results and discussion

3.3.2.1 Load vs. displacement curves

Figure 3.21 presents the load *vs*. cross-head displacement curves for all specimens from series EP and MG tested at different temperatures.

The overall pattern of the load *vs*. cross-head displacement curves of both series for all temperatures tested is similar, presenting three different branches: (i) an initial non-linear behaviour with increasing stiffness, due to adjustments of the test setup, (ii) a roughly linear response during most of the test; and (iii) an increasingly non-linear response with progressive stiffness reduction prior to failure.

Both series present a reduction of the (overall) stiffness and strength with increasing temperature, which is naturally due to the glass transition process underwent by the bonding materials and their consequent loss of stiffness. The comparison of both series shows that the magnitude of the above-

mentioned reduction is higher in series MG and moreover it occurs for lower temperatures, which is consistent with the DMA results. Accordingly, although at ambient temperature series EP and MG exhibit comparable overall stiffness and strength, for similar elevated temperatures, specimens from series EP present much better performance.

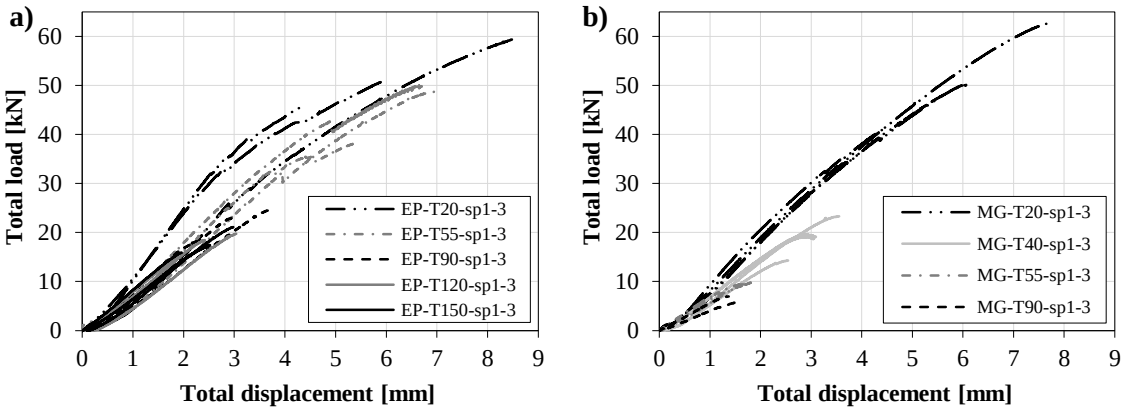

Figure 3.21: Load vs. cross-head deflection curves of specimens from series a) EP; and b) MG.

3.3.2.2 Load vs. slip curves

Figure 3.22 depicts the load *vs*. slip curves of a representative specimen from series EP and MG for all temperatures tested. As mentioned, the slip was measured at the top and bottom extremities of the CFRP strip (*cf*. Figure 3.18).

For series EP (Figure 3.22a), at ambient temperature, it can be seen that there was no slip at the bottom extremity of the CFRP strip (anchorage zone) for loads up to about 30 kN (approximately 2/3 of the maximum load); however, at this point, slip started to be measured, increasing non-linearly with the load level. This result was not expected, as the bonding length was much higher than the anchorage length recommended by ACI 440.2R-08 [56] (250 mm *vs*. 159 mm). Unsurprisingly, at the upper extremity of the CFRP strip, slip started to be measured since the beginning of the test, progressively (non-linearly) increasing with the applied load. For elevated temperatures, the load *vs*. slip curves at the bottom and top extremities generally exhibited a progressive stiffness reduction with increasing temperature. Compared to ambient temperature, the load *vs*. slip curves at elevated temperature present the following main differences: (i) slip started to develop at the bottom of the CFRP strip since the beginning of the test, although presenting very low magnitude; (ii) the slip measured at the top of the CFRP strip presents a variation closer to linear with the applied load, which is in agreement with the axial strain distributions (*cf*. section 3.3.2.3) that feature a much more uniform variation pattern with increasing load, compared to ambient temperature.

Regarding series MG, for all temperatures tested, the load *vs*. slip curves reflect a more markedly non-linear response. In general, for similar temperatures, specimens from series MG presented

lower stiffness and higher slip than those of series EP, particularly at the bottom extremity of the CFRP strip, in which relatively high slip was measured.

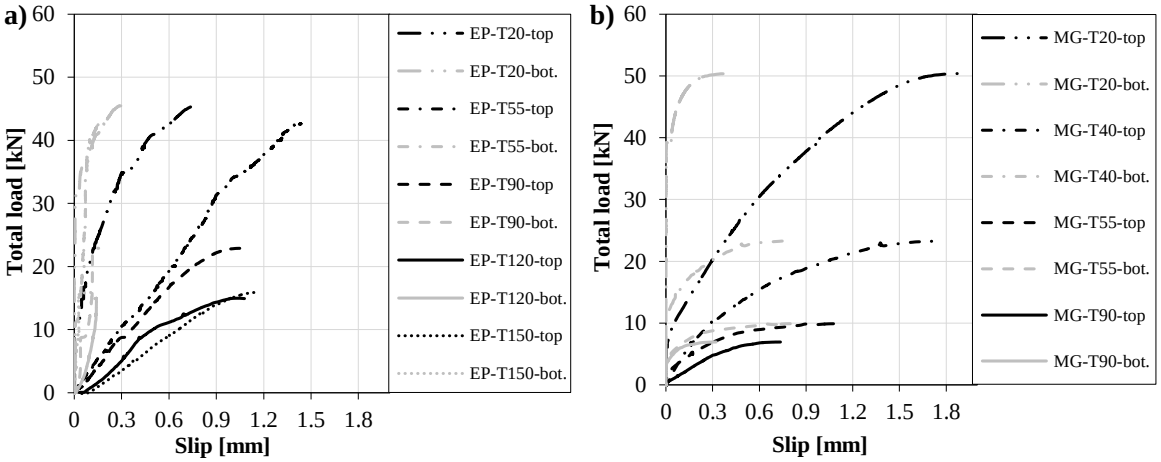

Figure 3.22: Load vs. slip curves of representative specimens from series a) EP; and b) MG.

3.3.2.3 Strain distributions

Figure 3.23 presents the axial strain distributions along the bonded length of representative specimens from series EP caused by the axial load (*i.e.* neglecting the residual strains developed during the heating stage), for different fractions of the failure load and for all temperatures tested. Although in all experiments at elevated temperature specimens were monitored with high-temperature strain gauges (and bonded with high-temperature adhesive), some measurements were not valid (when the strain gauge measurements exhibited erratic fluctuations or physically unexpected variation trends). In these (limited) cases, dotted lines are plotted in Figure 3.23.

At ambient temperature (Figure 3.23a), the axial strains present the typical non-linear distribution, with null deformations at the unloaded end of the CFRP strip (x = 250 mm) and a peak at the loaded extremity of the CFRP strip (x = 0). For higher load levels, the base of such peak progressively widens, with strains increasing in the central part of the bonded length prior to collapse. Results obtained also indicate that the effective bond length (EBL) was roughly 200 mm, *i.e.* lower than the bonded length. For elevated temperatures (Figure 3.23b-e) the overall magnitude of the axial strains consistently decreased with the temperature increase, which is naturally due to the strength and stiffness reduction of the materials, namely of the epoxy adhesive. It can also be seen that the axial strain distributions are closer to linear, no longer presenting a peak at the loaded extremity; this different pattern is due to the softening of the epoxy adhesive, which leads to more uniform shear stresses along the bonded length. Finally, it is also worth noting that the EBL increased for elevated temperatures; in fact, for a temperature of 55 ºC, it even became higher than the bonded length. In general, the above-mentioned behaviour is qualitatively similar to that described for the corresponding EBR specimens.

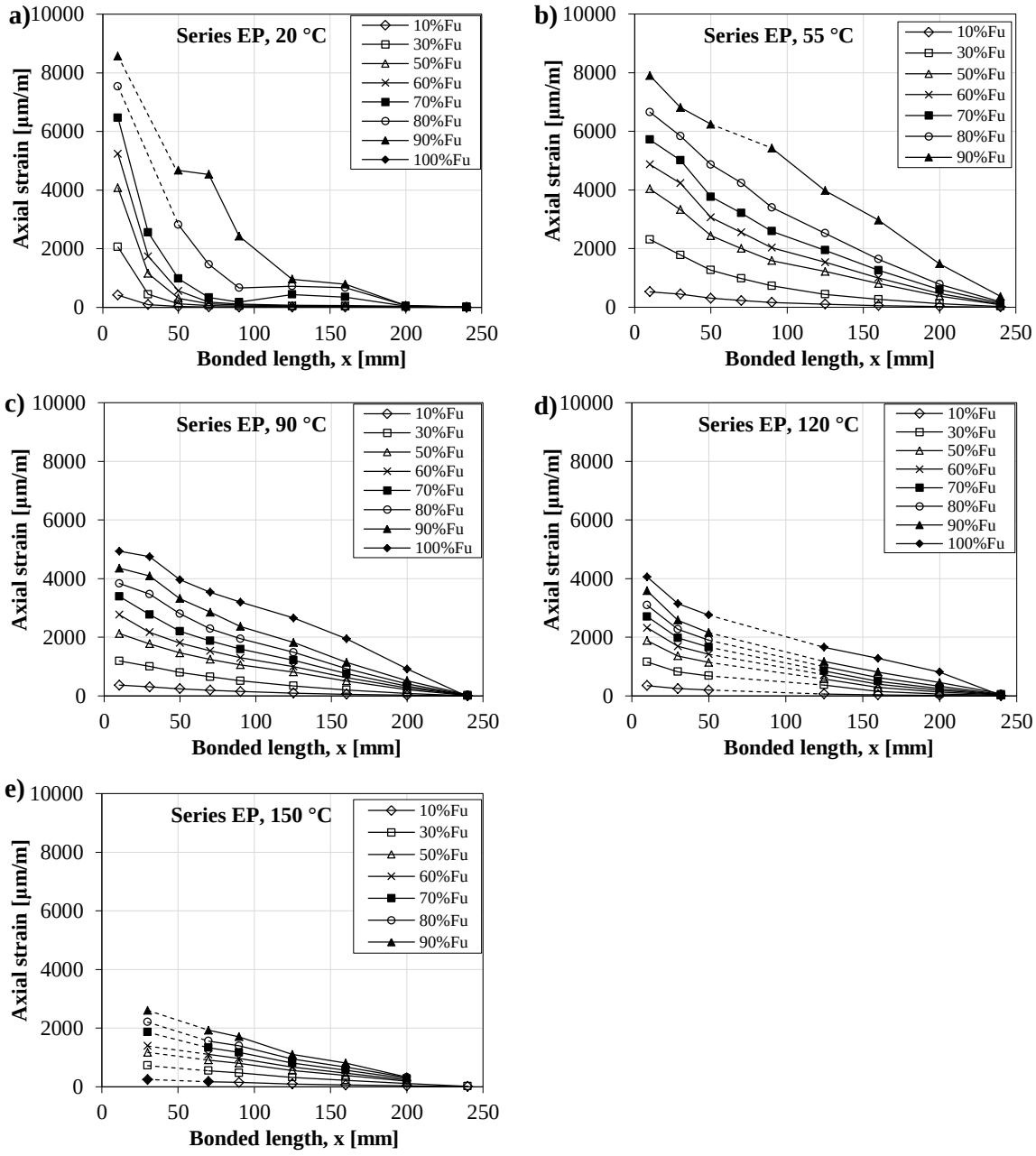

Figure 3.23: Axial strain distributions along the bonded length (x) of representative specimens from series EP for varying fractions of the failure load at temperatures of a) 20 ºC, b) 55 ºC, c) 90 ºC, d) 120 ºC, and e) 150 ºC.

Figure 3.24 presents the axial strain distributions along the bonded length of representative specimens from series MG caused by the mechanical load, for different fractions of the failure load and for all temperatures tested. As for series EP, some axial strain measurements were not valid. In these (limited) cases, dotted lines are plotted in Figure 3.24.

The axial strain distributions at ambient temperature of series MG (Figure 3.24a) are even closer to linear when compared to those of series EP; this difference stems from the lower stiffness of the mixed grout (compared to the epoxy adhesive), which promotes more uniform shear stress distributions along the bonded length. It is also relevant to note that unlike series EP, the EBL in

series MG is higher than the bonded length already at ambient temperature. For equivalent elevated temperatures (Figure 3.24b-d), compared to series EP, the magnitude of the axial strains in series MG is much lower, which is explained by the lower strength of the mixed grout at elevated temperature, thus considerably limiting the capacity of the bonded interface. As for series EP, in series MG, the axial strain distributions at elevated temperature are closer to linear when compared to ambient temperature; however, this difference is less pronounced, since the axial strains at ambient temperature are already closer to linear than those observed in series EP at the same temperature. As for ambient temperature, the EBL at elevated temperature is higher than the bonded length.

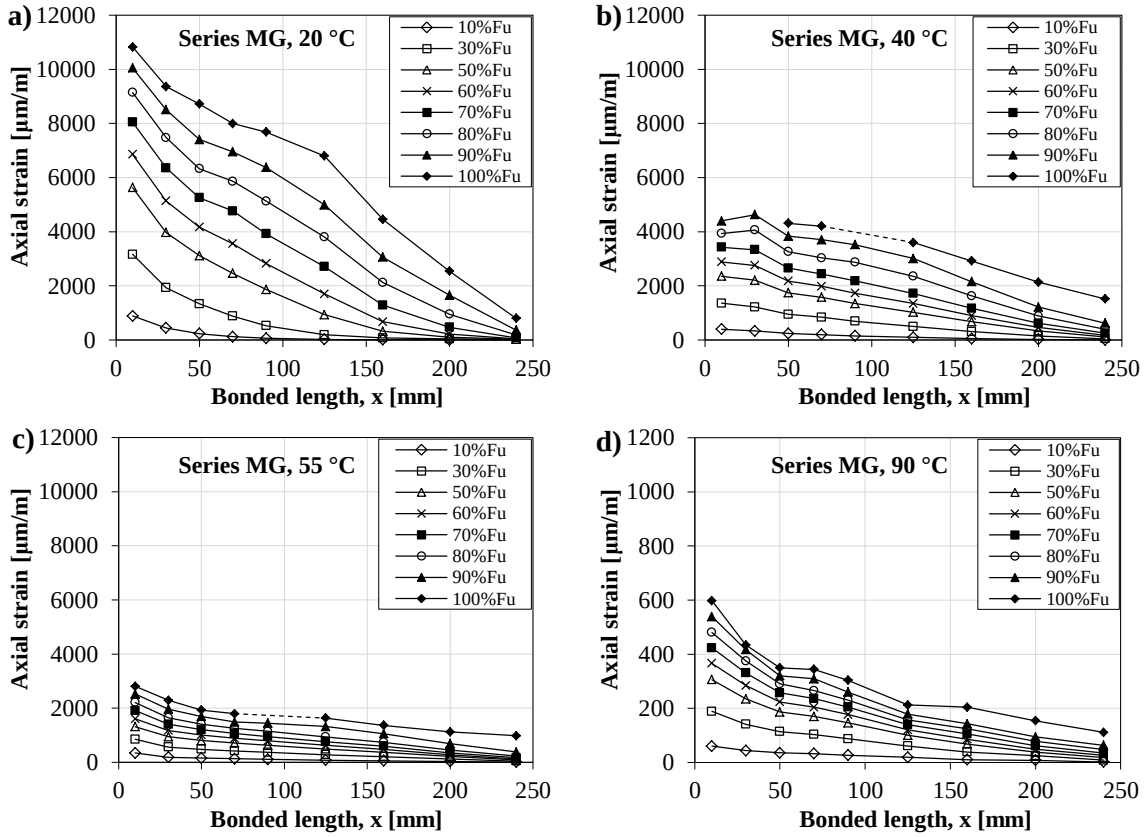

Figure 3.24: Axial strain distributions along the bonded length (x) of representative specimens from series MG for varying fractions of the failure load at temperatures of a) 20 ºC, b) 40 ºC, c) 55 ºC, and d) 90 ºC.

3.3.2.4 Bond vs. slip relationships

The shear stress (τ) *vs*. slip (s) relationships at different temperatures were determined based on the axial strain measurements, namely considering the results from pairs of adjacent strain gauges. This calculation was made according to the procedure suggested in [108], which was briefly described in section 3.2.2.4 (page 59). Figure 3.25 presents the bond-slip curves obtained for specimens from series EP and MG for all temperatures tested (as for the EBR specimens, since a high acquisition rate was adopted in the tests (10 Hz), the points were connected with lines in order to provide a

clear visualization of the those relations). The curves plotted in Figure 3.25 for a given temperature correspond to pairs of adjacent strain gauges (from all specimens) in which valid strain measurements were obtained. Again, it is worth noting that the strains were measured at the surface of the CFRP strips, therefore the slip measured with the LVDT located at $x = 0$ does not necessarily match the slip at the same position derived from the strain measurements. Actually, as mentioned for the EBR specimens, those results should differ as the latter slip measurement is also influenced by the overall flexibility of the CFRP-adhesive-concrete bonded connection, in particular by the distortion of the adhesive.

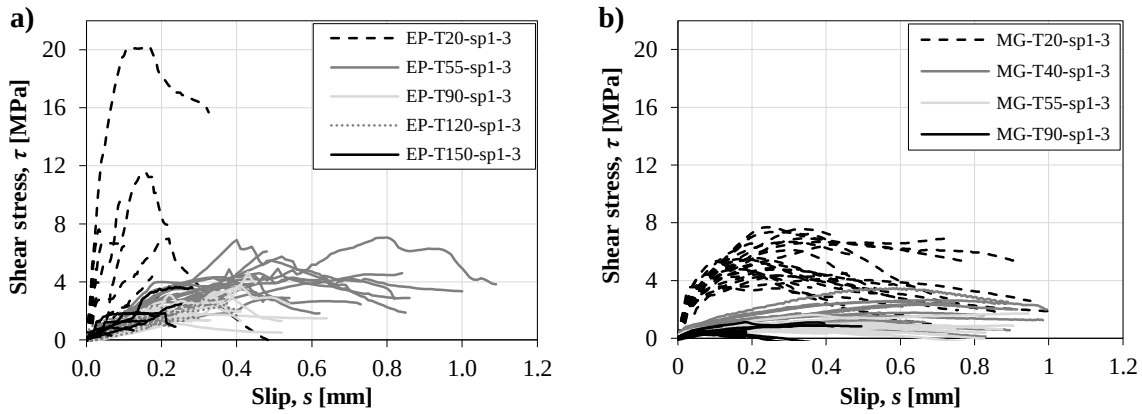

Figure 3.25: Shear stress vs. slip curves for series a) EP and b) MG for all temperatures tested.

The bond-slip curves at ambient temperature for series EP (Figure 3.25a) present a typical pattern, consistent with results published in the literature (*e.g.* [91, 109-111]), with well-defined ascending and descending branches. The several curves obtained present relatively high scatter, which can be explained by the local nature of the measurements, the non-uniformity of the adhesive thickness, causing a variation of the interface stiffness along the bonded length, and the possible (not confirmed) existence of small voids within the adhesive. With increasing temperature the bond-slip curves exhibit a consistent reduction of stiffness and maximum shear stress, especially when the temperature increases from 20 ºC to 55 ºC. It is interesting to note that for 55 ºC, the shear stress peak is attained for a slip that is higher than the one observed for all the other temperatures tested. This result indicates that at this temperature the EP adhesive softened considerably (but still retained enough strength), presenting its maximum distortion capacity, which is consistent with the measured slip at the top extremity of the CFRP strip (Figure 3.22a) at this temperature. Further increasing the temperature seems to cause a reduction of this distortion capacity.

For series MG, the bond-slip curves at ambient temperature (Figure 3.25b) are much more non-linear when compared to those of series EP, with lower stiffness and a flatter and lower shear stress peak. These differences naturally stem from the lower stiffness and strength of the mixed grout compared to the epoxy adhesive. As for series EP, the bond-slip curves of series MG exhibit a

considerable reduction of stiffness and maximum shear stress with increasing temperature, in this case already at a temperature of 40 ºC.

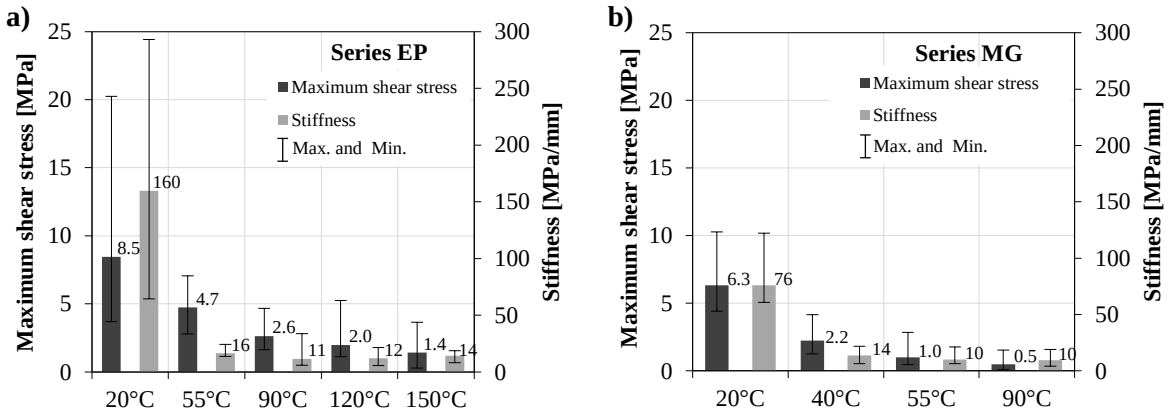

Figure 3.26: Average, maximum and minimum shear stress and stiffness (bond-slip relationships) from a) series EP and b) series MG.

Based on the individual bond-slip curves, Figure 3.26 summarizes the variation of the stiffness and the maximum shear stress with temperature for series EP and MG. The error bars correspond to the minimum and maximum values determined among the individual bond-slip curves at each temperature. Results plotted in Figure 3.26 (i) attest the better overall performance of series EP in terms of stiffness and maximum shear strength at ambient temperature, and (ii) indicate that the most considerable reductions of stiffness and maximum shear stress occur when temperature increases from 20 ºC to 55 ºC (series EP) or 40 ºC (series MG). The reductions in the maximum shear stress are much higher than those experienced by the corresponding bond strength (*cf.* section 3.3.2.6), particularly for series EP; this is explained by the change in the strain distribution along the bonded length (more pronounced in series EP), which tends to become closer to linear at elevated temperature.

3.3.2.5 Failure modes

Figure 3.27 illustrates the failure modes observed in series EP and MG, at both ambient and elevated temperatures.

For series EP, at ambient temperature collapse was caused by shear failure of the concrete block (Figure 3.27a), which was triggered close to the top extremity of the CFRP strip, where higher stress concentrations develop. In opposition, for all elevated temperatures, adhesive failure occurred at the CFRP-adhesive interface, with the slip being easily identified by the naked eye (Figure 3.27b).

For series MG, adhesive failure at the CFRP-adhesive interface occurred for both ambient (Figure 3.27c) and elevated temperatures (Figure 3.27d), highlighting the worse adhesive properties of this material. It is relevant to note that the failure mode illustrated in Figure 3.27c occurred due to the

CFRP slip at the CFRP-adhesive interface; the minor portion of adhesive (about 10 mm of length) attached to the CFRP strip showed in this figure corresponded to a localized phenomenon and was not representative of the overall failure mode of the bonded joint. The different failure mode at ambient temperature observed in series MG (compared to series EP) is not necessarily in disagreement with the similar bond strength provided by both bonding materials (*cf.* section 3.3.2.6). In fact, compared to the epoxy adhesive, the MG grout led to more uniform shear stress distributions along the bonded interface and thus caused lower maximum stresses in the concrete substrate (for the same load levels).

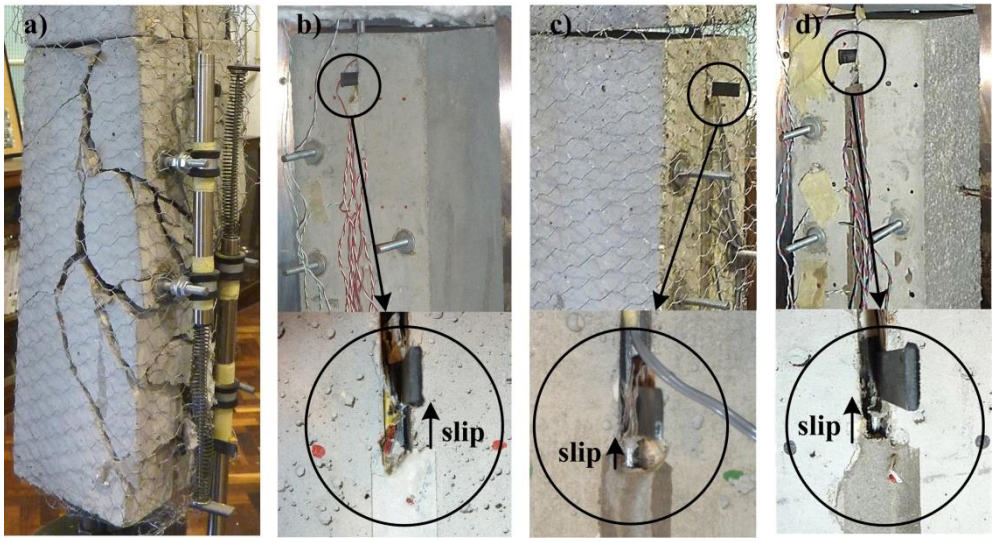

Figure 3.27: Failure modes for series EP at a) 20 ºC and at b) elevated temperature, and series MG at c) 20 ºC and at d) elevated temperature.

3.3.2.6 Bond strength

Figure 3.28 presents the failure load as a function of the interface temperature for specimens from both series EP and MG. The average failures loads obtained in both series are also presented in Table 3.3. Results obtained from double-lap shear tests performed on similar specimens to those of series EP, but with the CFRP strips installed according to the EBR technique (from series S1, *cf.* section 3.2), are also presented in Figure 3.28 for a comparison.

At ambient temperature, in spite of the relatively high scatter in terms of bond strength results, the performance of both adhesives was similar. For elevated temperature, both NSM series suffered a considerable reduction of bond strength, due to the glass transition process underwent by the bonding materials. In series MG, such reduction started for much lower temperatures and was much more pronounced compared to series EP. In fact, for the higher temperatures tested (90 ºC to 150 ºC), well above the T_g of the epoxy adhesive, the bond strength of series EP not only exhibited appreciable values but also seemed to stabilize. Since the glass transition process of the adhesive was complete (from a mechanical viewpoint) for those temperatures, it is likely that such relatively

high residual strength was promoted by chemical adhesion and friction forces at the CFRP-adhesive interface (an hypothesis that has already been put forward regarding the EBR specimens). In this regard, the lower residual bond strength of series MG should be attributed not only to the lower mechanical properties of the mixed grout at elevated temperature, but also to the probably lower friction forces developed with this material, which, as mentioned, presents much finer filler in its constitution.

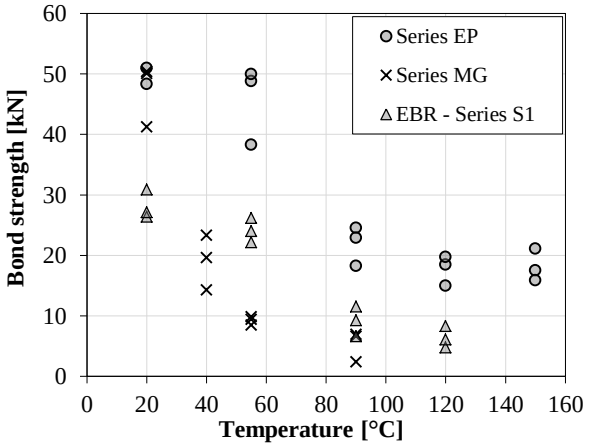

Figure 3.28: Bond strength vs. temperature for series EP and MG, together with data from series S1 for EBR interfaces (section 3.2).

Table 3.3: Failure load as a function of temperature obtained in NSM specimens (average ± standard deviation).

Series	Specimens	Failure load [kN]
EP	EP-T20	54.2 ± 8.0
	EP-T55	45.7 ± 6.4
	EP-T90	21.9 ± 3.2
	EP-T120	17.7 ± 2.5
	EP-T150	18.1 ± 2.7
MG	MG-T20	51.1 ± 8.8
	MG-T40	19.1 ± 4.5
	MG-T55	9.2 ± 0.7
	MG-T90	5.3 ± 2.5

The comparison between the results of series EP and those of series S1, also plotted in Figure 3.28, shows that for all temperatures tested the NSM technique provides much higher bond strength than the EBR technique (between 1.9 and 2.8 times).

Figure 3.29 plots the normalized bond strength of specimens from series EP and MG, *i.e.* the ratio between the bond strength at a given temperature and the corresponding strength at ambient temperature. The experimental data from both series (and the results of EBR specimens, series S1) are plotted together with the simulation curves fitted with the relaxation model proposed by Gibson

et al.'s [32] (already presented in section 2.2.3 – page 18; the corresponding fitted parameters are listed in Table 3.4). Figure 3.29 shows that, similarly to the EBR specimens, the normalized bond strength degradation of both NSM series is very well described by this relaxation law. Furthermore, both the experimental data and the simulation curves confirm that the bond strength reduction experienced by series MG starts at much lower temperatures (regardless of the T_g of the epoxy adhesive being only slightly higher to that of the mixed grout), is much steeper and presents much higher magnitude for similar temperatures. The comparison of the results of series EP with the data from series S1 shows that the bond strength reduction with temperature experienced with the NSM technique (16%, 60% and 67% respectively at 55 ºC, 90 ºC and 120 ºC) is generally lower when compared to that observed with the EBR technique (respectively 14%, 68% and 77%). It can also be seen that the strength reduction occurs roughly for the same temperature range, as attested by the similar $T_{g,mech}$ fitted parameters (Table 3.4). These results are consistent with the hypothesis discussed earlier of the residual bond at temperatures well above the T_g of the epoxy adhesive being promoted by friction forces at the CFRP-adhesive interface. In fact, the interfacial area when using the NSM technique is higher than when using the EBR technique.

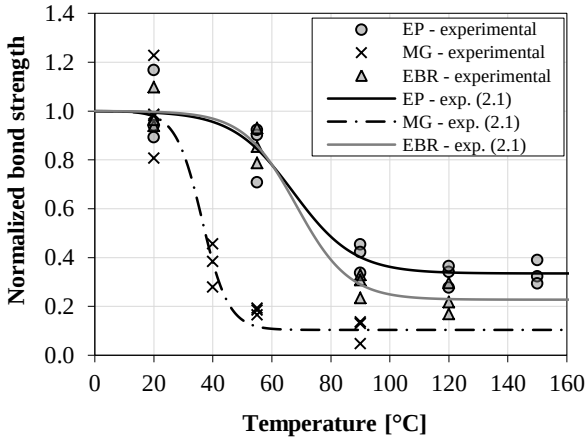

Figure 3.29: Normalized bond strength vs. temperature for series EP and MG: experimental data (including data from series S1 for EBR interfaces) and modelling.

Table 3.4: Fitted parameters of the bond strength as a function of temperature simulation curves (Gibson's model).

Series	k_m [-]	$T_{g,mech}$ [°C]	R^2 [-]
EP	0.048	67.3	0.92
MG	0.112	36.4	0.93
S1 (EBR)	0.0559	68.3	0.97

3.3.3 Summary of results

Section 3.3 presented an experimental study about the bond behaviour at high temperature between concrete and CFRP strips installed according to the NSM technique and bonded with either conventional epoxy adhesive or mixed grout. The following main results were obtained:

- The axial strains along the bonded length presented considerable changes from ambient temperature (non-linear distribution with a peak at the loaded end of the CFRP strip) to elevated temperatures (closer to linear distribution) due to the softening of the interface caused by the glass transition of the bonding materials. This change was more pronounced in series EP than in series MG, due to the higher stiffness of the epoxy adhesive at ambient temperature compared to that of the mixed grout.
- The effective bond length in series EP increased for elevated temperature, becoming higher than the bonded length. For series MG, the effective bond length was higher than the bonded length for all temperatures tested (including at ambient temperature), highlighting the worse performance of the mixed grout as a bonding material even at ambient temperature.
- The bond-slip curves obtained, although exhibiting relatively high scatter, indicate a consistent reduction of both stiffness and maximum shear stress with temperature. For all temperatures tested, the bond-slip curves obtained for series MG presented significantly lower stiffness (*e.g.* 10 MPa/mm at 55 °C *vs.* 16 MPa/mm in series EP at the same temperature) and much flatter and lower shear stress peaks (*e.g.* 1.0 MPa at 55 °C *vs.* 2.6 MPa in series EP at the same temperature), which was attributed to the lower stiffness of the mixed grout.
- For series EP, the temperature increase caused a change in the failure mode, from concrete shear failure (at ambient temperature) to adhesive failure at the CFRP-adhesive interface. For series MG, due to the worse adhesive properties of the mixed grout, failure at the CFRP-adhesive interface was observed for all temperatures.
- Both test series experienced a considerable reduction of bond strength when exposed to elevated temperatures, due to the glass transition process underwent by the bonding materials. In series MG, this reduction started for considerably lower temperatures and was much more pronounced (*e.g.* 82% reduction at 55 °C *vs.* 16% in series EP at the same temperature). Since the T_g of both bonding materials were of the same order of magnitude, this different behaviour was attributed mostly to the higher friction forces at the CFRP-epoxy adhesive interface, due to the much coarser filler particles of the epoxy adhesive. Gibson's relaxation law is able to simulate with good accuracy the bond strength degradation with temperature of both series.
- The bond strength of specimens strengthened according to the NSM technique is much higher than that of similar specimens strengthened according to the EBR technique for all temperatures tested (between 1.9 and 2.8 times). Furthermore, the strength reduction with temperature of NSM-strengthened specimens is lower than that experienced by comparable

EBR-strengthened specimens (*e.g.* 67% reduction at 120 °C *vs.* 77% in EBR specimens at the same temperature).

3.4 CONCLUDING REMARKS

This chapter presented experimental investigations on the bond between concrete and CFRP strengthening systems at moderately elevated temperatures (up to 150 °C) when installed according to either EBR (section 3.2) or NSM (section 3.3) techniques.

The results obtained for both strengthening techniques showed that elevated temperature causes significant changes in the strain distributions along CFRP-concrete bonded interfaces due to the stiffness reduction of the adhesives. In fact, at ambient temperature typical non-linear distributions were observed, while at elevated temperature the strain distributions were closer to linear.

Besides the changes in the strain distributions, the exposure to elevated temperature caused a continuous reduction of both stiffness and bond strength of the CFRP-concrete bonded connections; nevertheless, considerable bond strengths were kept for temperatures higher than the T_g of the adhesives, which were attributed to friction forces and chemical adhesion at the CFRP-concrete interfaces. The results also showed that the failure modes of the bonded connections changed from cohesive, at ambient temperature, to adhesive, at elevated temperatures (with the exception of the NSM-CFRP strips bonded with the mixed grout, where adhesive failures were also observed at ambient temperature). Finally, the better bond performance at elevated temperature of the NSM strengthening system (compared to EBR) was confirmed and quantified.

The experimental results presented herein, namely the bond strength reduction with temperature and the bond-slip relationships for the different tested temperatures, apart from their contribution to the understanding of the bond behaviour between CFRP strips and concrete at elevated temperatures, provide useful data that can be used on the numerical modelling of CFRP-strengthened RC members exposed to fire or simply to high temperatures. This aspect is assessed in the numerical investigations presented in chapters 4 and 8.

CHAPTER 4

BOND OF CFRP TO CONCRETE AT ELEVATED TEMPERATURE: NUMERICAL MODELLING

4.1 INTRODUCTION AND OBJECTIVES

This chapter presents numerical investigations on the bond between concrete and CFRP strengthening systems at moderately elevated temperatures. The study comprised the simulation of the double-lap shear tests presented in chapter 3 (only series S1 and EP). The main objective was to calibrate bond-slip laws representative of the overall behaviour of the CFRP-concrete interfaces for all temperatures tested and for both strengthening techniques (EBR and NSM, both with epoxy adhesive), which can then be implemented in numerical models of CFRP-strengthened RC structural members under elevated temperatures or fire (*cf.* chapter 8), thus allowing to predict their structural response.

In order to calibrate the bond-slip laws, three-dimensional finite element (FE) models of the test specimens were developed using the commercial package ABAQUS [112], in which the concrete blocks, the steel rebars and the CFRP strips were considered as isotropic materials. The CFRP-concrete interaction for each tested temperature was modelled assuming a cohesive damage behaviour defined by a bi-linear bond-slip law. These laws were derived for each tested temperature and strengthening technique based on an inverse analysis in order to minimize the relative differences between experimental and numerical results. A perfect bond between the steel rebars and the concrete was assumed.

4.2 DESCRIPTION OF THE NUMERICAL MODELS

4.2.1 Geometry and type of elements

Since material non-linear analyses were performed, a symmetry simplification of the model was introduced in order to reduce the computational costs (only one of the two blocks was simulated). In order to assembly the mesh, several parts were created for the concrete block (Figure 4.1). This was necessary in order to accurately simulate the contact zone between the concrete and the CFRP.

For the NSM strips, since there are two contact surfaces between concrete and CFRP, additional parts had to be created.

Figure 4.2 and Figure 4.3 illustrate the FE mesh of the specimens EBR and NSM, respectively. When generating the mesh for the concrete, CFRP and steel, 8-node hexahedral elements were used. These are isoparametric elements which are integrated by a tensor product Gauss quadrature rule. The mesh data for both FE models is presented in Table 4.1.

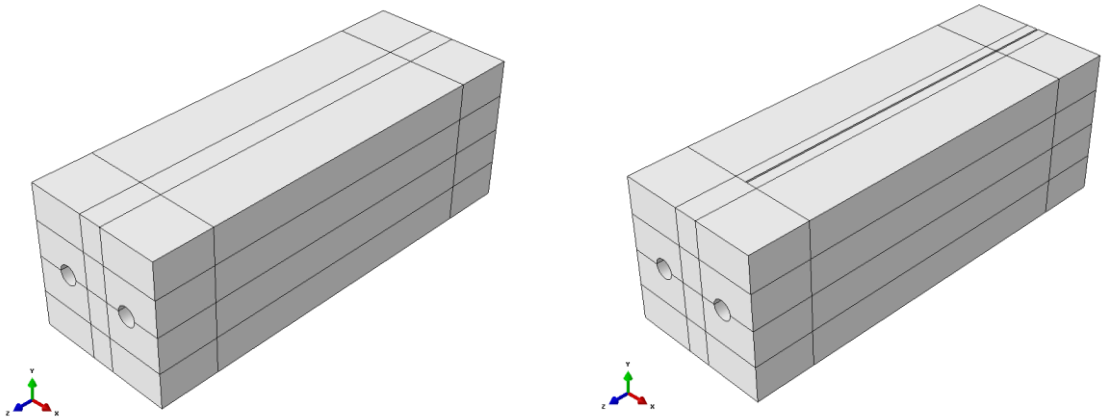

Figure 4.1: Different parts of the concrete blocks: a) EBR-CFRP-strengthened; b) NSM-CFRP-strengthened.

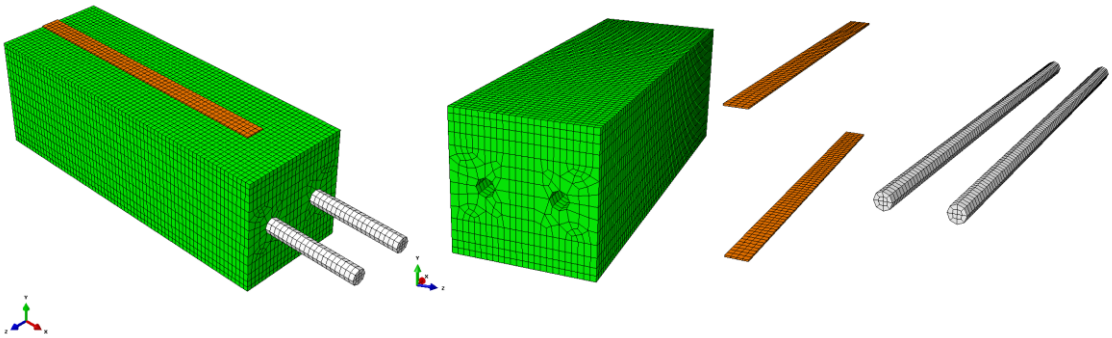

Figure 4.2: FE mesh of the EBR-CFRP-strengthened blocks (concrete-green; CFRP-orange; steel rebars-grey).

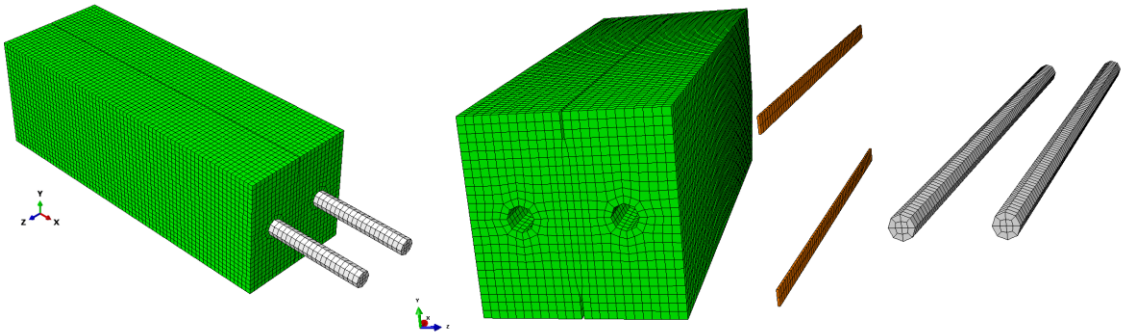

Figure 4.3: FE mesh of the NSM-CFRP-strengthened blocks (concrete-green; CFRP-orange; steel rebars-grey).

Table 4.1: Mesh data for the EBR and NSM FE models.

Parameter	EBR models	NSM models
Number of elements	26606	44862
Number of nodes	31326	51002
Number of Lagrange multipliers	510	816
Number of degrees of freedom	95508	155454

4.2.2 Material properties

A classical concrete damaged plasticity model [113] was used to simulate the concrete behaviour. This approach was considered to be adequate since for this study no crack concentrations (*e.g.* notches) existed. The mechanical properties adopted for the concrete at ambient temperature were the ones measured in the experimental campaign (*cf.* section 3.2.1.2 – page 48). Regarding the facture energy, a constant value with temperature of G_{cf} = 50 N/m was considered, based on the Fib Model Code 90 [96] recommendations for a concrete with similar mechanical properties and a maximum aggregate diameter of 8 mm. Concerning the U-shaped steel rebars (diameter of 16 mm, class A500NR), as the stress level due to the maximum load applied to the specimens was significantly lower than its yield strength (a stress of 240 MPa was measured for the maximum load), a classical linear elastic model was used, in which the following properties were considered: elastic modulus of E_s = 200 GPa and Poisson ratio of ν = 0.3. The variation with temperature of the mechanical properties of both concrete and steel were defined using data from [114].

Although the CFRP strips are orthotropic materials (comprising mainly a unidirectional reinforcement), in the present application they behave essentially in the longitudinal direction, hence, as a simplification, the CFRP was modelled as a linear elastic isotropic material, where ν = 0.3. The elastic modulus of the CFRP strip (E_f) was determined by a fitting procedure using the strain readings on the unbonded length of the specimens ("ext. 2", *cf.* Figure 3.2d – page 50) and the applied load data. The following values were determined for each tested temperature: E_f = 152.5 GPa[4] (20 °C and 55 °C); E_f = 147.0 GPa (90 °C); E_f = 140.0 GPa (120 °C); and E_f = 130.0 GPa (150 °C); this reduction with temperature is consistent with that proposed by Bisby [34].

4.2.3 Loading, boundary conditions and type of analyses

As referred in section 4.2.1, due to symmetry of the double-lap specimens, only one of the two blocks was modelled. Consequently, the vertical displacements of the loaded end of the CFRP

[4] The elastic modulus at 20 °C derived from the fitting procedure is different to that obtained from material characterization tests (*cf.* Section 3.2.1.2 – page 44), simply because these tests were carried out after the numerical investigations presented in this chapter. It was decided to maintain the value of 152.5 GPa (at ambient temperature) since its relative difference to that reported by the manufacturer (165 GPa) is less than 10%.

strips were restricted. To simulate the clamps of the testing machine, the nodes of extremities of the steel rebars were fixed in all directions.

The analysis was performed imposing applied displacements, allowing to control the post-peak responses during the softening stage [115, 116]. As the loading speed used in the experimental campaign was sufficiently low (0.2 or 0.6 mm/min), a static non-linear analysis was adopted.

4.2.4 Modelling of the interfaces - proposed bond-slip relationships

Figure 4.4a shows a scheme of a real CFRP-concrete bonded joint, in which two interfaces are identified: (i) the CFRP-adhesive interface; and (ii) the adhesive-concrete interface, whose actual behaviour can be defined by the corresponding non-linear bond-slip laws. As indicated in this figure, the structural response of the joint stems from the contribution of both interfaces together with the adhesive constitutive relationship (mainly its behaviour essentially under pure shear action). However, due to the complexity of the characterization of such interfaces and materials (especially at elevated temperatures), in this study the bond behaviour between concrete and CFRP is simulated by a single bond-slip law, representative of the overall response of the joint (as illustrated in Figure 4.4b). Note that this strategy has also been adopted in most previous numerical studies (for ambient temperature) reported in the literature (*e.g.* [117, 118]).

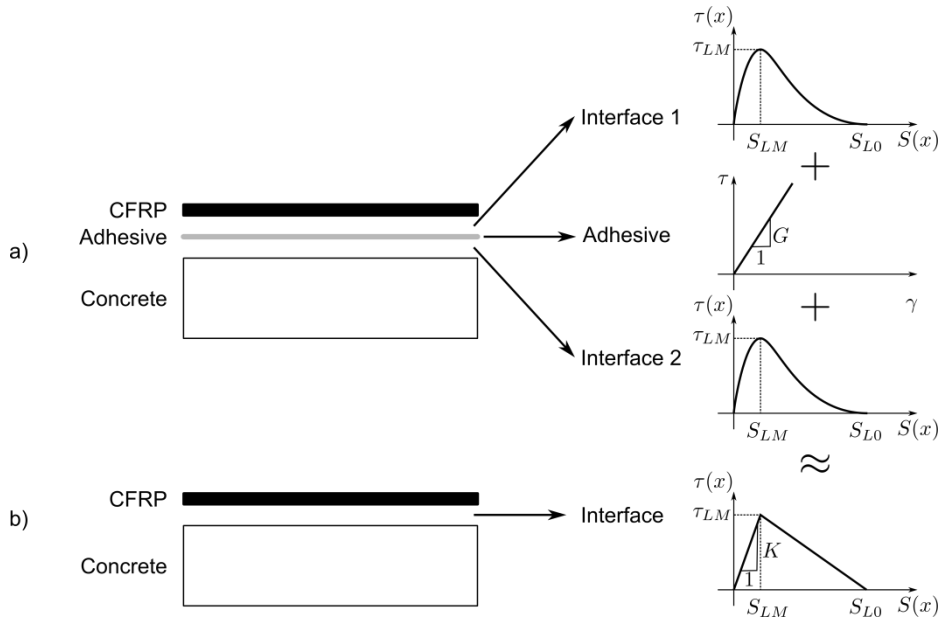

Figure 4.4: Global behaviour of CFRP-concrete bond, a) actual connection, and b) simulated connection described by a single bilinear relationship.

In the present study, the bond between the concrete and the CFRP strips was simulated by interface contact, in which a cohesive bi-linear constitutive relationship was implemented. In this formulation the damage initiation criterion is based on the maximum nominal stress for cohesive contact. The referred bi-linear relationship was defined by the following three parameters (*cf.*

Figure 4.4b): (i) stiffness, K; (ii) maximum shear strength, τ_{LM} (corresponding to the respective slip, s_{LM}); and (iii) ultimate slip, s_{L0}.

Table 4.2 presents the range of values admitted for each parameter in the numerical simulations of the EBR and NSM specimens (considering all temperatures tested). It can be seen that significantly wide ranges of variation were considered, which are in agreement with the high scatter of the bond-slip relationships experimentally obtained (*cf.* chapter 3).

Table 4.2: Range of values for interface parameters considered in the models.

Parameter	EBR models		NSM models	
	Minimum	**Maximum**	**Minimum**	**Maximum**
K [MPa/mm]	1	1500	2	1000
τ_{LM} [MPa]	0.5	25	1.5	20
s_{L0} [mm]	0.2	1.0	0.4	1.5

Figure 4.5a and Figure 4.5b plot the proposed bi-linear bond-slip relationships for the EBR and NSM specimens, respectively, for all the temperatures tested. As previously referred, these relationships were calibrated after carrying out an inverse analysis where the experimental and numerical results were compared (*cf.* section 4.3). Conceptually, the present analysis could be formulated in terms of a non-linear constrained optimization problem. The objective function to be minimized would be given by the weighted sum of the residuals of the three presented criteria (the presence of the weights is necessary in order to maintain the dimensional consistency of the terms). However, in practice, there are two main reasons that justify a different approach: (i) the difficulty in merging in the same objective function an extensive set of experimental data and a general purpose FE code, like ABAQUS[5]; (ii) the reduced number of parameters to be optimized (three). The alternative approach, followed here, was to perform this optimization from a practical point of view without precisely quantifying the objective function: the satisfaction of the criteria was assessed by inspection of the solution and comparison with the experimental data in terms of failure loads, load *vs.* slip responses, and strain distributions.

The parameters that define the proposed bond-slip laws (obtained using this procedure) are presented in Table 4.3. As expected, the laws for both strengthening techniques present consistent reductions of stiffness and maximum shear stress with increasing temperature, roughly similar to those observed in the experimental campaign (*cf.* chapter 3). However, it is important to point out that the experimental slip values were computed from the axial strain readings in the CFRP along the bonded length, hence not taking into account the distortion of the adhesive layer. For elevated temperatures, due to the

[5] It would be necessary to automatically generate the input files with the updated parameter values and to extract the results of the analysis in terms of the prescribed criteria. This output would then serve to evaluate the discrete (failure loads) and continuous (load *vs.* slip response and strain distributions along the bonded length) residuals of the objective function. Moreover, the value of the combination weights would have to be set.

adhesive softening, the distortion of the adhesive layer could be significantly high and, therefore, contribute for higher slip values (and, as result, lower stiffness) than those showed in chapter 3. Consequently, the values of parameters K and s_{L0} presented in Table 4.3 do not necessarily correlate directly with the curves showed in Figure 3.12 (page 60) and Figure 3.25 (page 75).

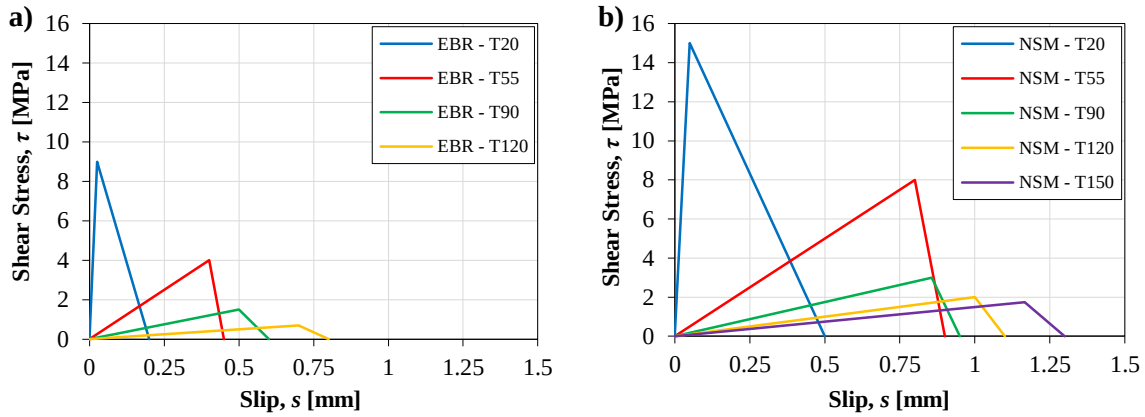

Figure 4.5: Proposed bond-slip relationships for a) EBR and b) NSM specimens for all temperatures tested.

Table 4.3: Proposed interface parameters for the cohesive model for all temperatures tested.

Parameter	EBR models				NSM models				
	20 °C	**55 °C**	**90 °C**	**120 °C**	**20 °C**	**55 °C**	**90 °C**	**120 °C**	**150 °C**
K [MPa/mm]	350	10	3	1	300	10	3.5	2	1.5
τ_{LM} [MPa]	9	4	1.5	0.7	15	8	3	2	1.75
s_{L0} [mm]	0.2	0.45	0.6	0.8	0.5	0.9	0.95	1.1	1.3

Figure 4.6 presents the normalized reduction with temperature of the stiffness and maximum shear stress of the proposed bond-slip laws for both strengthening techniques, together with the storage modulus of the epoxy adhesive (obtained from DMA, *cf.* Figure 3.1a – page 49). It can be seen that the stiffness reductions experienced by the CFRP-concrete interfaces for both EBR and NSM techniques (i) are very similar to each other and (ii) are comparable to the reduction exhibited by the adhesive storage modulus (although at 55 °C the latter property exhibited a slightly lower decrease). This result shows that, regardless of the strengthening technique, the CFRP-concrete interface stiffness is highly dependent of the adhesive behaviour with temperature. Concerning the maximum shear stresses, the reduction with temperature of the NSM bond-slip law is lower when compared to that of the EBR technique. This result was expected since in the former technique the CFRP-concrete interface (contact) area is higher and the confinement offered by the surrounding concrete provides a better bonding performance. It is also important to point out that for the higher temperatures tested (90 °C to 150 °C), well above the T_g of the epoxy adhesive, the residual maximum shear stresses are well above the corresponding values of the storage modulus. Since for those temperatures the glass transition process of the adhesive was completed, such relatively high

residual maximum shear stresses are attributed to friction forces at the concrete-adhesive and CFRP-adhesive interfaces.

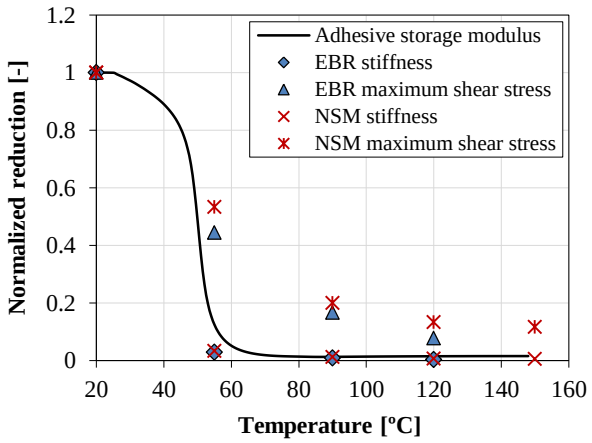

Figure 4.6: Normalized reduction with temperature of the adhesive storage modulus, stiffness and maximum shear stress of the proposed bond-slip relationships.

4.3 NUMERICAL RESULTS AND DISCUSSION

Sections 4.3.1 to 4.3.3 present the comparison between the experimental and numerical results, in terms of failure loads, load *vs*. slip curves and strain distributions, which were the parameters used to validate the proposed bond-slip relationships. It is worth mentioning that in the present study, the effects of possible thermal stresses induced during the heating phase were disregarded in the experimental data, hence were not considered in the calibration of the bond-slip laws. Next, section 4.3.4 presents the analysis of the inelastic strains. Finally, in section 4.3.5 one evaluates the influence of modelling concrete as a linear elastic material.

4.3.1 Failure load of the double-lap shear tests

Table 4.4 compares the experimental ($F_{u,exp}$) and numerical ($F_{u,num}$) failure loads and corresponding relative differences (Δ_{exp}) for the EBR and NSM specimens, respectively. It can be seen that the relative differences between predicted and experimental results are very low (average relative difference of 3%), confirming the accuracy of the proposed bond-slip relationships. The numerical results also confirm the higher effectiveness of the NSM strengthening technique, for which the predicted strength values are consistently higher when compared to the EBR counterparts (as observed in the tests).

4.3.2 Total load *vs.* slip curves

Figure 4.7a and Figure 4.7b depict the experimental (dotted lines) and numerical (continuous lines) load *vs*. slip curves (slip at the loaded end of the CFRP strip) of the EBR and NSM specimens, respectively, for the considered temperatures. At ambient temperature, for both strengthening

Table 4.4: Experimental vs. numerical failure loads.

Temperature	EBR models			NSM models		
	$F_{u,exp}$ [kN]	$F_{u,num}$ [kN]	Δ_{exp} [%]	$F_{u,exp}$ [kN]	$F_{u,num}$ [kN]	Δ_{exp} [%]
20 °C	25.9	25.8	-0.4	45.4	44.6	-1.8
55 °C	22.1	23.1	4.5	42.6	41.6	-2.3
90 °C	11.6	12.2	5.2	22.9	24.1	5.2
120 °C	4.8	5.2	8.3	19.7	19.6	-0.5
150 °C	-	-	-	17.5	17.7	1.1

techniques, the numerical models were able to accurately reproduce the non-linear behaviour of the curves, including the high stiffness reduction observed in the brink of collapse. The latter response was also observed at elevated temperatures, although in this case the slip at the top of the CFRP strip presents a variation closer to linear with the applied load, which is in agreement with the behaviour exhibited by the corresponding experimental curves plotted in Figure 4.7. With increasing temperature, the numerical curves presented a continuous stiffness reduction; however, for the EBR specimens at 55 °C and 90 °C and for the NSM specimens at 55 °C, this parameter is considerably higher when compared to the experimental data. This difference, especially at 55 °C, might be explained by the fact that the development of the glass transition process of the adhesive (*i.e.* the reduction of its mechanical proprieties) is concentrated mainly around this temperature. Despite these non-negligible differences (obtained for 3 cases), the numerical models were able to correctly simulate the structural response in terms of failure load (*cf.* section 4.3.1) and strain distributions (*cf.* section 4.3.3).

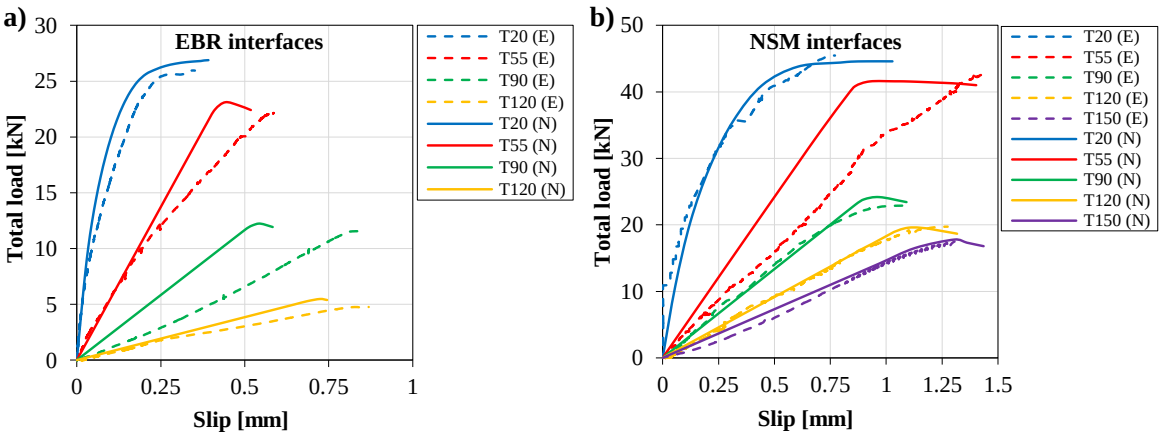

Figure 4.7: Numerical (N) and experimental (E) total load vs. slip curves at the CFRP load end: a) EBR and b) NSM specimens.

4.3.3 Strain distributions in the CFRP strips

Figure 4.8 and Figure 4.9 present the axial strain distributions along the CFRP bonded length of specimens EBR and NSM, respectively, for different fractions of the failure load and for

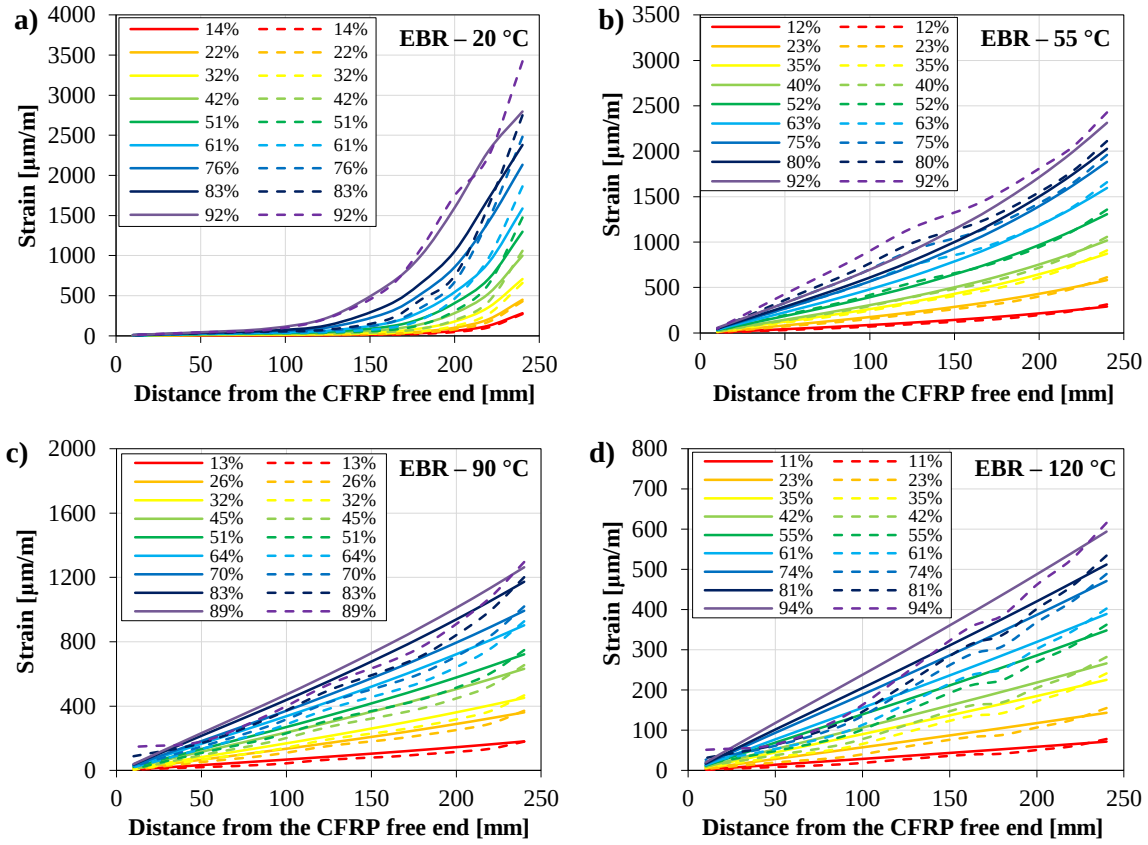

Figure 4.8: Experimental (dashed) and numerical (continuous) axial strains distributions in the EBR-CFRP strips for different fractions of the failure load and different temperatures: a) 20 °C; b) 55 °C; c) 90 °C; d) 120 °C.

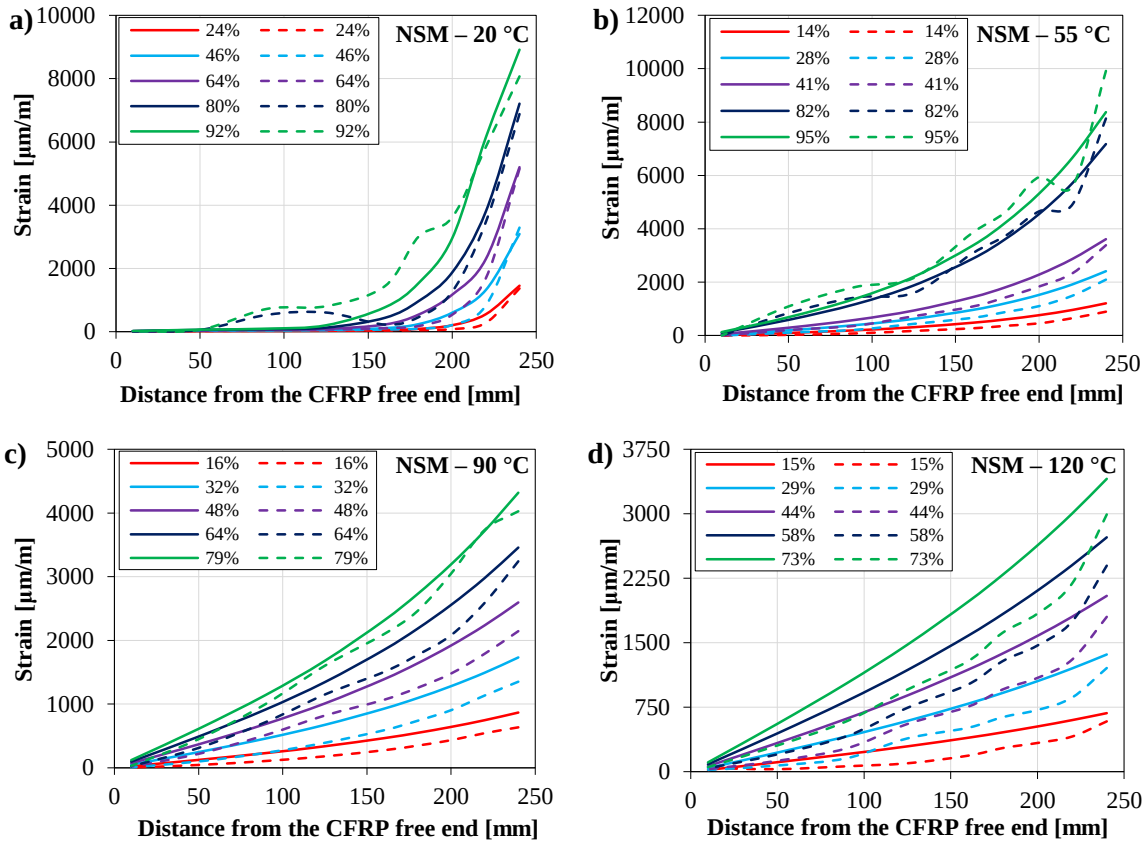

Figure 4.9: Experimental (dashed) and numerical (continuous) axial strains distributions in the NSM-CFRP strips for different fractions of the failure load and different temperatures: a) 20 °C; b) 55 °C; c) 90 °C; d) 120 °C.

temperatures up to 120 °C (again, the experimental results are plotted as dotted lines and the corresponding numerical curves as continuous lines). The results obtained at 150 °C (NSM specimens) are not displayed in these figures, due to the inconsistency in the strain readings of the tests performed at this temperature.

Figure 4.8a and Figure 4.9a show that at ambient temperature there is a good agreement between experimental and numerical results - the numerical models were able to simulate the non-linear response of the corresponding curves. At elevated temperatures, although the experimental curves exhibit a behaviour closer to linear (when compared to ambient temperature results) due to the adhesive softening, the experimental strain distributions are slightly more irregular than the corresponding numerical curves. This difference might be explained by the non-homogeneity of the surfaces in the interface layer (mainly the concrete surface, whose effect is more relevant at elevated temperature), which was not explicitly simulated in the models. Nevertheless, the numerical strain distributions are in close agreement with the measured distributions throughout the loading process, which further demonstrates the validity of the bond-slip laws proposed in section 4.2.4.

4.3.4 Inelastic strains and shear stress distributions

Figure 4.10a and Figure 4.10b present the inelastic maximum principal strains in the concrete of the EBR specimens due to the numerical failure load at 20 °C and 120 °C, respectively. The first figure shows high inelastic strains in a region located a few millimetres inside the concrete and along an area which is roughly the CFRP bonded length, *i.e.* there is a significant damage in the concrete along this highlighted volume. On the other hand, there are no visible inelastic strains in Figure 4.10b, indicating no damage in the concrete layer at 120 °C. These results are in close agreement with the failure modes observed in the experimental campaign, where a cohesive failure (within the concrete substrate) occurred at ambient temperature, in opposition to an adhesive failure at the concrete-adhesive interface (without concrete damage) at elevated temperatures. Regarding the NSM models, similar results and conclusion were obtained, with negligible inelastic strains in concrete at temperatures above 20 °C.

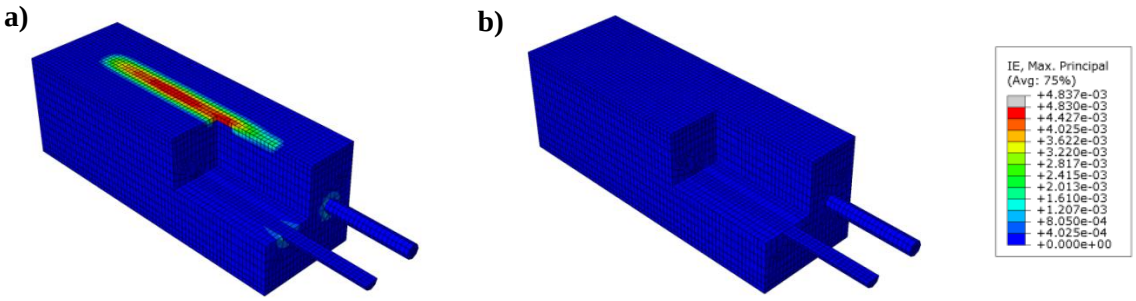

Figure 4.10: Inelastic maximum principal strains in the concrete at failure (EBR specimens): a) 20 °C; b) 120 °C.

Figure 4.11 and Figure 4.12 show for the EBR and NSM specimens, respectively, the evolution of the maximum principal inelastic strain in the concrete at ambient temperature and for different fractions of the failure load. In both figures, at first higher inelastic strains can be observed in the

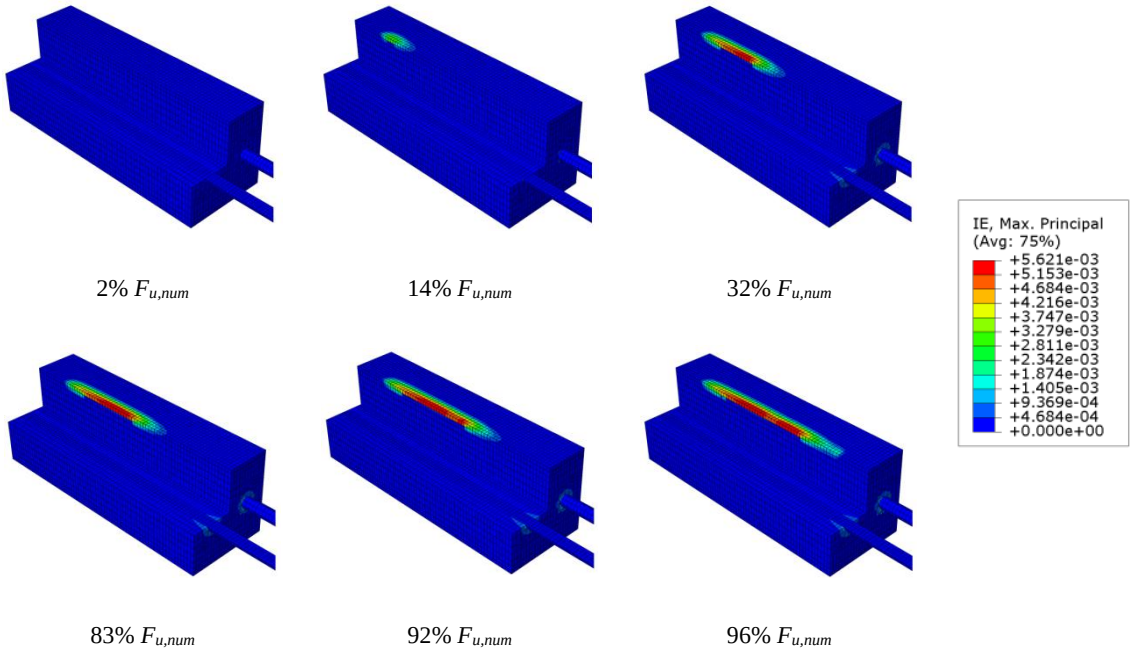

Figure 4.11: Inelastic maximum principal strain in the concrete for the EBR models at 20 ℃.

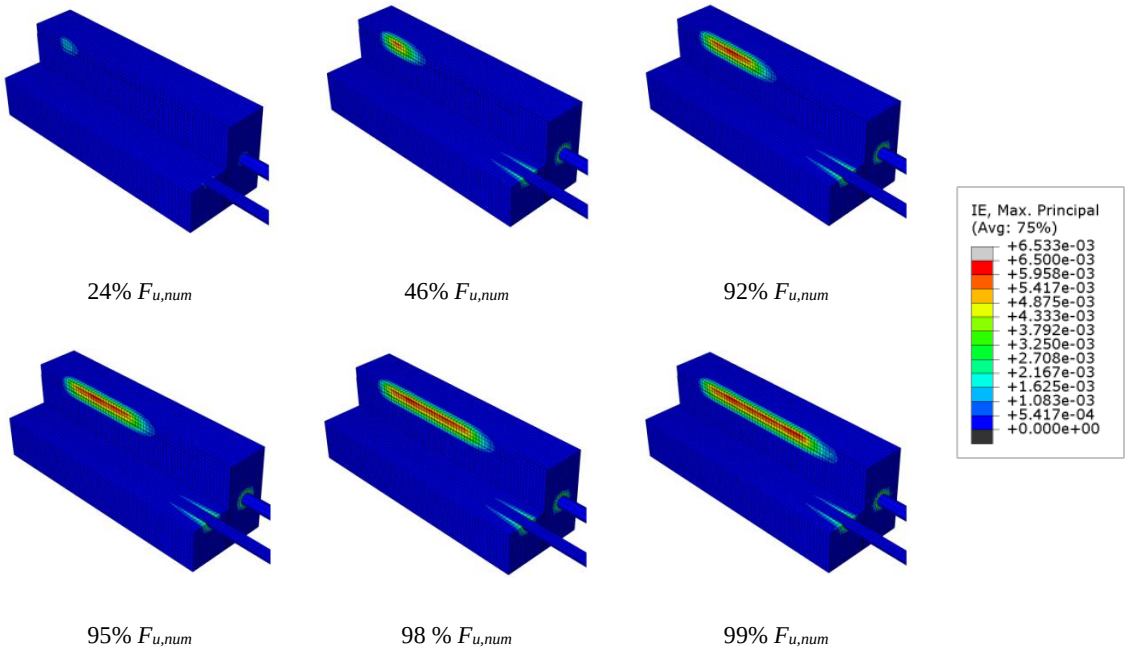

Figure 4.12: Inelastic maximum principal strain in the concrete for the NSM models at 20 ℃.

concrete located close to the loaded end of the CFRP strip, where stress concentrations develop; then, with increasing load, the damage in the concrete spreads from this area onwards and propagates along the bonded length. This behaviour is in agreement with the failure modes at 20 °C observed in the

experiments (as well as in several other similar studies, *e.g.* [119, 120]), which had been triggered close to the top (loaded) extremity of the CFRP strip. Furthermore, Figure 4.12 shows that for the NSM specimens the volume of concrete in which higher inelastic strains are observed is relatively deep and, as expected, surrounds the CFRP strip inserted into the slit, whereas the damage in the concrete observed in Figure 4.11 is much more superficial, explaining the failure modes recorded in the tests: debonding of the CFRP laminates in the EBR specimens, with the failure surface located a few millimetres inside the concrete substrate, and shear failure of the concrete block in the NSM specimens. This conclusion also provides additional validation to the numerical models and the proposed bond-slip relationships.

4.3.5 Effects of modelling concrete as a linear elastic material

As referred in the previous section, when simulating the specimens tested at elevated temperature the damage in the concrete is negligible. This result indicates that a simpler constitutive model might be used to simulate the concrete under those conditions, thus allowing reducing the computational costs.

Therefore, new models were developed, in which the concrete was modelled as a linear elastic material. In Figure 4.13, the total force *vs.* slip curves (slip at the loaded end of the CFRP strip) obtained with a linear (L) model (dotted lines) and a non-linear (NL) damage model for the concrete (continuous lines) for both strengthening techniques are compared with those already presented in Figure 4.7. As expected, at ambient temperature, when the concrete is modelled as a linear elastic material, the total force *vs.* slip curves present slightly higher stiffness (and a minor strength reduction), whereas at elevated temperatures the results obtained with both models are virtually equivalent. Therefore, these results show that when simulating the bond between concrete and CFRP strips at elevated temperatures, a linear elastic model can be implemented for the concrete with negligible precision losses, allowing for significant reduction of computational costs.

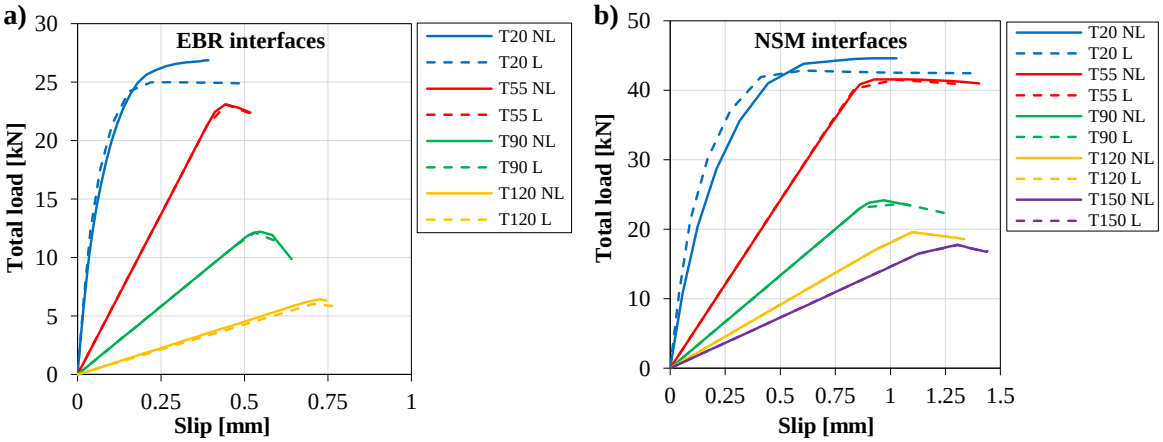

Figure 4.13: Total load vs. slip curves for the non-linear (NL) and linear (L) models: a) EBR models; b) NSM models.

4.4 CONCLUSIONS

This chapter presented numerical investigations about the bond between concrete and CFRP strips installed according to the EBR and NSM techniques when subjected to moderately elevated temperatures. The experimental double-lap shear tests described in chapter 3 (series S1 and EP) were simulated using a commercial software and the parameters of bi-linear bond-slip laws for temperatures up to 150 °C were proposed. These laws are representative of the overall behaviour of the CFRP-concrete joint and were derived for each predefined temperature based on an inverse analysis, in which the agreement between experimental and numerical results was evaluated in terms of the following criteria: (i) failure loads, (ii) load *vs.* slip response, and (iii) strain distributions. The results obtained allow drawing the following main conclusions:

- The proposed bond-slip laws for both strengthening techniques present consistent reductions of stiffness and maximum shear stress with increasing temperature, which are roughly similar to those determined in the experimental campaign.
- The stiffness reductions with increasing temperature of the proposed bond-slip laws are very similar for both strengthening techniques. Furthermore, they present a comparable variation with temperature to that experienced by the adhesive storage modulus (obtained from DMA experiments). This result shows that, regardless of the strengthening technique, at elevated temperature the CFRP-concrete interface stiffness is highly dependent of the adhesive behaviour.
- The maximum shear stress reductions with temperature of the proposed bond-slip laws for the NSM specimens is lower when compared to that observed with the EBR, which is in close agreement with the experimental results. Moreover, for both strengthening techniques the maximum shear stress reductions with temperature are well above the corresponding values of the adhesive storage modulus. This result indicates that chemical adhesion and friction forces at the concrete-adhesive and CFRP-adhesive interfaces at elevated temperature are relevant for this interface parameter.
- The proposed bond-slip laws provide a very good agreement between numerical results and experimental data for the mechanical criteria considered. Furthermore, it was also possible to accurately simulate the failure modes observed in the experimental campaign.
- In order to reduce the computational costs, when simulating the bond between concrete and CFRP strips at elevated temperatures, for the geometries and materials used in the present study, a linear elastic model can be adopted for concrete with negligible precision losses.

The proposed bond-slip laws, which were calibrated for representative strengthening techniques and materials, can be implemented in the numerical simulation of the thermo-mechanical response of CFRP-strengthened RC elements subjected to fire. In chapter 8 (page 173) this numerical

approach will be implemented in order to study the effects of different fire protection strategies/schemes in extending the fire endurance of CFRP strengthening systems applied to reinforced concrete beams.

Part III:
Fire behaviour of RC beams/slabs flexurally strengthened with CFRP strips

CHAPTER 5

DEVELOPMENT OF FIRE PROTECTION SYSTEMS FOR RC MEMBERS STRENGTHENED WITH CFRP STRIPS

5.1 INTRODUCTION

This chapter presents numerical investigations about the thermal behaviour of RC members flexurally strengthened with CFRP strips when subjected to fire. The main objective is to contribute for the development of a design methodology enabling the rational selection of fire protection systems. The first part of this chapter describes results of previous fire resistance tests on loaded RC beams strengthened with CFRP strips installed according to the EBR technique (which were also briefly described in section 2.4.3.1, page 29 - full details are presented in [5, 68]). The numerical study described in the second part of this chapter included the development of (i) two-dimensional (2D) finite element (FE) thermal models of the tested beams, whose results were compared with measured temperatures, and (ii) three-dimensional (3D) FE thermal models of CFRP-strengthened RC slabs. The latter numerical models were used to design different fire protection systems with thicker insulation layers applied in the anchorage zones of the strengthening system. In particular, the numerical study investigated the effect of the following parameters on the temperature distributions along the CFRP strengthening system: (i) geometrical configuration of the fire protection system, particularly in the anchorage zone; (ii) strengthening technique, namely EBR or NSM; and (iii) T_g of the adhesive.

5.2 PREVIOUS EXPERIMENTAL INVESTIGATIONS

5.2.1 Test programme and description of the specimens

Within the Master dissertation of the author [5], six fire resistance tests were conducted in an intermediate scale oven to investigate the fire behaviour of loaded CFRP strengthened RC beams, either unprotected (specimen CFRP) or protected with different passive fire protection systems. The fire protection systems were applied on the bottom surface of the beams and consisted of 25 mm or 40 mm thick calcium silicate (CS) boards (specimens CS25 and CS40, respectively) or vermiculite and perlite (VP) cement based mortar layers (specimens VP25 and VP40, respectively). As a reference, a non-strengthened RC beam (specimen RC) was also tested. The beams tested

were 2.10 m long, 0.10 m wide and 0.12 m deep, and the internal steel reinforcement, with a cover of 1 cm, consisted of four ϕ6 mm bars used as longitudinal reinforcement and ϕ5 mm distanced of 0.06 m used as transverse reinforcement. The CFRP strip (with a cross section of 50 × 1.2 mm) was installed in the bottom surface of the beams according to the EBR technique. The strip was 1.35 m long - such distance corresponded to the external width of the oven used in the fire resistance tests, guaranteeing that the anchorage zones were thermally insulated in a length of 0.20 m (thickness of the oven walls), as illustrated in Figure 5.1. In real applications, such insulation can be provided by applying very thick insulation layers in the anchorage zones, according to a procedure that is addressed in the numerical investigations (*cf.* section 5.3). In all tests, only the bottom surface of the beams was directly exposed to heat in a length of 0.95 m. The lateral faces were thermally insulated with mineral wool and CS panels, while the top face was exposed to ambient temperature. These test conditions actually simulate the behaviour of one-way slabs. The thermal loading followed the ISO 834 [6] time-temperature curve.

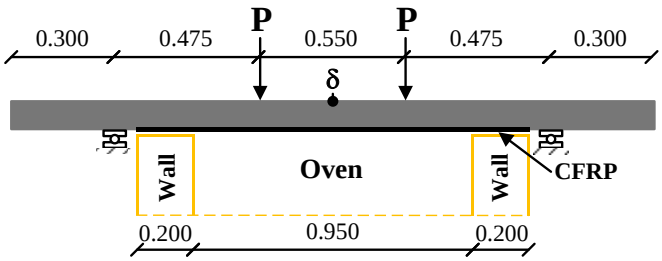

Figure 5.1: Test setup of previous fire resistance tests [5, 68] (not to scale, dimensions in m).

The aforementioned strengthening system provided a flexural strength increase of approximately 94%, which is higher than the limits established in most design recommendations (that normally indicate an upper limit ranging from 40% to 60% [56]). However, in several CFRP strengthening applications, namely those that are prior to the most recent design guidelines (*e.g.* [56, 99, 100]), the above mentioned limits were not respected.

In specimens CS25 and CS40, the CS boards (1.40 m long × 0.10 m wide, 25 mm or 40 mm thick) were mechanically fixed to the bottom soffit of the beams using four U-shaped thin steel plates. The VP mortar, with a water content of 0.67 l/kg was applied with a trowel (specimens VP25 and VP40) incorporating a 0.10 m wide steel wire netting (fixed to the bottom surface of the specimens) to improve its tensile strength and adherence to the concrete support.

All beams, with a simply supported span of 1.50 m, were tested in a four point bending configuration. A total gravity load of 10.2 kN (non-strengthened specimen RC, about 58% of its ambient temperature strength) or 16.3 kN (all 5 strengthened specimens, about 47% of their ambient temperature strength) was applied previously to the thermal loading. The vertical deflection and temperature distributions of all tested specimens were measured at midspan using a displacement transducer from *TML* (with 0.01 mm precision) and thermocouples type K,

respectively. In specimen CS40 two additional thermocouples were installed at one of the thermally insulated anchorage zones of the CFRP strip.

5.2.2 Summary of results

Figure 5.2 presents the variation of midspan deflection as a function of time for all specimens tested, in which the origin of the time scale (t = 0 min) corresponds to the beginning of the thermal loading. It can be concluded that the midspan deflection of specimen CFRP increased at a lower rate than that of specimen RC until the bond between the CFRP strip and concrete was lost. At that moment, the midspan deflection increased suddenly (due to the instantaneous loss of stiffness), and the mechanical properties of specimen CFRP became roughly similar to those of specimen RC. As the applied load in the strengthened beam was higher, its failure (due to tensile rupture of the steel reinforcement) occurred after a shorter period of exposure. As expected, the deflection increase rate in the protected specimens was lower than that observed in specimen CFRP (both before and after the failure of the strengthening system). It is also worth mentioning that in all strengthened beams, failure of the CFRP system was due to the loss of bond in the anchorage zone, *i.e.* tensile failure of the carbon fibres never occurred.

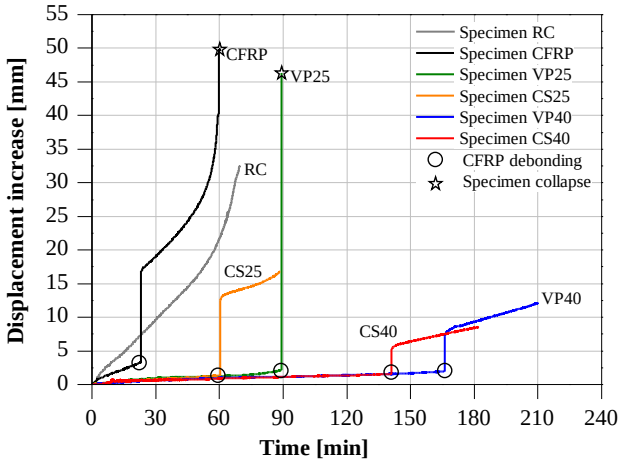

Figure 5.2: Increase of midspan deflection vs. *time, beams tested by Firmo et al. [68] (VP and CS identify the insulation material, vermiculite/perlite mortar and calcium silicate respectively, and the numbers indicate the corresponding insulation thickness in millimetres)*

As expected, the temperatures measured in the protected beams were considerably lower and so was their stiffness loss, when compared to the unprotected counterpart. As an example, the evolution of the temperatures measured at different depths of specimens CFRP and CS25 are presented in Figure 5.3, in which experimental results (*cf.* Figure 5.6, page 106 for thermocouples' position) are plotted together with numerical results (described in section 5.3.3).

The results obtained in the tests of the beams with passive protection show that when the strengthening system failed the average temperature at the CFRP-concrete interface at midspan section varied between 119 ºC and 187 ºC, while in specimen CFRP such temperature was 414 ºC;

these temperatures are well above the T_g of the epoxy adhesive (55 ºC). In addition, results obtained in the test of specimen CS40 indicate that when the bond between the CFRP strip and the concrete was lost, the average temperature along the insulated anchorage length (20 cm) of the CFRP strip was 52 ºC, which is roughly the T_g of the resin. These results indicate that the bond between the strengthening system and the beams was not significantly affected along the anchorage zones for a relatively long period of exposure to fire, and explain why the temperatures at midspan section were much higher than the T_g of the adhesive and the CFRP strengthening system was still effective.

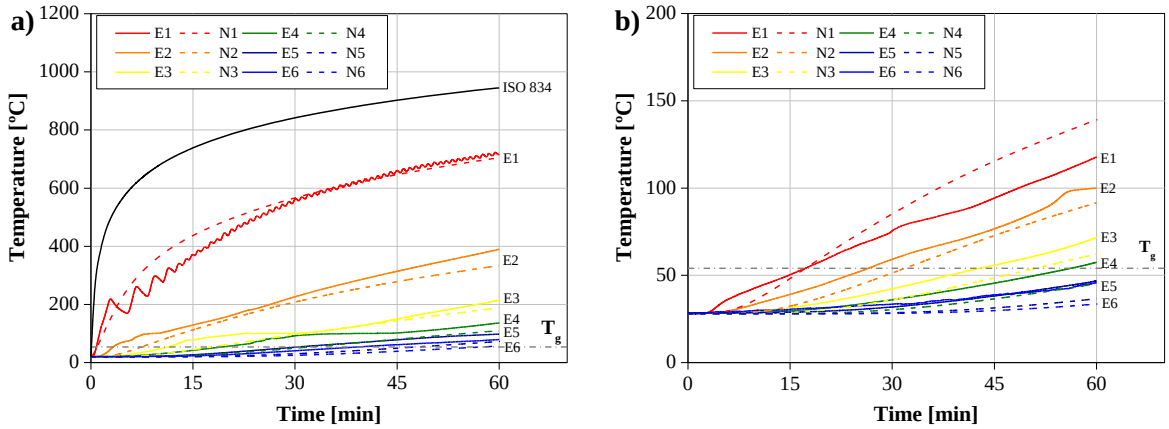

Figure 5.3: – Experimental (E) and numerical (N) temperature distributions along the cross sections of beams (a) CFRP and (b) CS25.

Post-fire assessments (Figure 5.4) showed that the heated length of the CFRP strip transformed into a "cable" fixed in the anchorage zones, where the CFRP-concrete bond remained relatively undamaged. As temperatures increased, the overall stiffness of the beams deteriorated and, consequently, the deflection increased together with the tensile force at the "cable". The strengthening system failed when one of the anchorage zones lost its bond strength, which, as already mentioned, could be associated to the average temperature in such zones attaining the adhesive T_g. The time for the CFRP strengthening system to fail was 23 min for specimen CFRP, 89 min for specimen VP25, 60 min for specimen CS25, 167 min for specimen VP40 and 137 min for specimen CS40.

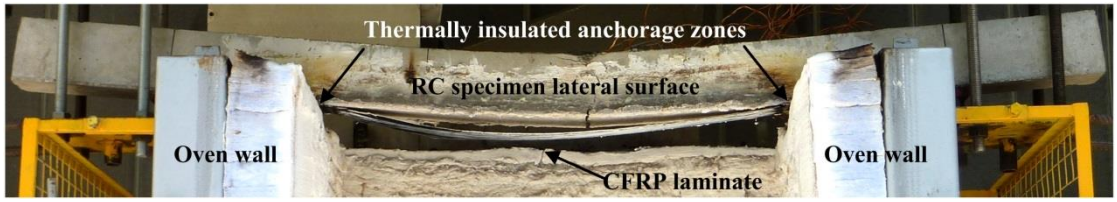

Figure 5.4: CFRP strip detached from the RC beam only at the central zone – "cable" behaviour (adapted from Firmo et al. [68]).

5.3 DESIGN OF FIRE PROTECTION SYSTEMS FOR CFRP-STRENGTHENED RC MEMBERS

5.3.1 General methodology and objectives

The methodology suggested herein for the design of fire protection systems to be used together with CFRP-strengthening systems entails the following two main requirements: (i) the temperature of the CFRP strengthening element in current zone must remain below a certain temperature, which may be defined based on the stress level installed on the CFRP strip together with its residual strength as a function of temperature; and (ii) the temperature of the CFRP-concrete interface along the anchorage zone must be kept below a "critical" temperature, hypothesized as being the T_g of the adhesive used in the strengthening system.

If passive fire protection systems are to be used, such as layers of insulation materials, the implementation of the above mentioned protection strategy will therefore provide a certain thickness in the current zone and an increased thickness along the anchorage zone.

In order to evaluate the feasibility of implementing the above mentioned strategy, in a first step, 2D FE thermal models of tested specimens CFRP and CS25 were developed (*cf.* section 5.3.3). The thermal analysis performed in those models was validated through the comparison of numerical and experimental temperatures.

In a second stage, the 2D geometry was generalised to 3D (*cf.* section 5.3.4), and the thermal response of entire RC slab sectors strengthened with CFRP strips using either the EBR or the NSM techniques was simulated. Results of the 3D numerical models were used to demonstrate the fire protection design based on the above mentioned strategy, namely the definition of the geometry of the thermal insulation in both current and anchorage zones. As already mentioned, the models were used to evaluate the influence of the geometrical configuration of the fire protection system, in both current and anchorage zones, of slabs strengthened according to either EBR or NSM techniques. In addition, the effect of T_g of the adhesive was also assessed.

The 3D models of both EBR- and NSM-strengthened slabs were used to define the minimum thickness and width of the fire protection system in the current zone that fulfilled the above mentioned temperature criterion. In the present study, it was considered that the temperature at the CFRP strip should remain below 500 ºC during 90 min of fire exposure, the reference period assumed for this study. In this regard, in what concerns the resistance of the strengthening material, according to Wang *et al.* [27], CFRP strips retain about 44% of their ambient tensile strength at 500ºC. Feih and Mouritz [121] reported 45% of tensile strength retention (compared to ambient temperature) in CFRP strips exposed to 600 ºC. Regarding the load installed in the CFRP strip, it is worth mentioning that for ultimate limit states design, most recommendations limit the CFRP stress

to 50% of its tensile strength, and the tensile stress installed in the CFRP in a fire situation is significantly lower than that value (the applied load in a fire situation is similar to that applied in a serviceability limit state). In the test of specimen CFRP, in which the strengthening ratio was relatively high, when the CFRP-concrete bond was lost the temperature of the CFRP strip was 541 ºC (calculated using the model described in section 5.3.3) and it did not present tensile failure, attesting the first design requirement.

In order to allow the behaviour of the strip as a "cable" (as described in section 5.2.2) different configurations of extra thermal insulation were defined along the anchorages zones to guarantee that the temperature at the epoxy bonded interface would remain below T_g for different periods of exposure. In this study, the anchorage length (l_a) was calculated according to ACI 440.2R-08 [56].

5.3.2 General description of the FE models

The 2D and 3D thermal models were developed using *ADINA-T* software [122]. The models comprise two procedures: (i) the finite element method to compute the temperature spatial distribution, and (ii) the finite difference method to compute the temporal temperature distribution (using a fully implicit scheme). No mechanical responses were modelled.

In all thermal models the convection and radiation modes of heat transfer were considered in both bottom and upper surfaces. The non-linearity introduced by the latter was explicitly considered. Based on studies developed earlier (*e.g.*, [5, 68, 123]), the convection coefficient (h_c) was considered to vary linearly with temperature, from 5 W/m^2 ºC at 20 ºC to 50 W/m^2 ºC at 1000 ºC. The variation with temperature of the thermal conductivity, the specific heat capacity and the density of the materials was also taken into account – the modelled properties are plotted in Figure 5.5. Only the emissivity was considered to be constant with temperature with values of 0.7 for concrete and CS [67] and 0.8 for the CFRP strip [124].

With the exception of the density of the CFRP and the CS boards, for which experimental results were used (reported in detail in [5] and [24], respectively), the variation of the thermo-physical properties of the materials was defined using data from the literature: concrete was modelled according to Eurocode 2 [67]; the CFRP strips were modelled based on results reported by Griffis *et al*. [95] and Miller and Weaver [124]; the adhesive properties were assumed to follow the same relation with temperature defined for the CFRP material. Regarding the CS boards, the thermal conductivity and the specific heat capacity at ambient temperature, as well as their variation with temperature, were considered as reported by the manufacturer [125]; the emissivity was considered to be constant with temperature, according to Mimoso [126].

The steel reinforcing bars were not modelled, due to their reduced influence in the evolution of temperatures at the CFRP-concrete interface, which was the region where the highest modelling accuracy was needed.

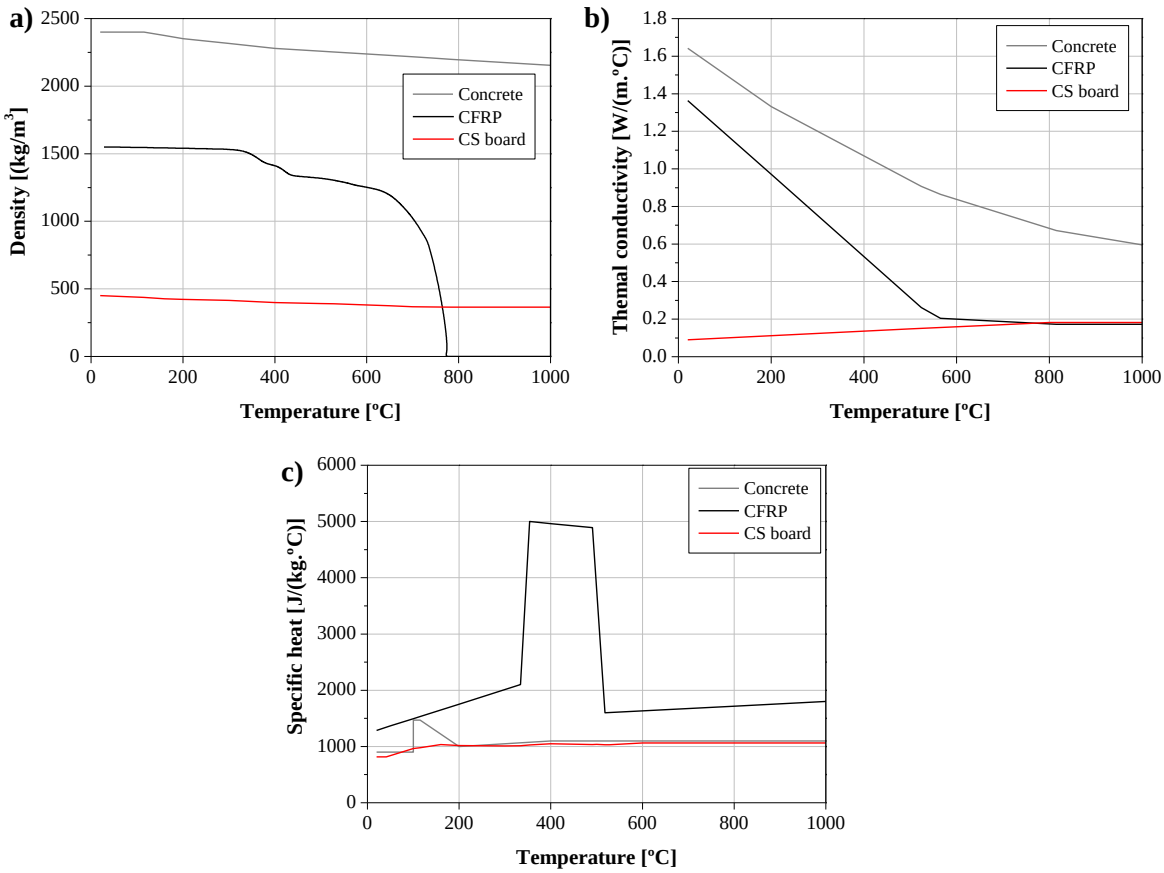

Figure 5.5: Thermo-physical properties of modelled materials as a function of temperature: a) density; b) thermal conductivity; c) specific heat.

5.3.3 Two-dimensional models (validation)

The 2D thermal models were developed to simulate specimens CFRP and CS25, strengthened with CFRP strips according to the EBR technique. The numerical models developed have the same geometry as the specimens tested, with the exception of the above mentioned simplifications.

The heat transfer in the fire exposed face is due to convection and radiation, following the temperature progression of the ISO 834 fire curve. The same modes of heat transfer were considered between the top face of the specimens and the laboratory environment, for which constant ambient temperatures of 20 ºC and 28 ºC were set for specimens CFRP and CS25, respectively (based on test measurements). The lateral faces were considered adiabatic, *i.e.* the heat transfer was null. The initial temperature of all models was considered to be 20 ºC in specimen CFRP and 28 ºC in specimen CS25, also based on test measurements.

A mesh of quadrangular elements with 9 nodes and maximum length of 1 mm was defined. Figure 5.6a) and b) shows the geometry of the cross-section and the position of the thermocouples in

specimens CFRP and CS, respectively, while Figure 5.6c) and d) shows the meshes and boundary conditions adopted in the models of those beams. The transient temperature distribution was computed using a time step of 10 seconds in each model.

The accuracy of the numerical models was assessed by comparing the results obtained from the 2D models with the corresponding experimental data. Figure 5.3 shows the experimental (E) and numerical (N) temperatures at different depths of midspan section of specimens CFRP and CS25 as a function of time. It can be seen that in both specimens the numerical models were able to simulate with fairly good accuracy the thermal response as a function of time. The relatively small deviations between measured and calculated temperatures are likely to stem from differences between the actual thermophysical properties of the materials and those considered in the models.

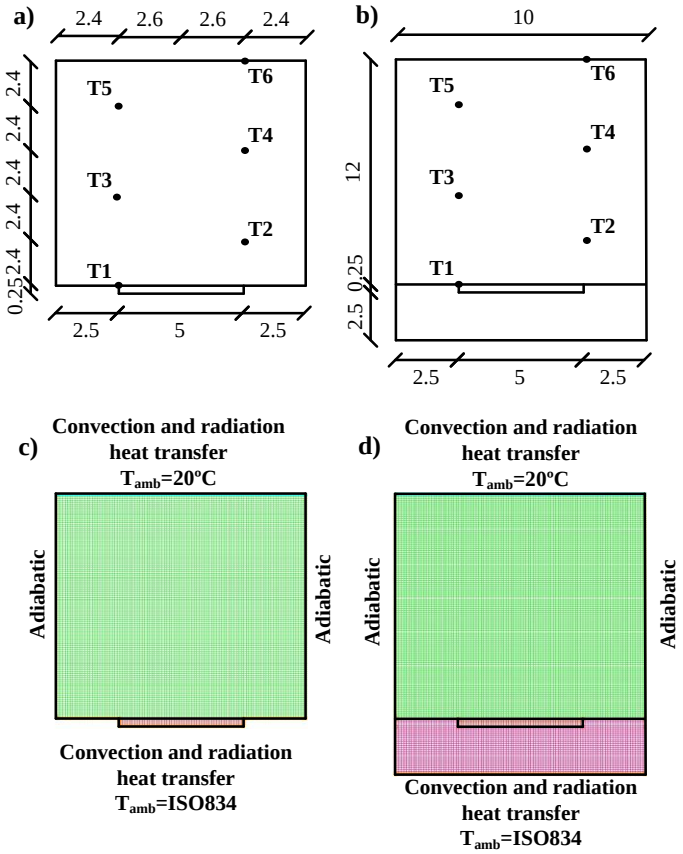

Figure 5.6: Geometry (in cm) and thermocouples' position in specimens a) CFRP and b) CS25. FE meshes and boundary conditions in the models of specimens c) CFRP and d) CS25.

5.3.4 Three-dimensional models

5.3.4.1 EBR-CFRP strengthened RC slab

The RC slab sector analysed is 5.20 m long, 0.50 m wide and 0.12 m deep. The CFRP strip has a cross section of 50 × 1.2 mm and is 4 m long. Due to the double symmetry of the model, only a quarter of the slab was analysed (Figure 5.7).

In the current zone, based on preliminary studies described in section 5.4.1, the CS insulation thickness was set as 0.02 m in order to guarantee that the temperature at the CFRP strip would be lower than 500 ºC after 90 minutes. Figure 5.8a shows the geometry of the cross-section of the slab modelled.

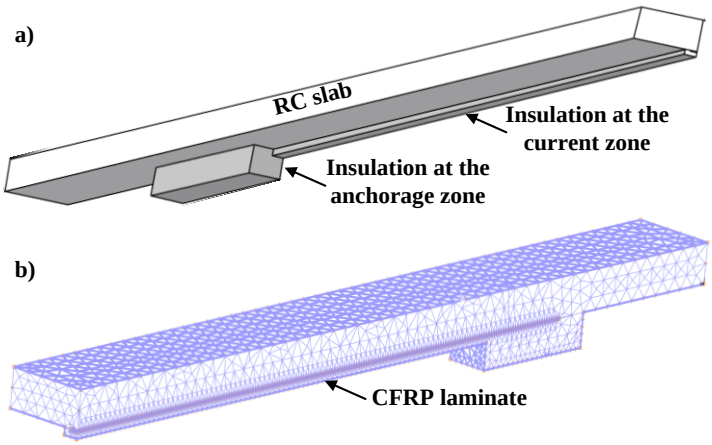

Figure 5.7: EBR-strengthened slab modelled: a) geometry (a quarter of the real slab) and b) FE mesh.

In the anchorage zone, the geometry of the CS insulation was considered to be variable in the three space dimensions according with parameters *L*, *T* and *W* (Figure 5.8b). Parameter *L* corresponds to the longitudinal dimension of the insulation material adjacent to l_a (anchorage length, *x*-direction), parameter *T* corresponds to the total thickness of the protection (*y*-direction), and parameter *W* corresponds to the distance between the lateral edge of the CFRP strip and that of the insulation (*z*-direction).

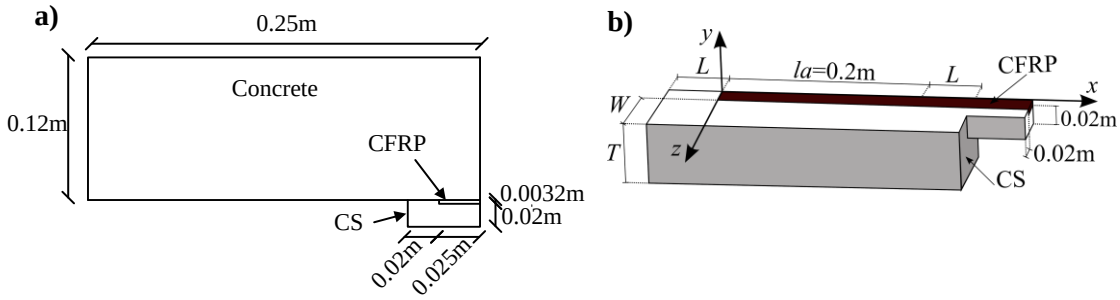

Figure 5.8: Geometry of the EBR flexurally strengthened slabs and CS protection: a) cross-section at midspan (in m); b) perspective of anchorage zone.

The width of the protection (*W*) was considered to be equal to its thickness (*T*) in order to maintain the relation that these parameters have in the current zone, which was defined based on a preliminary study (also described in section 5.4.1).

In a first stage, the influence of varying the ratio between the extended length of the insulation (*L*) and the corresponding thickness (*T*) in the anchorage zone was evaluated: three models were developed in which *L* varied from 2 cm to 6 cm, while maintaining *T* = 4 cm (models

EBR_L2T4W4, EBR_L4T4W4 and EBR_L6T4W4, the numbers refer respectively to the protection length, thickness and width in centimetres). In a second stage the influence of the total thickness of the protection in the anchorage zone was assessed: five models were developed in which *T* was varied between 2 cm and 10 cm in steps of 2 cm (models EBR_L2T2W2, EBR_L4T4W4, EBR_L6T6W6, EBR_L8T8W8 and EBR_L10T10W10).

Meshes of 10 node tetrahedral elements were used in all models. The maximum length of the elements was 0.05 m in the concrete slab, 0.02 m in the CS protection and 0.005 m in the CFRP strip/adhesive. These element dimensions were considered based on a mesh sensitivity study, in order to optimize the computational time and to obtain accurate results at the concrete-CFRP bonded interfaces. Table 5.1 summarizes the anchorage protection geometry and strengthening system for each model and the details of the slab meshes.

Table 5.1: Dimensions of the CS protection anchorage in the slabs flexurally strengthened according to the EBR and NSM techniques and total number of nodes and elements on the 2D and 3D models.

MODELS	**Geometry/system**	***L* (m)**	***T* (m)**	***W* (m)**	**Total elements**	**Total Nodes**
Specimen CFRP	2D/EBR	-	-	-	12.520	12.425
Specimen CS25		-	-	-	15.300	15.150
EBR_L2T2W2	3D/EBR	0.02	0.02	0.02	83.158	111.539
EBR_L2T4W4		0.02	0.04	0.04	85.408	114.153
EBR_L4T4W4		0.04	0.04	0.04	86.414	115.460
EBR_L6T4W4		0.06	0.04	0.04	83.619	111.414
EBR_L6T6W6		0.06	0.06	0.06	85.062	113.280
EBR_L8T8W8		0.08	0.08	0.08	84.979	113.254
EBR_L10T10W10		0.10	0.10	0.10	87.089	115.633
NSM_L2T2W4	3D/NSM	0.02	0.02	0.04	66.123	84.692
NSM_L6T6W12		0.06	0.06	0.12	43.770	57.689
NSM_L10T10W20		0.10	0.10	0.20	51.934	67.882

The following boundary conditions were considered: (i) convection and radiation heat transfer in the hot faces with an external temperature following the progression of the ISO 834 curve (identified in grey in Figure 5.3a); (ii) adiabatic boundary in the lateral faces; and (iii) convection and radiation heat transfer in the cold face with an external temperature of 20 ºC. The initial temperature of the models was set as 20 ºC.

As in the 2D models, in the 3D thermal models the transient temperature distributions were computed using the fully implicit scheme with a time step of 10 seconds.

5.3.4.2 NSM-CFRP strengthened RC slab

The RC slab sector analysed is also 5.20 m long, 0.5 m wide and 0.12 m deep. The RC slab sector was strengthened with a 4 m long CFRP strip with a cross section of 20 × 1.4 mm^2. The CFRP strip was introduced in a slit inside the concrete slab with a cross-section of 5 × 30 mm. Figure 5.9 shows the quarter of the slab that was modelled.

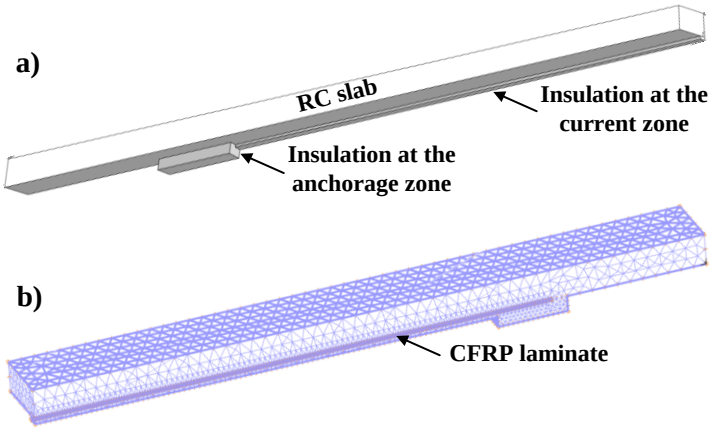

Figure 5.9: NSM-strengthened slab modelled: a) geometry (a quarter of the real slab) and b) FE mesh.

As for the EBR-strengthened slab, a preliminary study was carried out to determine the minimum CS insulation that guarantees a maximum average temperature of 500 ºC at the CFRP strip after 90 min (*cf.* section 5.4.1). Based on that study, a CS protection with (40 + 5 + 40) × 20 mm (width × thickness) was adopted. Figure 5.10a shows the geometry of the protection in the midspan section.

In the anchorage zone (Figure 5.10b), three different protection schemes were assessed, in order to evaluate the influence of the overall thickness of the fire insulation, which was varied between 2 cm and 10 cm in steps of 4 cm (models NSM_L2T2W4, NSM_L6T6W12 and NSM_L10T10W20, *cf.* Table 5.1). In these models, the ratio between parameters *W* and *T* was kept identical to that adopted in the current zone (*W* = 2 × *T*, set according to the preliminary study described in 5.4.1), while parameter *L* was set to be identical to parameter *T* (as adopted in the EBR models).

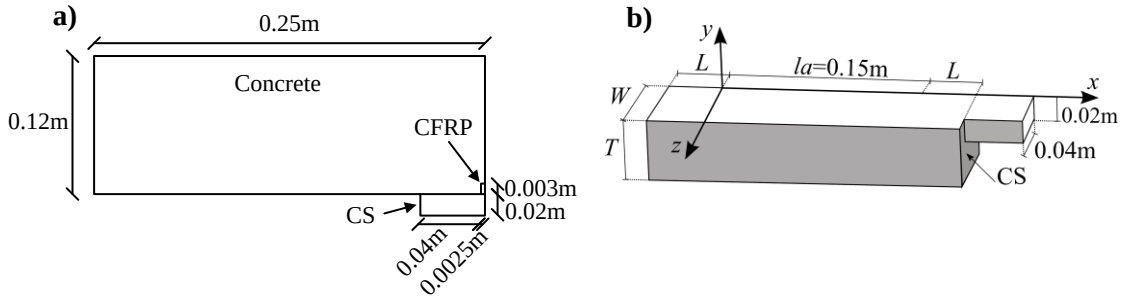

Figure 5.10: Geometry of the NSM flexurally strengthened slabs and CS protection: a) cross-section at midspan (in m); b) perspective of anchorage zone.

A mesh of 10 node tetrahedral elements was considered. Based on a mesh sensitivity study, the maximum length adopted for the elements was 0.05 m in the concrete slab, 0.02 m in the CS protection and 0.005 m in the CFRP/adhesive. The boundary conditions and time integration scheme were similar to those used in the EBR models.

5.4 RESULTS AND DISCUSSION

5.4.1 Preliminary studies (geometry in current zone)

As already mentioned, the geometry of the CS protection at midspan (current zone) was selected in order to guarantee that the temperature at the CFRP strip would be below 500 ºC for 90 min. Therefore, preliminary studies were developed for both the EBR and NSM strengthening systems in order to define (i) the relationship between the width (W) and the thickness (T) of the protection insulation, and (ii) the minimum insulation thickness in current zone.

In what concerns the influence of the width of the CS protection, based on preliminary numerical calculations, for the EBR strengthened slabs one decided to adopt a protection with the thickness equal to the width ($T = W$). In this case, numerical results showed that the principal heat flux influencing the CFRP strip developed mainly in the vertical direction (y axis, *cf.* Figure 5.8b). However, in the NSM strengthened slabs, it was observed that the heat flux in the transverse direction (z axis, *cf.* Figure 5.10b) had also an important influence in the CFRP temperature progression. For this reason, it was decided to assess the influence of the ratio between the thickness and the width of the protection, with the following ratios having been considered: W=T, W=2×T and W=3×T (T being kept constant and equal to 2 cm). Figure 5.11 shows the evolution of the average temperature in the CFRP strip for each relation. Based on cost-effectiveness considerations, a relation of W=2×T was set.

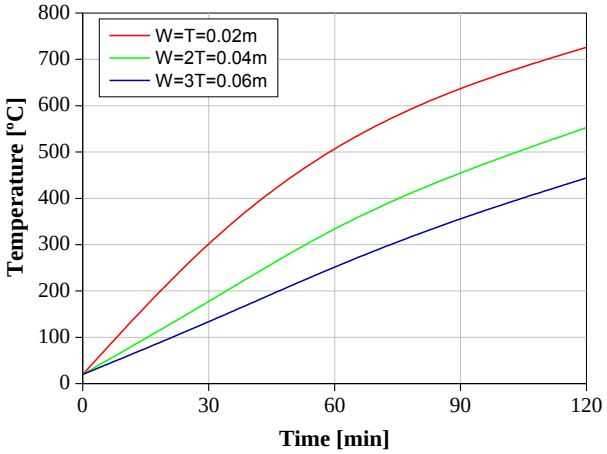

Figure 5.11: Average temperature at the CFRP laminate in NSM-strengthened slab: effect of varying the W/T ratio (T = 2 cm).

Regarding the definition of the minimum thickness of the protection layer at the current zone, Figure 5.12 shows the temperature distribution along the width of the CFRP strip at midspan for different periods of exposure. Based on the results obtained and on the above mentioned maximum temperature criterion, a thickness of 2 cm was adopted for both EBR and NSM strengthened slabs.

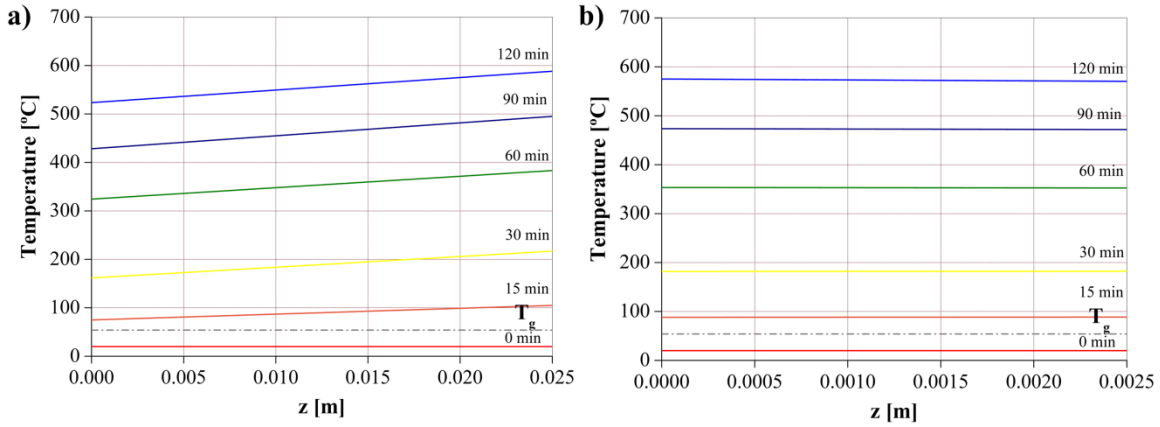

Figure 5.12: Average temperature along the width of the CFRP laminate (midspan section) for different periods of exposure for the slabs strengthened with the a) EBR and b) NSM systems.

5.4.2 Influence of the CS protection geometry in the anchorage zone

The influence of the longitudinal dimension of the insulation (L) compared to the thickness (T) in the temperature progression was first evaluated. The following ratios between those parameters were considered: $L=T/2$, $L=T$ and $L=1.5\times T$ (T being kept constant and equal to 4 cm). Figure 5.13 shows the temperature distribution in the CFRP strip (EBR-strengthened slab) along its anchorage length (l_a =20 cm) in the extreme (E, z=0.025m) and middle (M, z=0) fibres after 120 min of fire exposure for the different cases analysed.

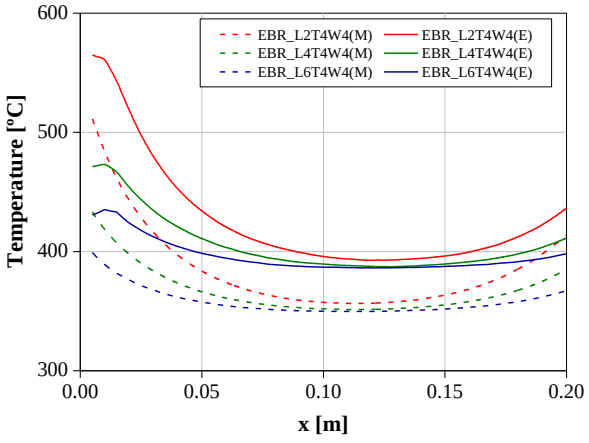

Figure 5.13: Temperature distribution along the anchorage length for the EBR-strengthened slab after 120 minutes of fire exposure (middle (M) and extreme (E) fibres).

Models EBR_L4T4W4 and EBR_L2T4W4 were compared and it was concluded that the latter model provides an average temperature reduction along the anchorage length of 5.2% in the extreme fibres and 5.8% in the middle fibres. In the same way, a comparison between models

EBR_L4T4W4 and EBR_L6T4W4 was carried out and it was concluded that the additional average temperature reduction along the anchorage length is now only 2.3%. Based on these results, it was decided to adopt a relation $L=T$ in the subsequent models.

The influence of the thickness of the insulation (T) was then evaluated. Figure 5.14 shows the temperature distribution along the CFRP strip of the EBR-strengthened slab (in a length of 0.5 m that includes the anchorage length of 0.2 m) after fire exposure periods of 30, 60 and 90 min.

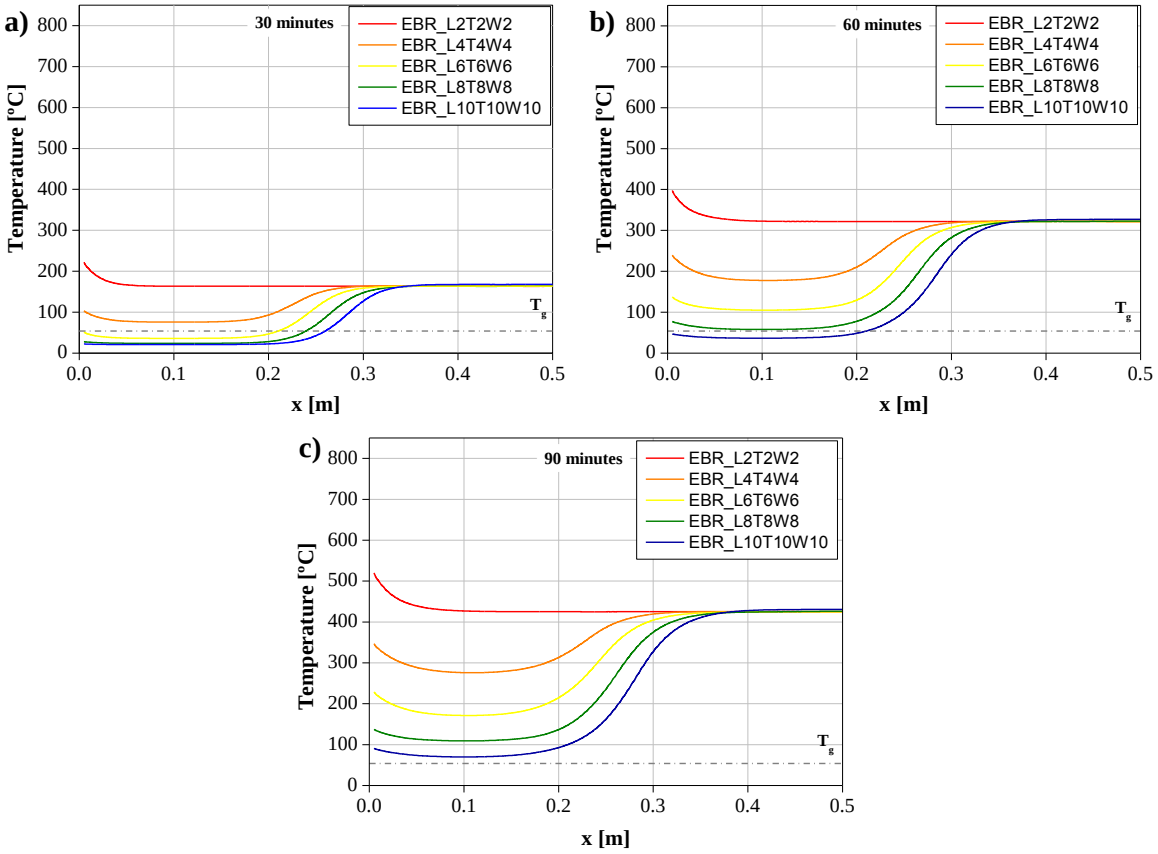

Figure 5.14: Numerical results for the EBR-strengthened slab after a) 30 minutes, b) 60 minutes, and c) 90 minutes of fire exposure.

The results presented in Figure 5.14 show that the influence of the increased insulation depth T in the anchorage zone is effective along *la* but becomes negligible between x = 0.3 m and x = 0.4 m. As expected, the increased insulation in the anchorage zone provided remarkable temperature reductions along the anchorage length. As an example, after 90 min of fire exposure, the temperature reduction in the anchorage zone of model EBR_L10T10W10 was 83% compared to model EBR_L2T2W2. Models EBR_L6T6W6 and EBR_L8T8W8 were able to maintain the average temperature at the interface below T_g (55 ºC according to [5, 68]) for 30 min, while only model EBR_L10T10W10 was able to guarantee such thermal insulation for 60 minutes.

In what regards the NSM-strengthened slab models, Figure 5.15 shows the temperature distribution along the first 0.5 m of the CFRP strip (which includes the l_a = 15 cm), also after fire exposure periods of 30, 60 and 90 min. As for the EBR-strengthened slabs, increasing the thermal insulation

thickness provided remarkable temperature reductions along the anchorage length. After 90 min of fire exposure, model NSM_L10T10W20 provided a temperature reduction of 91% in the anchorage zone compared with model NSM_L2_T2_W4 (without increased protection in the anchorage zone). Models NSM_L6T6W12 and NSM_L10T10W20 were both able to maintain the temperature at the CFRP-concrete interface below T_g during 60 minutes, while only the model NSM_L10T10W20 was able to keep such temperature along *la* below T_g for 90 minutes.

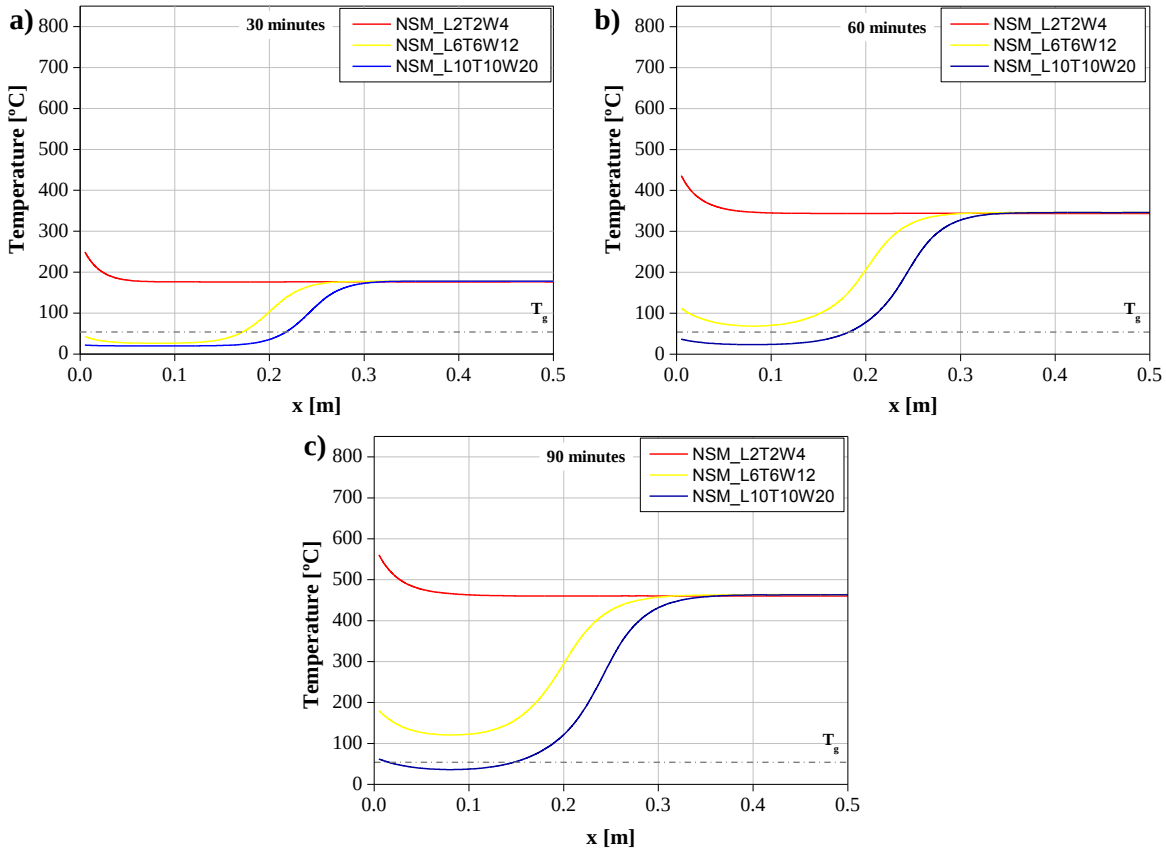

Figure 5.15: Numerical results for the NSM-strengthened slab after a) 30 minutes, b) 60 minutes, and c) 90 minutes of fire exposure.

5.4.3 Influence of the strengthening technique

The results plotted in Figure 5.14 and Figure 5.15 show that the strengthening technique affects the average temperature distribution in the CFRP strip. For similar protection thicknesses (with *L*=*T* equal to 2, 6 or 10 cm), the temperature distribution in the current zone is slightly lower in the NSM strengthened slab than in the EBR strengthened slab, in average about 8.6% after 90 min of fire exposure.

However, comparing the temperature distribution along the anchorage zone (*la*), it can be concluded that the NSM technique considerably improves the thermal protection compared with the EBR technique, in average about 26% and 42% (respectively for $T = 6$ and $T = 10$ cm) after 90 min of fire exposure. As an example, in the NSM-strengthened slab a 10 cm thick CS insulation

is able to maintain the average temperature at the CFRP-concrete interface below the T_g for 90 min; however, for the EBR-strengthened slab, such insulation provides a thermal protection of only 60 min.

5.4.4 Influence of the adhesive glass transition temperature

In order to evaluate the potential advantages of using epoxy adhesives with increased performance at elevated temperature, namely in extending the fire endurance of CFRP-strengthened slabs, the numerical models were used to calculate the time needed for the average temperature of the CFRP-concrete interface to attain the T_g along the l_a for different T_g values: 55 ºC (the one corresponding to the adhesive used in the experimental tests [5, 68]), 65 ºC and 75 ºC.

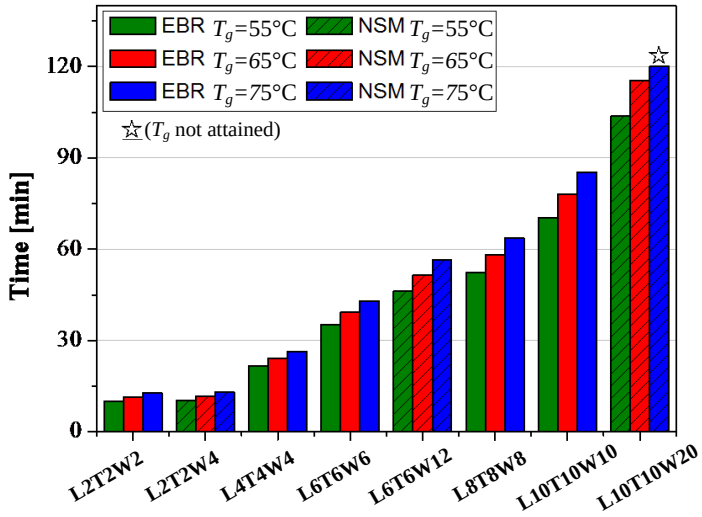

Figure 5.16: Time for the T_g to be attained along the anchorage length for all models developed.

The results obtained for all models analysed are depicted in Figure 5.16 in terms of the corresponding thermal endurance for each T_g. Results obtained show that using an epoxy adhesive with increased T_g can be an effective procedure to extend the thermal protection in the anchorage zone, as it can take considerably longer for the bonded interfaces to attain the T_g along the l_a. Compared with the adhesive used in the experiments (with a T_g of 55 ºC), average thermal protection increases of 12% and 22% were obtained when the T_g increased to 65 ºC and 75 ºC, respectively. As an example of such improvement, in model NSM_L10T10W20 the T_g = 75 ºC is not attained after 120 minutes of fire exposure (as marked in Figure 5.16). These results confirm that the use of an epoxy adhesive with a higher T_g, combined with the thermal insulation systems presented, is another possible solution to increase the fire endurance of CFRP strengthening systems.

5.5 CONCLUSIONS

This chapter presented numerical investigations about the fire behaviour of CFRP-strengthened RC members, aiming at the development of a methodology for the design of appropriate fire protection systems. The design strategy proposed involves guaranteeing that (i) the temperature of the CFRP strengthening strip in current zone remains below a certain temperature (in this case, 500 ºC), and (ii) the temperature of the CFRP-concrete interface along the anchorage zone is kept below a "critical" temperature, hypothesized as being the T_g of the adhesive (in this case, 55 ºC).

Results from previous fire resistance tests on CFRP-strengthened RC beams served as a proof of concept of the above mentioned strategy. In particular, it was confirmed that it is possible to attain considerable fire endurances, provided that adequate fire protection systems are used, including a thick thermal insulation of the anchorage zones.

The numerical thermal models developed, validated based on the good agreement with experimental data, were used to illustrate the application of the above mentioned design methodology, namely to define optimum fire insulation schemes, for both current and anchorage zones of building slabs. From the results obtained, the following conclusions are outlined:

- For current zone, protection schemes with geometries of $W = T$ and $W = 2T$ (W and T being the width and thickness of the thermal insulation) are suggested for EBR- and NSM-strengthened slabs, respectively. In addition, it has been shown that for both techniques T = 2 cm provides a thermal protection of 90 min.
- For the anchorage zones, insulation schemes for EBR-strengthened slabs with T = 6 cm and T = 8 cm are able to maintain the average temperature at the interface below the T_g of the adhesive used in the tests (55 ºC) for 30 min, while a thickness of T = 10 cm provides such thermal insulation for 60 min. For NSM-strengthened slabs, an insulation thickness of T = 6 cm provides thermal insulation in the anchorage zone during 60 min, while for 90 min of protection a thickness of T = 10 cm is needed.
- For similar insulation thicknesses, NSM-strengthening systems present better performance than their EBR counterparts, in terms of the time needed for the CFRP-concrete interfaces to attain the T_g. For the situations analysed here, the average thermal protection increase in the anchorage zone when using the NSM-strengthening technique was 2%, 31% and 45% (*w.r.t.* to equivalent EBR-strengthened slabs) for insulation thicknesses of 2, 6 and 10 cm, respectively.
- Using an epoxy adhesive with higher T_g is also a viable alternative or complementary strategy to increase the fire endurance of CFRP-strengthened RC slabs. In fact, within the range of commercially available epoxy adhesives, it is possible to increase considerably the thermal protection in the anchorage zone.

Finally, just one word to mention that the results from additional fire resistance tests (presented in chapter 7, page 143) will confirm the adequacy of the strategies suggested for the design of fire protection systems for CFRP-strengthened members, and, in particular, in what concerns the "critical" temperature for the CFRP anchorage zones, here hypothesized as being the T_g of the adhesive.

CHAPTER 6

PARTIALLY BONDED CFRP-STRENGTHENED RC BEAMS: FLEXURAL BEHAVIOUR AND APPLICATIONS TO FIRE PROTECTION SYSTEMS DESIGN

6.1 INTRODUCTION

Previous experimental investigations about the fire resistance behaviour of CFRP-strengthened RC beams (*cf.* section 5.2, page 99) proved that CFRP strengthening systems are able to attain considerable fire endurance, provided that adequate fire protection systems are used. In a fire event, even though a CFRP strip may rapidly debond from the central part of the beam in which it is installed, if sufficiently thick insulation is applied in the anchorage zones, the strip transforms into a cable fixed at the extremities, thus maintaining a considerable contribution to the mechanical response of the strengthened beam. Departing from these experimental observations, a preliminary methodology for the design of fire protection systems (comprising thicker insulation at the CFRP extremities) was proposed in chapter 5. It is worth mentioning that the proposed methodology assumes that during fire it is possible exploit the CFRP mechanical contribution through a cable behaviour; however, such behaviour is still not completely understood and characterized.

This chapter presents experimental and numerical investigations on CFRP-strengthened RC beams with the objective of understanding in further depth their fire resistance behaviour, namely the influence of the above mentioned cable behaviour on the mechanical response of the beams. Moreover, this study aims at confirming the possibility of taking such behaviour into account when designing fire protection systems for CFRP-strengthened RC members, serving as a proof of concept of the strategy proposed in chapter 5.

In the first part of this chapter, flexural tests performed at room temperature on small-scale RC beams strengthened according to the EBR and NSM techniques are presented. In these tests, described in section 6.2, the effects of fully or partially bonding CFRP strips (only in the anchorage zones, thus simulating the cable effect) to the bottom soffit of RC beams were investigated, namely in what concerns the mechanical performance reduction of those beams. Alongside the experimental campaign, a numerical study was performed (presented in section 6.3), in which the

mechanical response of the beams tested was simulated by means of non-linear finite element (FE) models.

In the second part of the chapter (*cf.* section 6.4, page 128), the numerical models are extended to full-scale beams, in which the influence of the CFRP bonded length and the loading type (point or uniformly distributed) on the strength reduction was evaluated. These results are then incorporated in the simplified procedure that is proposed for the design of fire protection systems of CFRP-strengthened RC flexural members (*cf.* section 6.4.4, page 137), which is founded on the methodology presented in chapter 5.

6.2 EXPERIMENTAL PROGRAMME ON SMALL-SCALE BEAMS

6.2.1 Test series

The experimental programme comprised small-scale 4-point bending tests on five types of beams: (i) one reference unstrengthened beam (beam RC); two beams strengthened with CFRP strips externally bonded, (ii) fully or (iii) partially (beams EBR-F and EBR-C, respectively); and two beams strengthened with CFRP strips inserted into the concrete cover, also (iv) fully or (v) partially bonded (beams NSM-F and NSM-C, respectively). Table 6.1 summarizes the characteristics of all beams tested. The beams' designation is related to the strengthening technique used (EBR or NSM) and bonded length of the strip (F - fully bonded or C - cable, partially bonded). The bonded length adopted in beams EBR-C and NSM-C (0.20 m) was slightly longer than the anchorage length (l_a) specified on ACI 440.2R [56] (0.197 m and 0.159 m, respectively for EBR and NSM) and corresponded to the insulated length of the strip adopted on previous fire resistance tests, as referred in section 5.2 (page 99). The comparison of the results obtained from beams EBR-F and NSM-F with those from beams EBR-C and NSM-C, respectively, allowed evaluating the effect of fully *vs.* partially bonding the CFRP strip.

Table 6.1: General characteristics of beams tested.

Beam	Strengthening technique	CFRP strip length [m]	Bonded length [m]
RC	-	-	-
EBR-F	EBR	1.10	1.10
EBR-C			0.20 (× 2)[1]
NSM-F	NSM	1.10	1.10
NSM-C			0.20 (× 2)[1]

[1] 0.20 m of the strip bonded to concrete at each anchorage zone.

6.2.2 Specimen geometry, materials and test setup

The cross-section and reinforcement of the beams tested is depicted in Figure 6.1. The internal steel reinforcement consisted of four ϕ6 mm bars (longitudinal reinforcement) and ϕ6 mm stirrups distanced of 0.06 m (transverse reinforcement). The nominal length of the beams was 1.50 m and the concrete cover was set as 15 mm. The RC beams were produced using standard Portland cement concrete (average compressive and splitting tensile strengths at the age of testing of f_{cm} = 30.5 MPa and f_{ctm} = 2.5 MPa, respectively, elastic modulus of E_{cm} = 30 GPa) and A500NR steel bars with diameter of 6 mm (characteristic yielding strength of f_{syk} = 546 MPa, average failure stress of f_{sum} = 703 MPa, and average elastic modulus of E_{sm} = 193 GPa, all provided by the manufacturer). The average tensile properties of the CFRP strips (*S&P Strips CFK 150/2000*) and of the epoxy adhesive (*S&P Resin 220*) were presented in section 3.2.1.2 (page 48).

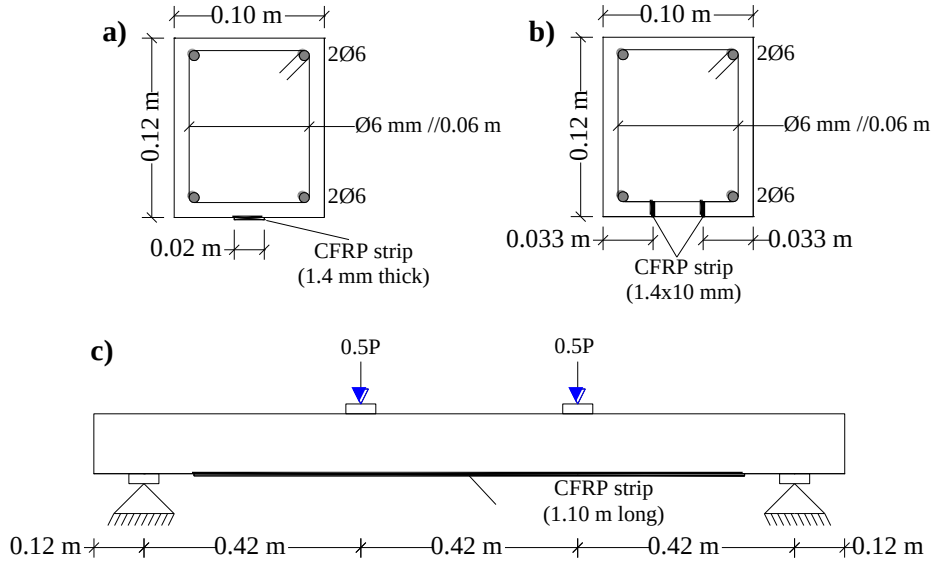

Figure 6.1: a) EBR-CFRP strengthened RC beams' cross section; b) NSM-CFRP strengthened RC beams' cross section; c) geometry of the beams (longitudinal) and load positions.

The EBR-strengthened RC beams were prepared as follows (similar procedure to that used in the EBR specimens for the bond tests, *cf.* section 3.2.1.3, page 49): the superficial layer of the concrete was removed with needle scalers, exposing the first layer of aggregates; the residues from the previous procedure were removed with compressed air; the epoxy adhesive was applied on both the concrete surface and the strips (total thickness of about 2 mm); and the strips were then applied and pressed against the concrete surface. For the NSM-strengthened RC beams the following procedure was adopted (similar to that used in the NSM specimens for bond tests, *cf.* section 3.3.1.3, page 67): slits (5 mm wide and 15 mm deep) were made on the concrete surface using a diamond blade cutter; the slits were cleaned with compressed air; the slits were filled with epoxy adhesive; and the strips were manually introduced into the slits.

The test setup is schematically shown in Figure 6.1c. All beams were tested in a 4-point bending configuration with a span of 1.26 m. The vertical deflection at the midspan section of the beams was measured with an *APEK* displacement transducer. The total applied load was also measured and recorded with a *Novatech* load cell. The tests were conducted under load control at an average speed of 0.06 kN/s.

6.2.3 Results and discussion

The total load *vs.* midspan deflection curves of all beams tested are depicted in Figure 6.2. Beam RC presented the typical behaviour of RC flexural members, sequentially exhibiting (i) an elastic uncracked branch (up to a load of roughly 4 kN), (ii) an elastic cracked branch (up to a load of about 15 kN) and, finally, (iii) a plastic yielding plateau. The load *vs.* deflection curves of beams EBR and NSM presented in Figure 6.2 are also typical of CFRP-strengthened RC beams. Results obtained show that all strengthened beams were considerably stiffer than the reference one in the elastic cracked branch, with such stiffness progressively decreasing until a sudden load decrease occurred. In general, the strengthened beams did not exhibit any plastic branch, but the deformation capacity of NSM-strengthened beams was considerably higher than that of EBR-strengthened beams. As expected, the ultimate load of the strengthened beams was considerably higher than that of beam RC, particularly when using the NSM technique.

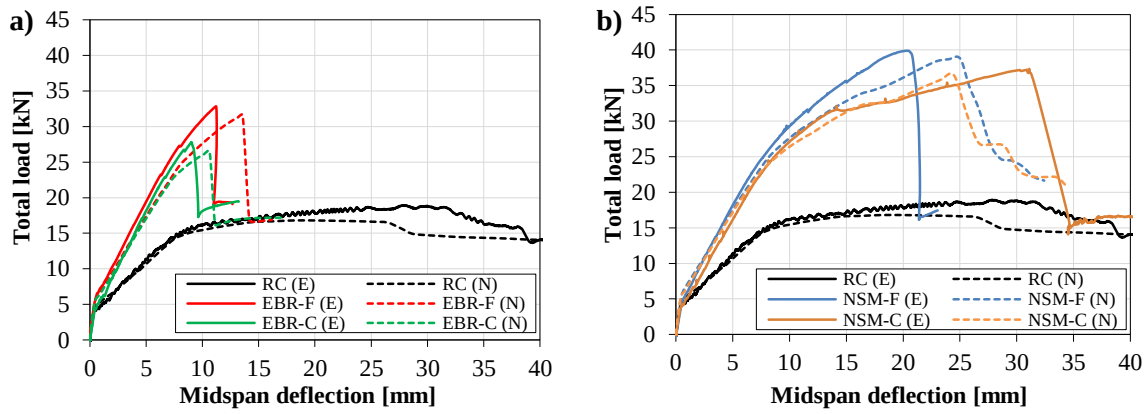

Figure 6.2: Experimental (E) and numerical (N) load vs. midspan deflection curves for a) EBR-strengthened and b) NSM-strengthened beams.

Failure of the reference beam RC occurred due to concrete crushing at the midspan section, as shown in Figure 6.3a), after considerable yielding of the longitudinal steel rebars. The failure of both EBR-strengthened beams was caused by the sudden debonding of the CFRP strips at the concrete-adhesive interface (Figure 6.3b and Figure 6.3c); in beam EBR-C (Figure 6.3c) debonding occurred partially at the CFRP-adhesive interface. The failure of beam NSM-F (Figure 6.3d) occurred due to concrete cover separation (concrete peeling-off) along a significant length of the beam, whereas in beam NSM-C concrete crushing was observed at midspan section (Figure 6.3e) following a progressive slip at the CFRP-adhesive interface (Figure 6.3f). In all strengthened

beams, either fully or partially bonded, the failure of the strengthening system occurred due to the end debonding phenomenon; intermediate cracked-induced debonding failure was not observed in any of the tested beams. Table 6.2 summarises the main results obtained in the experiments, in terms of stiffness (computed within the elastic cracked branch of the load *vs*. midspan deflection curves) and failure load. As expected, regardless of the bonding length, the NSM strengthening technique was the most effective, providing strength increases compared to the RC beam of 111% and 98% when respectively full and partial bonding were adopted. In the beams strengthened according to the EBR technique, those strength increases were respectively 74% and 47%.

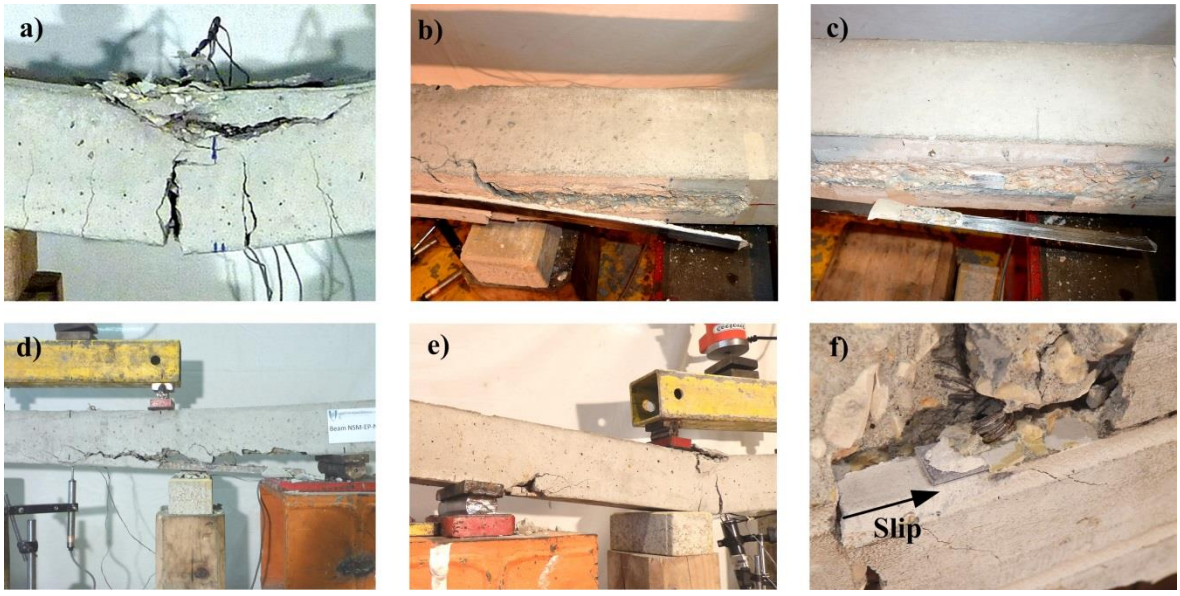

Figure 6.3: Failure modes of tested beams: a) RC - concrete crushing; b) EBR-F and (c) EBR-C – debonding of the CFRP strip; d) NSM-F – concrete peeling-off; e) NSM-C – concrete crushing at the midspan section after slip at the CFRP-adhesive interface; f) NSM-C – detailed view of the slip between the CFRP and the adhesive.

Table 6.2: Summary of experimental (stiffness, failure load and ratio between failure loads with partial and full bonding) and numerical results (Δ_{exp} – relative difference to test data).

Beam	Experimental			Numerical		
	Stiffness [kN/mm]	**Failure load [kN]**	**Partial/full ratio [%]**	**Failure load [kN]**	Δ_{exp} **[%]**	**Partial/full ratio [%]**
RC	1.6	18.9	-	-	-	-
EBR-F	3.0	32.9	84.5	31.6	-3.81	83.9
EBR-C	3.0	27.8		26.5	-4.71	
NSM-F	2.5	39.9	93.7	38.8	-2.73	94.1
NSM-C	2.5	37.4		36.5	-1.72	

In what concerns the influence of the bonding length on overall stiffness, beams EBR-F and EBR-C both presented an average stiffness of 3.0 kN/mm (computed within the elastic cracked branch). Similar results were obtained for the beams strengthened according to the NSM technique - beams NSM-F and NSM-C both presented an average stiffness of 2.5 kN/mm. These results show

that partially bonding the CFRP strips had no consequence on the beams' stiffness. Regarding the influence of the bonding length on strength, the ultimate load of beam EBR-C (27.8 kN) was only 15% lower than that observed on beam EBR-F (32.9 kN). For the NSM-strengthened beams, the strengths of beams NSM-F and NSM-C were respectively 39.9 kN and 37.4 kN – thus, for this technique, the partial bonding led to a strength decrease of only about 6%. It should be noted that the low strength reductions induced by the partial bond observed in both strengthening techniques is related to fact that the failure mode of the strengthening system remained unchanged (end debonding).

The results presented above show that bonding the CFRP strip only along the anchorage length (l_a = 0.20 m) did not have a significant influence on the structural responses of the CFRP-strengthened RC beams tested - strength reductions were relatively low (6 to 15%). Furthermore, it is worth mentioning that the load applied in a fire situation (similar to that corresponding to a serviceability limit state) is significantly lower than the ultimate load capacity of the RC member. This indicates that in the event of a fire the cable behaviour of the strengthening system may in fact ensure the required load bearing capacity provided that the mechanical properties of the materials (and interfaces) are not excessively reduced due to thermal degradation. In order to prevent such degradation, especially along the anchorage length, a fire protection system must be duly designed and applied, which may be done according to the procedure presented in chapter 5.

6.3 NUMERICAL SIMULATION OF THE TESTS ON SMALL-SCALE BEAMS

6.3.1 Description of the FE models

The numerical study comprised the development of non-linear finite element (FE) models of all beams tested at ambient temperature and strengthened with both systems, with the CFRP strips fully or partially bonded. The FE models were developed using the commercial software ATENA, developed by *Cervenka Consulting* [127]. This software has been fully tested with success in the simulation of RC structures using smeared fracture mechanics [128] and was used to simulate the behaviour of a wide range of RC members incorporating FRP composites (*e.g.* [129-133]).

6.3.1.1 Geometry, type of elements and boundary conditions

Since physically non-linear analyses were performed in the present study, in order to reduce the computational costs, only half of the beams span was simulated, with a total length of 0.65 m. Due to the test conditions, a simple plane stress analysis was deemed adequate to simulate the behaviour of the beams tested. For this reason, only plane finite elements were used to describe the concrete behaviour.

Figure 6.4 illustrates the FE mesh of the strengthened beams EBR and NSM. When generating the mesh for the concrete, plane quadrilateral elements with 4 nodes were used. These are isoparametric elements integrated by Gauss quadrature at 4 integration points for the case of bilinear interpolation. In the models of the EBR-strengthened beams, the CFRP strips were also simulated with plane elements, but using 3-node constant strain triangular elements. These elements were implemented directly over the bottom face of the beams. In the models of the NSM-strengthened beams, the CFRP strips were simulated with classical frame elements. As plane elements were used to model concrete, the two CFRP strips applied in the concrete cover were simulated by a single frame element, considering the equivalent thickness and contact area. The horizontal steel rebars, with a diameter of 6 mm, were also modelled with frame elements positioned in two different vertical levels at a distance of 2.4 cm from the top and bottom faces of the beams. The vertical shear stirrups were implemented using a membrane element ("smeared reinforcement"), with only vertical stiffness, which corresponds to a uniform distribution of shear rebars.

In the right end of the beam model the horizontal displacements and the rotations were restricted throughout the edge height. To simulate the pinned support in the left end and in order to avoid any stress concentration effects, a rectangular elastic support was adopted. The same simplification was adopted for the applied load.

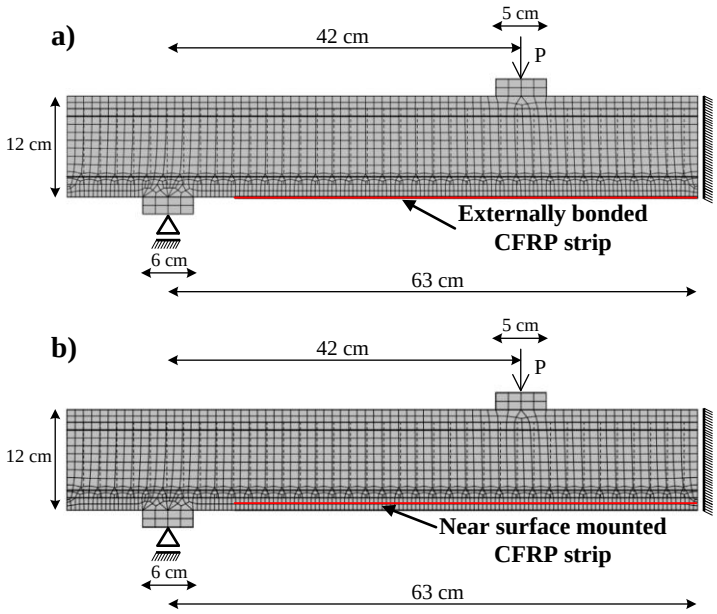

Figure 6.4: Geometry of the finite element mesh of a) EBR-F and EBR-C beams (CFRP strips modelled with plane elements) and b) NSM-F and NSM-C beams (CFRP strips modelled with frame elements).

6.3.1.2 Material properties

A classical smeared crack model was used to simulate the concrete behaviour. The mechanical properties adopted for the concrete were the ones measured in the experimental campaign:

f_{ctm} = 2.5 MPa, f_{cm} = 30.5 MPa and E_{cm} = 30 GPa. For the shear behaviour a rotated crack model was used, with variable shear retention factor and linear tension-compression interaction. The rotated crack model was adopted in order to correctly simulate the debonding of the CFRP. For compression, concrete was simulated using a classical fictitious compression model. A fictitious crack model (such as the rotated crack one) is based on a tension stress *vs*. crack opening law with certain fracture energy and this formulation has been found to be suitable to model crack propagation in concrete. It is used in combination with the crack band theory in order to prevent mesh dependency using the exponential crack opening law. A fracture energy of G_{cf} = 50 N/m was adopted according to the Fib Model Code 90 [96] (for a concrete class C25/30 and for a maximum aggregate diameter of 8 mm).

The CFRP strips were modelled as linear elastic, with E_f = 170 GPa. For the steel rebars a classical elastoplastic multi-linear model with hardening was adopted with the following material parameters: E_s = 200 GPa (elastic); yielding stress f_{sy} = 600 MPa; E_{sy} = 20 GPa (post-hardening); ultimate yielding stress f_{syu} = 690 MPa, with E_{su} = 0 GPa.

6.3.1.3 CFRP-concrete interfaces constitutive relations

The constitutive relations of both EBR and NSM beams were defined based on bi-linear bond-slip curves (as those presented in chapter 4) defined by the maximum shear strength (τ_{LM}), the corresponding slip (s_{LM}) and the ultimate slip (s_{L0}). Table 6.3 summarizes the values adopted for these parameters, which are also illustrated in Figure 6.5a) and Figure 6.5b) for the EBR and NSM beams, respectively. These constitutive relations were calibrated based on the comparison between experimental and numerical load *vs.* deflection curves of the beams, but also taking into account results of double lap shear tests presented in chapter 3. Figure 6.5a) and Figure 6.5b) show the shear stress *vs*. slip curves obtained from those tests carried out on EBR and NSM-strengthened concrete blocks, respectively. Note that each curve was obtained through the readings of consecutive strain gauges glued along the CFRP strips. Although the data scatter is high (which is typical in this type of tests), these results provided a variation range for the simplified bond-slip curves. It can be seen that the bi-linear bond-slip curves adopted in the numerical models are well within the variation range obtained in the double-lap shear tests. It is worth mentioning that the bond *vs.* slip relations calibrated in chapter 4 (*cf*. Figure 4.5, page 88) for ambient temperature were not adopted here, because the present FE models were developed prior (chronologically) to the definition of such relations; nevertheless the differences between these two proposals are not substantial (and are also within the variation range experimentally obtained).

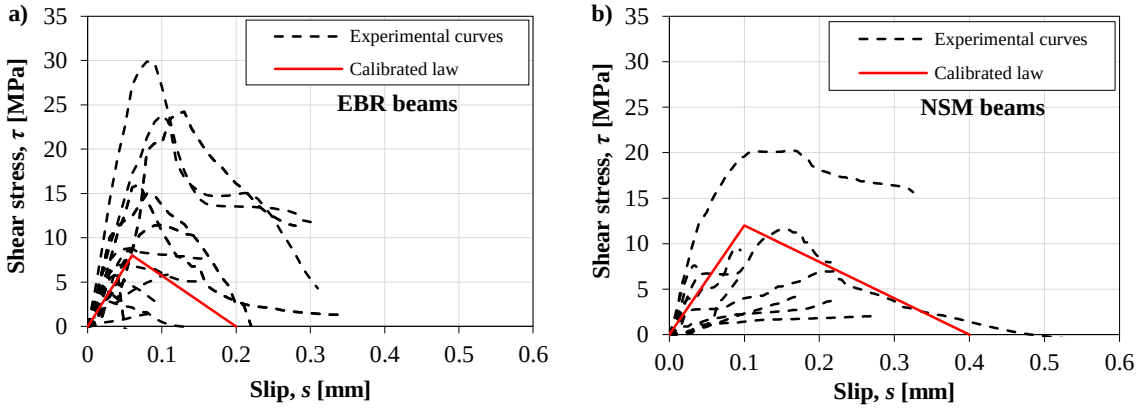

Figure 6.5: Adopted constitutive relations for the CFRP-concrete interfaces of a) EBR beams and b) NSM beams.

Table 6.3: Parameters of the bond-slip laws adopted for ambient temperature conditions.

Parameter	EBR models	NSM models
τ_{LM} [MPa]	8	12
s_{LM} [mm]	0.06	0.10
s_{L0} [mm]	0.20	0.40

Other proposals for bond-slip curves (for room temperature) are available in the literature for both EBR and NSM systems (*e.g.* [105, 108, 134, 135]). The definition of such laws, which should take into account the mechanical properties of concrete, FRP strips and bonding adhesive, as well as the preparation procedure of the concrete surface, is still an open and very challenging issue.

For the EBR-strengthened beams the adherence between CFRP and concrete was modelled using an interface element, with a width of 20 mm (identical to that of the CFRP strip), with a cohesive Mohr-Coulomb bi-linear constitutive relation (Figure 6.6). The respective elastic tangential and normal stiffnesses were set as k_t = 133.3 GPa/m and k_n = 1000 GPa/m, respectively. While the tangential stiffness corresponds to the one computed on the ascending branch of the calibrated bond-slip law (presented in Figure 6.5a and defined in Table 6.3), the value of the normal stiffness had to be reduced (compared to the ratio between the adhesive elastic modulus and thickness) in order to avoid numerical instabilities (however, this simulation procedure does not affect the overall response of the beams, as reported by Neto *et. al* [136]). The following parameters were defined for the failure surface: friction coefficient of $\Phi = 10^{o}$ (as suggested in [137]); normal tensile resistance of f_t = 17 MPa (corresponding the tensile strength of the epoxy adhesive, determined in [68][6]); cohesion of c = 8 MPa (the maximum shear stress of the calibrated bond-slip law); parameter Δv_c = 0.14 mm (defined based on S_{LM} = 0.06 mm and slip S_{L0} = 0.20 mm of the calibrated bond-slip law, $\Delta v_c = 0.20 - 0.06 = 0.14$ mm). For the EBR-strengthened beam with cable

[6] The tensile strength of the epoxy adhesive mentioned in chapter 3 (14.2 MPa) was experimentally determined after the conclusion of this numerical investigation. Therefore, in the FE models described herein a value of 17 MPa (determined in a previous experimental investigation) was adopted.

behaviour only normal stiffness was considered, *i.e.* the shear stiffness at the interface was set to null.

For the NSM-strengthened beams, the CFRP-concrete adherence was modelled by implementing explicitly the above mentioned bond-slip interaction law (calibrated curve depicted in Figure 6.5b) between the frame and the concrete plane elements (as suggested in [137]). In this model, only the shear interaction was considered to simulate the debonding effect (interaction with normal stresses was not accounted for). Since in this strengthening technique the CFRP strip has two contact surfaces with the concrete, a total contact perimeter of 40 mm was considered.

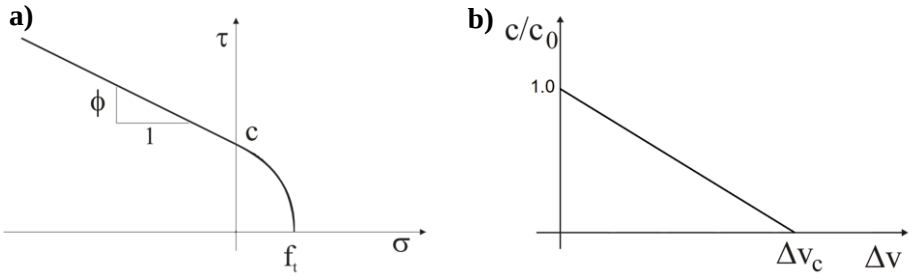

Figure 6.6: a) Failure surface for interface elements using Mohr-Coulomb; b) bi-linear softening law for cohesive Mohr-Coulomb.

6.3.1.4 Type of analysis

One of the objectives of this investigation was to simulate the load *vs.* displacement curve of the beams up to the post-failure softening regime. Therefore, in order to control the post-peak responses during the softening stage, the analyses were performed using applied displacements [116]. As the load rate used in the experimental campaign was sufficiently slow, static non-linear analyses were performed.

6.3.2 Results and discussion

Figure 6.2a and Figure 6.2b (page 120) show the comparison between numerical (dashed lines identified by the letter "N") and experimental load *vs.* deflection curves obtained for the EBR and NSM-strengthened beams, respectively.

It can be seen that the numerical models were able to simulate the experimentally observed mechanical response of both EBR and NSM-strengthened beams, with very high accuracy. In terms of cracked stiffness, experimental and numerical curves exhibit an equivalent slope, with experimental curves presenting slightly higher stiffness. This (slight) difference may be due to the effect of some horizontal friction in the pinned supports, which was impossible to completely eliminate during the tests.

Table 6.2 (page 121) summarizes the numerical failure loads of all strengthened beams and the corresponding ratios between those loads for full (EBR-F and NSM-F) and partial bonding (EBR-C

and NSM-C). The relative differences to experimental results are very low (lower than 4%), confirming the accuracy of numerical predictions. Accordingly, the numerical strength reductions stemming from the partial bonding are also in agreement with experimental data – reductions of 16% and 6% were obtained for the EBR and NSM beams, respectively (those figures compare with experimental reductions of 15% and 6%).

Figure 6.7 illustrates the deformed shape and the final crack distribution of the EBR-strengthened beams, after the debonding of the CFRP strip. Results are coherent with the ones observed in the experimental campaign. This figure illustrates the debonding of the CFRP strip, which led to a considerable softening of the load *vs*. displacement curve. Figure 6.8 depicts the deformed shapes of the NSM-strengthened beams, illustrating an explicit horizontal debonding at the end of the CFRP strip. This failure mode was expected since the frame element with bond-slip relationship does not allow simulating the vertical debonding of the strip. Although in this case the failure mode was not rigorously reproduced (due to the aforementioned reason), the numerical models were able to predict with success the overall behaviour of the NSM-strengthened beams.

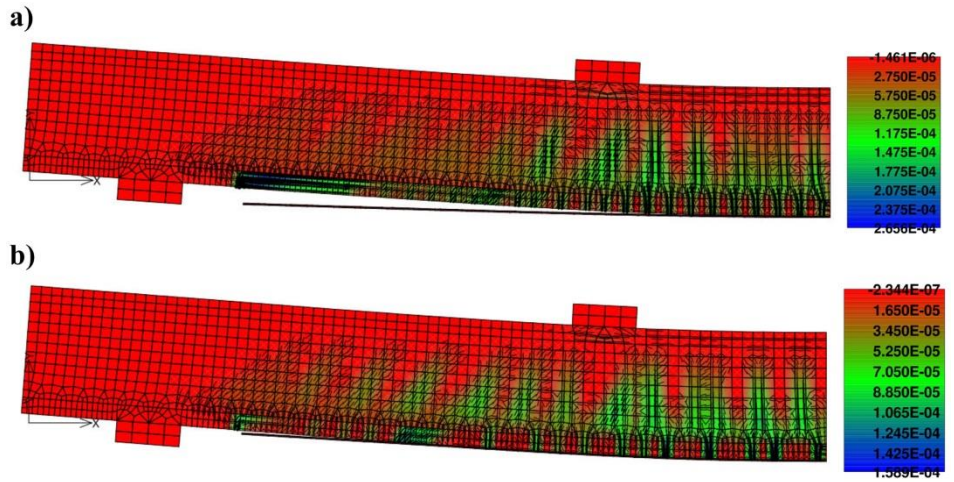

Figure 6.7: Deformed shape and final crack distribution [m] of beams a) EBR-F and b) EBR-C.

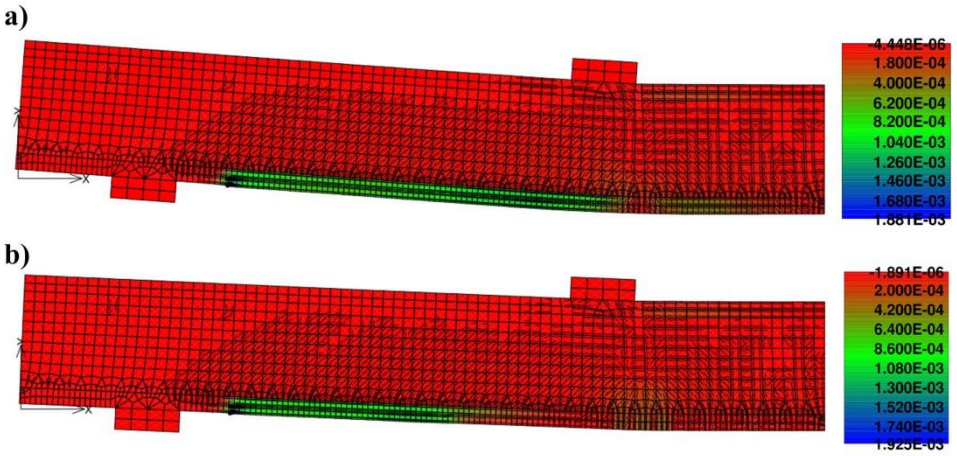

Figure 6.8: Deformed shape and final crack distribution [m] of beams a) NSM-F and b) NSM-C.

The good agreement between the numerical simulations and experimental data provides further validation about the cable effect, *i.e*. the preservation of most of the contribution of the partially bonded CFRP strip to the structural response of the beams, provided that it remains fully bonded in the anchorage zones.

6.4 NUMERICAL SIMULATIONS ON FULL-SCALE BEAMS

6.4.1 Objectives and procedure

This section presents numerical investigations about the flexural behaviour of full-scale RC beams strengthened with CFRP strips partially bonded along their length at ambient temperature conditions. The main objective of this study is to propose a simplified procedure for the design of fire protection systems for CFRP strengthened-RC beams, complementing the preliminary methodology already presented in chapter 5. As a first step towards the validation of this procedure, the models presented in section 6.3 (corresponding to small scale beams subjected to point loads) were extended for different beam geometries, with different spans (L), in which the influence of the CFRP bonded length (l_a) and the loading type (point or uniformly distributed) on the mechanical response was evaluated. The numerical results obtained (*cf.* section 6.4.3), namely the relations between the strength reduction due to the partial bonding and the l_a/L ratio were then included in a simplified procedure for the design of fire protection systems for CFRP strengthening systems (presented in section 6.4.4). The results obtained in this section allowed establishing the minimum CFRP bonded length or, in other words, the minimum length of the thicker insulation layer to be applied in the anchorage zones. The thickness of this insulation, in both central and anchorage zones of the strengthening system, can be defined based on the criteria indicated in chapter 5 (also detailed in section 6.4.4).

6.4.2 Description of the numerical models

6.4.2.1 Geometry and boundary conditions

The 2D FE models of small-scale CFRP-strengthened RC beams presented in section 6.3 were extended here for different beam geometries with spans varying from 2 m to 5 m. The geometry of the beams' cross sections, namely the relationship between the height (h), thickness (b) and free span (L), was similar to that of the small-scale beams tested previously (described in section 6.2 – page 118). Figure 6.9 presents the parameters that define the longitudinal dimensions of the models for the two loading types, point (Figure 6.9a) and uniformly distributed (Figure 6.9b). Note that in this figure only half of the beams' length is represented; in fact, using symmetry, and in order to reduce the computational costs, only half of the beams length was modelled. In this figure, a represents the length of the supports, c identifies the distance from the extremity of the beam to the

CFRP strip (beginning of the bonded length), r is the concrete cover and l_a is the bonded length. For all the models the following geometrical ratios were considered: L/h = 10; L/b = 16; L/a = 16; and $c = a + 0.05$ (dimensions in meters). Table 6.4 shows the values of the geometrical parameters adopted for all the beams (with the exception of l_a), regardless of the strengthening technique adopted.

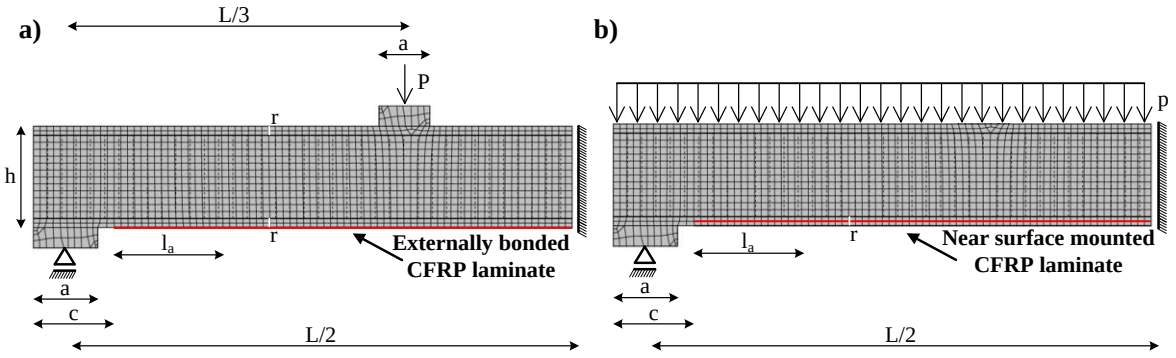

Figure 6.9: Geometry of the FE mesh of the beams (with the 2 m span) strengthened according with the a) EBR and b) NSM techniques and parameters of the models for point and uniformly distributed loads, respectively.

Table 6.4: Geometrical parameters adopted for both types of beams, EBR and NSM.

Span (*L*) [m]	**Height (*h*) [m]**	**Thickness (*b* = *a*) [m]**	***c* [m]**	***r* [cm]**
2.0	0.2	0.13	0.18	1.5
3.0	0.3	0.19	0.24	1.5
4.0	0.4	0.25	0.30	2.0
5.0	0.5	0.31	0.36	2.5

The steel-concrete ratios and the percentage of flexural strength increase provided by the CFRP strengthening system were also similar to those of the small-scale beams presented in section 6.2. Table 6.5 presents the details of the steel reinforcement and the CFRP strips adopted for each beam. The tensile steel reinforcement area ($A_{S,inf}$) was approximately 0.5% of the cross section area, whereas that of the compression one ($A_{S,sup}$) was approximately 0.18% (higher than the minimum reinforcement specified in the Eurocode 2 [138]). As the objective of this study involves assessing the failure of the strengthening system, the area of shear reinforcement ($A_{S,w}$) was designed in order to avoid shear failure of the strengthened beams. The shear reinforcement was uniformly spaced along the beams and the corresponding areas are listed in Table 6.5. Regarding the CFRP strips (A_f represents the cross section area, b_f the width and t_f the thickness), when installed according to the EBR technique, a 35% flexural strength increase (when compared to the non-strengthened beam) was set and estimated based on the procedure indicated in the CNR-DT200/2013 [100]; for the NSM technique, a 50% strength increase was considered and evaluated according with the ACI guidelines [56]. The bonded length (l_a) of the CFRP strips adopted for both strengthening techniques varied from the recommended anchorage length (l_e) (determined as suggested in [100]

for the EBR system and in [56] for the NSM) to $7 \times l_e$. The referred parameters and strengths were computed using the material properties presented in section 6.2.2.

Concerning the boundary conditions, as only half of the beams' length was modelled (*cf.* Figure 6.9), the horizontal displacements throughout the edge height in the right end of the beams were restricted. To simulate the pinned support in the left end, and in order to avoid any stress concentration effects, a rectangular elastic support was adopted. For the beams subjected to a point load, the same simplification was adopted for the applied load.

Table 6.5: Details of the steel reinforcement and CFRP strips adopted for both EBR and NSM beams (diameter ϕ in mm, spacing // in m)

Span *(L)* [m]	Both EBR and NSM beams			EBR beams		NSM beams	
	$A_{S,inf}$	$A_{S,sup}$	$A_{S,w}$	A_f [n° × b_f × t_f ; in mm]	l_e[1] [m]	A_f [n° × b_f × t_f ; in mm]	l_e[2] [m]
2.0	2 ϕ10	2 ϕ6	ϕ6 //0.20	1 × 30 × 1.4	0.22	2 × 10 × 1.2	0.16
3.0	3 ϕ12	2 ϕ8	ϕ6 //0.10	1 × 70 × 1.4	0.22	3 × 15 × 1.2	0.16
4.0	4 ϕ12	3 ϕ8	ϕ6 //0.10	1 × 100 × 1.4	0.22	3 × 15 × 1.4	0.19
5.0	4 ϕ16	3 ϕ10	ϕ6 //0.10	1 × 150 × 2.0	0.26	4 × 25 × 1.2	0.17

[1] determined according with CNR-DT200/2013 [100] guidelines.

[2] determined according with ACI440-2R-08 [56] guidelines.

6.4.2.2 Type of elements and materials properties

Figure 6.9 illustrates the FE mesh of the beams (with the 2 m span) strengthened according with the EBR and NSM techniques. For the remaining beams, proportional FE meshes were adopted. The type of elements used in the models, as well as the material properties adopted, were already described in sections 6.3.1.1 and 6.3.1.2, respectively.

6.4.2.3 CFRP-concrete interfaces constitutive relations and type of analysis

The bi-linear bond-slip relations described in section 6.3.1.3 were adopted for the CFRP-concrete interfaces of both EBR and NSM beams. However, it is worth mentioning that it is widely reported in the literature that in EBR systems the width of the CFRP strips (b_f) has a significant influence on the maximum shear strength (τ_{LM}); increasing b_f reduces the value of τ_{LM} (although the stiffness of the ascending branch of the bond-slip law does not change). In fact, the CNR-DT200/2013 [100] suggests the following geometrical factor (k_b) to take into account this phenomenon,

$$k_b = \sqrt{\frac{2 - \frac{b_f}{b}}{1 + \frac{b_f}{400}}} \tag{6.1}$$

where b represents the width of the RC beam. As the bi-linear bond-slip law presented in Figure 6.5a was calibrated for b_f = 20 mm and b = 12 cm, corrections to the values of τ_{LM} were performed taking into account the dimensions presented in Table 6.5 for the EBR-strengthened beams. Table 6.6 presents the corrected values that were adopted in the present study.

Table 6.6: Parameters of the adopted bond-slip relations.

Span *(L)* [m]	EBR-Strengthened beams			NSM-Strengthened beams		
	τ_{LM} [MPa]	s_{LM} [mm]	s_{L0} [mm]	τ_{LM} [MPa]	s_{LM} [mm]	s_{L0} [mm]
2	7.9	0.059	0.200	12.0	0.100	0.400
3	7.5	0.056				
4	7.2	0.054				
5	6.7	0.050				

In the present investigation, the mechanical behaviour of the CFRP-strengthened RC beams is studied in terms of the load *vs.* displacement curves up to the post-failure softening regime. Therefore, in order to control the post-peak responses during the softening stage (CFRP debonding), the numerical simulation of the beams subjected to an uniformly distributed load was performed using the arc-length technique [115]. For the beams subjected to a point load, since the analyses were performed using applied displacements, the classical Newton-Raphson technique was deemed appropriate to capture the post-peak response after the CFRP debonding. As the load rate admitted in this study was sufficiently slow, a static non-linear analysis was adopted.

6.4.3 Numerical results

6.4.3.1 Load vs. deflection response of EBR beams

Figure 6.10 shows the load *vs.* deflection curves obtained for the unstrengthened (identified as RC) and EBR-strengthened beams with free spans varying from 2 m (Figure 6.10a) to 5 m (Figure 6.10d) and subjected to a point loading. Similar results obtained in beams subjected to a uniformly distributed load are plotted in Figure 6.11. In these figures the corresponding curves of the beams with fully (EBR-F) and partially bonded (EBR-C, simulating the cable behaviour) CFRP strips are represented. For the latter beams, the results obtained for bonded lengths between l_e (beam EBR-C-le) and 7 × l_e (beam EBR-C-7le) are also showed (l_e is defined in Table 6.5).

In both figures, the unstrengthened beams (beams RC) presented the typical behaviour of RC flexural members, sequentially exhibiting (i) an elastic uncracked branch, (ii) an elastic cracked branch and, finally, (iii) a plastic yielding plateau. The corresponding results of all strengthened beams (with either fully or partially bonded CFRP) were considerably stiffer than the reference ones (beams RC) in the elastic cracked branch, with such stiffness progressively decreasing until a

sudden load decrease occurred (corresponding to the loss of the strengthening system), which was more pronounced when the beams were subjected to a uniformly distributed load (Figure 6.11).

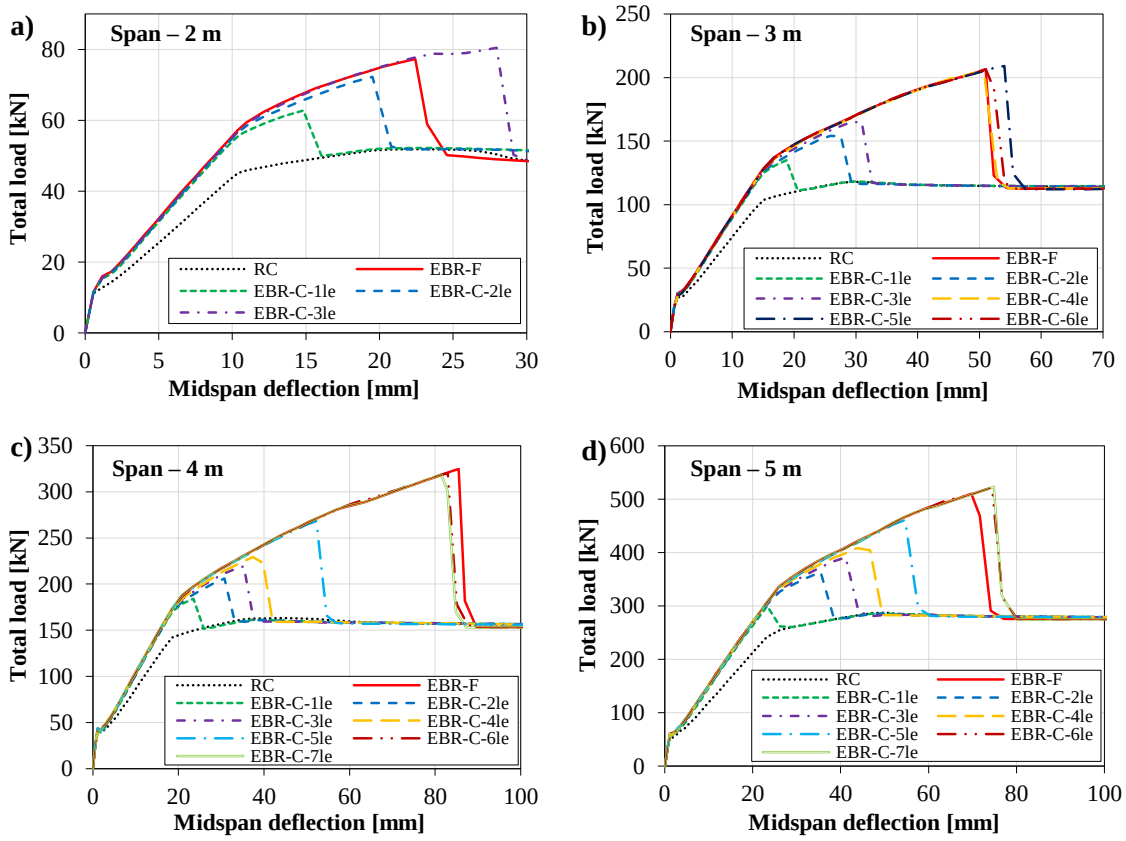

Figure 6.10: EBR CFRP-strengthened beams subjected to point load: total load vs. midspan deflection curves for spans of a) 2 m, b) 3 m, c) 4 m, and d) 5 m.

After the CFRP debonding, the behaviour of all strengthened beams tends to the one exhibited by the reference beams. As expected, the results obtained showed that: (i) the maximum load of the strengthened beams was considerably higher than the ones exhibited by the reference beams; (ii) the beams subjected to an uniformly distributed load presented higher failure loads than the corresponding ones subjected to a point load; and (iii) for both loading types, the beams strengthened with partially bonded CFRP strips exhibited higher strength with increasing bonded lengths. Regarding the influence of the partially bonded strengthening system, a slight increase in the strength and deformation capacity was observed when higher bonded lengths were used (mainly in beams with 2.0 m of free span). This is consistent with previous results reported in the literature (*e.g.* [139-141]). It is worth mentioning that, in general, the calculated flexural strength increase provided by the externally bonded CFRP strips was considerably higher than the theoretical value of 35% (based on CNR-DT200/2013 [100]), considered to design the CFRP area in each beam. The comparison between these analytical flexural strength predictions and the corresponding numerical results is out of the scope of the present chapter; however, these results showed that, for the modelled beams, the CNR-DT200/2013 [100] underestimates their flexural

strength (as showed in section 6.3.2, the numerical models were able to correctly simulate the flexural behaviour of CFRP-strengthened beams). Figure 6.12 shows the relationship between the strength reduction due to the partial bonding (when compared to the strength of the fully bonded CFRP) and the ratio "bonded length (l_a)"/"span (L)" for all the spans considered and for both loading cases, point (Figure 6.12a) and uniformly distributed (Figure 6.12b). Note that l_a represents the bonded length adopted only at one extremity of the CFRP strip, *i.e.* when this ratio is 0.5 the strengthening system is fully bonded along its length. As expected, the strength reduction decreases when the ratio l_a/L increases for both loading cases. Despite the curves obtained for the different spans were not perfectly coincident (which may be due to some mesh dependence), no strength reduction was observed on the beams subjected to point loads (Figure 6.12a) when the CFRP bonded length is higher than 30% of the span, whereas for the uniformly distributed load the same bonded length caused a strength reduction lower than 20%. These small reductions indicate that the cable behaviour of the strengthening system can ensure the required load bearing capacity even when the structural element is subjected to elevated loads. As mentioned, the numerical data plotted in Figure 6.12 will be incorporated in a simplified procedure for the design of fire protection systems for CFRP strengthening systems (*cf.* section 6.4.4).

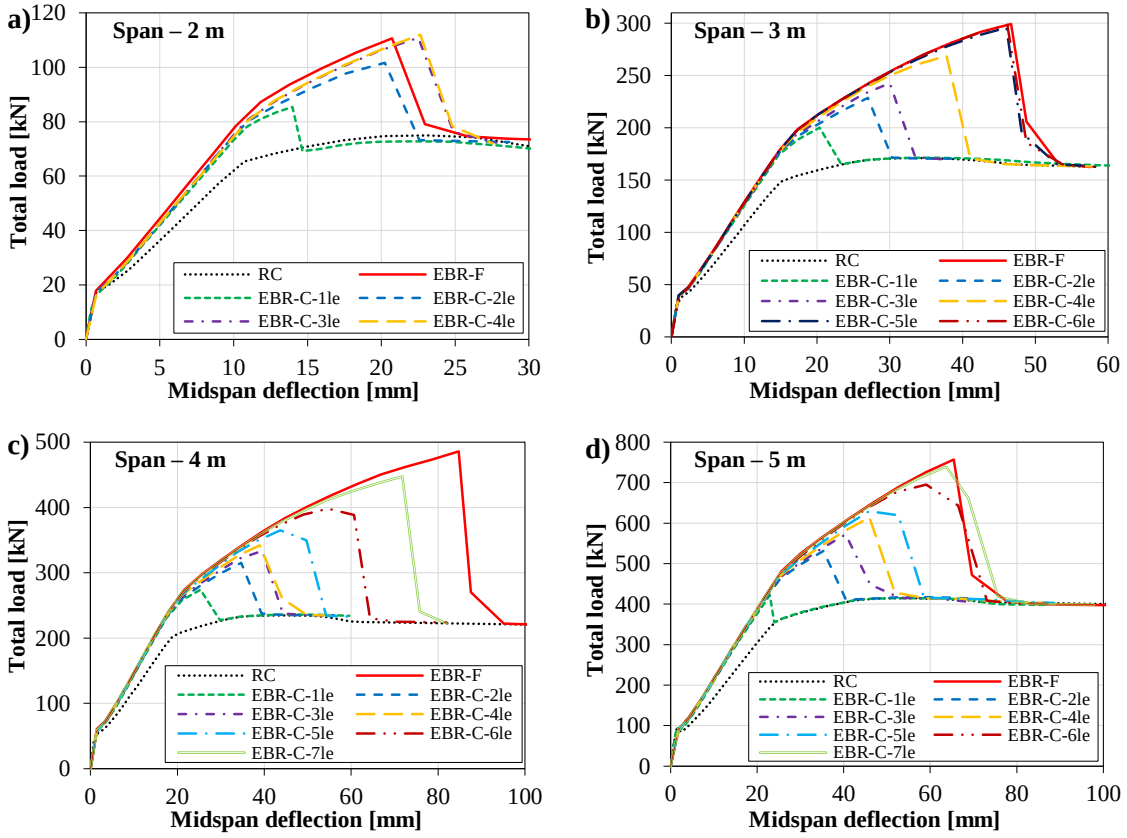

Figure 6.11: EBR CFRP-strengthened beams subjected to uniformly distributed load: total load vs. midspan deflection curves for spans of a) 2 m, b) 3 m, c) 4 m, and d) 5 m.

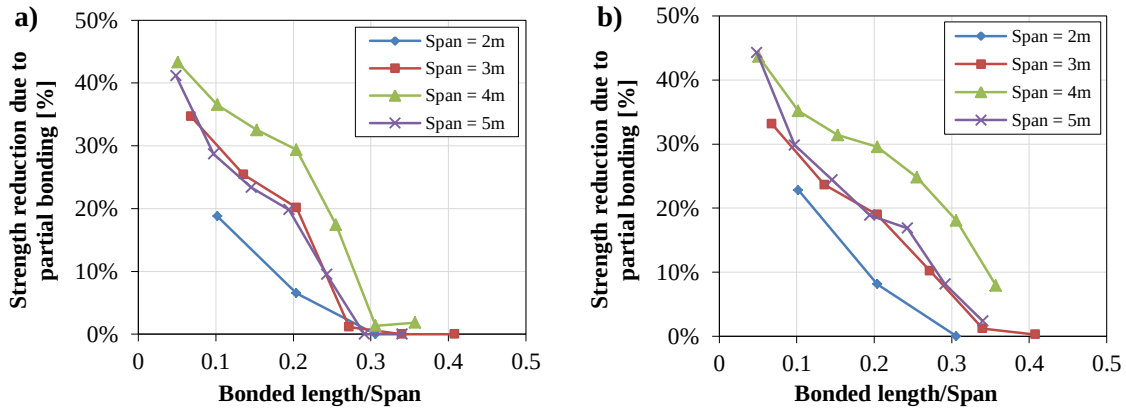

Figure 6.12: EBR CFRP-strengthened beams subjected to (a) point load and (b) uniformly distributed load: Strength reduction due to partial bonding vs. bonded length/span.

6.4.3.2 Load vs. deflection response of NSM beams

Figure 6.13 and Figure 6.14 show the load *vs.* deflection curves obtained in the reference beams (beams RC) and in the NSM-strengthened beams subjected to point and uniformly distributed loads, respectively. The nomenclature adopted in these figures is similar to the one used in the previous section: NSM-F stands for the beams strengthened according to the NSM technique, in which the CFRP strip is fully (F) bonded along its length; NSM-C-2le identify the beams strengthened with partially bonded NSM CFRP strips, in which the bonded length was $2 \times l_e$ (l_e defined in Table 6.5 – page 130). In these figures it can be seen that the deformation capacity of both fully and partially bonded NSM-strengthened beams is considerably higher than the EBR-strengthened counterparts (*cf.* Figure 6.10 and Figure 6.11). Furthermore, the stiffness in the elastic cracked branch exhibited by the former beams is slightly lower due to the partially bonded CFRP; however, it increases with longer bonded lengths. Moreover, the stiffness reduction along the elastic cracked branch (until the CFRP debonding) is more progressive than that observed in the EBR-strengthened beams. It is also important to point out that the flexural strength increase provided by the fully bonded NSM-CFRP strips was, in general, slightly lower than the one obtained in the EBR-strengthened beams. In fact, the flexural strength increase in the NSM-strengthened beam models presents a reasonable agreement with the value of 50% (computed based on ACI 440.2R-08 [56]) considered for designing the CFRP area. As mentioned in section 6.4.3.1, the higher flexural strength increase obtained in the EBR-strengthened beams is related to the fact that the CNR-DT200/2013 [100] underestimated their strength.

The results presented in Figure 6.13 and Figure 6.14, which are in general agreement with those obtained for the EBR-strengthened beams, showed that (i) the beams subjected to an uniformly distributed load presented slightly higher strength than those subjected to a concentrated load, and (ii) for both loading types, the beams strengthened with partially bonded CFRP strips exhibited higher strength with increasing bonded lengths.

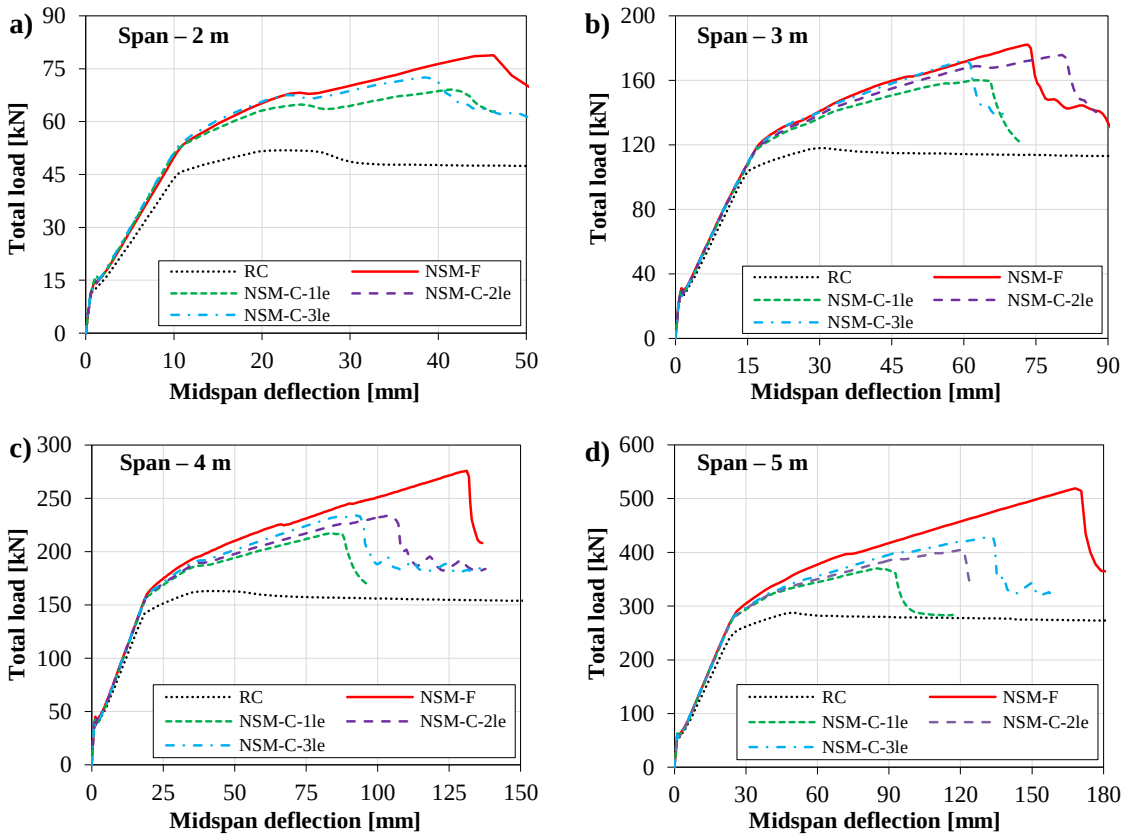

Figure 6.13: NSM CFRP-strengthened beams subjected to point load: total load vs. midspan deflection curves for spans of a) 2 m, b) 3 m, c) 4 m, and d) 5 m.

In Figure 6.15 the relationship between the strength reduction due to the partial bonding and the l_a/L ratio is illustrated for both loading cases and all spans. As expected, it can be concluded that the partial bonding procedure is considerably more effective in the NSM strengthening system compared to the EBR, *i.e.*, for similar l_a/L ratios the strength reduction experienced in the NSM-strengthened beams is lower than that of the EBR counterparts. As an example, when the CFRP bonded length is only 10% of the free span length (l_a/L = 0.10), the strength reduction for the NSM varied between 7% and 22%, whereas that for the EBR it ranged between 20% and 40%. Figure 6.15 also shows that, despite the curves obtained for the different beam lengths were not perfectly coincident, the relationship between the strength reduction due to the partial bonding and the l_a/L ratio followed a similar behaviour for all the geometries tested. As for the numerical results obtained in EBR-strengthened beams (*cf.* section 6.4.3.1), the data presented in Figure 6.15 will be also used in a simplified methodology for the design of fire protection systems (*cf.* section 6.4.4).

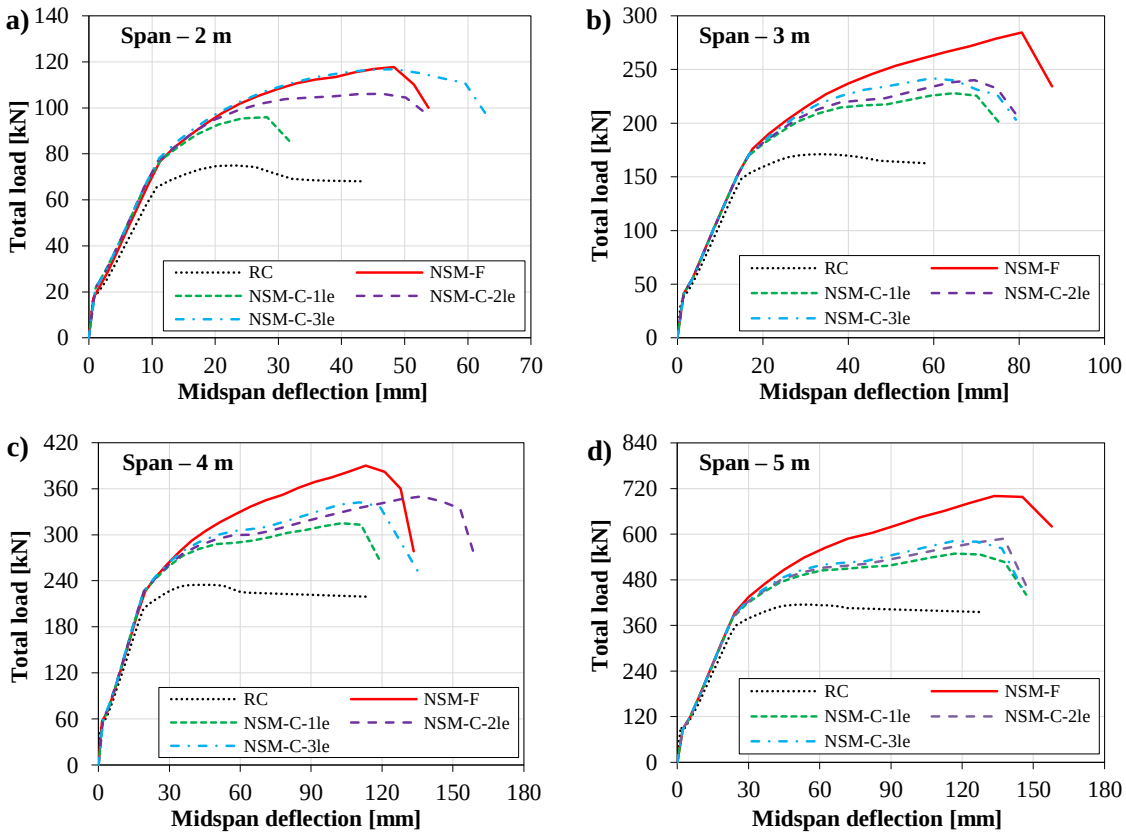

Figure 6.14: NSM CFRP-strengthened beams subjected to uniformly distributed load: total load vs. midspan deflection curves for spans of a) 2 m, b) 3 m, c) 4 m, and d) 5 m.

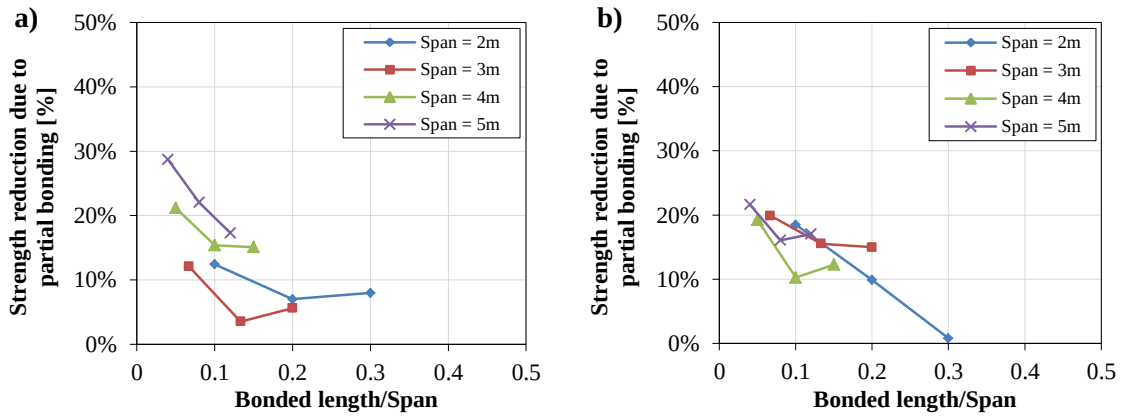

Figure 6.15: NSM CFRP-strengthened beams subjected to a) point load and b) uniformly distributed load: strength reduction due to partial bonding vs. bonded length/span.

6.4.3.3 Crack distribution and failure modes

The crack distribution and failure modes obtained in the numerical simulations performed at ambient temperature, although not providing direct input for the design procedure of fire protection systems (*cf.* section 6.4.4), allow understanding in further depth the effects on the structural response of the RC beams associated with the cable behaviour of the strengthening system. Figure 6.16a and Figure 6.16b illustrate the deformed shape and the final crack distribution of the fully

and partially bonded EBR-strengthened beams (with 2 m of span and subjected to a point load), respectively, at the instant when the CFRP strip debonded. Similar results were obtained for the longer beams and uniformly distributed loads. Both figures illustrate the debonding of the CFRP strip, which led to a considerable softening of the load *vs.* displacement curves. As expected, in the partially bonded strengthened beams more cracks developed in the concrete along the unbonded length of the CFRP, together with a concentrated damage on the CFRP bonded length (Figure 6.16b), whereas in the fully bonded strengthened beams (Figure 6.16a), less cracks and a more uniform damage along the beam length were found.

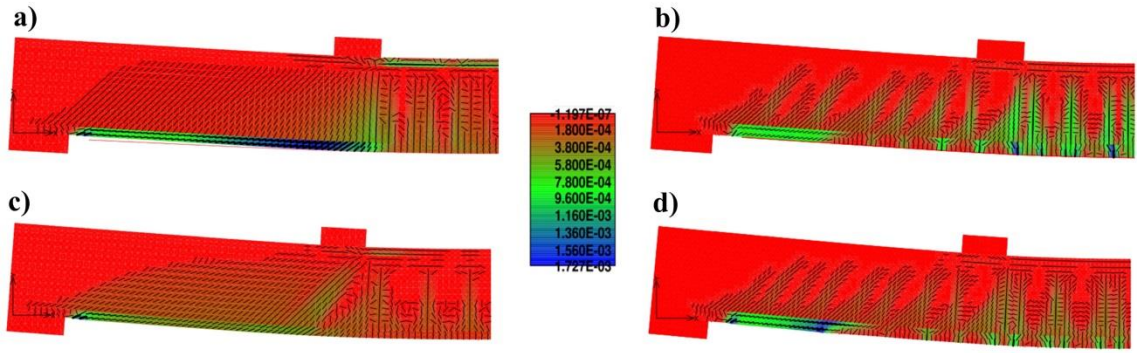

Figure 6.16: Crack opening distribution (in [m]) before the collapse load for strengthened beams: a) EBR-F; b) EBR-C-1le; c) NSM-F and d) NSM-C-1le.

Figure 6.16c and Figure 6.16d illustrate the corresponding deformed shapes and the final crack distribution of the fully and partially bonded NSM-strengthened beams (also with 2 m of span and subjected to a point load), respectively. Similar crack distributions to the ones described for the EBR beams can be observed in these figures. Regarding the failure mode, in both figures an explicit horizontal debonding at the tip of the CFRP strip is shown; this behaviour was expected since the frame element with bond-slip relationship does not allow simulating the vertical debonding of the strip.

6.4.4 Application to the design of fire protection systems

Figure 6.17a and Figure 6.17b show, for both loading cases, the relationship between the strength reduction due to the partial bonding and the ratio l_a/L obtained in the models of the EBR- and NSM-strengthened beams, respectively, plotted together with the proposed relations between the referred parameters; these relations were fitted to the numerical data using the minimum least square criterion.

The proposed relations provide a reasonable agreement with the numerical results and prompt the following comments: (i) the strength reduction decreases when the ratio l_a/L increases; (ii) the loading type does not present a relevant influence on the strength reduction of the partially bonded beams; and (iii) for similar l_a/L ratios, the strength reduction experienced by the NSM-strengthened

beams is considerably lower than that of the EBR-strengthened beams. It is worth mentioning that although the proposed relations have been determined based on numerical results of CFRP-strengthened beams with different spans and loading types, the strengthening levels were approximately constant. Further research is needed regarding the influence of the strengthening level on these relations.

The numerical results presented herein confirm that regardless of the strengthening technique used, the type of loading and the beam's dimension (namely at the full-scale level), partially bonded CFRP strengthening systems can in fact provide a considerable load bearing capacity, which can be significantly improved by increasing the bonded length at the extremities of the CFRP strips (*cf.* Figure 6.17). As the load applied in a fire situation is significantly lower than the ultimate load capacity of the structural member (typically, it ranges between 45% and 70% of the design load [16]), the results obtained in this investigation at ambient temperature provide further confirmation that a protection scheme that enables the strengthening system to behave as a cable during fire exposure (*i.e.* with thicker insulation in the anchorage zones) may ensure the required load bearing capacity for a certain period of time, provided that the mechanical properties of the materials (and interfaces) are not excessively reduced due to thermal degradation. It is worth pointing out that the CFRP debonding (from the concrete substrate) is expected to take place (based on previous tests [5, 68]) when the temperature at the epoxy adhesive reaches its glass transition temperature (typically around 45-60 ºC). Although higher temperatures occur along the central part of the beams (where thinner insulation is proposed) up to the instant when the CFRP system is lost (due to debonding at one of the anchorages zones), the influence of thermal effects on both concrete and steel reinforcement is not expected to be large; in fact, during the previous fire resistance tests [5, 68] (described in section 5.2 – page 99, in which similar insulation schemes were used), it was observed that in most cases the maximum temperature in the tensile steel rebars was lower than 100 °C.

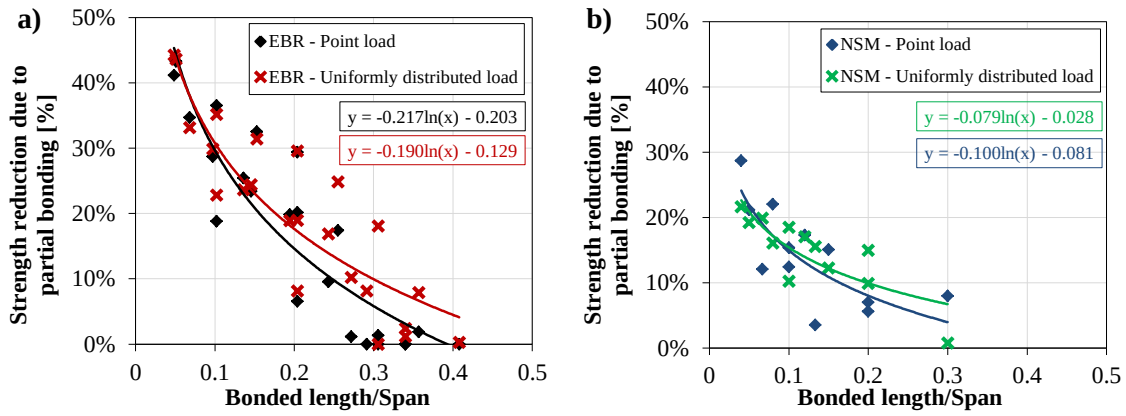

Figure 6.17: Proposed expression for the strength due to partial bonding vs. bonded length/span: (a) EBR-strengthened beams; (b) NSM-strengthened beams.

The methodology for the design of the thickness of the fire protection system is based on the following two main requirements, put forward in chapter 5: (i) the temperature of the CFRP strip along the central zone must remain below a certain temperature, which may be defined based on the developed stress level, together with its residual strength as a function of temperature; and (ii) the temperature of the CFRP-concrete interface along the anchorage length must be kept below a critical temperature, hypothesized as the T_g of the adhesive used in the strengthening system.

Based on the above mentioned requirements and on the numerical results obtained in the present study, the following design procedure is proposed:

1. The first step involves defining the load level that should be considered during the fire exposure, P_{fire}. For example, the simplified method described in the Eurocode 2 [16] suggests taking $P_{fire} = 0.7 \times P_d$, where P_d is the design load.
2. Then, for that load level, the maximum tensile stress in the CFRP strip at the central zone can be computed; this result, together with the data available in the literature about the residual strength of the CFRP material as a function of temperature (*e.g.* Wang *et al*. [27]), will allow for an approximate[7] definition of the maximum temperature this material may be subjected to, preventing its tensile rupture during a fire event.
3. A minimum thickness of the insulation system at the central zone of the strengthening system should then be prescribed (using a simple thermal model as the one described in chapter 5) in order to guarantee that the maximum allowed temperature in the CFRP is not achieved before the required time of fire exposure.
4. Regarding the thickness of the insulation system, in the anchorage zones of the CFRP strips, a similar design procedure should be employed; however, such insulation should be able to keep the temperature in the adhesive below its T_g. The length of this thicker insulation can be defined based on the ratio P_{fire}/P_d and the results presented in this section, namely the proposed relations plotted in Figure 6.17. In fact, as observed in [5, 68], the thicker insulation in the anchorage zones will impose the cable behaviour of the CFRP. In other words, during fire exposure, the strengthening system, which was initially fully bonded along its length, will behave as a partially bonded system and, therefore, will exhibit a certain strength reduction. Consequently, considering the defined ratio P_{fire}/P_d (0.7, as an example), a complementary value of the strength reduction due to the partial bonding (0.30 in the example) can be used to compute the required bonded length that will provide the necessary load bearing capacity during the pre-defined time of fire exposure (for the example above, according with the proposed equation in Figure 6.17a for point load, $l_a = 0.10\ L$).

[7] The term "approximate" is used because during fire exposure the initial stress level in the CFRP laminate is likely to present some variation due to the changes in the material properties with temperature, as well as the effects of damage progression. In this respect, further results are obtained and discussed in chapter 8 of this thesis.

6.5 CONCLUSIONS

The first part of this chapter (sections 6.2 and 6.3) presented an experimental and numerical study that allowed understanding in further depth the mechanical behaviour of CFRP-strengthened RC beams subjected to fire, namely in what concerns the cable behaviour observed in previous fire resistance tests. The results obtained allow drawing the following conclusions:

- Results of flexural tests on small-scale beams showed that at room temperature the influence of partially bonding the CFRP strips (only along the anchorage length) on the beam's stiffness is negligible, regardless of the strengthening technique (EBR or NSM).
- Results of those experimental tests showed also that for both strengthening techniques, the strength reduction at room temperature caused by partially bonding the CFRP strips is very limited: 15% and 6% for EBR and NSM strengthening techniques, respectively; in this regard, it is relevant that the failure mode of the strengthening system remained unchanged (end debonding phenomenon) for both EBR and NSM beams.
- The above mentioned slight reduction of mechanical performance confirms that during a fire the cable behaviour exhibited by CFRP-strengthening systems can in fact provide the necessary load bearing capacity, provided that the mechanical properties of the materials (in current zone) and interfaces (in the anchorages) are not excessively deteriorated due to elevated temperature. This points out the need to use appropriate insulation schemes, namely in the anchorage zones.
- Results of numerical simulations presented a very good agreement with experimental data, in terms of load *vs*. deflection curves, stiffness and strength, thereby providing further demonstration of the cable behaviour.

The second part of this chapter (section 6.4) presented numerical investigations about the mechanical behaviour at ambient temperature of full-scale CFRP-strengthened RC beams. The results obtained provided relevant data that was incorporated in a simplified methodology for the design of fire protection systems of CFRP-strengthened RC flexural members. The following main conclusions are drawn from this study:

- The numerical results presented a similar tendency to experimental data previously obtained at the small-scale level (section 6.2), confirming the main consequences of partially bonding the CFRP strips: limited effect on the beam's stiffness and relatively small strength reduction, regardless of the strengthening technique (EBR or NSM), confirming that the CFRP cable behaviour can in fact provide a considerable load bearing capacity.
- Although the beams subjected to a uniformly distributed load presented slightly higher failure loads than the ones subjected to a point loading (either fully or partially bonded), for

the beam geometries considered, the strength reduction due to the partial bonding presents a similar relationship with the l_a/L ratio (bonded length/free span) for both load configurations.

- The partially bonded NSM-strengthened beams were significantly more effective than the EBR counterparts: when the CFRP bonded length was 10% of the free span length (l_a/L = 0.10), the strength reduction with NSM varied between 7% and 22%, whereas with EBR such reduction varied between 20% and 40%.
- Relations between the strength reduction due to the partial bonding and the l_a/L ratio (bonded length/free span) were calibrated for both loading cases and strengthening techniques at ambient temperature conditions. These relations, together with the previous recommendations proposed in chapter 5, were incorporated in a simplified procedure for the design of fire protection systems of full-scale RC beams strengthened with CFRP strips according to different application techniques (EBR or NSM) and loading types (uniformly distributed or point loading).

The next step in the current thesis comprises (i) fire resistance tests on CFRP-strengthened RC beams thermally insulated according to the procedure proposed (chapter 7) and (ii) the numerical simulations of those tests, considering the actual thermal degradation of the materials and interfaces (chapter 8). Those experimental and numerical investigations are expected to provide further confirmation of the adequacy of the safety concepts and strategies for the design of fire protection systems suggested in the present chapter.

CHAPTER 7

FIRE RESISTANCE TESTS ON RC BEAMS FLEXURALLY STRENGTHENED WITH CFRP STRIPS

7.1 INTRODUCTION

The research presented in this chapter aims at (i) improving the understanding of the fire behaviour of CFRP-strengthened beams, namely the structural effectiveness of the strengthening system during fire, (ii) validating the strategy for the design of fire protection systems proposed in chapter 5, in particular with regard to the "critical temperature" in the anchorage zones (*i.e.*, the temperature for which the strengthening system loses its structural effectiveness), and (iii) comparing the fire performance of the EBR-strengthening technique with that of the alternative NSM. To this end, fire resistance tests were performed on RC beams flexurally strengthened with CFRP strips installed according to both EBR and NSM techniques. Different fire protection schemes were studied, comprising thinner insulation layers along the bottom soffit of the beams and thicker ones in the CFRP anchorage zones. Additionally, the (potential) beneficial effects of (i) applying mechanical anchorages at the extremities of the EBR-CFRP strips, (ii) using a high T_g adhesive on the fire performance of the EBR strengthening system, and (iii) using a mixed grout with cement and epoxy binders as bonding agent in NSM-strengthened beams were also evaluated.

The first part of this chapter (section 7.2) presents the experimental campaign on EBR-CFRP-strengthened RC beams, whereas in the second part (section 7.3) results from similar tests carried out on RC beams strengthened with NSM-CFRP strips are presented and compared with those obtained in the EBR counterparts.

7.2 EBR-STRENGTHENED RC BEAMS

7.2.1 Test specimens

The experimental programme consisted of nine fire resistance tests conducted in an intermediate scale furnace on RC beams flexurally strengthened with CFRP strips installed according with the EBR technique. As a reference, an unstrengthened RC beam (beam RC) was also tested. The beams were 1.50 m long, 0.10 m wide, 0.12 m deep (*cf.* Figure 7.1a to c) and were cast with ready-mixed

concrete, produced in a concrete plant with limestone aggregates and Portland cement type CEM II/A-L 42.5R. The following average mechanical properties of concrete were determined at an age representative of the fire resistance tests (279 days): average compressive strength in cylinders of f_{cm} = 37 MPa, average splitting tensile strength of f_{ctm} = 3.6 MPa, and average elastic modulus of E_{cm} = 31 GPa. The internal steel reinforcement, with a cover of 1.5 cm, consisted of four ϕ6 mm longitudinal rebars and ϕ6 mm transverse stirrups distanced of 0.06 m (*cf.* Figure 7.1b and c), presenting the following mechanical properties (provided by the manufacturer): characteristic yielding strength of f_{syk} = 546 MPa, average failure stress of f_{sum} = 703 MPa, and average elastic modulus of E_{sm} = 193 GPa.

The strengthening system for flexure comprised CFRP strips, epoxy bonding adhesives (two different adhesives were used, epoxy 1 and epoxy 2) and, in two of the tested beams (beams A-0-0 and A-50-25), bolted steel plates as mechanical anchorages for the CFRP strips (as illustrated in Figure 7.1a and Figure 7.1c). Epoxy 1 is a conventional adhesive used in CFRP strengthening systems and epoxy 2 is a high T_g adhesive. A detailed description of the strengthening system and constituent materials is provided in section 7.2.2.

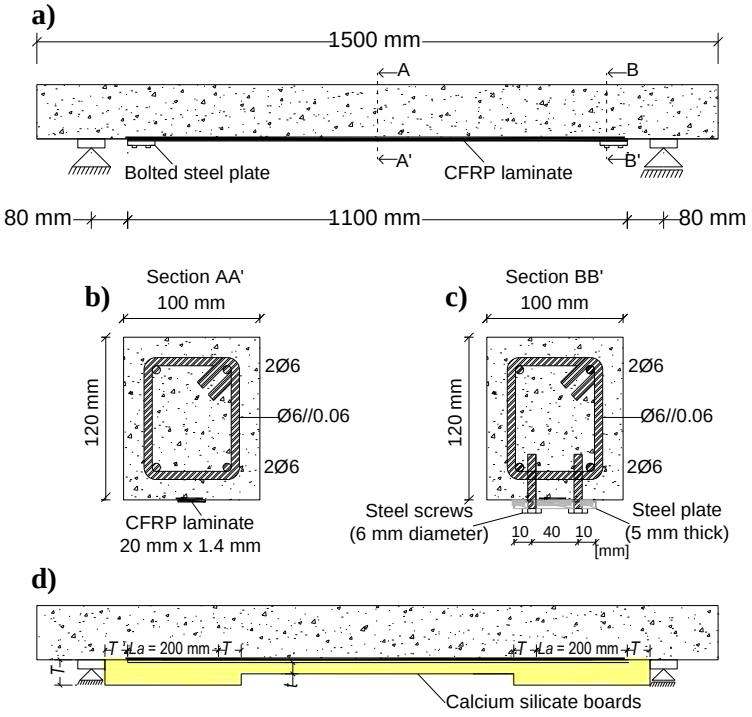

Figure 7.1: Geometry of the EBR-strengthened beams: a) longitudinal view of the specimen with mechanical anchorages on the CFRP strip extremities; b) current cross section; c) cross section with mechanical anchorage; d) longitudinal geometry of the fire protection system.

The fire insulation systems consisted of calcium silicate (CS) boards, with thicknesses ranging from 25 mm to 75 mm, applied on the bottom surface of the beams. As depicted in Figure 7.1d, and according to the fire protection strategy described in chapter 5, the passive fire protection systems

used in this study exhibited variable thickness along the length, being typically thicker in the anchorage zones of the CFRP strips (thickness *T* in Figure 7.1d) and thinner at the central zone (thickness *t* in Figure 7.1d). In section 7.2.3, a more comprehensive description of the fire insulation systems is provided.

The nomenclature adopted for the CFRP-strengthened beams (Table 7.1) is related to the following characteristics: (i) geometry of the insulation system applied (dimensions *T* and *t*); (ii) type of adhesive used (epoxy 1 – conventional adhesive, or epoxy 2 – high T_g adhesive); and (iii) presence of mechanical anchorages at the strip extremities. The first number of the nomenclature (*cf.* Table 7.1) corresponds to the dimension *T* and the second one to the dimension *t* (*cf.* Figure 7.1d - both in millimetres). As observed in Table 7.1, different combinations of the parameters *T* and *t* were tested, which allowed for a systematic evaluation of the effectiveness of applying thicker insulation in the CFRP anchorage zones on the fire resistance of the strengthening system (*i.e.* the time of fire exposure until the CFRP system loses its structural effectiveness). When the high T_g adhesive (epoxy 2) was used, the corresponding beam was identified by the suffix "T_g". The presence of bolted steel plates at the CFRP strip extremities was identified by the letter "A".

Table 7.1: Details of the EBR-strengthened beams tested under fire.

Beam	**Adhesive type**	**Mechanical anchorage**	**Fire protection thickness [mm]**	
			Anchorage zone (*T*-Figure 7.1d)	**Current zone (*t*-Figure 7.1d)**
RC	-	-	-	-
0-0	Epoxy 1[1]	-	0	0
25-0			25	0
25-25			25	25
50-25			50	25
75-25			75	25
75-50			75	50
50-25-Tg	Epoxy 2[2]		50	25
A-0-0	Epoxy 1[1]	Bonded steel plate	0	0
A-50-25			50	25

[1] Conventional epoxy adhesive for CFRP strengthening systems; commercial designation *S&P Resin 220* (detailed description provided in section 3.2.1.2, page 48).

[2] High T_g epoxy-based adhesive; commercial designation *Araldite 2014-1* (detailed description provided in section 7.2.2).

7.2.2 Strengthening system

The CFRP strips used as externally bonded reinforcement, with the commercial designation *S&P Laminates CFK 150/2000*, have a cross-section of 20 mm (width) × 1.4 mm (thickness), and a total length of 1100 mm (*cf.* Figure 7.1a). The adopted CFRP length, besides being in agreement with

the guidelines for detailing EBR-CFRP systems [56, 99, 100], allowed exposing directly to heat the entire length of the strengthening system during the fire resistance tests (a detailed description of the test setup is provided in section 7.2.4). The CFRP strips are constituted by unidirectional carbon fibres (about 70% in weight) embedded in an epoxy resin matrix. Their average tensile properties and T_g (88 °C) were already presented in section 3.2.1.2 – page 48.

The epoxy 1 is a two-component epoxy-based adhesive currently used for CFRP strengthening applications, with the commercial designation *S&P Resin 220*. The average tensile properties, the T_g (47 °C) and T_d (380 °C) of this ambient temperature curing adhesive were also presented in section 3.2.1.2 – page 48.

The epoxy 2 is also a two-component epoxy-based adhesive, with the commercial designation *Araldite 2014-1*, which is typically used for bonding metals or FRP components exposed to relatively high temperatures. Its tensile modulus and strength are respectively E_a = 4.4 GPa and f_{at} = 26 MPa (determined by the manufacturer according to ISO-527-2 [102]). The manufacturer reports a T_g of 85 ºC, determined through differential scanning calorimetry (DSC) tests performed according to ISO-11357-2 [142]. This T_g, which cannot be directly compared with those determined through DMA tests, was obtained on adhesive specimens cured for 24 hours at 20 ºC plus 1 hour at 80 ºC. These curing conditions were also adopted for beam 50-25-Tg, in which this adhesive was used.

The CFRP-strengthened RC beams were prepared as follows (in a similar procedure to that used in EBR specimens for the bond tests, *cf.* section 3.2.1.3 – page 49): the superficial layer of the concrete was removed with needle scalers, exposing the first layer of aggregates; the residues from the previous procedure were removed with compressed air; the bonding adhesive was applied on both the concrete surface and the strips (total thickness of about 2 mm); the strips were then applied and pressed against the concrete surface. In beams A-0-0 and A-50-25, the anchorage systems comprised a square steel plate (class S235, 60 mm × 60 mm, 5 mm thick), which was fixed to the concrete by means of 4 self-screwing steel bolts (grade 19MnB4, diameter of 6 mm, and positioned as showed in Figure 7.1c) while the epoxy adhesive was still wet. These screws were tightened with a torque of 20 N.m and the center of the anchoring plate was positioned at a distance of 3 cm from the end of the CFRP strip. This mechanical anchorage system was similar to that used in the experimental campaign presented in section 3.2 – page 48.

Four point bending tests performed at ambient temperature in beams similar to those presented here (with epoxy 1 and without mechanical anchorages, presented in section 6.2 – page 118), showed that the CFRP strengthening system provided a flexural strength increase of 74% (when compared to the RC beam). This strengthening level is higher than the limits established in most design recommendations (40-60%); however, in several CFRP strengthening applications, namely those

that are prior to the most recent design guidelines, the above-mentioned limits were not respected. Furthermore, in the present study, the authors intended to simulate a situation in which the CFRP contribution for the load level applied during fire is needed to prevent the beam's failure, as discussed in section 7.2.4.2.

7.2.3 Fire insulation systems

The fire insulation systems comprised CS boards, with the commercial designation *Promatect-L500*, which are made of agglomerated calcium silicate. The CS boards were bonded to the bottom soffit of the beams with fire resistance mastic and mechanically fixed using U-shaped thin steel plates distanced of approximately 0.20 m. These plates were fixed to the lateral faces of the beams with small metallic screws. According to the technical sheet of the supplier [125], the CS boards exhibit the following properties at ambient temperature (20 °C): dry density of ρ_{CS} = 450 kg/m^3; thermal conductivity of λ_{CS} = 0.09 W/(m.K); and specific heat capacity of $C_{p,CS}$ = 815 J/(kg.K). The variation with temperature of these properties, also provided by the manufacturer, can be found in chapter 5 (Figure 5.5 – page 105). It is worth mentioning that the fire insulation systems were applied only at the bottom surface of the beams due to the fact that only this area was directly exposed to heat (*cf.* section 7.2.4.1). The thickness of the insulation varied between 25 mm and 75 mm, in some cases being different in the anchorages zones of the strengthening system and in the central part of the beam, as described in Table 7.1. As mentioned, the adopted insulation schemes aimed at validating the strategy for the design of fire protection systems suggested in chapter 5, namely exploiting the CFRP cable behaviour by preventing (i) the tensile rupture of the CFRP strip at the central zone, and (ii) the CFRP debonding in the anchorage zones. Regarding the length of the thicker insulation in the anchorage zones, it was decided to protect a length of l_a = 200 mm (*cf.* Figure 7.1d), which is approximately the recommended anchorage length (l_e) determined as suggested in CNR-DT200 guidelines [100].

7.2.4 Test setup, instrumentation, and procedure

7.2.4.1 Thermal loading

The fire resistance tests were performed on a vertical furnace powered by propane gas, with external dimensions of 1.35 m (length) × 1.20 m (width) × 2.10 m (height). The tested beams were placed over the opened top of the furnace, as showed in Figure 7.2. The beam's supports (6 cm long × 10 cm wide) were positioned over metallic plates, above the furnace's external walls (Figure 7.2b). Those metallic plates were suspended with four ϕ24 mm steel rods on a steel reaction frame, which was erected surrounding the furnace (Figure 7.2a).

Concerning the thermal boundary conditions, the bottom face of the beams was directly exposed to the standard fire time-temperature curve defined in ISO 834 [6], whereas their top face was submitted to ambient temperature. In order to seal the lateral openings of the furnace, two insulation covers made of ceramic wool were placed adjacently to the beams (Figure 7.2c). A preliminary test (performed at ambient temperature before the fire tests) demonstrated that the lateral insulation did not restrict the vertical displacement of the beams. At the beginning of the fire resistance tests, the bottom surface of this lateral insulation system was located approximately 5 cm below the bottom surface of the beams. Consequently, although the vertical deflection of the beams increased with heating (*cf.* section 7.2.5.3), only their bottom face was directly exposed to heat; these test conditions actually simulate the thermal exposure typically found on one-way slabs.

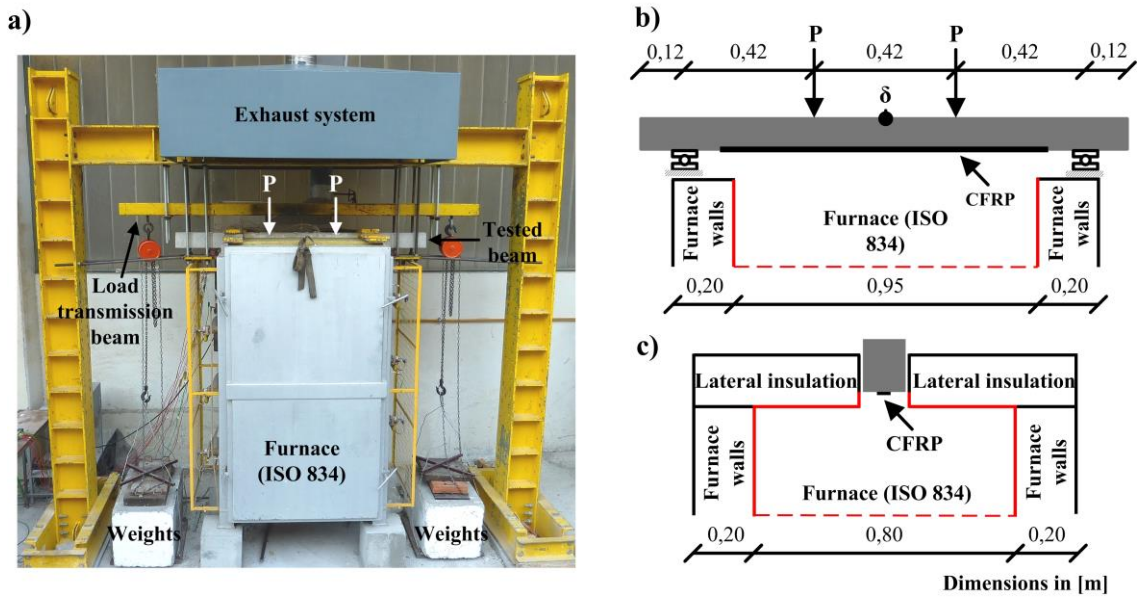

Figure 7.2: Test setup: a) general view of the furnace tests; b) longitudinal and c) transversal schematic views of the test setup.

7.2.4.2 Structural loading

During the fire resistance tests all the specimens were simply supported and loaded in a four point bending configuration, as illustrated in Figure 7.2a and b. The mechanical (gravity) load was applied by means of two sets of weights, suspended at the ends of a load transmission steel beam with pulley blocks (Figure 7.2a), which guaranteed a constant load during the test. The load transmission beam, placed over the tested beams, transferred the load to the top surface of the concrete beams through two tubular steel profiles with a contact area of 5 cm long × 10 cm wide.

The total load applied in the fire resistance tests (P_{fire}, Table 7.2) was defined based on the recommendations of Eurocode 2 (part 1-2) [16], which suggest that the mechanical action during fire can be simply determined as 70% of the design load at ambient temperature (P_d, Table 7.2),

corresponding to a load level that is slightly lower than the maximum value indicated in the standard (75% of P_d).

In the present study the design load for the unstrengthened beam (P_d^{RC}, Table 7.2) was computed based on the Eurocode 2 (part 1-1) [138], whereas that of the RC beams flexurally strengthened with EBR-CFRP strips was determined based on the CNR-DT200 Italian guidelines [100]. Table 7.2 shows the total load applied during fire (P_{fire}), the design load (P_d), the failure load (P_u) obtained at ambient temperature (with a similar test setup, *cf.* section 6.2 – page 118) and the ratios between those load values for both types of beams (unstrengthened and strengthened beams). It is worth pointing out that the beam's self-weight (very low, about 0.4 kN) was not included in those figures. As observed in Table 7.2, the load level applied during the fire resistance tests when compared to the failure load at ambient temperature (exemplified by the ratio P_{fire}/P_u) was similar in both unstrengthened and strengthened beams (0.38 and 0.36, respectively). The ratio $P_{fire}/P_u^{RC} = 0.62$ for the strengthened beams indicates that the loss of the CFRP strengthening system would not necessary mean the structural failure of the beam, since the failure load of the unstrengthened beam (at ambient temperature) is higher than the load applied during the fire tests (in fact, as discussed later, when the CFRP system debonds the thermal degradation in the unstrengthened member is relatively low). Regarding the ratio P_{fire}/P_d^{RC} for the strengthened beams, it can be observed that such ratio is higher than 1.0, which means that in a typical design scenario the unstrengthened beam would not be able to guarantee the necessary load bearing capacity when subjected to the fire load combination (P_{fire}). This result is due to the high flexural strength increase provided by the strengthening system (74%, above the design guidelines recommendations) which, as mentioned in section 7.2.2, was intentionally set to make it necessary to take into account the CFRP mechanical contribution during fire.

The total load applied during fire (P_{fire}) imposed a maximum CFRP strain of $\varepsilon_f = 1.1$ ‰ (measured at ambient temperature), which corresponds to 10% of its ultimate strain (also at ambient temperature). This means that, as expected, for the fire load combination, the strain/stress installed in the CFRP strip was relatively low (208 MPa).

Table 7.2: Design load (P_d) and (average) failure load (P_u) at ambient temperature, total load applied during the fire tests (P_{fire}) and corresponding ratios (excluding the beams' self-weight).

Specimen	Design load at 20 °C (P_d) [kN]	Failure load at ambient temperature (P_u) [kN]	Fire load (P_{fire}) [kN]	P_{fire}/P_d^{RC}	P_{fire}/P_u	P_{fire}/P_u^{RC}
Control beam (beam RC)	10.3[1]	18.9	7.2	0.70	0.38	0.38
Strengthened beams (EBR)	16.7[2]	32.9	11.7	1.14	0.36	0.62

[1] Computed based on the Eurocode 2 (part 1-1) [138];

[2] Computed based on the CNR-DT200 Italian guidelines [100].

7.2.4.3 Instrumentation

The instrumentation of the tested beams consisted of an electrical displacement transducer (from *TML*, model *CDP*-500 with a stroke of 500 mm) for measuring the midspan displacement at the top (cold part) of the beam (δ, in Figure 7.2b) and a set of 15 thermocouples (type K, with external diameter of 1 mm), whose nomenclature and location are shown in Figure 7.3. These sensors were used in all tested beams to measure the temperatures in the concrete, steel rebars and air above the top surface at the midspan section (thermocouples T1 to T7, *cf.* Figure 7.3b), and in the adhesive along the bonded length (thermocouples T8 to T14, *cf.* Figure 7.3a and Figure 7.3b). An additional thermocouple was placed between the CFRP strip and the CS boards at the midspan section (thermocouples T15, *cf.* Figure 7.3b).

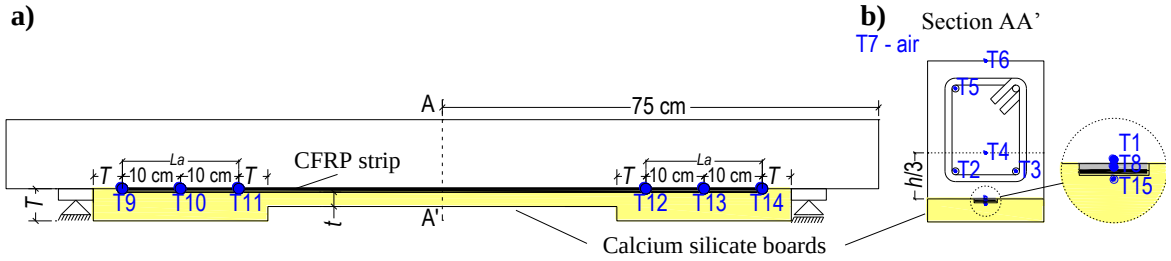

Figure 7.3: Position of the thermocouples a) in the adhesive along the bonded length and b) in the midspan section.

7.2.4.4 Test procedure

The fire resistance tests started with the application of the structural loading, as showed in Figure 7.2a. After a period of about 30 min, set in order to guarantee the stabilization of the deflections[8], the bottom surface of the beams started to be thermally loaded, as detailed in section 7.2.4.1 and showed in Figure 7.2c. The burners of the furnace were turned off a few minutes after the CFRP strengthening system lost its structural effectiveness; as discussed in section 7.2.5.3, the debonding of the strengthening system was clearly detected on the midspan displacement *vs*. time curves. Note that in the unstrengthened beam (beam RC), the test was carried out for approximately 90 min; this test duration provided sufficient data (in terms of midspan displacement) as a comparative reference for the strengthened beams.

7.2.5 Results and discussion

7.2.5.1 Temperatures vs. time of fire exposure

Figure 7.4 illustrates the temperatures measured as a function of the time of fire exposure at different positions of two representative beams, 25-0 (Figure 7.4a) and A-50-25 (Figure 7.4b). As illustrated in Figure 7.4a, the furnace temperature accurately followed the ISO 834 [6] standard fire

[8] In most cases the stabilization of the deflections was observed after shorter periods.

curve (although presenting some differences in the first instants, the deviation is well within the bounds defined in the test standard). In all the remaining tests, the furnace temperature *vs.* time curves presented a similar behaviour to that showed in Figure 7.4a. Regarding the temperatures at the bottom steel rebars (thermocouples T2 and T3, *cf.* Figure 7.3b) measured in beam 25-0 (Figure 7.4a), it can be observed that in both rebars the temperature increased at a similar rate, exhibiting a small plateau at 100 °C (between 11 minutes and 13 minutes) caused by the water vaporization in the surrounding concrete. During the test of beam 25-0, the maximum temperature attained in the steel rebars was lower than 300 °C and when the CFRP strengthening system debonded such temperature was 126 °C. In fact, in all the tested beams, when the CFRP system lost its structural effectiveness the temperatures in the steel rebars were always lower than 126 °C (*cf.* Table 7.3), and therefore the thermal-induced degradation on its mechanical properties can be considered negligible [16]. Concerning the temperature in the adhesive at the midspan section of beam 25-0 (measured by T8, *cf.* Figure 7.4a), it increased at a significantly higher rate compared to the anchorage zones (measured by T10 and T13), where a 25 mm thick CS board was applied. In this beam, at the midspan section the adhesive T_g was exceeded after less than 2 minutes of fire exposure, however the CFRP strengthening system kept its structural effectiveness for up to 15 min. At that duration, the temperature in the adhesive was approximately 400 °C at midspan (T8), whereas in the anchorages zones (T10 and T13) the temperatures were in the range of the adhesive T_g, as showed in Figure 7.4a. These temperatures indicate that along the uninsulated length of the beam the bond between the CFRP and the concrete was lost in an early stage of fire; however, the CFRP system maintained its effectiveness through a cable behaviour, with the CFRP strip fixed in the anchorages zones, where the temperatures at the CFRP-concrete interface were much lower, remaining below the adhesive T_g for a longer period of fire (further demonstration of this behaviour is provided in section 7.2.5.4 – page 155). It is worth mentioning that the CFRP temperature at the midspan was not sufficiently high to induce its tensile failure, allowing the CFRP to behave as a cable until the debonding of the strengthening system (as discussed in section 7.2.5.4 – page 155). Such temperature was not directly measured in this particular beam, hence it was estimated to lie between the adhesive temperature (T8, lower bound) and the furnace temperature (upper bound), being more likely closer to the former.

For the beams comprising insulation with varying thickness, Table 7.3 shows a similar relationship between the adhesive temperature at the midspan section (T8) and in the anchorage zones to that observed in beam 25-0. As expected, when a thin insulation was applied at the central zone of the beams, the temperatures measured in the adhesive in such location were considerably lower than those observed in beams where that length was left uninsulated. This table also lists the temperature range in the CFRP strip at the debonding instant. The results presented attest the efficacy of the

insulation schemes in limiting the maximum temperature in the CFRP strip at the current zone, which prevented its tensile failure (as discussed in section 7.2.5.4 – page 155).

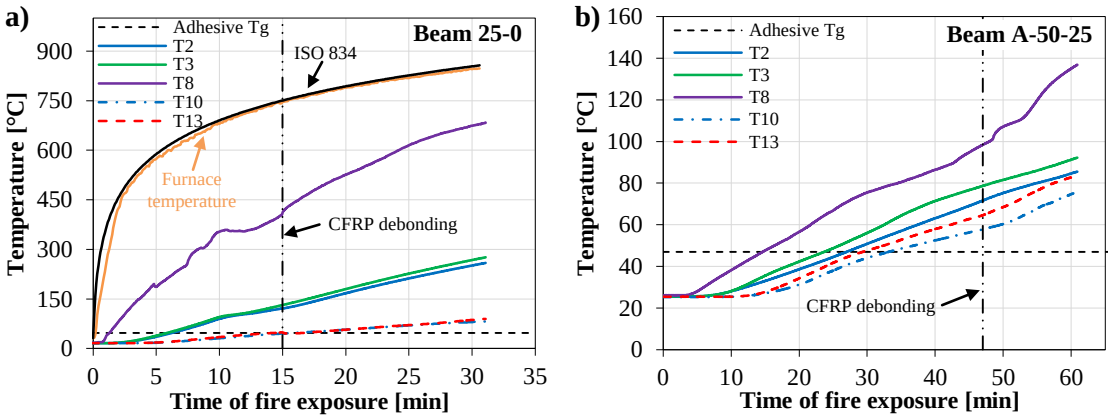

Figure 7.4: Examples of measured temperature vs. time of fire exposure: a) beam 25-0 and b) beam A-50-25.

Table 7.3: Temperatures when the EBR-CFRP strengthening system debonded - midspan section of the beams (tensile steel rebars and adhesive) and anchorage zones (in the adhesive); corresponding time of fire exposure for the debonding of the CFRP strengthening system.

Beam	Temperatures at the midspan when the CFRP system debonded [°C]			Temperatures in the anchorage zones when the CFRP system debonded [°C]		Time for the debonding of the CFRP strengthening system [min]
	Tensile steel rebars (average T2, T3)	Adhesive (T8)	CFRP strip (temperature range)	Left anchorage (average T9, T10, T11)	Right anchorage (average T12, T13, T14)	
0-0	24	114	114[1] – 437[2]	69	63	2
25-0	126	405	405[1] – 742[2]	58	63	15
25-25	48	72	72[1] – 114[3]	46	58	18
50-25	92	107	107[1] – 181[3]	43	71	40
50-25-Tg	107	167	167[1] – 216[3]	77	84	65
75-25	83	114	114[1] – 149[3]	55	66	62
75-50	74	91	91[1] – 96[3]	42	58	70
A-0-0	32	161	161[1] – 468[2]	93	96	4
A-50-25	76	99	99[1] – 172[3]	64	68	47

[1] Adhesive temperature at the midspan (T8);

[2] Furnace temperature;

[3] Temperature between the CFRP strip and the CS boards at the midspan section (T15).

Figure 7.4b exemplifies the effects on the temperature distribution of combining a thin insulation at the central zone of the beam (25 mm CS board) with a thicker one (50 mm CS board) in the CFRP anchorage zones. Compared to Figure 7.4a, it can be seen that temperatures in the steel rebars and in the adhesive were lower and increased at a lower rate, explaining why the effectiveness of the CFRP strip was lost after a longer period of fire exposure (47 min). Similarly to what was observed

in beam 25-0, when the strengthening system of beam A-50-25 lost its structural effectiveness, temperatures in the CFRP-concrete interface at the central zone of the beam were considerably higher than the adhesive T_g, again suggesting that the CFRP strip behaved as a "cable" following the loss of bond with concrete along the central zone. In this beam, the debonding of the CFRP strip from the anchorage zones occurred when the adhesive temperature in those zones (measured by thermocouples T10 and T13, Figure 7.4b) was slightly higher than its T_g (around 60 °C). Although it would be expected that in this beam the mechanical anchorages applied at the CFRP ends would improve the bond performance of the strengthening system, these temperatures were only slightly higher than those measured in the beams without these devices (*cf.* Table 7.3).

7.2.5.2 Temperatures along the bonded interface when the CFRP system debonded

Figure 7.5a shows for all beams tested the temperatures along the bonded interface (measured by the thermocouples T8 to T14) when the CFRP strengthening system debonded from the beams' soffit. As expected, beams with thicker insulation at the CFRP anchorages zones (compared to the current zone) exhibited higher temperatures at the central zone, in most cases considerably higher than the adhesive T_g (47 °C), indicating higher thermal degradation of the adhesive layer; in beam 25-0 this result could be clearly noticed.

Regarding the temperatures obtained in beam A-0-0, it can be observed that the overall temperature distribution is, in general, above the temperature recorded in the remaining beams. In fact, it was expected that the mechanical anchorage would improve the bond performance of the CFRP system under fire, therefore allowing the adhesive to experience higher temperatures before the CFRP system would lose its mechanical effectiveness. However, in beam A-50-25 the mechanical system was not so effective as in beam A-0-0, since in the former specimen the temperatures at the CFRP-concrete interface were only slightly higher than those obtained in the beams without mechanical anchorage. This result can also be observed in Figure 7.5b, where the average temperature along the hotter anchorage zone at the debonding instant is plotted for all the tested specimens (also listed in Table 7.3): 96 °C ($2.0 \times T_g$) in beam A-0-0 *vs.* 68 °C ($1.4 \times T_g$) in beam A-50-25.

With the exception of beam 50-25-Tg, in which the average temperature in the anchorage zone was approximately the adhesive T_g (85 °C, determined from DSC), the remaining beams exhibited average temperatures in the anchorage zones that are slightly to moderately higher than the adhesive T_g (47 °C, determined from DMA), ranging from 58 °C ($1.2 \times T_g$) to 69 °C ($1.5 \times T_g$).

In what concerns the maximum temperatures in the CFRP strip attained in the current zone, due to the protection schemes used, they were much higher than in the anchorage zones: maximum values attained ranged between 405 and 702 ºC, without causing tensile failure of the CFRP strip in any of the beams tested (as discussed in section 7.2.5.4).

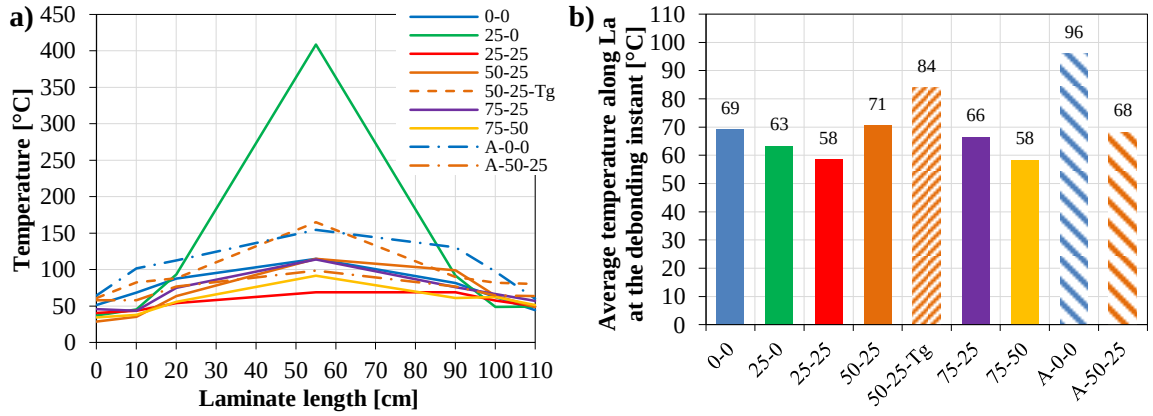

Figure 7.5: Temperatures in the adhesive when the EBR-CFRP system debonded: a) along the bonded interface; b) average along the anchorage length.

7.2.5.3 Midspan displacement increase

Figure 7.6 presents the midspan displacement increase of all CFRP-strengthened beams as a function of the time of fire exposure, in which the origin of the time scale corresponds to the beginning of the thermal exposure. The evolution of midspan displacement of the unstrengthened beam (beam RC) up to 50 min is also shown as a reference. As expected, the beams' midspan displacement increased with time (and temperature rise), due to stiffness (and strength) decrease of the materials.

The midspan displacement of beam 0-0 presented an instantaneous increase at 2 min of fire exposure due to the CFRP debonding (as addressed in section 7.2.5.4.), after which the mechanical properties of this beam became roughly similar to those of beam RC. Although the applied load in the strengthened beams was higher than that in beam RC (*cf.* Table 7.2 – page 149), the midspan displacement increase in beam 0-0 was approximately similar to that observed in the latter. The behaviour of beam A-0-0 (uninsulated with mechanical anchorages at the CFRP ends) was comparable to that of beam 0-0; however the CFRP debonding occurred 2 min later and was more progressive.

In the thermally insulated beams, the temperatures in the midspan zone were considerably lower (*cf.* section 7.2.5.1) and so was the stiffness (and strength) reduction. Therefore, accordingly, the midspan increase rate was lower than that observed in the uninsulated beams, both before and after the CFRP debonding. It is worth pointing out that in beam 25-0 the midspan increase rate was similar to that of beam 0-0, since the insulation system was applied only along the anchorage zone of the CFRP strip (*cf.* Table 7.1 – page 145), with the central zone remaining unprotected.

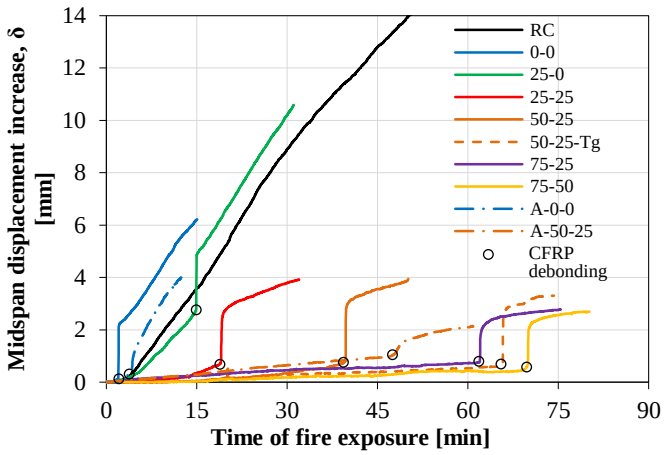

Figure 7.6: Midspan displacement increase vs. time of fire exposure.

7.2.5.4 Failure modes and post-fire assessment

Figure 7.7 illustrates three strengthened beams (specimens 0-0, 25-0 and A-0-0) after the fire resistance tests, illustrating the different failure modes of the CFRP system observed in the tests. The bottom face of beam 0-0 (Figure 7.7a) presented signs of thermal degradation, with the dark coloration being mostly due to the combustion of the CFRP system. This figure also shows that the strengthening system debonded at the left anchorage, where a cohesive failure occurred along about 10 cm of the CFRP extremity (failure surface located a few millimetres inside the concrete), with an adhesive failure being visible from that length towards the central zone of the beam. When the CFRP strip debonded, although the temperature distribution along the adhesive layer was approximately uniform (as showed in Figure 7.5a), slightly lower temperatures were measured at the CFRP extremities, therefore the adhesive preserved higher bond strength in the anchorage zones compared to the central zone, explaining the mixed cohesive-adhesive failure mode observed in beam 0-0. It is worth mentioning that this failure mode was observed only in this beam.

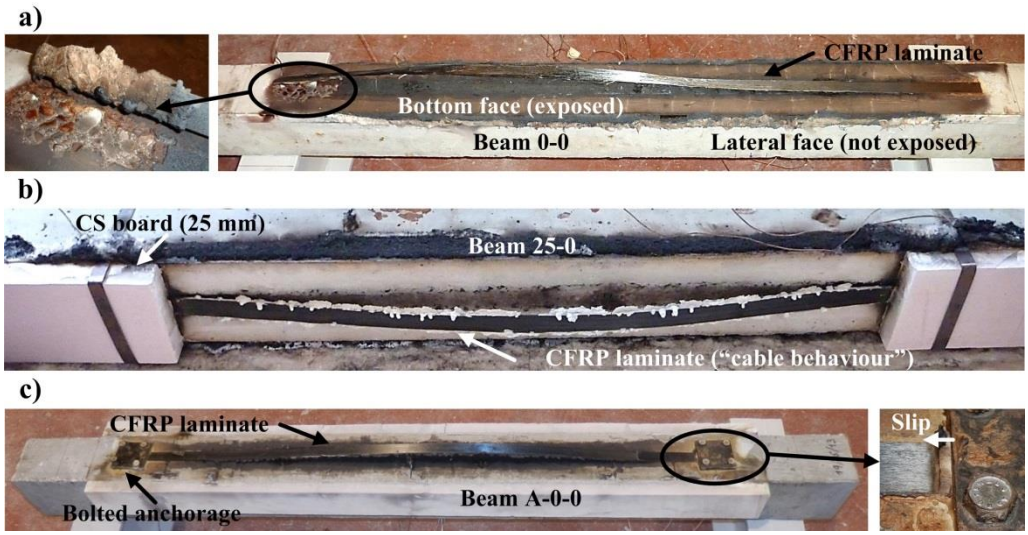

Figure 7.7: Examples of the failure modes of the CFRP strengthening system: a) beam 0-0; b) beam 25-0; c) beam A-0-0.

Figure 7.7b shows that in beam 25-0 the length of the CFRP strip that was directly exposed to the thermal action was completely detached from the concrete substrate after the test. As discussed in section 7.2.5.1 and showed in Figure 7.4a (page 152), the adhesive T_g at the midspan section was exceeded after only 2 min of fire exposure, therefore the CFRP-concrete bond was severely damaged since an early stage of the test. However, the CFRP strengthening system kept its structural effectiveness for up to 15 min. These results, together with Figure 7.7b, demonstrate that the CFRP strip transformed into a "cable" fixed in the anchorage zones, where the thermal degradation of the bonded interface was delayed by the 25 mm thick CS boards. As temperatures increased, the flexural stiffness of the beam decreased and, as a consequence, the midspan displacement increased (*cf.* Figure 7.6), as well as the tensile force in the "cable". The strengthening system of beam 25-0 lost its structural effectiveness after 15 min due to adhesive failure at the hotter anchorage zone; as showed in Table 7.3 (page 152), the average temperature in the adhesive in that anchorage zone was slightly higher than the adhesive T_g, more precisely $1.3 \times T_g$. Excluding specimens A-0-0 and A-50-25, similar behaviour and failure modes of the strengthening system were observed in all insulated beams.

Regarding the beams with mechanical anchorages applied at the CFRP ends (A-0-0 and A-50-25), the failure of the strengthening system was caused by the progressive slip of the CFRP strip under the anchorage plate (Figure 7.7c), which took place after the occurrence of adhesive failure at the concrete-adhesive interface at the central zone of the beams, with the CFRP strip also exhibiting the cable behaviour described above. This type of failure mode is in agreement with those observed in the double-lap shear tests presented in chapter 3 (*cf.* Figure 3.14 – page 62), where similar materials were used. In these beams the loss of structural effectiveness of the CFRP system was slightly delayed (between 2 and 7 min, compared to equivalent beams without anchorage system), which is associated mostly to the friction provided by the steel anchoring plates.

None of the beams tested presented tensile failure of the CFRP strips, in other words, the anchorage zone always governed the fire endurance of the strengthening system. This fact, together with the maximum temperatures attained in the CFRP strip in current zone (namely in beam 25-0) validate the methodology proposed for the design of fire protection systems.

7.2.5.5 Structural effectiveness of the EBR strengthening system during fire

The results presented in the previous sections allowed determining the exact instant when the strengthening system lost its structural effectiveness (Figure 7.6) and the corresponding temperature distributions along the CFRP bonded interface (Figure 7.5). The efficacy of the strategy adopted for the fire protection of the CFRP strengthening system can be assessed in Figure 7.8, which plots the time of fire exposure until the loss of the CFRP system. As observed in this figure, in the unprotected beam 0-0 the CFRP debonding occurred after only 2 min, confirming its

high susceptibility when exposed to fire. When the 25 mm-thick CS board was applied only in the CFRP anchorage zones (beam 25-0), the fire resistance of the strengthening system was considerably improved (to 15 min). When this insulation board was applied along the entire CFRP length (beam 25-25), the fire endurance of the CFRP system presented a small further increase (3 min to 18 min). With increasing thickness of CS board insulation, particularly in the CFRP anchorage zones (combined with a thinner layer at the midspan), the fire resistance of the strengthening system presented consistent and significant improvements. As an example, in beam 75-50 the debonding occurred after 70 min of fire.

As expected, the fire performance of the CFRP strengthening system improved when the high T_g adhesive was used (beam 50-25-Tg), as the reduction of its properties takes place at higher temperatures (compared to the conventional epoxy 1). The application of a mechanical anchorage allowed the CFRP system to retain its structural effectiveness for slightly longer periods of exposure, with fire endurances of 4 and 47 min being obtained respectively in beams A-0-0 and A-50-25.

The results presented herein confirm that is possible to exploit the structural effectiveness of CFRP strengthening systems during fire exposure. The application of thicker layers of insulation material in the anchorage zones of the CFRP strips allowed extending considerably the structural effectiveness of the strengthening system by exploiting the referred cable behaviour. These results provide an experimental validation to the strategy for designing fire protection systems for CFRP-strengthened RC members proposed in chapter 5 (which had been supported on numerical simulations). The temperature criterion for designing the thickness of insulation layers along the CFRP anchorage zones considered in chapter 5 consisted of limiting the adhesive temperature to its T_g in order to prevent the CFRP debonding for the required time of fire exposure. The results obtained in the present investigation show that this criterion is reasonably conservative: the debonding of the strengthening system occurred when the average temperature in the adhesive attained values from $1.2 \times T_g$ to $1.5 \times T_g$ (excluding the results of beams A-0-0, A-50-25 and 50-25-Tg), thus demonstrating that the "critical" temperature in the anchorage zones is slightly to moderately higher than the adhesive T_g. This can be further confirmed in Figure 7.9, which shows that in all beams tested the time for the adhesive T_g (obtained from DMA tests and computed based on the onset curve of the storage modulus) to be attained in the anchorage zones was always lower than the corresponding time for the loss of the CFRP system. Regarding beam 50-25-Tg, although a good agreement is also plotted, note that its T_g was obtained from a different method (DSC) compared to the remaining beams.

One last word to mention that the conclusions concerning the structural effectiveness of the strengthening system were drawn based on results of fire resistance tests in which the load level of all strengthened beams was maintained constant. However, as mentioned in section 7.2.4.2, the

adopted load level is only 5% lower than the maximum value suggested in Eurocode 2 (part 1-2) [16]. Consequently, the referred conclusions might be conservative, since in most cases the load level in fire situations should be lower than that adopted here. Additional experimental investigations are needed in order to obtain further understanding about the stress-temperature dependency of CFRP strengthening systems at elevated temperatures.

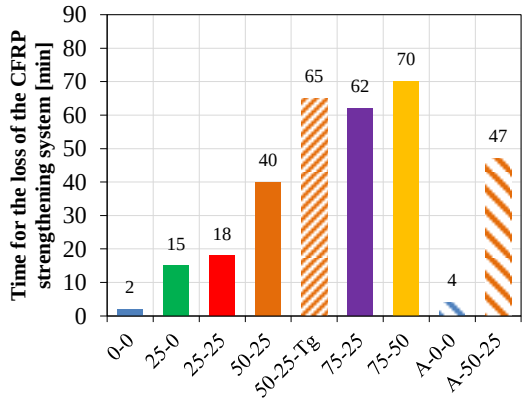

Figure 7.8: Fire resistance of the strengthening system.

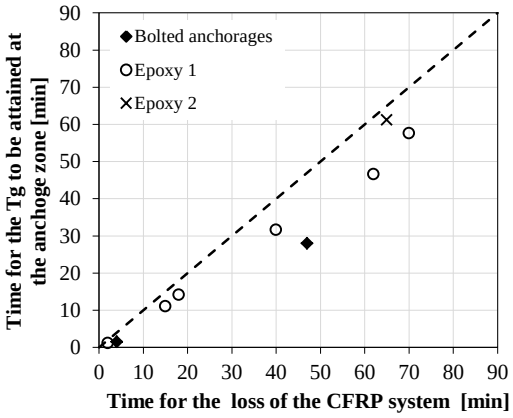

Figure 7.9: Comparison between the time for the adhesive T_g to be attained in the anchorage zone with the time for the loss of the CFRP system.

7.2.6 Summary of results

This section presented the results of fire resistance tests on RC beams flexurally strengthened with externally bonded (EBR) CFRP strips simultaneously subjected to a sustained load and the standard ISO 834 fire. The main results obtained were as follows:

- The fire resistance test conducted on the uninsulated EBR-strengthened beam confirmed the susceptibility of CFRP strengthening systems when exposed to high temperatures/fire; in this beam, the CFRP strip debonded after only 2 minutes of fire.
- When insulation boards were applied at the CFRP ends, the EBR strengthening system retained its structural effectiveness through a cable behaviour after the bonded interface was damaged in the central zone.
- The structural effectiveness of the CFRP strengthening system was considerably extended by applying thicker insulation boards in the CFRP anchorage zones and making use of the referred cable behaviour: with 25 mm thick CS boards applied only in those zones, the CFRP strip debonded after 15 min of fire exposure. When the thicker insulation at the CFRP extremities was combined with a thinner one along the central zone, a considerable improvement on the fire behaviour of the strengthening system was observed: in beam 75-50, the CFRP strip debonded after 70 min of fire exposure.
- Using a high T_g adhesive combined with the proposed fire insulation schemes allowed extending further the fire resistance of the CFRP system: in beam 50-25-Tg the debonding

of the strengthening system occurred 25 minutes later than in beam 50-25, where a conventional epoxy adhesive was used.

- The application of the mechanical anchorage at the CFRP ends, combined with the proposed fire insulation schemes, provided a slight improvement to the fire endurance of the strengthening system: the loss of structural effectiveness of the CFRP system was delayed through the friction provided by the steel anchoring plates; however the critical temperature in the anchorage zones was found to be only slightly higher compared to that of the corresponding beams without mechanical anchorage.
- For the beams tested and insulation schemes adopted, the debonding of the EBR-strengthening system occurred when the average temperature in the adhesive in the anchorage zones attained values ranging from $1.2 \times T_g$ to $1.5 \times T_g$, thus demonstrating that the critical temperature in the anchorage zones is slightly to moderately higher than the adhesive T_g (determined from DMA tests and based on the onset of the storage modulus curve).

7.3 NSM-STRENGTHENED RC BEAMS

7.3.1 Test specimens and materials

Eight fire resistance tests were conducted in an intermediate scale furnace to investigate the fire behaviour of RC beams flexurally strengthened with NSM-CFRP strips and thermally insulated with calcium silicate (CS) boards. The geometry of the specimens and the nomenclature adopted are shown in Figure 7.10 and Table 7.4, respectively. The test variables included: (i) the adhesive type (conventional epoxy adhesive - specimens identified by "EP", or a mixed grout made of cement and epoxy binders - specimens identified by "MG"), and (ii) the fire protection scheme, which comprised different insulation thicknesses at the central zone of the beams (from 0 to 25 mm – dimension *t*, *cf.* Figure 7.10a) and in the CFRP anchorage zones (from 0 to 50 mm – dimension *t*, *cf.* Figure 7.10a). The first number of the nomenclature adopted corresponds to the dimension *T* and the second one to the dimension *t* (both in millimetres). As observed in Table 7.4, different combinations of the parameters *T* and *t* were tested in order to evaluate the effectiveness of applying thicker insulation in the CFRP anchorage zones on the fire resistance of the NSM strengthening system (*i.e.* the time of fire exposure until the CFRP system loses its structural effectiveness).

The ready-mixed concrete and steel reinforcement bars used in the NSM-strengthened beams were similar to those adopted in the EBR- counterparts (section 7.2); the characteristics and properties of these materials were already described in section 7.2.1.

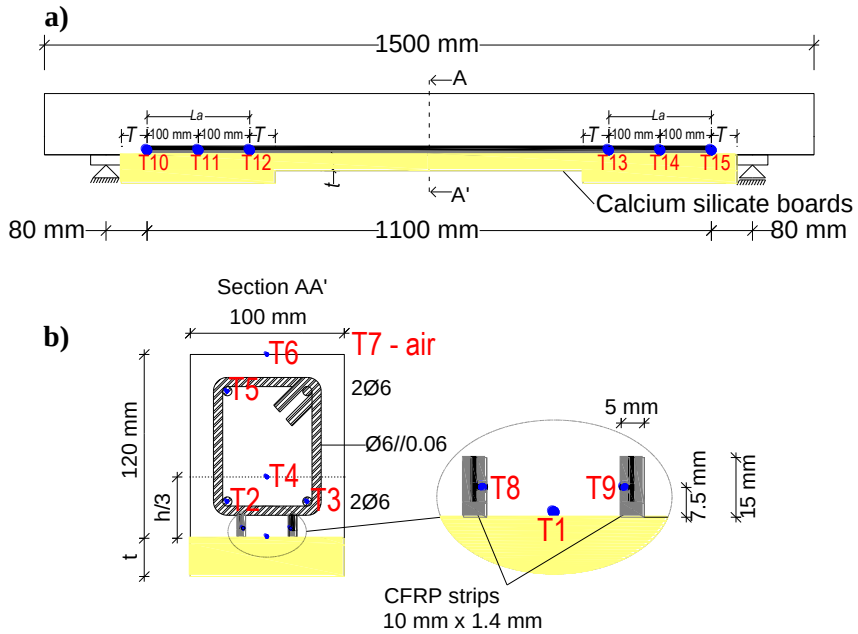

Figure 7.10: Geometry of the NSM-strengthened beams and position of the thermocouples: a) longitudinal view; b) midspan cross section (A-A').

Table 7.4: Details of the NSM-strengthened beams tested under fire.

Beam	Adhesive type	Fire protection thickness [mm]	
		Anchorage zone (*T*-Figure 7.10a)	Current zone (*t*-Figure 7.10a)
EP-0-0	Epoxy[1]	0	0
EP-25-0		25	0
EP-25-25		25	25
EP-50-25		50	25
MG-0-0	Mixed grout[2]	0	0
MG-25-0		25	0
MG-25-25		25	25
MG-50-25		50	25

[1] Conventional epoxy adhesive for CFRP strengthening systems; commercial designation *S&P Resin 220* (detailed description provided in section 3.2.1.2, page 48).

[2] Mixed epoxy-cement grout; commercial designation of *AT Floor ER* (detailed description provided in section 3.3.1.2, page 66)

The CFRP strips used as NSM reinforcement (commercial designation *S&P Laminates CFK 150/2000*) have cross-section of 10 mm (width) × 1.4 mm (thickness) and total length of 1100 mm (*cf.* Figure 7.10a). An anchorage length (l_a, as represented in Figure 7.10d) of 200 mm was considered, which is slightly higher than the value recommended in ACI440.2R-08 [56] (180 mm) for the geometry of the beams and the referred material properties. The epoxy adhesive, with the commercial designation *S&P Resin 220*, is currently used for CFRP strengthening applications. The mixed grout, with the commercial designation *ATFloor ER*, was used as an alternative to the

epoxy adhesive. These three materials were also adopted to strengthen the concrete blocks used for the bond tests presented in chapter 3 – their properties were already described in sections 3.2.1.2 (page 48) and 3.3.1.2 (page 66).

The NSM-strengthening system was installed in the beams soffit according to the following procedure (similar to that used in NSM specimens for the bond tests, *cf.* section 3.3.1.3 – page 67): the slits (5 mm wide and 15 mm deep) were made on the concrete surface using a diamond blade cutter; the slits were cleaned with compressed air and then filled with adhesive; the strips were manually introduced into the slits and the adhesive in excess was removed.

Four point bending tests performed at ambient temperature in beams similar to those presented here (results presented in section 6.2 – page 118), showed that the NSM-CFRP strengthening system provided a flexural strength increase of 111%, when compared to an unstrengthened beam (beam RC). This strengthening level is considerably higher than the limits established in most design recommendations (40-60%); however, the author intended to simulate a situation in which the CFRP contribution to strength during fire is needed to prevent the beams' failure (further discussion is provided in the next section).

The fire protection systems consisted of CS boards (commercial designation *Promatect-L500*) bonded over the strengthening system with fire resistance mastic and mechanically fixed using U-shaped thin steel plates (fixed to the lateral faces of the beams with small metallic screws) distanced of approximately 0.20 m. As described in Table 7.4, the thickness of the insulation varied between 25 mm and 50 mm, in some cases being different in the anchorages zones of the strengthening system and in the central part of the beam. This insulation material is similar to that used in the EBR-strengthened beams – its properties and additional details were described in section 7.2.3.

7.3.2 Test setup, instrumentation and procedure

The fire resistance tests on NSM-strengthened RC beams were conducted under the same conditions to those of the EBR- counterparts (*cf.* section 7.2.4 – page 147).

Regarding the load applied during the fire tests (P_{fire}), it was defined as 70%[9] of the design load at ambient temperature (P_d), according with the recommendations of Eurocode 2 (part 1-2) [16]. The design load for the RC beams flexurally strengthened with NSM-CFRP strips was determined based on ACI 440 guidelines [56].

Table 7.5 lists the values of P_{fire}, P_d, the (average) failure load (P_u) at ambient temperature (obtained using a similar test setup, *cf.* section 6.2 – page 118) and the ratios between those load

[9] This value corresponds to a load level that is slightly lower than the maximum admissible value indicated in Eurocode 2 Part 1-2 (75% of P_d).

values, for both unstrengthened and NSM-strengthened beams (all excluding the beam's self-weight, very low, about 0.4 kN). As observed in this table, the ratio P_{fire}/P_u was similar in both types of beams (0.38 and 0.37). In fact, the load applied during fire (P_{fire}) imposed a maximum CFRP strain of ε_p = 2.4 ‰ (measured at ambient temperature), which corresponds to 15% of its ultimate tensile strain (also at ambient temperature). This means that, as expected, for the fire load combination, the strain/stress installed in the CFRP strip was relatively low. The fraction $P_{fire}/P_u^{RC} = 0.78$ for the strengthened beams indicates that the loss of the CFRP strengthening system would not necessary cause the structural failure of the beam, since the failure load of the unstrengthened beam (P_u^{RC}, at ambient temperature) is higher than the load applied during the fire tests (P_{fire}). Regarding the ratio P_{fire}/P_d^{RC} for the strengthened beams, it can be observed that such ratio is considerably higher than 1.0, which means that in a typical design scenario the unstrengthened beam would not be able to guarantee the necessary load bearing capacity when subjected to the fire load combination (P_{fire}). As for the EBR-strengthened beams, this result is due to the high flexural strength increase provided by the NSM-strengthening system (111%, above the design guidelines recommendations), which was intentionally set to make it necessary to take into account the CFRP mechanical contribution during fire.

Table 7.5: Design load (P_d) and (average) failure load (P_u) at ambient temperature, total load applied during the fire tests (P_{fire}) and corresponding ratios (excluding the beams' self-weight).

Specimen	Design load at 20 °C (P_d) [kN]	Failure load at ambient temperature (P_u) [kN]	Fire load (P_{fire}) [kN]	P_{fire}/P_d^{RC}	P_{fire}/P_u	P_{fire}/P_u^{RC}
Control beam (beam RC)	10.3[1]	18.9	7.2	0.70	0.38	0.38
Strengthened beams (NSM)	21.1[2]	39.9	14.8	1.44	0.37	0.78

[1] Computed based on the Eurocode 2 (part 1-1) [138];

[2] Computed based on the ACI 440.2R-08 guidelines [56].

Regarding the instrumentation, similar measuring devices to those used in the EBR-strengthened beams were adopted. The temperature distributions were measured with a set of 15 thermocouples (type K, with external diameter of 1 mm), whose nomenclature and location are shown in Figure 7.10 (page 160). The midspan section was instrumented with 9 of these sensors (T1 to T9, *cf.* Figure 7.10b), whereas the temperature in the bonding adhesive along both anchorage zones of the CFRP was measured through thermocouples T10 to T15 (*cf.* Figure 7.10a). It is worth pointing out that all the thermocouples in the adhesive were located at mid-depth of the slits (*cf.* Figure 7.10b).

The midspan displacement at the top (cold part) of the beams was measured with an electrical displacement transducer (from *TML*, model *CDP*-500 with a range of 500 mm).

7.3.3 Experimental results and discussion

7.3.3.1 Temperatures vs. time of fire exposure

Figure 7.11 plots the evolution of the furnace temperature and at different positions of two representative beams (EP-25-0 in Figure 7.11a and EP-25-25 in Figure 7.11b) as a function of the time of fire exposure, namely at one of the bottom steel rebars (T2) and in the adhesive at the midspan section (average of readings from thermocouples T8 and T9), and in the two anchorage zones (T11 and T14). It can be seen that the furnace temperature, although presenting some deviation to the standard fire curve (yet well within the bounds defined in the test standard), accurately followed the ISO 834 [6] time-temperature curve. A good agreement was also obtained in all the remaining tests.

The temperature at the bottom steel rebar (thermocouple T2, *cf.* Figure 7.10b) measured at the midspan section in beam EP-25-0 (Figure 7.11a) presented the following behaviour with time of fire exposure: (i) increased almost linearly up to 100 °C, (ii) exhibited a small plateau at this temperature due to the water vaporization in the surrounding concrete, and (iii) presented a final branch in which the temperatures continuously increased up to the end of the test, attaining a maximum value around 330 °C (when the CFRP strengthening system debonded, the temperature in the steel rebars was lower, therefore its residual stiffness and strength was relatively high). In fact, in all the tested beams, when the CFRP system lost its structural effectiveness the temperatures in the steel rebars were always lower than 274 °C (*cf.* Table 7.6), and therefore the thermal-induced degradation on its mechanical properties can be considered to be negligible [16]. In beam EP-25-25 (Figure 7.11b), due to the 25 mm thick CS board applied along the entire length of the beam soffit, the temperature at the tensile steel rebar increased almost linearly and at a lower rate than that observed in beam EP-25-0.

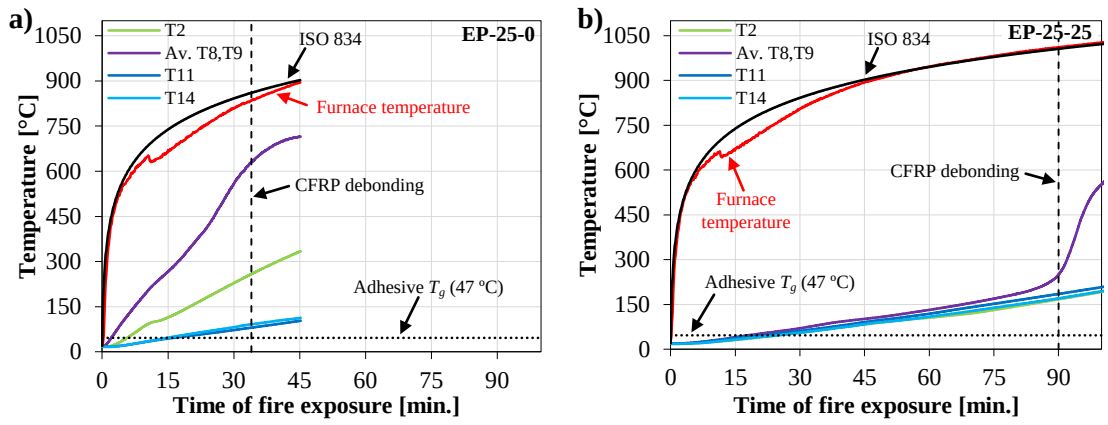

Figure 7.11: Examples of measured temperature vs. time of fire exposure: a) beam EP-25-0 and b) beam EP-25-25.

Figure 7.11a shows that the average temperature in the adhesive (average between T8 and T9) at the midspan section of beam EP-25-0 exceeded the corresponding T_g after less than 3 minutes of

fire exposure and increased at a significantly higher rate compared to the anchorage zones (measured by T11 and T14), which were protected by a 25 mm thick CS board. Although along the central (unprotected) length of this beam the bond between the CFRP and the concrete was severely damaged since early stages of the test, the strengthening system kept its structural effectiveness up to 34 min through a cable behaviour: the CFRP strips continued to carry tensile forces as suspended cables fixed in the anchorages zones, where the CFRP-concrete bond was significantly less affected (further discussion is provided in section 7.3.3.4). Regarding the temperatures in the adhesive measured in beam EP-25-25 (Figure 7.11b), as expected, a similar thermal behaviour was observed at the central and anchorages zones of the CFRP strips, with temperatures increasing almost linearly with the time of exposure up to 80 min. After this instant, the adhesive temperature at the midspan section increased more rapidly until the end of the fire test, due to cracks developed at the CS boards (*cf.* section 7.3.3.4). When the CFRP debonded, in both beams the maximum temperatures in the adhesive in the anchorage zones were considerably higher than the corresponding T_g (between 105 °C and 219 °C, *cf.* Table 7.6). This result confirmed that NSM-CFRP-strengthening systems present considerable bond strength retentions when exposed to temperatures higher than the adhesive T_g. This result is in agreement with the double-lap shear tests (*cf.* section 3.3 – page 66) carried out on specimens with similar materials, which exhibited considerable bond strength retentions at temperatures well above the adhesive T_g (*e.g.* 40% at 90 °C and 30% at 150 ºC).

Table 7.6: Temperatures measured at the midspan section of the beams (tensile steel rebars and adhesive) and anchorage zones (in the adhesive) when the CFRP strengthening system debonded, and corresponding time of fire exposure.

Beam	Temperatures at the midspan when the CFRP system debonded [°C]		Temperatures in the anchorage zones when the CFRP system debonded [°C]		Time for the debonding of the CFRP strengthening system [min]
	Tensile steel rebars (average T2, T3)	Adhesive (averageT8, T9)	Left anchorage (average T10, T11, T12)	Right anchorage (average T13, T14, T15)	
EP-0-0	135	315	239	234	18
EP-25-0	274	630	105	117	34
EP-25-25	167	249	178	219	90
EP-50-25	218	282	130	201	114
MG-0-0	207	353	269	289	17
MG-25-0	208	437	81	96	22
MG-25-25	210	259	190	198	85
MG-50-25	221	280	137	156	92

It is worth mentioning that the CFRP temperature at the midspan of beam EP-25-0 (which should be similar to that measured in the adhesive by thermocouples T8 and T9), although attained 630 °C immediately before the CFRP lost its mechanical contribution, was not sufficiently high to induce

its tensile failure, thus allowing the CFRP to behave as a cable until the debonding of the strengthening system (as discussed in section 7.3.3.4). It is also worth reminding that the initial CFRP stress level due to the applied load was very low (*cf.* section 7.3.2), therefore, although the stresses in the CFRP may vary during fire exposure (an aspect that is analysed in chapter 8), based on [27], one expected the CFRP strip to withstand considerable thermal-induced degradation before its tensile failure.

7.3.3.2 Temperatures along the bonded interface when the CFRP system debonded

Figure 7.12a shows for all beams the temperatures along the bonded interface (measured by thermocouples T8 to T15, *cf.* Figure 7.10a) when the CFRP strengthening system lost its structural effectiveness, with such instants being detected on the midspan displacement *vs*. time curves (*cf.* section 7.3.3.3). As expected, beams with CS boards applied only in the anchorage zones of the NSM strengthening system (specimens EP-25-0 and MG-25-0) exhibited very high temperatures at the central zone (left uninsulated) and considerably lower temperatures in the CFRP anchorage zones. For beams EP-50-25 and MG-50-25, a similar relationship between the adhesive temperature at the midspan section and in the anchorage zones was observed, although lower temperatures were measured at the central zone (when compared to those of the two previous beams). The temperature distributions obtained in the uninsulated beams (EP-0-0 and MG-0-0) and those protected by a 25 mm thick CS board along the entire length of the CFRP system (EP-25-25 and MG-25-25) were roughly uniform, presenting lower temperatures at the CFRP ends (thermocouples T10 and T15, *cf.* Figure 7.10a) due to the vicinity of the furnace walls. Although all the above-mentioned distributions were expected, Figure 7.12a shows that the temperatures in the anchorage zones (which, as discussed in section 7.3.3.4, governs the fire endurance of the strengthening system) presented relatively high scatter. This scatter is clearly noticed in Figure 7.12b, where the average temperature along the hotter anchorage zone at the debonding instant is plotted for all the tested specimens (these temperatures are also listed in Table 7.6). This figure highlights the complexity of the behaviour of NSM-strengthened systems under fire exposure, which is related to (i) the thermal gradient existing along the depth of the slits (inducing a non-uniform thermal degradation in its depth), and also to (ii) the confinement effect on the strengthening system caused by thermal expansion of the surrounding concrete.

Apart from the above mentioned aspects, Figure 7.12b shows that, in general, the debonding of the CFRP system with epoxy adhesive occurred for higher temperatures than those measured when the mixed grout was used, indicating a better performance of the former material. In the unprotected beams an opposite result was obtained, however, the debonding of the CFRP system occurred after very short periods of fire exposure (*cf.* Table 7.6), corresponding to a test stage in which the furnace temperatures increased at a very high rate and exhibited some variability compared to the

nominal curve (*cf.* Figure 7.11). A relevant finding of this test campaign is that the debonding of the strengthening systems occurred when the temperature in the anchorages zones was considerably higher than the corresponding adhesive T_g: ranging from 117 °C (2.5 × T_g) to 239 °C (5.1 × T_g) for the epoxy adhesive, and from 96 °C (2.2 × T_g) to 289 °C (6.6 × T_g) for the mixed grout.

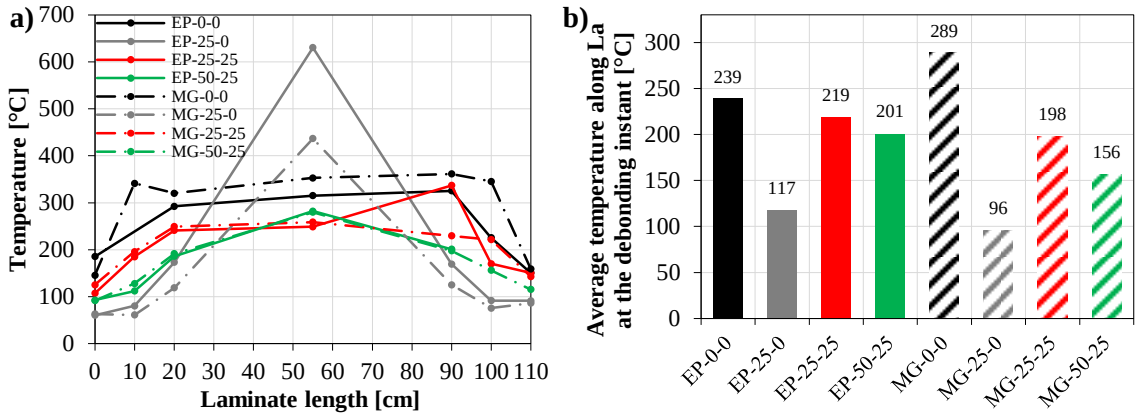

Figure 7.12: Temperatures in the adhesive when the NSM-CFRP system debonded: a) along the bonded interface; b) average along the anchorage length.

As observed in Figure 7.12b, in the beams with the 25-0 insulation scheme (EP-25-0 and MG-25-0) the CFRP lost its structural effectiveness for considerably lower temperatures in the anchorage zones (compared to the remaining beams). This result might be related to the very high temperatures recorded along their central zone (unprotected length), where the CFRP-concrete bond was severely damaged, therefore increasing the bond stresses in the CFRP anchorage zones and thus explaining the occurrence of CFRP debonding for lower temperatures. In the beams protected with the 50-25 insulation scheme, although it is very likely that stresses in the anchorage zones also increased during fire exposure, such increase must have been less significant due to the lower temperatures observed at the central zone (compared to the 25-0 insulation scheme, *cf.* Figure 7.12a). Further research is needed about this stress transfer phenomenon and its influence in the critical temperature in the anchorage zones. This aspect is assessed in the numerical investigations presented in chapter 8.

7.3.3.3 Midspan displacement increase

The midspan displacement increase of the unstrengthened beam (beam RC, already presented in section 7.2.5.3 – page 154) and of all CFRP-strengthened beams as a function of the time of fire exposure are plotted in Figure 7.13, in which the origin of the time scale corresponds to the beginning of the thermal exposure. As expected, the beams' midspan displacement increased with time (and temperature) due to the stiffness (and strength) decrease of the materials. The loss of structural effectiveness of the CFRP strengthening system is marked in this figure, and can be clearly identified by an increase on the slope of the curves; is most cases a progressive slope increase was observed, with the instant of the CFRP loss being considered at its initial stage. After

the debonding of the strengthening system, the mechanical properties of the beams became roughly similar to those of beam RC. As the applied load in the strengthened beams was higher than that in beam RC (*cf.* Table 7.5 – page 162), the midspan displacement increase rate in the unprotected beams (EP-0-0 and MG-0-0) and in those with most of their length left uninsulated (EP-25-0 and MG-25-0) was significantly higher than that observed in the reference beam. The insulation systems applied along the strengthening system (beams 25-25 and 50-25) delayed the thermal induced degradation on the materials during the entire test, explaining their lower midspan displacement increase rate (before and after the CFRP loss).

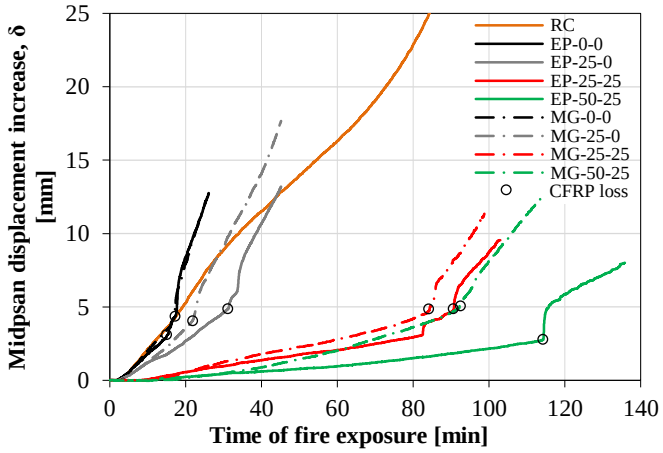

Figure 7.13: Midspan displacement increase vs. time of fire exposure.

7.3.3.4 Failure modes and post-fire assessment

Figure 7.14 illustrates the beams with the epoxy adhesive after the fire resistance tests, showing some of the effects of high temperature exposure. The bottom face of beam EP-0-0 (Figure 7.14a) presented signs of thermal degradation, with the dark coloration being mostly due to the combustion of the CFRP system. The loss of structural effectiveness of the strengthening system was caused by the bond failure at the CFRP-adhesive interface, causing the CFRP slip inside the slits. In this figure a considerable number of concrete cracks can also be observed, most of them having probably developed after the loss of the strengthening system. In one of those cracks (marked in Figure 7.14a) some CFRP broken fibres can be observed. Again, it is likely that such partial CFRP rupture occurred after its debonding, since at that instant the temperature inside the slit (similar to that of the CFRP) was not sufficiently high to induce the CFRP tensile failure (as discussed in section 7.3.3.1). It is worth mentioning that this partial CFRP tensile rupture was observed only in this beam.

Similar failure modes of the strengthening system to that describe for beam EP-0-0 were observed in all the remaining specimens (CFRP slip inside the slits); however, in the beams protected with thicker CS boards in the CFRP anchorage zones (beams EP-25-0, EP-50-25, MG-25-0 and MG-50-25) the loss of bond of the strengthening system was significantly delayed (when

compared, respectively, to beams EP-0-0, EP-25-25, MG-0-0 and MG-25-25) and occurred in the hotter anchorage zone. As discussed in section 7.3.3.1, the CFRP-concrete bond was severely damaged at the central zone of these beams at earlier stages of the test, but the NSM-CFRP strengthening system kept its structural effectiveness through a cable behaviour for a longer period of fire exposure (further discussion about the efficacy of the adopted insulation system is provided in section 7.3.3.5).

Figure 7.14c to d show that although the CS boards presented some cracks, their mechanical fastening successfully prevented the insulation system to detach from the beams' soffit, remaining effective during the entire duration of the tests. As mentioned in section 7.3.3.1, such insulation cracks caused a localized temperature increase in the bonding adhesive at the end of the tests (*cf.* Figure 7.11b).

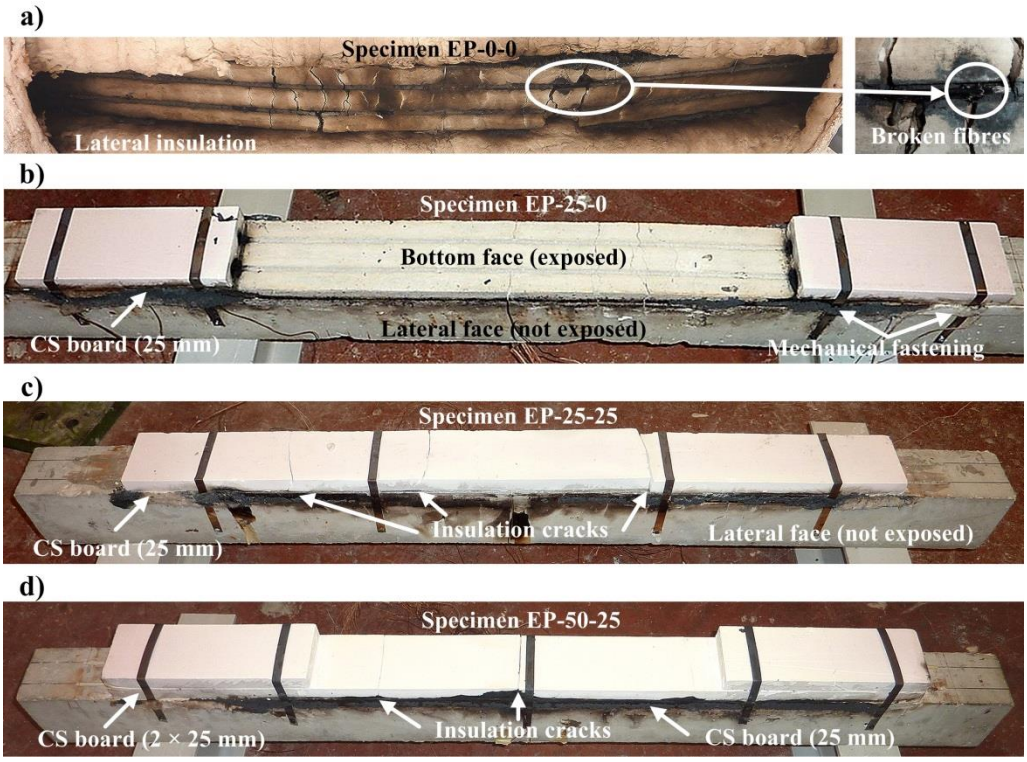

Figure 7.14: Post-fire observations: a) beam EP-0-0; b) beam EP-25-0; c) beam EP-25-25; d) beam EP-50-25.

7.3.3.5 Structural effectiveness of the NSM strengthening system during fire

The results presented in the previous sections allowed determining the exact instant when the strengthening system lost its structural effectiveness (Figure 7.13) and the corresponding temperature distributions along the CFRP bonded interface (Figure 7.14). Figure 7.15 plots the time of fire exposure until the loss of the CFRP system, allowing assessing the efficacy of the fire protection strategy adopted. Additionally, the fire performance of the strengthening system using the two different adhesives can also be compared. As observed in this figure, in all beams where the mixed grout was used, the strengthening system lost its mechanical contribution after shorter

periods of fire exposure when compared to the analogous beams with epoxy adhesive. These results, together with the data presented in Figure 7.12b (showing lower temperatures in the anchorage zones in most of the beams with the mixed grout), confirmed the worse performance of this bonding adhesive.

Regarding the results obtained in the beams where the epoxy adhesive was used, Figure 7.15 shows that when the strengthening system was unprotected (beam EP-0-0) the CFRP debonded after only 18 min, confirming its high susceptibility when exposed to fire. When the 25 mm-thick CS board was applied in the CFRP anchorage zones (beam EP-25-0), the fire resistance of the strengthening system was improved (to 34 min, almost doubling compared to beam EP-0-0). However, when such insulation board was applied along the entire CFRP length (beam EP-25-25), the fire endurance of the CFRP system presented a further significant increase (attaining 90 min), showing the importance of applying a thin insulation layer over the entire length of the NSM-strengthening system. With increasing thickness of CS board insulation in the CFRP anchorage zones (combined with a thinner layer at the midspan - beam EP-50-25), the fire resistance of the strengthening system increased up to 114 min.

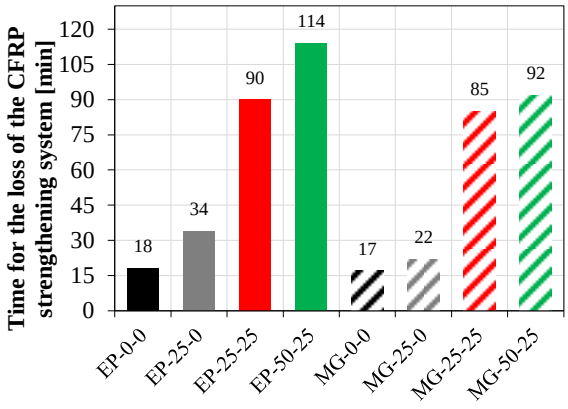

Figure 7.15: Fire resistance of the NSM strengthening systems.

The results presented herein confirm that is possible to exploit the structural effectiveness of NSM-CFRP strengthening systems during fire exposure. The application of thicker layers of insulation material in the anchorage zones of the CFRP strips allowed extending the structural effectiveness of the strengthening system by exploiting the referred cable behaviour. These results provide an experimental validation to the strategy for designing fire protection systems for CFRP-strengthened RC members proposed in chapter 5 (which was based only on numerical thermal simulations). The temperature criterion for designing the thickness of insulation layers along the CFRP anchorage zones considered in chapter 5 consisted of limiting the adhesive temperature in the anchorage length to its T_g in order to prevent the CFRP debonding for the required time of fire exposure. However, the results obtained in the present experimental campaign show that this criterion is too

conservative: in fact, the debonding of the NSM-strengthening system occurred when the average temperature in the adhesive along the anchorage length ranged between 2.2 × T_g and 6.6 × T_g.

7.3.4 Comparison with EBR-strengthened RC beams

The fire behaviour of EBR-CFRP strengthened beams was assessed in section 7.2, in which similar materials, fire insulation schemes and test conditions were adopted. Figure 7.16 shows the comparison between the fire performance of comparable beams (only using the conventional epoxy adhesive) in terms of (i) average temperature in the adhesive along the anchorage zone at the debonding instant (Figure 7.16a), and (ii) time of fire exposure until the loss of the CFRP strengthening system (Figure 7.16b). As illustrated in Figure 7.16a, with the EBR-strengthening system the CFRP debonding occurred for significantly lower temperatures in the anchorage zones, which ranged from 1.2 × T_g to 1.5 × T_g, therefore being only slightly higher than the adhesive T_g. This critical temperature range in the anchorage zones is significantly lower than that observed for the NSM-strengthening technique. The worse fire performance of the EBR technique is also illustrated in Figure 7.16b, where it is shown that for all insulation schemes, the fire resistance of the EBR-strengthened beams is considerably lower than that of the NSM counterparts. This figure reveals that increasing the insulation thickness in the anchorage zones of the EBR-CFRP beams is more effective than in the NSM-CFRP ones (*e.g.* comparing beams 0-0 with beams 25-0, the relative increase of the time of fire exposure until CFRP debonding is higher in the EBR-strengthened specimens). Furthermore, in the NSM-strengthened beams the fire resistance of the strengthening system was considerably improved by applying a thin insulation layer along the current zone, whereas in the EBR-strengthened beams such increase was almost negligible. This is particularly clear by comparing the results shown in Figure 7.16b for beams with the insulation schemes 25-0 and 25-25: in the EBR-strengthened beams the fire resistance of the strengthening system increased from 15 min (insulation 25-0) to 18 min (insulation 25-25), whilst in the NSM counterparts such resistance increased from 34 min to 90 min. These results should be related to the different stress transfer mechanisms between the central and anchorage zones of the strengthening systems during the development of the cable behaviour. Further investigations are still needed to fully understand this phenomenon.

The comparison presented above, besides confirming the better performance under fire of NSM-CFRP strengthened beams, shows that a different criterion should be adopted for the design of fire protection schemes of NSM- and EBR-strengthened beams, particularly when defining the thickness of insulation to be applied along the CFRP anchorage zones in order to prevent the CFRP debonding (for the required time of fire exposure). If for the EBR technique the adhesive T_g seems to be an adequate criterion (not excessively conservative), for the NSM technique 2 × T_g seems to be more adequate. Regarding the thickness of the insulation layer applied along the current zone of

the strengthening system, the same criterion should be adopted for both EBR and NSM techniques, and it consists of maintaining the CFRP at sufficiently low temperatures (defined based on the applied tensile stress and strength-temperature data reported in the literature - *e.g.*, [27]) in order to prevent the tensile rupture of the CFRP strip, allowing it to behave as a cable until the debonding of the strengthening system in the anchorage zones.

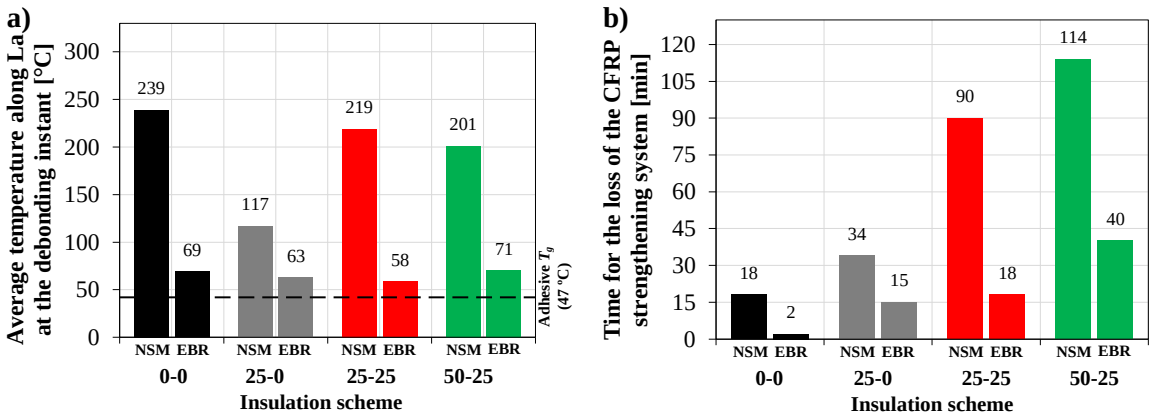

Figure 7.16: Comparison between the fire performance of EBR and NSM strengthening systems (using the same epoxy adhesive): a) average temperature along the anchorage length when the CFRP system debonded; b) fire resistance of the strengthening system.

7.3.5 Summary of results

Section 7.3 presented the results of fire resistance tests on RC beams flexurally strengthened with NSM-CFRP. The following main results are highlighted:

- The fire resistance tests confirmed the susceptibility of NSM-CFRP strengthening systems to fire. In the uninsulated strengthened beams the mechanical contribution of the NSM-CFRP strips was lost after only 18 and 17 min of fire exposure, using respectively the epoxy adhesive and the mixed grout.
- The NSM-CFRP strips bonded with the mixed grout presented a worse fire performance than those bonded with the epoxy one: with the former adhesive, the strengthening system lost its mechanical contribution after shorter periods of fire exposure and generally for lower adhesive temperatures.
- When the 25 mm thick CS boards were applied only in the CFRP anchorage zones, the fire resistance of the strengthening system (CFRP bonded with epoxy adhesive) increased from 18 min to 34 min. Although the CFRP-concrete bond became highly damaged along the central zone (unprotected), the CFRP strips maintained its structural effectiveness through a cable behaviour.
- The structural effectiveness of the NSM-CFRP strengthening system was considerably further extended by combining a thinner insulation layer (25 mm) along its current zone

with a thicker one (50 mm) in the anchorage zones. With this insulation scheme the CFRP mechanical contribution was lost after 114 min of fire exposure.

- For the beams tested and the insulation schemes adopted, the strengthening system lost its structural effectiveness when the average temperature in the adhesive in the anchorage zones attained values ranging from 2.2 × T_g to 6.6 × T_g.

7.4 CONCLUDING REMARKS

This chapter presented experimental investigations on the fire behaviour of RC beams flexurally strengthened with CFRP strips installed according to both EBR and NSM techniques. The results obtained from the tests on uninsulated CFRP-strengthened beams confirmed the susceptibility of CFRP strengthening systems (either EBR or NSM) when exposed to high temperatures/fire - the CFRP strips debonded after very short periods of fire exposure (between 2 and 18 min).

When insulation boards were applied at the CFRP ends, the strengthening systems retained their structural effectiveness through a cable behaviour after the bonded interface was damaged in the central zone; considerable improvements were obtained when the thicker insulation at the CFRP extremities was combined with a thinner one along the central zone – in some cases the strengthening systems retained their structural effectiveness for more than 90 min of fire exposure, which meet most of the building codes requirements.

The experimental campaign allowed obtaining a direct comparison between the fire behaviour of similar EBR- and NSM-strengthened RC beams, where the better performance of the latter strengthening technique was confirmed. In fact, in the EBR-strengthened beams the CFRP debonding occurred after considerably shorter periods of fire exposure and for much lower average temperatures in the adhesive in the anchorage zones. Moreover, it was also shown that the fire resistance of the NSM strengthening system was considerably improved by applying a thin insulation layer along the current zone (together with the insulation of the anchorage zones), whereas the effectiveness of the EBR system during fire exposure was improved mostly by increasing the insulation thickness in the anchorages zones, with the influence of the insulation applied along the current zone being much less important.

The results presented in this chapter provide an experimental validation to the strategy for designing fire protection systems for CFRP-strengthened RC members proposed in chapter 5. Furthermore, it was shown that for the test conditions used in this study (namely, strengthening ratios and load levels) the critical temperature in the CFRP anchorage zones can be considered (at least) as T_g and 2 × T_g, respectively for EBR- and NSM-strengthened RC beams (with T_g being determined from DMA tests on the adhesive and defined based on the onset of the corresponding storage modulus curve). Further validation will be pursued using the numerical models presented in the next chapter.

CHAPTER 8

NUMERICAL SIMULATION OF THE FIRE BEHAVIOUR OF EBR-CFRP-STRENGTHENED RC BEAMS

8.1 INTRODUCTION

This chapter presents numerical investigations about the thermal and structural responses of insulated RC beams flexurally strengthened with EBR-CFRP strips subjected to fire. The objective is two-fold: (i) to improve the understanding about the fire behaviour of CFRP-strengthened beams, namely concerning the cable behaviour observed in the fire resistance tests (*cf.* chapter 7), and (ii) to further validate the strategy for the design of fire protection systems (comprising thicker insulation layers in the CFRP anchorage zones) proposed in chapter 5 and experimentally assessed in chapter 7, more specifically regarding the critical temperature in the CFRP anchorage zones. To this end, 2D FE models of EBR-CFRP-strengthened RC beams with different fire insulation schemes were developed, considering the variation with temperature of the thermal and mechanical properties of the constituent materials. The CFRP-concrete interaction was also modelled using the bond-slip laws presented in chapter 4 that were (independently) derived, for different temperatures, based on numerical and experimental investigations. Numerical predictions of (i) temperature distributions, (ii) midspan displacement increase, and (iii) time for the loss of structural effectiveness of the EBR-CFRP strengthening systems were compared with test results presented in chapter 7 in order to assess the accuracy of the FE models. These calibrated models provided additional data that generally cannot be measured during fire resistance tests[10], namely the stresses/strains in both the CFRP strip and the CFRP-concrete interface, as well as the stress transfer between the central and anchorage zones of the strengthening system during the development of the cable behaviour. In summary, the main goal of this numerical study was to improve the understanding about the structural effectiveness of the CFRP system during fire exposure and to validate the above mentioned insulation strategy.

[10] Such difficulty stems from the relatively low temperature operation limits for deflection and strain measuring sensors.

8.2 DESCRIPTION OF THE NUMERICAL MODELS

8.2.1 Geometry and type of elements

Two-dimensional FE models of the simply supported RC beams flexurally strengthened with EBR-CFRP strips subjected to fire resistance tests (*cf.* chapter 7) were developed using the commercial package ABAQUS. As a reference, an unstrengthened RC beam (beam RC) was also modelled. The geometry of the models was similar to that of the beams tested: 1.50 m long, 0.10 m wide and 0.12 m deep (*cf.* Figure 8.1a and b). In order to reduce the computational costs, only half of the beams' length was simulated, as depicted in Figure 8.1c.

The internal steel reinforcement, with a cover of 1.5 cm, consisted of four ϕ6 mm longitudinal bars and ϕ6 mm transverse stirrups distanced of 0.06 m (*cf.* Figure 8.1a). Regarding the strengthening system, CFRP strips with a cross section of 20 mm (width) × 1.4 mm (thickness) and a total length of 1100 mm (*cf.* Figure 8.1) were considered to be bonded to the surface of the beams' soffit. The 2 mm thick adhesive layer was not explicitly modelled.

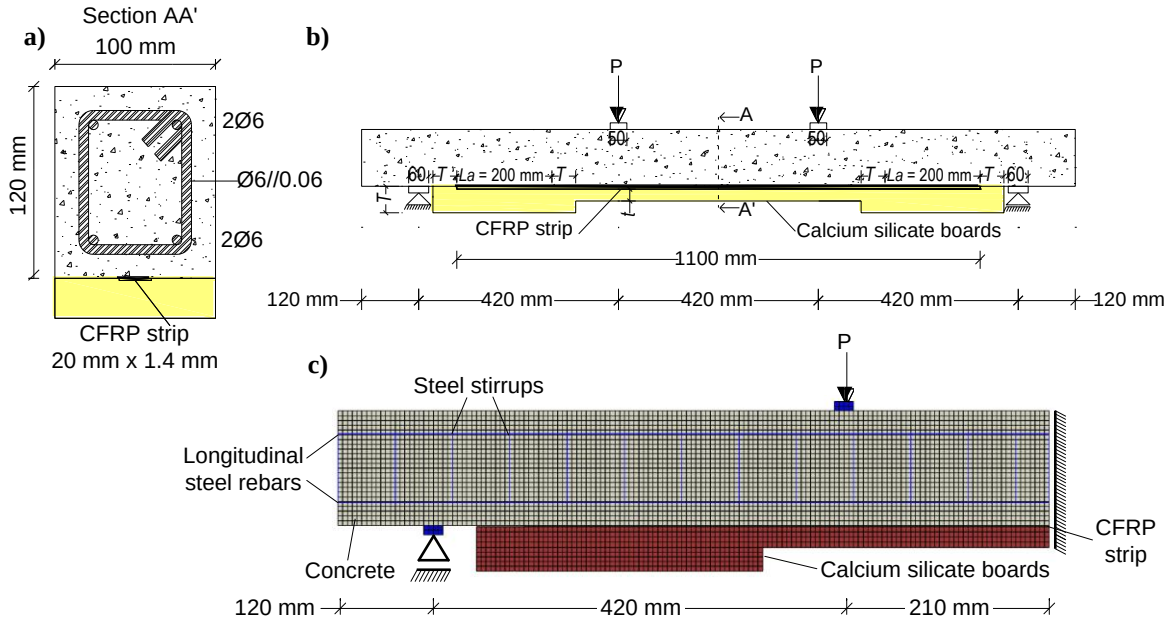

Figure 8.1: Geometry of the beams: a) midspan cross section; b) longitudinal view of the tested beams; c) FE mesh of the beams' models (example of the model 50-25).

The fire insulation systems consisted of calcium silicate (CS) boards, with thicknesses ranging from 25 mm to 75 mm, applied on the bottom surface of the beams. As depicted in Figure 8.1, the passive fire protection systems exhibited variable thickness along the beam's length, being typically thicker in the anchorage zones of the CFRP strips (thickness *T*, *cf.* Figure 8.1b) and thinner along the central zone (thickness *t*, *cf.* Figure 8.1b). As for the beams tested, the nomenclature adopted for the beams' models (Table 8.1) is related to those thicknesses: the first

number corresponds to the dimension *T* and the second one to the dimension *t* (*cf.* Figure 8.1b - both in millimetres).

Figure 8.1c exemplifies the FE mesh (with maximum dimension of 5 mm) adopted for the models of the insulated CFRP-strengthened beams. Four-node isoparametric plane quadrilateral elements (DC2D4 and CPS4 for the thermal and mechanical analyses, respectively) were used to model concrete, CFRP strips and CS boards. For the steel rebars 2-node truss elements (DC1D2 and T2D2 for the thermal and mechanical analyses, respectively) were adopted.

Table 8.1: Nomenclature adopted for the models.

Beam model	Fire protection thickness [mm]	
	Anchorage zone (*T*-Figure 8.1b)	Central zone (*t*-Figure 8.1b)
RC	-	-
0-0	0	0
25-0	25	0
25-25	25	25
50-25	50	25
75-25	75	25

8.2.2 Temperature-dependent material properties

The temperature-dependency of the properties of all materials (Figure 8.2) was incorporated in the models due its significant influence on the thermal and structural responses of the CFRP-strengthened RC beams subjected to fire. As the models' calibration was based on the agreement with the experimental results presented in chapter 7, some of the material properties determined in that investigation (most of them at ambient temperature) were incorporated in the present models. These data were complemented with proposals available in the literature for the temperature-dependency of those properties. A detailed description of the variation with temperature of the thermo-physical properties of the materials was provided in chapter 5.

The variation with temperature of concrete's density (Figure 8.2a), specific heat capacity (Figure 8.2b) and thermal conductivity (Figure 8.2c) was defined according to Eurocode 2 [16]. The emissivity was considered to present a constant value with temperature of 0.7 (also according to Eurocode 2). For the mechanical behaviour simulation, a classical concrete damaged plasticity model [113] was adopted. This approach was deemed as adequate since the simulated beams presented no crack concentrations (*e.g.*, notches). The following mechanical properties of concrete at ambient temperature (experimentally determined) were considered: average compressive strength in cylinders of f_{cm} = 37 MPa, average splitting tensile strength of f_{ctm} = 3.6 MPa, and average elastic modulus of E_{cm} = 31 GPa. The reduction with temperature of these properties was

assumed to follow the relationships suggested in Eurocode 2 (Figure 8.2d). A fracture energy of G_{cf} = 65 N/m was assumed at ambient temperature according to the Fib Model Code 1990 [96] recommendations for a concrete with similar mechanical properties to that used in the present study. According to Bamonte and Fellicetti [22], this property was considered to be constant with temperature.

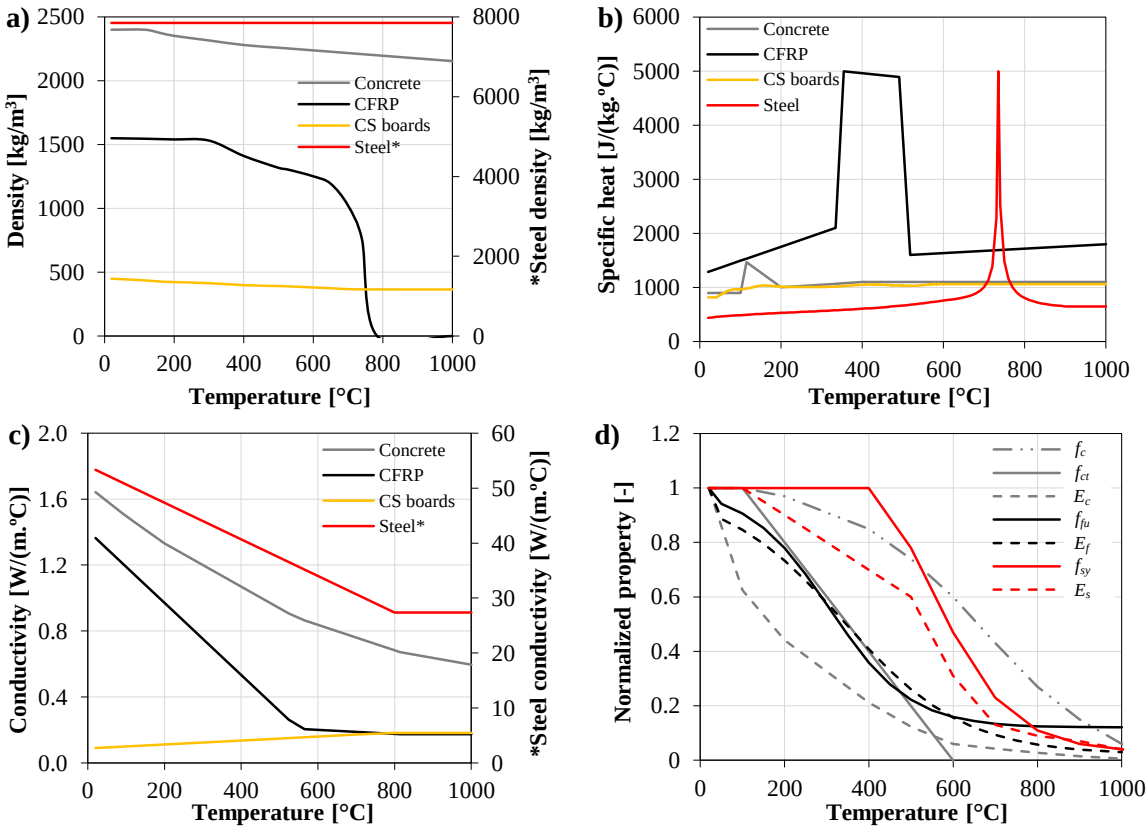

Figure 8.2: Thermo-physical (a, b and c) and mechanical properties (d) of the materials as a function of temperature.

The thermo-physical properties of the steel reinforcement as a function of temperature (Figure 8.2a to c) were also defined according to Eurocode 2 [16]. For the mechanical behaviour simulation, although the (initial) stress level in the steel reinforcement was significantly lower than its yield strength (the models predicted less than 180 MPa), a perfect elasto-plastic model was adopted, with the following properties: average elastic modulus of E_{sm} = 193 GPa, yield strength of f_{sy} = 546 MPa; Poisson's ratio of ν = 0.3; the temperature reductions of these properties defined in Eurocode 2 (Figure 8.2d) were included in the models. Regarding the steel-concrete interaction, a perfect bond was assumed.

With the exception of the CFRP density (Figure 8.2a), for which experimental results were used (reported in [5]), the variation with temperature of its thermal properties was defined using data from the literature [95, 124]; note that the CFRP emissivity (0.7) was considered to be constant with temperature [124]. Regarding their mechanical behaviour, although the CFRP strips are orthotropic (comprising mainly a unidirectional reinforcement), in the present application they

behave essentially in the longitudinal direction; hence, as a simplification, the CFRP was modelled as a linear elastic isotropic material, with $\nu = 0.3$. The average tensile properties at ambient temperature (experimentally determined, *cf.* section 3.2.1.2 – page 48) are as follows: tensile strength of f_{fu} = 2076 MPa, Young's modulus of E_f = 189 GPa; the models considered the reduction with temperature of those properties (Figure 8.2d), as suggested by Yu and Kodur [29].

Regarding the CS boards, the thermal conductivity and the specific heat capacity at ambient temperature (λ_{CS} = 0.09 W/(m.K) and $C_{p,CS}$ = 815 J/(kg.K), respectively), as well as their variation with temperature (Figure 8.2c and d, respectively), were considered as reported by the manufacturer [125]; the emissivity (0.7) was considered constant with temperature, according to Mimoso [126]. As for the CFRP, the variation with temperature of the CS boards' density (Figure 8.2a) was experimentally determined (reported in [24]). The mechanical contribution of the fire insulation system was not considered, since it was estimated to be negligible.

8.2.3 Thermal degradation of the CFRP-concrete bond

The CFRP-concrete bond is severely affected for moderate temperatures, since it is usually ensured by epoxy-based adhesives cured at ambient temperature, with low T_gs (typically ranging from 40 °C to 80 °C). Therefore, in order to provide accurate predictions of the fire behaviour of CFRP-strengthened RC members, the CFRP-concrete bond degradation with temperature must be carefully considered. In the present study the bond between the concrete and the CFRP strips was simulated by bi-linear global laws with an ascending elastic branch and a descending softening branch that can be defined, for each temperature, by the following three parameters (*cf.* section 4.2.4 – page 86): (i) stiffness, K; (ii) maximum shear strength, τ_{LM} (corresponding to the respective slip, s_{LM}); and (iii) ultimate slip, s_{L0}. These parameters were independently determined in a numerical investigation presented in chapter 4, in which bond-slip laws were derived for temperatures up to 120 ºC based on an inverse analysis. Figure 4.5 (page 88) plots the bi-linear bond-slip relationships obtained in that investigation and adopted here to simulate the CFRP-concrete bond at elevated temperatures. The parameters that define those relationships are listed in Table 4.3 (page 88). It is worth pointing out that for temperatures ranging between those listed in Table 4.3, the models perform a linear interpolation to define the corresponding parameters, whereas for temperatures above 120 °C, the CFRP-concrete interaction is considered to be null.

8.2.4 Boundary conditions, thermal and structural loadings

8.2.4.1 Thermal boundaries

In order to accurately simulate the test conditions adopted in the tests, the bottom face of the beams' models between the structural supports (*cf.* Figure 8.1) was directly exposed to the time-

temperature fire curve defined in ISO 834 standard [6], whereas the remaining length of the bottom face and the top face were submitted to a constant ambient temperature (20 °C in all models). The lateral faces were thermally insulated during the tests, therefore in the models these faces were considered adiabatic, *i.e.*, the heat transfer was null. These boundary conditions actually correspond to the thermal exposure of one-way slabs (as adopted in the tests). Radiation and convection heat transfer modes were considered on both top and bottom faces; a convection coefficient (h_c) of 25 W/m^2 ºC (constant with temperature) was adopted, as suggested in [16]. The initial temperatures of the models were defined according to the measurements made in the beams tests (ranging from 15 °C to 25 °C).

8.2.4.2 Structural boundaries and loading

The EBR-CFRP-strengthened beams tested were simultaneously subjected to the ISO 834 standard fire and to a mechanical (gravity) load applied in a 4-point bending configuration (*cf.* Figure 8.1a). As only half of the beams' length was modelled (*cf.* Figure 8.1c), in the right end of the beams models (midspan) the horizontal displacements throughout the section height were restricted. The pinned support in the left end was simulated by a rectangular elastic support to avoid any stress concentration effects; a similar simplification was adopted for the applied load.

The structural fire load (P_{fire}) was defined based on the recommendations of Eurocode 2 (part 1-2) [16] (*cf.* section 7.2.4.2– page 148) - the corresponding applied loads were P_{fire} = 7.2 kN and P_{fire} = 11.7 kN, respectively for the unstrengthened and strengthened beams. It is worth pointing out that those figures do not include the beams' self-weight (very low, about 0.4 kN).

8.2.5 Type of analysis

The FE models described above simulated the fire behaviour of the CFRP-strengthened RC beams by means of a sequentially uncoupled thermo-mechanical procedure: the heat transfer analysis was first performed to obtain the temperature distributions, and was followed by a mechanical analysis that considered the thermal data calculated in the previous step. It is worth pointing out that the same FE mesh was used in both steps. The temperature distributions were computed using the fully implicit scheme with a maximum time step of 10 seconds.

For simulating the mechanical response, a geometrical and material non-linear analysis comprising a two-stage procedure was performed: (i) the fire load (P_{fire}) was first applied to the beams' models at ambient temperature, inducing an initial deflection (computed with maximum load increments of $0.01 \times P_{fire}$), (ii) the temperature distributions with time (previously determined in the thermal analysis) were then imposed to the loaded beams for a duration similar to that observed in the tests; in this last stage the time increment (0.01 seconds) was considerably shorter than that adopted in

the thermal analysis, therefore the temperatures between steps of 10 seconds were computed by linear interpolation.

8.3 RESULTS AND DISCUSSION

8.3.1 Flexural response at ambient temperature

Results from flexural tests on CFRP-strengthened RC beams performed at ambient temperature (*cf.* section 6.2 – page 118) were used to evaluate the accuracy of the FE models in simulating their mechanical response. These beams, similar to those used in the fire resistance tests (including all materials and dimensions), were monotonically loaded up to failure in a similar setup to that depicted in Figure 8.1b (4-point bending).

Figure 8.3a shows the comparison between numerical (dashed lines, identified as "N") and experimental (continuous lines, identified as "E") load *vs.* deflection curves obtained for a reference unstrengthened beam (beam RC) and for a EBR-CFRP-strengthened beam (beam CFRP). As observed, the numerical models were able to simulate the mechanical response of both beams with reasonable accuracy. The slightly higher stiffness obtained in the numerical models (particularly the cracked stiffness of the strengthened beam) may be related to some horizontal friction in the pinned supports, not considered in the FE models, and also due to the intrinsic experimental scatter in this type of tests and structural systems. The predicted failure loads (18.5 kN and 30.1 kN for beams RC and CFRP, respectively) also presented a good agreement with the experimental counterparts (18.7 kN and 32.9 kN for beams RC and CFRP, respectively).

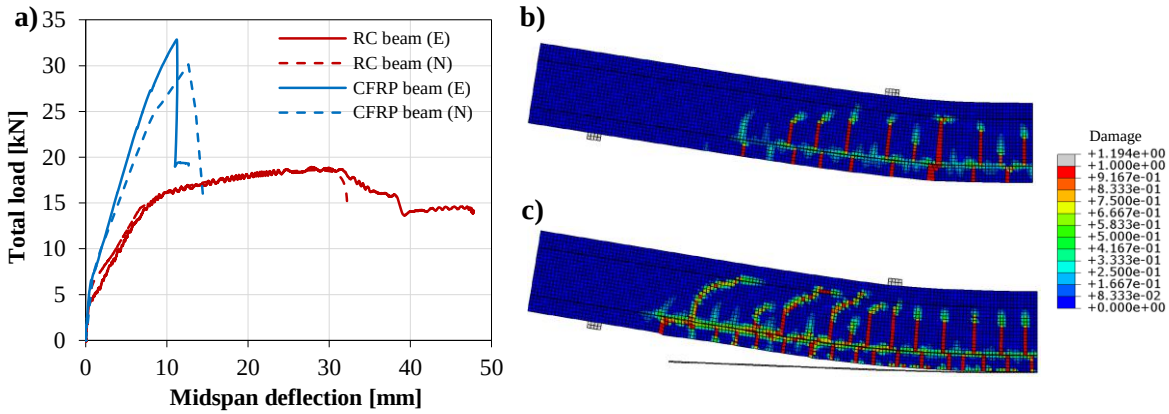

Figure 8.3: a) Experimental (E) and numerical (N) load vs. midspan deflection curves of unstrengthened (RC) and CFRP-strengthened (CFRP) beams tested at ambient temperature (cf. section 6.2 – page 118); damage at failure of b) beam RC, and c) beam CFRP.

Figure 8.3b and c illustrate respectively for beams RC and CFRP the calculated deformed shape with concrete damage distribution at failure. The numerical results in terms of crack distribution

are fairly similar to the observations made in the experimental campaign, further confirming the accuracy of the models to simulate the structural response of the beams at ambient temperature.

8.3.2 Thermal response

8.3.2.1 Temperatures vs. time of fire exposure

Temperatures of the CFRP-strengthened RC beams subjected to fire were measured at 15 different locations, whose nomenclature and location were presented in Figure 7.3 (page 150).

Figure 8.4 shows the comparison between experimental (E) and numerical (N) temperatures as a function of time of fire exposure at different locations (*cf.* Figure 8.4h) in the midspan section and in one of the CFRP anchorage zones (similar temperatures were measured in the opposite anchorage zone) of the different beams tested. Overall, all models provided a good estimate of the temperatures evolution in the corresponding beams. It can be seen that the numerical time-temperature curves exhibit a more regular temperature increase compared to the experimental counterparts, which are more irregular. In beams RC and 25-0 (Figure 8.4a and c) the experimental curves from thermocouple T4 (located in the concrete, *cf.* Figure 8.4h) exhibited a small plateau at 100 °C caused by the water vaporization, which was not accurately predicted by the models. These (small) relative differences between experimental and numerical results may stem from differences between actual and modelled thermo-physical responses of the materials (most thermo-physical properties were modelled according to the literature).

In beam 50-25 temperatures at the end of the fire resistance tests increased at a higher rate than those measured during earlier stages of the fire exposure; this behaviour, which was not predicted by the models, was caused by the development of cracking in the insulation material. As referred above, the numerical procedure did not account for reverse dependencies; therefore the effect of cracking in the insulation (and in the concrete) on the heat penetration was not simulated. Furthermore, in the fire resistance tests it was not possible to fully insulate the lateral faces of the beams, hence there was some (limited) heat transfer through these faces (in the modelling these were considered as adiabatic boundaries), which can also explain some of the differences observed.

8.3.2.2 Temperatures along the bonded interface when the CFRP system debonded

Figure 8.5a shows the comparison between predicted and measured temperatures along the bonded interface (measured by thermocouples T8 to T14, *cf.* Figure 8.4h) when the CFRP strengthening system lost its structural effectiveness due to the debonding from the beams' soffit in the anchorage zones. It is worth mentioning that this debonding was clearly detected on both experimental and

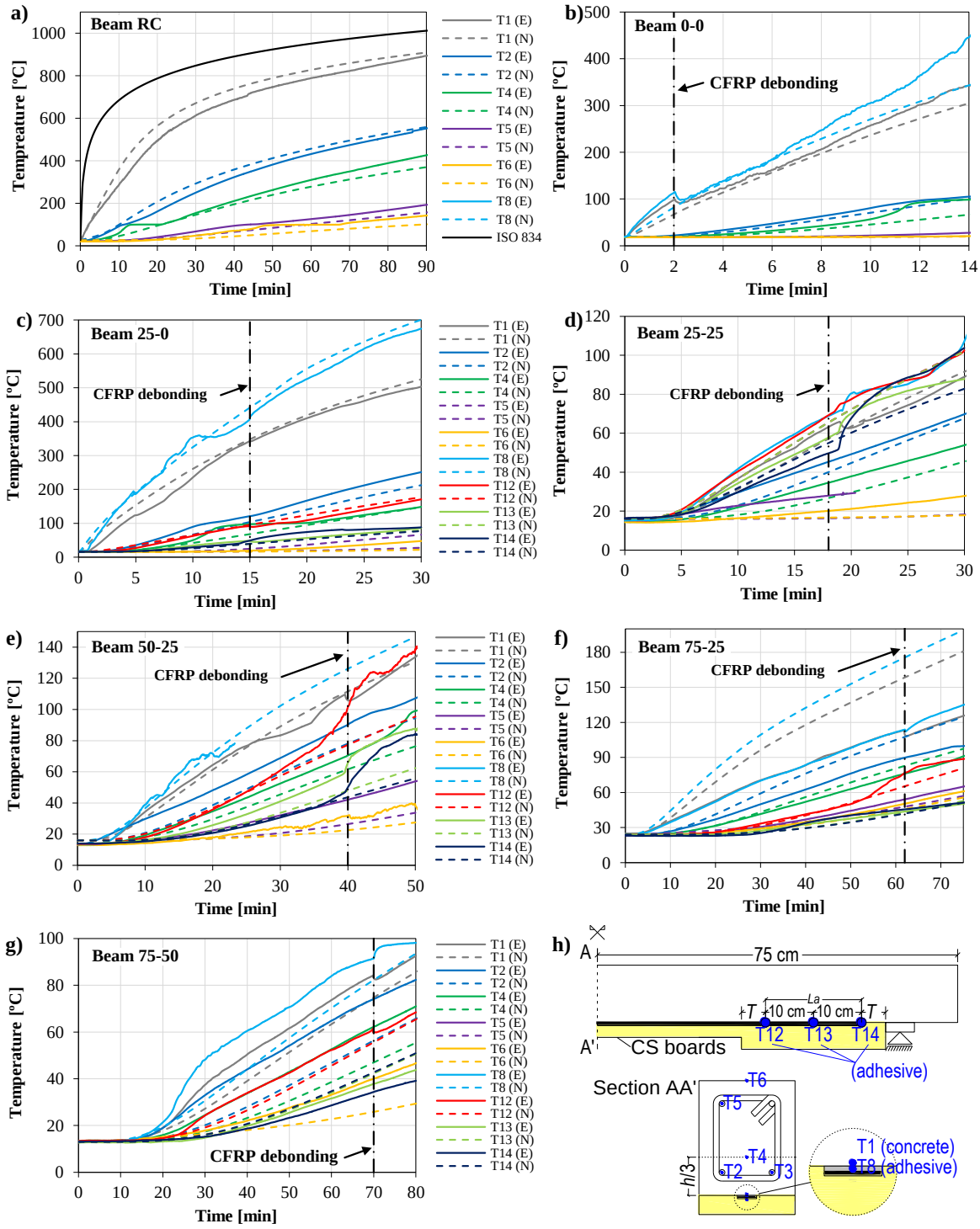

Figure 8.4: Measured (E) and predicted (N) temperatures at different location as a function of time of fire exposure in beams (a) RC, (b) 0-0, (c) 25-0, (d) 25-25, (e) 50-25, (f) 75-25, (g) 75-50, (h) location of the thermocouples. (in very limited cases the experimental curves are not available for the entire tests' duration).

numerical midspan displacement *vs.* time curves, as discussed in section 8.3.3.1 (further details about this failure mode are provided in section 8.3.3.2). Figure 8.5a shows that the beams with thicker insulation in the CFRP anchorage zones (compared to the current zone) exhibited higher temperatures at the central zone, in most cases considerably higher than the adhesive T_g (47 °C, determined from DMA), therefore indicating higher thermal degradation of the adhesive layer in

this zone; in beam 25-0 this result could be clearly noticed. Overall, the numerical curves presented a similar behaviour, although in beams 50-25 and 75-25 the FE models overestimated the temperature at the midspan section (laminate length = 55 cm); none of the models predicted tensile failure of the CFRP strips (*cf.* section 8.3.3.2 for further information), which is in agreement with the experimental observations and provided further validation to the fire protection strategy adopted. With the exception of beam 0-0 (uninsulated), the models accurately predicted the temperatures in the CFRP anchorages zones; the good agreement between measured and predicted temperatures is illustrated in Figure 8.5b, where the average temperature along (both) the anchorage zones at the debonding instant is plotted for all specimens. It can be observed that the average temperatures in the anchorage zones of the insulated beams (*i.e.*, excluding beam 0-0) are slightly to moderately higher than the adhesive T_g, ranging from 50 °C ($1.1 \times T_g$) to 61 °C ($1.3 \times T_g$) in the experiments, which compares (very well) with 53 °C ($1.1 \times T_g$) to 65 °C ($1.4 \times T_g$) in the models. As expected, the predicted temperatures for the uninsulated beam (beam 0-0) are constant along the bonded interface (Figure 8.5a) presenting a value of 118 °C (Figure 8.5b); this temperature distribution is significantly different from the measured one, in which lower temperatures were obtained, in particular in the CFRP anchorage zones (Figure 8.5b). This difference may be due to the fact that the CFRP debonding occurred after only 2 min of the fire exposure; in fact, in such initial stages of the fire resistance tests, the air temperature in the furnace presented a considerable delay compared to the standard fire time-temperature curve.

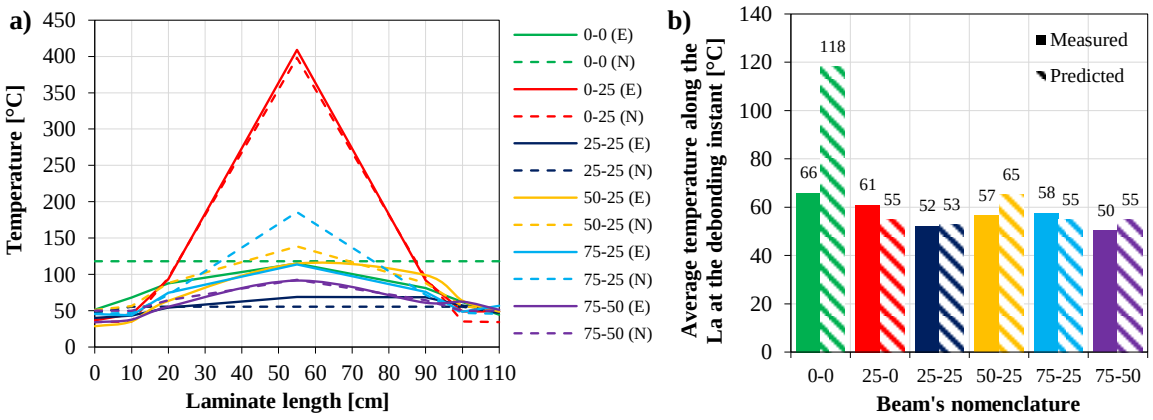

Figure 8.5: Measured (E) and predicted (N) temperatures in the adhesive when the CFRP strengthening system lost its structural effectiveness: (a) along the bonded interface; (b) average along the anchorage length (L_a).

Despite the above-mentioned deviations between experimental and numerical temperatures, the results discussed in this section confirm the ability of the 2D models to accurately simulate the thermal response of insulated EBR-CFRP-strengthened RC beams subjected to fire.

8.3.3 Structural response

8.3.3.1 Midspan displacement increase

Figure 8.6 presents the measured and predicted midspan displacement increase of all CFRP-strengthened beams as a function of the time of fire exposure, in which the origin of the time scale corresponds to the beginning of the thermal exposure. As observed in the fire resistance tests, the predicted midspan displacement increased with time (and temperatures) due to the materials' stiffness (and strength) decrease. As expected, the beams protected with thicker insulation layers presented lower midspan increase rates compared to beams 0-0 and 25-0, since temperatures in the midspan zone of the former beams were considerably lower (*cf.* section 8.3.2.1) and so was their stiffness (and strength) reduction. However, numerical curves exhibited slightly higher deflection increase rates than those measured during the tests, which may stem from (i) some horizontal friction in the pinned supports (already mentioned, not considered in the FE models), and (ii) differences between the actual temperature dependencies of the materials' mechanical properties and those considered in the FE models (as referred in section 4.2.2, data from the literature was mostly used). Nevertheless, all numerical and experimental curves exhibit a similar instantaneous midspan deflection increase, corresponding to the loss of structural effectiveness of the strengthening system, after which the mechanical properties of the beams become roughly similar to those of an unstrengthened one. As observed in Figure 8.6, the models were able to predict the loss of the CFRP system with reasonable accuracy. Further discussion about the structural effectiveness of the strengthening system is provided in the next section.

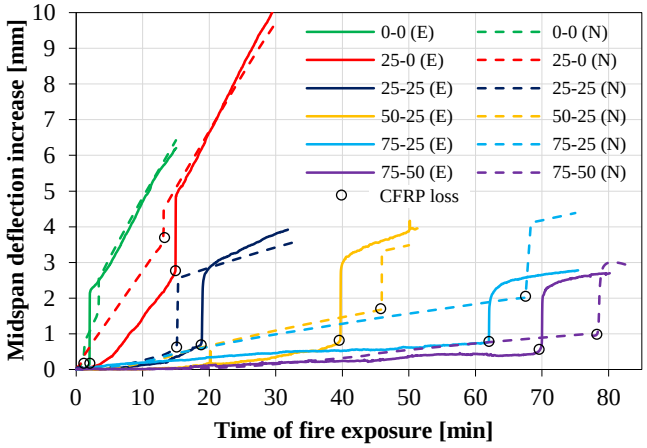

Figure 8.6: Measured (E) and predicted (N) midspan deflection increase vs. time of fire exposure.

8.3.3.2 Structural effectiveness of the strengthening system

Figure 8.6 indicates the instant when the structural effectiveness of the CFRP strengthening system of the different beams was lost. The corresponding failure mode can be evaluated from the numerical results presented in Figure 8.7, where the variation of the average bond stress at the

CFRP-concrete interface (along the CFRP anchorage length and central length, Figure 8.7a), the CFRP tensile stress at the midspan section (Figure 8.7b), as well as the normalized tensile stress in the bottom steel rebars at the midspan section (Figure 8.7b), all shown as a function of the time of fire exposure; again, the origin of the time scale corresponds to the beginning of the thermal exposure. For time = 0 min, as expected, Figure 8.7a shows (i) similar bond stresses in all beams (considering the same location), and (ii) higher average bond stresses along the anchorage length of the strengthening system (l_a, *cf.* Figure 8.1b) compared to those along the central length. Regarding the variation of bond stresses with time, two different behaviours are observed: (i) in beams 0-0 and 25-25 (null and constant insulation thickness, respectively) the average bond stresses along the CFRP anchorage length and the central zone are approximately constant during a relatively short period (about 0.7 MPa and 0.4 MPa, respectively) and then both suddenly decrease to zero, with such instants matching those when instantaneous increases in the displacement curves were observed (*cf.* Figure 8.6), *i.e.*, corresponding to the loss of structural effectiveness of the CFRP system; (ii) in the remaining beams (all with thicker insulation in the CFRP anchorage zones) average bond stresses in the anchorage and central zones were approximately constant during the initial stages of fire (in some case presenting slight increases), after which stresses along the central length decreased to zero, whereas those along the CFRP anchorage length increased at a high rate, then presented a less pronounced increase and finally decreased to zero, with such instant matching the loss of the CFRP system (*cf.* Figure 8.6). These results confirmed that the thicker insulation boards applied in the CFRP extremities promote bond stress transfer from the central part of the strengthening system to the anchorage zones, allowing the CFRP strip to retain its structural effectiveness through a cable behaviour - the CFRP-concrete bond is first damaged by the thermal action along the central length (less insulated), with the composite action in the CFRP anchorage length being preserved for longer periods of fire exposure.

Figure 8.7b shows that in all beams the CFRP tensile stress at the midspan section increased with the time of fire exposure; as temperatures/time increased, the flexural stiffness of the beams decreased and, as a consequence, the midspan displacement increased, as well as the tensile force/stress in the CFRP. In beams with thicker insulation, as expected, the stress increase rate was lower than that in less insulated beams. All beams exhibited a sudden CFRP stress decrease with such instant corresponding to the debonding of the CFRP strip in one of the anchorage zones, already identified in Figure 8.6 (and in Figure 8.7a). Figure 8.7b also shows that the CFRP normalized tensile stress (ratio between the stress level and the corresponding strength at a given temperature, based on test data by Wang *et al.* [27]) was very low in all beams, confirming that in the FE models no tensile failure occurred. Indeed, from the numerical results presented in Figure 8.7a and b it was possible to conclude that the failure mode of the strengthening system consisted

of the loss of bond between the CFRP strip and concrete (in the anchorage), which is in agreement with the post-fire observation of the tested beams (*cf.* Figure 7.7 – page 155).

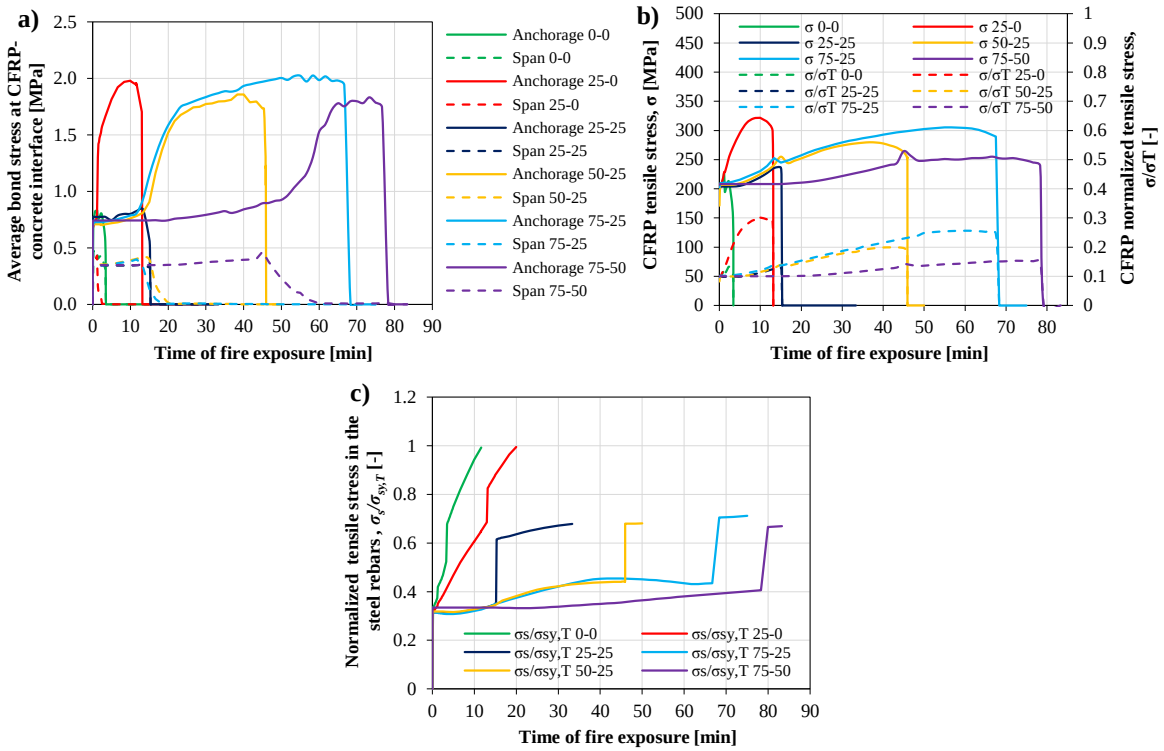

Figure 8.7: (a) Average bond stress at the CFRP-concrete interface (along the CFRP anchorage length and central zone) vs. time of fire exposure; (b) CFRP tensile stress at midspan vs. time of fire exposure; (c) normalized tensile stress in the steel rebars at the midspan section vs. time of fire exposure.

Regarding the variation of the tensile stress in the bottom steel rebars at the midspan section (depicted in Figure 8.7c; normalized with the temperature-dependent yield strength), as expected a sudden increase was observed in all beams when the strengthening systems lost their structural effectiveness. Figure 8.7c also shows that in beams 0-0 and 25-0 the steel rebars attained the yield stress a few minutes after CFRP debonding; in the remaining beams the calculated stresses were lower, since the stiffness (and strength) decrease of the materials was considerably reduced due to the insulation layers applied at the central zone. It is worth noting a slight reduction of the tensile stress in steel rebars of beam 75-25 after 45 min of fire exposure. Such stress reduction is related to (i) the thermal degradation of the elastic modulus of steel and to (ii) the fact that the thermal expansion of those rebars is restrained by the surrounding concrete (due to the different coefficients of thermal expansion of concrete and steel), resulting in localised compression effects. The latter phenomenon, also reported in [97], was not noticed in the remaining beams as the temperatures in the steel rebars were lower (*cf.* Figure 8.4).

The efficacy of the strategy adopted for the fire protection of the CFRP strengthening system can be assessed in Figure 8.8, which plots the predicted (numerical) and observed (experimental) times of fire exposure until the CFRP debonding in the anchorage zone. This figure shows that the FE

models were able to accurately predict the fire resistance of the CFRP systems. In the unprotected beam 0-0 the CFRP debonding occurred after only 3 min (*vs.* 2 min in the tests), confirming its high vulnerability when exposed to fire. When the 25 mm-thick CS board was applied only in the CFRP anchorage zones (beam 25-0), the predicted fire resistance of the strengthening system increased to 13 min (*vs.* 15 min in the tests). When this insulation board was applied along the entire CFRP length (beam 25-25), the predicted fire resistance of the CFRP system presented a small further increase up to 15 min (*vs.* 18 min in the tests). With increasing insulation thickness, particularly in the CFRP anchorage zones, consistent and significant improvements were observed: as an example, in beam 75-50 the CFRP debonding was predicted to occur after 79 min of fire (*vs.* 70 min in the tests).

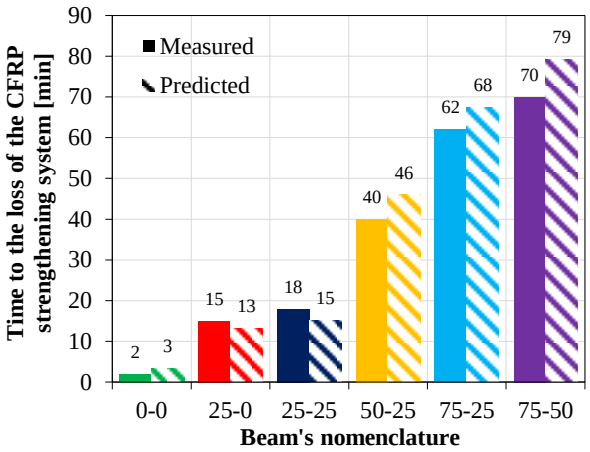

Figure 8.8: Predicted and observed time to complete debonding of the CFRP strengthening system.

8.4 CONCLUSIONS

This chapter presented a numerical study about the fire behaviour of RC beams flexurally strengthened with externally bonded CFRP strips simultaneously subjected to a service load and to the standard fire time-temperature curve of ISO 834. The results obtained from 2D FE models provided a better understanding about the structural effectiveness of EBR-CFRP systems when subjected to fire, allowing drawing the following conclusions:

- The thermal response of the insulated CFRP-strengthened RC beams subjected to fire was accurately predicted, in particular the temperature distribution along the CFRP-concrete interface.
- The structural fire response of the insulated CFRP-strengthened RC beams was also predicted with reasonable accuracy, in particular the loss of structural effectiveness of the CFRP system (due to CFRP debonding from the anchorages zones), showing that the global bond-slip laws for the CFRP-concrete interaction proposed in chapter 4 are adequate for simulating the behaviour of the EBR-CFRP strengthening systems under fire exposure.

- The numerical models confirmed that the application of a thicker insulation layer in the CFRP anchorage zones allows exploiting the CFRP mechanical contribution during fire even after the CFRP-concrete bond is destroyed along its central length; those insulation systems allow making use of the CFRP cable behaviour and therefore extend the fire resistance of the strengthening system, in some cases for more than 1 hour.
- The models predicted the occurrence of CFRP debonding in the anchorage zones when the average temperature in the CFRP-concrete interface attains values ranging from $1.1 \times T_g$ to $1.4 \times T_g$, which is in close agreement with previous experimental observations, thus demonstrating that the critical temperature in the anchorage zones is slightly to moderately higher than the adhesive T_g (determined from DMA tests and based on the onset of the storage modulus curve).

The results presented in this chapter also provided further validation to the strategy proposed in chapter 5 for the design of fire protection systems, which is based on the fulfillment of two main requirements: (i) the temperature of the CFRP strengthening element along the central zone must remain below a certain critical temperature, avoiding the tensile rupture of the CFRP; and (ii) the temperature of the CFRP-concrete interface along the anchorage length must be kept below the T_g of the adhesive to prevent the CFRP debonding for the required time of fire exposure. Furthermore, this chapter showed that current FE models can be used as an auxiliary tool for the design of fire protection systems for CFRP-strengthened RC structural members.

Part IV:

Conclusions and future developments

CHAPTER 9

CONCLUSIONS AND RECOMMENDATIONS FOR FUTURE RESEARCH

9.1 CONCLUSIONS

CFRP materials have been successfully used to strengthen civil engineering structures over the past 25 years due to their well-known advantages over traditional materials. Although the structural efficacy of strengthening techniques incorporating CFRPs at ambient temperature has been widely confirmed in numerous investigations, their performance at elevated temperatures continues to hinder a more widespread application in bridges subject to high service temperatures, and especially in buildings, where the fire action has to be considered at design. In fact, there is clear evidence that the strength, stiffness and bond properties of both CFRP and polymeric adhesives are severely deteriorated at moderately elevated temperature, namely when approaching their T_gs. These concerns are reflected in the current design guidelines for FRP-strengthening of RC structures that provide the following two recommendations when designing for the fire load combination: (i) to neglect the contribution of the CFRP systems, or (ii) to account for the contribution of the CFRP strengthening system, provided that it can be proven that these systems remain effective during the period of time required for a certain type of structural member and use. However, the guidelines provide absolutely no information on how to perform this verification.

In the context described above, the main objectives of this thesis were to provide in-depth understanding about the behaviour at elevated temperatures and under fire exposure of RC structures strengthened with CFRP materials and to develop a design method for the definition of tailored fire protection systems. Consequently, the research was developed along the two following domains:

1. Bond behaviour of CFRP-concrete interfaces at elevated temperature;
2. Fire behaviour of RC beams/slabs flexurally strengthened with CFRP strips.

The objectives initially defined for this thesis were accomplished. The main conclusion drawn from the research developed is that with the fire protection schemes proposed, comprising thicker thermal insulation in the anchorage zones, it is possible to exploit the mechanical contribution of the CFRP strengthening system during considerably long periods of fire exposure, thus allowing to

meet building codes requirements for most applications. Specific conclusions related to the above mentioned research domains are presented in the following two sections.

9.1.1 Bond behaviour of CFRP-concrete interfaces at elevated temperature

In the first research domain of the thesis, comprehensive experimental and numerical studies on the bond behaviour of CFRP-concrete interfaces at elevated temperature were performed.

The experimental programme (*cf.* chapter 3) allowed obtaining a significant amount of data, which were scarce (in some cases inexistent) in the literature. These data include the bond strength and stiffness degradation with temperature of CFRP-concrete interface for different strengthening techniques (EBR and NSM) and bonding agents (epoxy and mixed epoxy-cement adhesives, in the NSM technique), as well as the influence of applying mechanical anchorages (in EBR strips) in those interface properties.

The experimental results showed that regardless of the strengthening technique (NSM or EBR), with increasing temperatures the effective bond length consistently increases, the bond strength is continuously reduced and the strain distributions along the CFRP-concrete bonded interface become closer to linear. These results were attributed mostly to the softening of the bonding adhesives. Furthermore, it was shown that the influence of the test procedure adopted (steady-state or transient conditions) was negligible.

The results obtained from the NSM specimens with mixed epoxy-cement adhesive were not satisfactory as its performance at both ambient and elevated temperatures was worse than that of the conventional epoxy adhesive, pointing out the need to improve this type of inorganic adhesives. On the other hand, the incorporation of mechanical anchorages on EBR-strengthened specimens improved the performance of the bonded connection for both ambient and elevated temperatures, although these specimens experienced equivalent strength reductions with temperature when compared to those without such constructive detail.

The experiments showed that the bond strength of CFRP-concrete specimens strengthened according to the NSM technique is much higher (between 1.9 and 2.8 times) than that of similar specimens strengthened according to the EBR technique for all temperatures tested. Furthermore, the strength reduction with temperature of NSM-strengthened specimens is lower than that experienced by comparable EBR-strengthened specimens (*e.g.* 67% reduction at 120 °C *vs.* 77% in EBR specimens at the same temperature). Additionally, it was shown that for both strengthening techniques significant bond strength is kept for temperatures higher than the T_g of the adhesive and this was attributed to friction forces and chemical adhesion at the concrete-adhesive interface. This result is particularly relevant for practical applications, since it indicates that for both service and

fire conditions a critical temperature higher than the adhesive T_g can be defined, depending on the stress level installed on the strengthening system.

The numerical investigations on the CFRP-concrete bond at elevated temperature (*cf.* chapter 4) allowed deriving global bi-linear bond *vs.* slip laws for temperatures up to 150 °C (for both EBR and NSM techniques), that were then successfully implemented in the numerical simulation of the thermo-mechanical response of CFRP-strengthened RC elements subjected to fire (*cf.* chapter 8).

9.1.2 Fire behaviour of RC beams/slabs flexurally strengthened with CFRP strips

The second research topic of the thesis included experimental and numerical investigations about the fire behaviour of RC beams/slabs flexurally strengthened with CFRP strips. These investigations provided an in-depth understanding about the structural effectiveness of CFRP strengthening systems during exposure to fire. A methodology for the design of appropriate fire protection systems was also proposed and validated.

In a first stage of this research topic (*cf.* chapter 5), a strategy for designing insulation schemes for RC members flexurally strengthened with CFRP strips (installed according either EBR or NSM techniques) was proposed. This insulation strategy was based on results from preliminary fire resistance tests (carried out within the author's Master dissertation [5]) that showed that it is possible to exploit the CFRP mechanical contribution during fire through a cable behaviour, provided that its anchorage zones remain sufficiently cold. Therefore, the design methodology proposed involves applying thicker insulation layers in the CFRP anchorage zones to maintain the temperature of the CFRP-concrete interface below a critical temperature (first hypothesized as the T_g of the adhesive) avoiding CFRP debonding, and thinner ones along its central length, with the purpose of preventing the tensile rupture of the CFRP by maintaining its temperature below a certain temperature (defined based on the stress level installed on the CFRP together with the data available in the literature about its residual strength as a function of temperature). Numerical thermal models were developed and validated based on the good agreement with experimental data, and then used to illustrate the application of the above mentioned design methodology, namely to define optimum fire insulation schemes, for both EBR and NSM-strengthened RC slabs. The numerical results obtained showed that for similar insulation thicknesses NSM-strengthening systems present better performance than their EBR counterparts, in terms of the time needed for the CFRP-concrete interfaces to attain the adhesive T_g. Additionally, it was shown that using an epoxy adhesive with higher T_g is also a viable alternative or a complementary strategy to increase the fire endurance of CFRP-strengthened RC members.

The methodology proposed in chapter 5 for the design of fire insulation systems assumed that during fire it is possible to exploit the CFRP mechanical contribution through a cable behaviour; however, such behaviour was still not completely understood and characterised. In chapter 6, experimental and numerical investigation were performed at ambient temperature conditions with the objective of understanding in further depth the influence of the above mentioned cable behaviour on the mechanical response of CFRP-strengthened RC beams and, in particular, to confirm the possibility of taking such behaviour into account when designing fire protection systems, hence, serving as a proof of concept of the methodology proposed. The experimental results obtained on small-scale beams with partially bonded CFRP strips (NSM or EBR) – thus simulating the cable behaviour – showed that for both strengthening techniques, the strength reduction caused by partially bonding the strips is very limited, confirming that during a fire the cable behaviour exhibited by CFRP-strengthening systems can in fact provide the necessary load bearing capacity, provided that the mechanical properties of the materials (in current zone) and interfaces (in the anchorages) are not excessively deteriorated due to elevated temperature. The results obtained from the numerical models, first calibrated based on the agreement with experimental data, confirmed the main consequences of partially bonding the CFRP strips: limited effect on the beam's stiffness and strength, regardless of the CFRP strengthening technique (EBR or NSM) and loading type (point or uniformly distributed). Moreover, the numerical results allowed calibrating relations between the strength reduction due to the partial bonding and the l_b/L ratio (CFRP bonded length/free span). These relations were incorporated in a simplified procedure for the design of fire protection systems that improved/complemented the previous methodology (proposed in chapter 5).

In a second stage of the second research topic (*cf.* chapter 7), fire resistance tests were performed on RC beams flexurally strengthened with either EBR- or NSM-CFRP strips, comprising different fire insulation schemes (with thicker protection in the anchorage zones). These tests allowed tracing the thermal and mechanical responses of the beams, providing very relevant and comprehensive experimental data, and allowing understanding in further depth their thermo-mechanical behaviour, namely the effectiveness at high temperature of the CFRP strengthening systems. These tests also validated the above mentioned strategy for the design of fire protection systems – as expected, the thicker insulation layers applied in the CFRP anchorage zones allowed extending the structural effectiveness of the CFRP strengthening system by making use of the referred cable behaviour. Additional experimental results demonstrated that using a high T_g adhesive combined with the proposed fire insulation schemes allowed extending further the fire resistance of the CFRP system (the CFRP debonding occurred 25 minutes later than in a comparable conventional epoxy adhesive), as well as the application of the mechanical anchorage at the CFRP ends, although in this case only slight improvements were obtained. Nevertheless, this

experimental campaign demonstrated that is possible to exploit the mechanical contribution of EBR-CFRP strengthening systems during fire exposure, in some case for more than 90 min. Such fire resistances meet most of the building codes requirements.

The results obtained from the fire resistance tests performed on EBR-strengthened RC beams showed that the debonding of the strengthening system occurred when the average temperature in the adhesive in the anchorage zones attained values ranging from $1.2 \times T_g$ to $1.5 \times T_g$, thus demonstrating that the critical temperature in the anchorage zones is slightly to moderately higher than the adhesive T_g (determined from DMA tests and based on the onset of the storage modulus curve). These results confirm that the critical temperature considered in the methodology for the design of fire insulation systems (firstly hypothesized as the adhesive T_g) is slightly conservative.

The results obtained from NSM-strengthened RC beams showed that with the insulation systems proposed the strengthening system lost its structural effectiveness when the average temperature in the adhesive in the anchorage zones attained values ranging from $2.2 \times T_g$ to $6.6 \times T_g$, providing an important conclusion related to the design of tailored fire protection schemes: for NSM-strengthened members the critical temperature in the anchorage zone can be considered, at least, as $2 \times T_g$, with T_g being determined as mentioned above. Furthermore, the comparison between the fire behaviour of similar EBR- and NSM-strengthened RC beams confirmed the better performance of the latter strengthening technique: in fact, with the former technique, the CFRP debonding occurred after considerably shorter periods of fire exposure and for much lower average temperatures in the adhesive in the anchorage zones. Additionally, it was also shown that the fire resistance of NSM strengthening system was considerably improved by applying a thin insulation layer along the current zone (together with the insulation of the anchorage zones), whereas in the EBR system the influence of the insulation thickness in the current zone was much less significant.

In chapter 8 the 2D FE models of the insulated EBR-strengthened RC beams were able to simulate both thermal and mechanical responses of the beams tested under fire conditions. The loss of structural effectiveness of the CFRP system (due to CFRP debonding from the anchorages zones) was predicted with considerable accuracy, showing that the global bond-slip laws for the CFRP-concrete interaction proposed in chapter 4 are adequate for simulating the behaviour of the EBR-CFRP strengthening systems under fire exposure. Furthermore, the numerical results confirmed that the application of thicker insulation layers in the CFRP anchorage zones allows exploiting the CFRP mechanical contribution during fire even after the CFRP-concrete bond is destroyed along its central length (cable behaviour), providing further validation to the methodology put forward for the design of fire protection systems.

Finally, it is worth pointing out that the above mentioned conclusions, besides being important for the scientific community, have practical relevance regarding the application of CFRP strengthening

systems in RC structures likely to be subjected to fire (buildings), which may ultimately allow to widespread their use in building applications.

9.2 RECOMMENDATIONS FOR FUTURE RESEARCH

The experimental and numerical investigations presented in this thesis provided a better understanding of the behaviour at elevated temperatures and under fire exposure of RC structures strengthened with CFRP strips. Although a relevant number of innovative developments and conclusions have been drawn, several topics remain to be investigated. This section describes the recommendations for future investigations in this field, which were organized according to the two research domains developed in the present thesis.

9.2.1 Bond behaviour of FRP-concrete interfaces at elevated temperature

In what concerns the bond of FRP materials to concrete at elevated temperatures further research should focus on the following aspects:

- Bond tests with different types of (i) FRP strengthening materials (basalt or glass fibre composites), (ii) FRP configurations (sheets or bars), (iii) FRP surface finishing (sand coated, ribbed, external wound fibres), (iv) concrete surface preparation (sand blasting, grinding, high pressure water jetting), and (v) concrete strength.
- Development of analytical formulations to provide temperature-dependent global bond *vs.* slip laws for the different strengthening techniques, FRP materials and concrete properties.
- Additional bond tests to provide an in-depth understanding about the importance of considering the thermal strains developed during the heating phase of the specimens, as well as to assess the influence of its duration and the potential occurrence of post-curing phenomena.
- Development of improved cement-based adhesives (less prone to thermal degradation) capable of providing adequate mechanical performance at ambient temperature conditions and superior behaviour under exposure to elevated temperatures/fire.
- Assessing the influence of thermal cycles and sustained stress on the FRP-concrete interface properties at elevated temperature.

9.2.2 Fire behaviour of RC members incorporating FRPs

With regard to the fire behaviour of RC members strengthened with FRP materials and the development of fire protection systems, the following aspects worth further investigation:

- Additional fire resistance tests on RC members strengthened with the FRP strengthening materials/shapes mentioned in the previous section (first and fourth bullets).

- Assessing the potential beneficial effect of post-curing on the performance of the FRP strengthening systems when exposed to elevated temperatures or fire.
- Development of 3D FE models capable of simulating the thermo-mechanical response of insulated FRP-strengthened RC members under fire exposure, modeling in particular the structural effectiveness of NSM-CFRP strengthening systems during fire (not addressed in the numerical study presented in chapter 8).
- Additional experimental and numerical investigations on CFRP-strengthened RC beams with both bottom and lateral faces subjected to fire, allowing validating the fire protection schemes proposed in the present thesis for different thermal boundary conditions.
- Post-fire bending tests on FRP-strengthened RC members previously exposed to certain durations of fire exposure without FRP debonding, allowing determining their residual strength and the feasibility of repair.
- Development of innovative detailing solutions able to improve the anchoring capacity of the FRP systems at elevated temperature (*e.g.* bending their extremities into the RC member), delaying FRP debonding and therefore allowing exploiting the FRP cable behaviour for longer periods of fire exposure (with less insulation material).
- Additional fire resistance tests on full-scale CFRP-strengthened RC beams in order to confirm the efficacy of the methodology proposed for the design of fire protection schemes.
- Evaluating the fire behaviour of RC members shear-strengthened with FRP systems, either externally bonded, near surface mounted or embedded through the section.
- Studying the influence of (i) the strengthening level, (ii) the loading configuration (point or uniformly distributed), (iii) the axial restriction, and (iv) the type of thermal exposure (real or standard fire) on the fire response of FRP-strengthened RC members.
- Addressing the effect of high temperature or fire exposure on the mechanical response of RC members strengthened with prestressed FRP systems – the effect of the adhesive softening is expected to present a major influence in the FRP pre-stress level.

The above-mentioned recommendations are natural developments of the work presented in this thesis. The following suggestions are more general and include further research on the fire behaviour of FRP materials and RC structures reinforced with FRP bars:

- Experimental characterization of the temperature dependent thermo-physical properties of both FRP's and insulation materials, which are presently very scarce in the literature.
- Experimental determination of the mechanical properties of various FRP materials (with different shapes/configurations and types of fibres) and adhesives at elevated temperatures (high temperature properties) and after high temperature exposure (residual properties).

- Experimental and numerical investigations on the fire behaviour of RC structures reinforced with FRP bars, assessing the feasibility of exploiting the cable behaviour of the FRP bars by extending its extremities to cold regions and/or applying thicker insulations in their anchorage zones, as well as evaluating the influence of FRP bar surface finishing, lap splices and type of end anchors.
- Assessing the fire behaviour of concrete members reinforced with hybrid steel-FRP prestressed bars, which have shown good performance at ambient temperature conditions (*e.g.* [143]), but whose performance at elevated temperature has not yet been investigated.

BIBLIOGRAPHY

[1] C. Bakis, L. Bank, V. Brown, E. Cosenza, J. Davalos, J. Lesko, A. Machida, S. Rizkalla, T. Triantafillou, Fiber-reinforced polymer composites for construction: state-of-the-art review, *Journal of Composites for Construction*, Vol. 6, No. 2, pp. 73-87, 2002.

[2] V. Karbhari, J. Chin, D. Hunston, B. Benmokrane, T. Juska, R. Morgan, J. Lesko, U. Sorathia, D. Reynaud, Durability gap analysis for fiber-reinforced polymer composites in civil infrastructure, *Journal of Composites for Construction*, Vol. 7, No. 3, pp. 238-247, 2003.

[3] K. A. Harries, M. L. Porter, J. Busel, FRP materials and concrete - research needs, *Concrete International*, Vol. 25, No. 10, pp. 49-54, 2003.

[4] L. A. Bisby, M. F. Green, V. K. R. Kodur, Response to fire of concrete structures that incorporate FRP, *Progress in Structural Engineering and Materials*, Vol. 7, No. 3, pp. 136-149, 2005.

[5] J. P. Firmo, *Fire Protection System for Reinforced Concrete Beams Strengthened with CFRP Laminates*, MSc dissertation in Civil Engineering, Instituto Superior Técnico - Universidade de Lisboa, Lisbon, Portugal, 2010.

[6] ISO 834-1, *Fire-Resistance Tests - Elements of Building Construction - Part 1: General Requirements*, International Organization for Standardization, Geneve, Switzerland, 1999.

[7] J. P. Firmo, C. López, C. Tiago, Desenvolvimento de sistemas de protecção ao fogo para elementos de betão armado reforçados com laminados de CFRP, *Construção Magazine*, Vol. 49, pp. 10-17, 2012.

[8] J. P. Firmo, J. R. Correia, Comportamento da ligação betão-CFRP a temperaturas elevadas: estudo experimental, *Construção Magazine*, Vol. 64, pp. 16-20, 2014.

[9] J. P. Firmo, D. Pitta, J. R. Correia, M. Arruda, H. Vallé, H. Cruz, Effect of elevated temperature on the bond of CFRP-concrete interfaces, In *2nd International Conference on the Structural Adhesive Bonding (AB2013)*, Porto, Portugal, 2013.

[10] J. P. Firmo, D. Pitta, J. R. Correia, M. R. T. Arruda, C. Tiago, Experimental and numerical study on the bond behaviour of CFRP-concrete in interfaces at elevated temperature, In *7th International Conference on FRP Composites in Civil Engineering (CICE 2014)*, R. El-Hacha, Vancouver, Canada, 2014.

[11] J. P. Firmo, M. R. T. Arruda, J. R. Correia, Contribution to the understanding of the mechanical behaviour of CFRP-strengthened RC beams in fire: experimental and numerical

assessment, In *11th International Sympoisum on Fiber Reinforced Polymer for Reinforced Concrete Structures (FRPRCS-11)*, Barros J. A. O., Sena-Cruz J., University of Minho, Guimarães, 2013.

[12] C. López, J.P. Firmo, C. Tiago, J.R. Correia, Fire protection systems for reinforced concrete beams and slabs strengthened with CFRP laminates, In *6th International Conference on FRP Composites in Civil Engineering (CICE 2012)*, Rome, Italy, 2012.

[13] J. P. Firmo, J. R. Correia, P. França, S. Cabral-Fonseca, Fire protection systems for reinforced concrete beams strengthened with CFRP laminates, In *16th International Conference on Composite Structures (ICCS 16)*, Porto, Portugal, 2011.

[14] J. P. Firmo, J. R. Correia, C. Tiago, Comportamento ao fogo de vigas de betão armado reforçadas com laminados de CFRP. Estudo experimental, In *5as Jornadas Portuguesas de Engenharia de Estruturas (JPEE 2014)*, LNEC, Lisboa, Portugal, 2014.

[15] J. P. Firmo, J. R. Correia, C. Tiago, Comportamento ao fogo de vigas de betão armado reforçadas à flexão com laminados de CFRP colados exteriormente. Estudo experimental, In *4as Jornadas de Segurança aos Incêndios Urbanos*, Bragança, Portugal, 2014.

[16] CEN, *Eurocode 2: Design of Concrete Structures - Part 1-2: General Rules - Structural Fire Design*, EN 1992-1-2, European Committe for Standardization, Brussels, Belgium, 2010.

[17] FIB, *The fib Model Code for Concrete Structures*, Model Code 2010, International Federation for Structural Concrete (FIB), Laussanne, Switzerland, 2010.

[18] ACI Committee 216, *Guide for Determining the Fire Endurance of Concrete Elements*, ACI-216R-89, American Concrete Institute, Farmington Hills, MI, USA, 1989.

[19] ACI/TMS Committee 216, *Code Requirements for Determining Fire Resistance of Concrete and Masonry Construction Assemblies*, ACI-216.1-07, American Concrete Institute, Farmington Hills, MI, USA, 2007.

[20] ASCE Committee on Fire Protection - Structural Division, *Structural Fire Protection*, Manual of Practice No. 78, American Society of Civil Engineers, New York, USA, 1992.

[21] Z. P. Bazant, M. F. Kaplan, *Concrete at High Temperatures: Material Properties and Mathematical Models*, Concrete Design and Construction Series, Longman, 412p., London, UK, 1996.

[22] P. Bamonte, R. Felicetti, High-temperature behaviour of concrete in tension, *Structural Engineering International*, Vol. 22, No. 4, pp. 493-499, 2012.

[23] L. Phan, N. Carino, Review of mechanical properties of HSC at elevated temperature, *Journal of Materials in Civil Engineering*, Vol. 10, No. 1, pp. 58-65, 1998.

[24] J. R. Correia, *GFRP Pultruded Profiles in Civil Engineering: Hybrid Solutions, Bonded Connections and Fire Behavior*, PhD thesis in Civil Engineering, Instituto Superior Técnico - Universidade de Lisboa, Lisbon, Portugal, 2008.

[25] A. P. Mouritz, A. G. Gibson, *Fire Properties of Polymer Composite Materials*, Springer, 394p., Dordrecht, Netherlands, 2006.

[26] C. Shenghu, W. Zhis, W. Xin, Tensile properties of CFRP and hybrid FRP composites at elevated temperatures, *Journal of Composite Materials*, Vol. 43, No. 4, pp. 315-330, 2009.

[27] K. Wang, B. Young, S. T. Smith, Mechanical properties of pultruded carbon fibre-reinforced polymer (CFRP) plates at elevated temperatures, *Engineering Structures*, Vol. 33, No. 7, pp. 2154-2161, 2011.

[28] E. U. Chowdhury, R. Eedson, L. A. Bisby, M. F. Green, N. Benichou, Mechanical characterization of fibre reinforced polymers materials at high temperature, *Fire Technology*, Vol. 47, No. 4, pp. 1063-1080, 2011.

[29] B. Yu, V. K. R. Kodur, Effect of temperature on strength and stiffness properties of near-surface mounted FRP reinforcement, *Composites Part B: Engineering*, Vol. 58, pp. 510-517, 2014.

[30] W. D. Bascom, R. L. Cottington, Effect of temperature on the adhesive fracture behavior of an elastomer-epoxy eesin, *The Journal of Adhesion*, Vol. 7, No. 4, pp. 333-346, 1976.

[31] O. Moussa, A. P. Vassilopoulos, J. de Castro, T. Keller, Time–temperature dependence of thermomechanical recovery of cold-curing structural adhesives, *International Journal of Adhesion and Adhesives*, Vol. 35, pp. 94-101, 2012.

[32] A. G. Gibson, Y. S. Wu, J. T. Evans, A. P. Mouritz, Laminate theory analysis of composites under load in fire, *Journal of Composites Materials*, Vol. 40, No. 7, pp. 639-658, 2006.

[33] C. A. Mahieux, K. L. Reifsnider, S. W. Case, Property modeling across transition temperatures in PMC's: Part I. Tensile properties, *Applied Composite Materials*, Vol. 8, No. 4, pp. 217-234, 2001.

[34] L. A. Bisby, *Fire Behaviour of Fibre-Reinforced Polymer (FRP) Reinforced or Confined Concrete*, PhD thesis in Civil Engineering, Queen's University, Kingston, Ontario, Canada, 2003.

[35] H. Blontrock, *Analysis and Modeling of the Fire Resistance of Concrete Elements with Externally Bonded FRP Reinforcement*, PhD thesis in Civil Engineering, Ghent University, Ghent, Belgium, 2003.

[36] E. L. Klamer, D. A. Hordijk, H. J. M. Janssen, The Influence of temperature on the debonding of externally bonded CFRP, In *7th International Symposium on Fiber-Reinforced (FRP) Polymer*

Reinforcement for Concrete Structures, C. K. Shield, J. P. Busel, S. L. Walkup, D. D. Gremel, New Orleans, USA, 2005.

[37] E. L. Klamer, *Influence of Temperature on Concrete Beams Strengthened in Flexure with CFRP*, PhD thesis in Civil Engineering, Eindhoven University of Technology, Eindhoven, Netherlands, 2009.

[38] Z. S. Wu, K. Iwashita, S. Yagashiro, T. Ishikawa, Y. Hamaguchi, Temperature effect on bonding and debonding behavior between FRP sheets and concrete, *Journal of the Society of Materials Science, Japan*, Vol. 54, No. 5, pp. 474-480, 2005.

[39] J. C. P. H. Gamage, M. B. Wong, R. Al-Mahadi, Performance of CFRP strengthened concrete members under elevated temperatures, In *Proceeding of the International Sysposium on Bond Behaviour of FRP in Structures (BBFS 2005)*, J. F. Teng, J. G. Chen, Hong Kong, China, 2005.

[40] M. Leone, S. Matthys, M. A. Aiello, Effect of elevated service temperature on bond between FRP EBR systems and concrete, *Composites Part B: Engineering*, Vol. 40, No. 1, pp. 85-93, 2009.

[41] J. P. Firmo, D. Pitta, J. R. Correia, C. Tiago, M. R. T. Arruda, Experimental characterization of the bond between externally bonded reinforcement (EBR) CFRP strips and concrete at elevated temperatures, *Cement and Concrete Composites*, Vol. 60, pp. 44-54, 2015.

[42] A. Palmieri, S. Matthys, L. Taerwe, Bond behavior of NSM FRP bars at elevated temperatures, In *First Middle East Conference on Smart Monitoring Assessment and Rehabilitation of Civil Structures (SMAR 2011)*, M. Motavalli, B. Havranek, E. Saqan, Dubai, 2011.

[43] P. J. Burke, L. A. Bisby, M. F. Green, Effects of elevated temperature on near surface mounted and externally bonded FRP strengthening systems for concrete, *Cement and Concrete Composites*, Vol. 35, No. 1, pp. 190-199, 2013.

[44] B. Yu, V. K. R. Kodur, Effect of high temperature on bond strength of near-surface mounted FRP reinforcement, *Composite Structures*, Vol. 110, pp. 88-97, 2014.

[45] J. P. Firmo, D. Pitta, J. R. Correia, C. Tiago, M. R. T. Arruda, Bond behavior at high temperatures between near surface mounted (NSM) CFRP strips and concrete, *Journal of Composites for Construction*, (accepted for publication - doi: 10.1061/(ASCE)CC.1943-5614.0000535), No. pp., 2014.

[46] W. Gao, J. G. Teng, J. Dai, Effect of temperature variation on the full-range behavior of FRP-to-concrete bonded joints, *Journal of Composites for Construction*, Vol. 16, No. 6, pp. 671-683, 2012.

[47] J. Dai, W. Gao, J. G. Teng, Bond-slip model for FRP laminates externally bonded to concrete at elevated temperature, *Journal of Composites for Construction*, Vol. 17, No. 2, pp. 217-228, 2013.

[48] H. Yuan, J. G. Teng, R. Seracino, Z. S. Wu, J. Yao, Full-range behavior of FRP-to-concrete bonded joints, *Engineering Structures*, Vol. 26, No. 5, pp. 553-565, 2004.

[49] J. Dai, T. Ueda, Y. Sato, Development of the nonlinear bond stress–slip model of fiber reinforced plastics sheet–concrete interfaces with a simple method, *Journal of Composites for Construction*, Vol. 9, No. 1, pp. 52-62, 2005.

[50] L. A. Bisby, V. K. R. Kodur, M. F. Green, Fire endurance of fiber-reinforced polymer-confined concrete columns, *ACI Structural Journal*, Vol. 102, No. 6, pp. 883-891, 2005.

[51] E. U. Chowdhury, L. A. Bisby, M. F. Green, V. K. R. Kodur, Investigation of insulated FRP-wrapped reinforced concrete columns in fire, *Fire Safety Journal*, Vol. 42, No. 6–7, pp. 452-460, 2007.

[52] V. K. R. Kodur, L. A. Bisby, M. F. Green, Experimental evaluation of the fire behaviour of insulated fibre-reinforced-polymer-strengthened reinforced concrete columns, *Fire Safety Journal*, Vol. 41, No. 7, pp. 547-557, 2006.

[53] N. Bénichou, D. Cree, E. U. Chowdhury, M. F. Green, L. A. Bisby, Fire testing of FRP strengthened reinforced concrete columns, In *International Conference on Durability & Sustainability of FRP Composites for Construction and Rehabilitation (CDCC 2011)*, Quebec, Canada, 2011.

[54] ISIS, *Strengthening Reinforced Concrete Structures with Externally Bonded Fiber Reinforced Polymers*, Intelligent Sensing for Innovative Structures Canada, Winnipeg, Manitoba, Canada, 2001.

[55] ASTM International Subcommitte E05.11, *Standard Methods of Fire Test of Building Construction and Materials, American Society for Testing and Materials*, ASTM E119-14 American Society for Testing and Materials, West Conshohocken, USA, 2014.

[56] ACI Committee 440, *Guide for the Design and Construction of Externally Bonded FRP Systems for Strengthening Concrete Structures*, ACI 440.2R-08, American Concrete Institute, Farmington Hills, MI, USA, 2008.

[57] H. Blontrock, L. Taerwe, P. Vandevelde, Fire testing of concrete slabs strengthened with fibre composite laminates, In *Proceedings of the 5th Annual Symposium on Fibre-Reinforced-Plastic Reinforcement for Concrete Structures*, London, UK, 2001.

[58] B. Williams, L. A. Bisby, V. K. R. Kodur, M. F. Green, E. C. Chowdhury, Fire insulation schemes for FRP-strengthened concrete slabs, *Composites Part A: Applied Science and Manufacturing*, Vol. 37, No. 8, pp. 1151-1160, 2006.

[59] M. Adelzadeh, M. F. Green, N. Bénichou, Behaviour of fibre reinforced polymer-strengthened T-beams and slabs in fire, *Structures and Buildings*, Vol. 165, No. SB7, pp. 361-371, 2012.

[60] T. J. Stratford, M. Gillie, J. F. Chen, A. S. Usmani, Bonded fibre reinforced polymer strengthening in a real fire, *Advances in Structural Engineering*, Vol. 12, No. 6, pp. 867-878, 2009.

[61] M. Deuring, *Brandversuche an Nachtraglich Verstarkten Tragern aus Beton*, Research report EMPA no. 148,795, Swiss Federal Laboratories for Materials Testing and Research, Dubendorf, Switzerland, 1994

[62] N. Grace, M. Bebawy, Fire protection for beams with fiber-reinforced polymer flexural strengthening systems, *ACI Structural Journal*, Vol. 111, No. 3, pp. 537-548, 2014.

[63] B. Williams, V. K. R. Kodur, M. F. Green, L. A. Bisby, Fire endurance of fiber-reinforced polymer strengthened concrete T-beams, *ACI Structural Journal*, Vol. 105, No. 1, pp. 60-67, 2008.

[64] H. Blontrock, L. Taerwe, P. Vandevelde, Fire tests on concrete beams strengthened with fibre composites laminates, In *Proceedings of the 3rd International PhD Symposium in Civil Engineering*, Konrad Bergmeister, Vienna, Austria, 2000.

[65] H. Kexu, H. Guisheng, L. Fan, Experimental study on fire protection methods of reinforced concrete beams strengthened with carbon fiber reinforced polymer, *Frontiers of Architecture and Civil Engineering in China*, Vol. 1, No. 4, pp. 399-404, 2007.

[66] A. Ahmed, V. K. R. Kodur, The experimental behavior of FRP-strengthened RC beams subjected to design fire exposure, *Engineering Structures*, Vol. 33, No. 7, pp. 2201-2211, 2011.

[67] CEN, *Eurocode 1: Actions on Structures - Part 1-2: General Actions - Actions on structures Exposed to Fire*, EN 1991-1-2, European Committee for Standardization, Brussels, Belgium, 2010.

[68] J. P. Firmo, J. R. Correia, P. França, Fire behaviour of reinforced concrete beams strengthened with CFRP laminates: Protection systems with insulation of the anchorage zones, *Composites Part B: Engineering*, Vol. 43, No. 3, pp. 1545-1556, 2012.

[69] J. P. Firmo, J. R. Correia, Fire behaviour of thermally insulated RC beams strengthened with EBR-CFRP strips: experimental study, *Composite Structures*, Vol. 122, No. pp. 144-154, 2015.

[70] A. Palmieri, S. Matthys, L. Taerwe, Experimental investigation on fire endurance of insulated concrete beams strengthened with near surface mounted FRP bar reinforcement, *Composites Part B: Engineering*, Vol. 43, No. 3, pp. 885-895, 2012.

[71] A. Palmieri, S. Matthys, L. Taerwe, Fire endurance and residual strength of insulated concrete beams strengthened with near-surface mounted reinforcement, *Journal of Composites for Construction*, Vol. 17, No. 4, pp. 454-462, 2013.

[72] H. Zhu, G. Wu, L. Zhang, J. Zhang, D. Hui, Experimental study on the fire resistance of RC beams strengthened with near-surface-mounted high-Tg BFRP bars, *Composites Part B: Engineering*, Vol. 60, pp. 680-687, 2014.

[73] B. Yu, V. K. R. Kodur, Fire behavior of concrete T-beams strengthened with near-surface mounted FRP reinforcement, *Engineering Structures*, Vol. 80, pp. 350-361, 2014.

[74] J. P. Firmo, J. R. Correia, Fire behaviour of thermally insulated RC beams strengthened with NSM-CFRP strips: experimental study, *Composites Part B: Engineering*, Vol. 76, pp. 112-121, 2015.

[75] L. A. Bisby, M. F. Green, V. K. R. Kodur, Modeling the behavior of fiber reinforced polymer-confined concrete columns exposed to fire, *Journal of Composites for Construction*, Vol. 9, No. 1, pp. 15-24, 2005.

[76] C. A. Griffis, R. A. Masumura, C. I. Chang, Thermal response of graphite epoxy composite subjected to rapid heating, *Environmental effects on composite materials, Technomic, Lancaster*, Vol. 2, pp. 245-260, 1984.

[77] M. Spoelstra, G. Monti, FRP-confined concrete model, *Journal of Composites for Construction*, Vol. 3, No. 3, pp. 143-150, 1999.

[78] E. C. Chowdhury, L. A. Bisby, M. F. Green, N. Bénichou, V. K. R. Kodur, Heat transfer and structural response modelling of FRP confined rectangular concrete columns in fire, *Construction and Building Materials*, Vol. 32, pp. 77-89, 2012.

[79] W. F. Chen, T. Atsuta, *Theory of Beam-Columns*, McGraw Hill, New York, USA, 1976.

[80] G. Luciano, A. Vignoli, Strength and ductility of HSC and SCC slender columns subjected to short-term eccentric load, *ACI Structural Journal*, Vol. 105, No. 3, pp. 259-269, 2008.

[81] Z. Tao, Q. Yu, Behaviour of CFRP-strengthened slender square RC columns, *Magazine of Concrete Research*, Vol. 60, No. 7, pp. 523-533, 2008.

[82] T. T. Lie, J. L. Woollerton, *Fire resistance of reinforced concrete columns: test results*, IRC Internal Report No. 569, National Research Council of Canada, Ottawa, Canada, 1998.

[83] C. López, J. P. Firmo, J. R. Correia, C. Tiago, Fire protection systems for reinforced concrete slabs strengthened with CFRP laminates, *Construction and Building Materials*, Vol. 47, pp. 324-333, 2013.

[84] J. P. Firmo, M. R. T. Arruda, J. R. Correia, C. Tiago, Flexural behaviour of partially bonded carbon fibre reinforced polymers strengthened concrete beams: Application to fire protection systems design, *Materials & Design*, Vol. 65, pp. 1064-1074, 2014.

[85] R. A. Hawileh, M. Naser, W. Zaidan, H. A. Rasheed, Modeling of insulated CFRP-strengthened reinforced concrete T-beam exposed to fire, *Engineering Structures*, Vol. 31, No. 12, pp. 3072-3079, 2009.

[86] N. Wang, J. T. Evans, Collapse of continuous fibre composite beams at elevated temperatures, *Composites*, Vol. 26, No. 1, pp. 56-61, 1995.

[87] H. Varastehpour, P. Hamelin, Strengthening of concrete beams using fiber-reinforced platics, *Materials and Structures*, Vol. 30, No. 3, pp. 160-166, 1997.

[88] V. K. R. Kodur, A. Ahmed, Numerical model for tracing the response of FRP-strengthened RC beams exposed to fire, *Journal of Composites for Construction*, Vol. 14, No. 6, pp. 730-742, 2010.

[89] A. Ahmed, V. K. R. Kodur, Effect of bond degradation on fire resistance of FRP-strengthened reinforced concrete beams, *Composites Part B: Engineering*, Vol. 42, No. 2, pp. 226-237, 2011.

[90] V. K. R. Kodur, B. Yu, Evaluating the fire response of concrete beams strengthened with near-surface-mounted FRP reinforcement, *Journal of Composites for Construction*, Vol. 17, No. 4, pp. 517-529, 2013.

[91] J. Sena-Cruz, J. A. O. Barros, Bond between near-surface mounted carbon-fiber-reinforced polymer laminate strips and concrete, *Journal of Composites for Construction*, Vol. 8, No. 6, pp. 519-527, 2004.

[92] A. Katz, N. Berman, L. Bank, Effect of high temperature on bond strength of FRP rebars, *Journal of Composites for Construction*, Vol. 3, No. 2, pp. 73-81, 1999.

[93] H. A. Rasheed, R. R. Harrison, R. J. Peterman, T. Alkhrdaji, Ductile strengthening using externally bonded and near surface mounted composite systems, *Composite Structures*, Vol. 92, No. 10, pp. 2379-2390, 2010.

[94] J. Dai, W. Gao, J. G. Teng, Finite element modeling of insulated FRP-strengthened RC beams exposed to fire, *Journal of Composites for Construction*, Vol. 19, No. 2, pp., 2015.

[95] C. A. Griffis, R. A. Masumura, C. I. Chang, Thermal response of graphite epoxy composite subjected to rapid heating, *Journal of Composite Materials*, Vol. 15, No. 5, pp. 427-442, 1981.

[96] FIB, *The fib Model Code for Concrete Structures*, Model Code 1990, International Federation for Structural Concrete (FIB), Lausanne, Switzerland, 1993.

[97] W. Y. Gao, Jian-Guo Dai, J. G. Teng, G. M. Chen, Finite element modeling of reinforced concrete beams exposed to fire, *Engineering Structures*, Vol. 52, pp. 488-501, 2013.

[98] CSA, *Design and Construction of Building Structures with Fibre-Reinforced Polymers*, CAN/CSA-S806-12, Canadian Standards Association / National Standard of Canada, Rexdale, Ontario, Canada, 2012.

[99] FIB, *Externally Bonded FRP Reinforcement for RC Structures*, Bulletin 14, International Federation for Structural Concrete, Lausanne, Switzerland, 2001.

[100] CNR, *Guide for the Design and Construction of Externally Bonded FRP Systems for Strengthening Existing Structures*, CNR-DT200/2013-R1, National Research Council - Advisory Committee on Technical Recommendations for Construction, Rome, Italy, 2013.

[101] ISO, *Plastics - Determination of Tensile Properties - Part 5: Test Conditions for Unidirectional Fibre-Reinforced Plastic Composites*, ISO 527-5, International Organization for Standardization, Geneve, Switzerland, 2009.

[102] ISO, *Plastics - Determination of Tensile Properties - Part 2: Test Conditions for Moulding and Extrusion Plastics*, ISO 527-2, International Organization for Standardization, Geneve, Switzerland, 2012.

[103] ISO, *Plastics - Diffential Scanning Calorimetry (DSC) - Part 1: General Principles*, ISO 11357-1, International Organization for Standardization, Geneve, Switzerland, 2009.

[104] C. Mazzotti, M. Savoia, B. Ferracuti, An experimental study on delamination of FRP plates bonded to concrete, *Construction and Building Materials*, Vol. 22, No. 7, pp. 1409-1421, 2008.

[105] X. Z. Lu, J. G. Teng, L. P. Ye, J. J. Jiang, Bond–slip models for FRP sheets/plates bonded to concrete, *Engineering Structures*, Vol. 27, No. 6, pp. 920-937, 2005.

[106] L. Bizindavyi, K. Neale, Transfer lengths and bond strengths for composites bonded to concrete, *Journal of Composites for Construction*, Vol. 3, No. 4, pp. 153-160, 1999.

[107] T. Vallée, *Adhesively Bonded Lap Joints of Pultruded GFRP Shapes*, PhD thesis in Civil Engineering, École Polytechnique Fédérale de Lausanne, Lausanne, Switzerland, 2004.

[108] B. Ferracuti, M. Savoia, C. Mazzotti, Interface law for FRP–concrete delamination, *Composite Structures*, Vol. 80, No. 4, pp. 523-531, 2007.

[109] L. De Lorenzis, A. Nanni, Bond between near-surface mounted fiber-reinforced polymer rods and concrete in structural strengthening, *ACI Structural Journal*, Vol. 99, No. 2, pp. 123-132, 2002.

[110] R. Seracino, N. Jones, M. Ali, M. Page, D. Oehlers, Bond strength of near-surface mounted FRP strip-to-concrete joints, *Journal of Composites for Construction*, Vol. 11, No. 4, pp. 401-409, 2007.

[111] S. S. Zhang, J. G. Teng, T. Yu, Bond strength model for CFRP strips near-surface mounted to concrete, *Journal of Composites for Construction*, Vol. 18, No. 3, pp. Special Issue - 10th Anniversary of IIFC - A4014003 2014.

[112] SIMULIA, *ABAQUS 6.11 - Analysis User's Manual, Dassault Systèmes*, Rhode Island, USA, 2011.

[113] J. M. Lee, G. L. Fenves, Plastic-damage model for cyclic loading of concrete structures, *Journal of Engineering Mechanics*, Vol. 124, No. 8, pp. 892-900, 1998.

[114] S. V. Saidu, G. Hadjisophocleous, S. Craft, *Fire Safety - Properties of Materials at Elevated Temperatures*, CIB-W014, International Council for Research and Innovation in Building and Construction, Delft, Netherlands, 2010.

[115] M. A. Crisfield, *Non-Linear Finite Element Analysis of Solids and Structures*, Volume 2: Advanced Topics, John Wiley & Sons, 1997.

[116] M. A. Crisfield, *Non-Linear Finite Element Analysis of Solids and Structures*, Volume 1: Essentials, John Wiley & Sons, 1991.

[117] B. Ferracuti, M. Savoia, C. Mazzotti, A numerical model for FRP–concrete delamination, *Composites Part B: Engineering*, Vol. 37, No. 4–5, pp. 356-364, 2006.

[118] G. Chen, J. Teng, J. Chen, Finite-element modeling of intermediate crack debonding in FRP-plated RC beams, *Journal of Composites for Construction*, Vol. 15, No. 3, pp. 339-353, 2010.

[119] A. Bilotta, F. Ceroni, M. Di Ludovico, E. Nigro, M. Pecce, G. Manfredi, Bond efficiency of EBR and NSM FRP systems for strengthening concrete members, *Journal of Composites for Construction*, Vol. 15, No. 5, pp. 757-772, 2011.

[120] W. Xue, L. Zeng, Y. Tan, Experimental studies on bond behaviour of high strength CFRP plates, *Composites Part B: Engineering*, Vol. 39, No. 4, pp. 592-603, 2008.

[121] S. Feih, A. P. Mouritz, Tensile properties of carbon fibres and carbon fibre–polymer composites in fire, *Composites Part A: Applied Science and Manufacturing*, Vol. 43, No. 5, pp. 765-772, 2012.

[122] ADINA R&D Inc., *Automatic Dynamic Incremental Non linear Analysis (ADINA), User's Manual, Version 8.8*, MA, USA, 2012.

[123] C. Tracy, *Fire Endurance of Multicellular Panels in an FRP Building System*, PhD thesis in Civil Engineering, École Polytechnique Fédérale de Lausanne, Lausanne, Switzerland, 2005.

[124] J. R. Miller, P. M. Weaver, Temperature profiles in composite plates subject to time-dependent complex boundary conditions, *Composite Structures*, Vol. 59, No. 2, pp. 267-278, 2003.

[125] Promat, Promatect-L500 technical data sheet. 2012.

[126] J. M. Mimoso, *Theoretical bases for building applications - Technical information for buildings*, LNEC, Lisboa, Portugal, 1987.

[127] Cervenka Consulting, *Advaced Tool for Engineering Nonlinear Analysis (ATENA) Software - Version 4.2.2*, Prague, Czech Republic, 2009.

[128] J. Červenka, V. K. Papanikolaou, Three dimensional combined fracture–plastic material model for concrete, *International Journal of Plasticity*, Vol. 24, No. 12, pp. 2192-2220, 2008.

[129] S. Hashemi, R. Al-Mahaidi, Experimental and finite element analysis of flexural behavior of FRP-strengthened RC beams using cement-based adhesives, *Construction and Building Materials*, Vol. 26, No. 1, pp. 268-273, 2012.

[130] M. R. Aram, C. Czaderski, M. Motavalli, Debonding failure modes of flexural FRP-strengthened RC beams, *Composites Part B: Engineering*, Vol. 39, No. 5, pp. 826-841, 2008.

[131] F. Schladitz, M. Frenzel, D. Ehlig, M. Curbach, Bending load capacity of reinforced concrete slabs strengthened with textile reinforced concrete, *Engineering Structures*, Vol. 40, pp. 317-326, 2012.

[132] B. Matos, J. R. Correia, L. M. S. Castro, P. França, Structural response of hyperstatic concrete beams reinforced with GFRP bars: Effect of increasing concrete confinement, *Composite Structures*, Vol. 94, No. 3, pp. 1200-1210, 2012.

[133] P. Duarte, J. R. Correia, J. G. Ferreira, F. Nunes, M. R. T. Arruda, Experimental and numerical study on the effect of repairing reinforced concrete cracked beams strengthened with CFRP laminates, *Canadian Journal of Civil Engineering*, Vol. 41, No. 3, pp. 222-231, 2014.

[134] A. Bilotta, C. Faella, E. Martinelli, E. Nigro, Indirect identification method of bilinear interface laws for FRP bonded on a concrete substrate, *Journal of Composites for Construction*, Vol. 16, No. 2, pp. 171-184, 2012.

[135] F. Ceroni, M. Pecce, A. Bilotta, E. Nigro, Bond behavior of FRP NSM systems in concrete elements, *Composites Part B: Engineering*, Vol. 43, No. 2, pp. 99-109, 2012.

[136] P. Neto, J. Alfaiate, J. R. Almeida, E. B. Pires, The influence of mode II fracture on concrete strengthened with CFRP, *Computers & Structures*, Vol. 82, No. 17–19, pp. 1495-1502, 2004.

[137] F. Buyle-Bodin, E. David, E. Ragneau, Finite element modelling of flexural behaviour of externally bonded CFRP reinforced concrete structures, *Engineering Structures*, Vol. 24, No. 11, pp. 1423-1429, 2002.

[138] CEN, *Eurocode 2: Design of Concrete Structures - Part 1-1: General Rules and Rules for Buildings*, EN 1992-1-1, Brussels, Belgium, 2010.

[139] J. M. Lees, J. Burgoyne, Experimental study of influence of bond on flexural behaviour of concrete beams pretensioned with aramid fiber reinforced plastic, *ACI Structural Journal*, Vol. 96, No. 3, pp. 377-386, 1999.

[140] H. T. Choi, J. S. West, K. A. Soudki, Analysis of the flexural behavior of partially bonded FRP strengthened concrete beams, *Journal of Composites for Construction*, Vol. 12, No. 4, pp. 375-386, 2008.

[141] H. T. Choi, J. S. West, K. A. Soudki, Partially bonded near-surface-mounted CFRP bars for strengthened concrete T-beams, *Construction and Building Materials*, Vol. 25, No. 5, pp. 2441-2449, 2011.

[142] ISO, *Plastics - Diffential Scanning Calorimetry (DSC) - Part 2: Determination of Glass Transition Temperature and Glass Transition Step Height*, ISO 11357-2, Geneve, Switzerland, 2013.

[143] F. Soltanzadeh, H. Mazaheripour, J. A. O. Barros, T. Mahsa, J. Sena-Cruz, Experimental study on shear behavior of HPFRC beams reinforced by hybrid pre-stressed GFRP and steel bars, In *7th International Conference on FRP Composites in Civil Engineering (CICE 2014)*, R. El-Hacha, Vancouver, Canada, 2014.